STARS

University of Central Florida
STARS

Electronic Theses and Dissertations, 2004-2019

2018

Trace Element Analysis of Human Dentition from the Elite Meroitic Cemetery at Sedeinga, Sudan to Determine Dietary Consumption and Cultural Behaviors

Tiffany Lee
University of Central Florida

Part of the Archaeological Anthropology Commons
Find similar works at: https://stars.library.ucf.edu/etd
University of Central Florida Libraries http://library.ucf.edu

This Masters Thesis (Open Access) is brought to you for free and open access by STARS. It has been accepted for inclusion in Electronic Theses and Dissertations, 2004-2019 by an authorized administrator of STARS. For more information, please contact STARS@ucf.edu.

STARS Citation

Lee, Tiffany, "Trace Element Analysis of Human Dentition from the Elite Meroitic Cemetery at Sedeinga, Sudan to Determine Dietary Consumption and Cultural Behaviors" (2018). *Electronic Theses and Dissertations, 2004-2019*. 6374.
https://stars.library.ucf.edu/etd/6374

TRACE ELEMENT ANALYSIS OF HUMAN DENTITION FROM THE ELITE MEROITIC CEMETERY AT SEDEINGA, SUDAN TO DETERMINE DIETARY CONSUMPTION AND CULTURAL BEHAVIORS

by

TIFFANY M. LEE
B.A. University of Hawaii West Oahu, 2015

A thesis submitted in partial fulfillment of the requirements
for the degree of Master of Arts
in the Department of Anthropology
in the College of Sciences
at the University of Central Florida
Orlando, Florida

Summer Term
2018

© 2018 Tiffany M. Lee

ABSTRACT

Minimal research has been conducted on the human skeletal remains from this site, and this research is aimed toward adding knowledge of the Nubian culture for the period between the 1st c. AD to the 4th c. AD, particularly focusing on answering the following questions: 1) Was intra- individual variation present in dietary consumption or cultural behaviors based on elements found within an individual's multiple molars after analysis; 2) Was an inter-individual variation apparent, based on developmental age through permanent molars, that indicated a distinction between dietary consumption against all individuals; and 3) Based on known medicinal and cosmetic use of kohl in neighboring societies, as well as archaeological evidence found at Sedeinga, if individuals will have used kohl based on observed increased levels of lead or antimony? A trace element analysis was performed on an archaeological sample from 13 individuals consisting of 21 first, second, and third permanent molars excavated from the elite Nubian Meroitic Cemetery of Sedeinga, located in northern Sudan.

Elemental analysis was performed using Laser Ablation-Inductively Coupled Plasma-Mass Spectrometry (LA-ICP-MS). A total of 13 trace elements including Ca^{44} and P^{31}; minor elements Mg^{24}, S^{32}, C^{13}, and Sr^{88}; metals Fe^{56}, Cu^{63}, Zn^{66}, Sb^{121}, and Pb^{208}; and La^{139} and U^{238} were analyzed for each sample with concentration values mapped and analyzed. The data collected during laser ablation was utilized to create two-dimensional detection and concentration maps of each tooth using MATLAB® software. Analysis of concentration values confirmed dietary change from early childhood to late adolescence across the population. Probable use of antimony and lead-based kohl was determined from high concentration values

mapped in dentition. Two-dimensional mapping of trace elements within teeth have revealed cultural and dietary changes across the population.

ACKNOWLEDGMENTS

I am very grateful to all that have helped me during my journey through graduate school. With the help of my graduate committee I have become a better writer, researcher, problem solver, and overall person. It is through their hard work and their commitment to instill success in their students that I have finished my first stretch of graduate school as a competent and credible individual within my field of study. I would especially like to thank my advisor, Dr. Tosha Dupras, for her words of encouragement while navigating me through the deep waters of graduate school. Her belief in my abilities to succeed gave me the confidence I needed to succeed, not only academically, but professionally as well. I would also like to thank my committee members, Dr. Lana Williams and Dr. John J. Schultz, both of which pushed me to become a better student through their encouraging words, motivational talks, and continual guidance throughout the last two years.

I would also like to thank Dr. Mauro Labrador for his patience and assistance in preparing and analyzing my research sample. I am truly grateful that he was able to share his time and knowledge with me throughout my research process. I would also like to thank Dr. Matthieu Baudelet for sharing his resources and knowledge as well.

I would also like to thank Dr. Vincent Francigny and Dr. Claude Rilly for the opportunity to perform my research by utilizing a sample from their archaeological site of Sedeinga. Their knowledge, hard-work, and detailed excavations have made my research possible.

Lastly, I would also like to thank my family and friends for pushing me through some of the more challenging times of graduate school. Their motivational speeches came when I needed

them the most. The overall support I received gave me the confidence I needed to not only finish but continue with school at the doctoral level.

Nyaweñha and Mahalo to everyone I have met throughout this journey.

TABLE OF CONTENTS

LIST OF FIGURES xxi
LIST OF TABLES xxiv
LIST OF ABBREVIATIONS xxv
CHAPTER ONE: INTRODUCTION 1
Research Questions 2
CHAPTER TWO: ARCHAEOLOGICAL SAMPLE BACKGROUND 5
Sedeinga 5
Tomb Structure 9
Diet 11
Kohl 12
CHAPTER THREE: LITERATURE REVIEW 14
Dentition 14
Dental Composition 14
Enamel 15
Dentin 16
Incremental lines 17
Chronology of Tooth Formation 18
Element absorption 20
Trace Elements 21
Major Elements 25
Calcium 25
Phosphorus 26
Minor elements 27
Magnesium 27
Sulfur 29
Carbon 30
Trace Metals 31

Iron 31
Copper 32
Zinc 33
Strontium 34
Laser Ablation-Inductively Coupled Plasma-Mass Spectrometry (LA-ICP-MS) 35
Advantages of LA-ICP-MS 36
CHAPTER FOUR: METHODS AND MATERIALS 38
Documentation 38
Individual Dental Age Assessment 39
IIT 160-01 41
IIT 160-02 41
IIT 178-01 42
IIT 190-01 43
IIT 197-01 44
IIT 213-01 44
IIT 217-01 45
IIT 220-01 46
IIT 236-01 47
IIT 263-01 48
IIT 312-01 49
IIT 315-01 49
IIT 316-01 50
Sample Preparation 51
LA-ICP-MS Analysis 55
Standard Solutions 57
Mapping 62
CHAPTER FIVE: RESULTS 66
Two-dimensional Maps 66
Individual IIT 160-01 67
First molar 67
Carbon (C13) 67

Magnesium (Mg^{24}) 67
Phosphorus (P^{31}) 68
Sulfur (S^{32}) 68
Calcium (Ca^{44}) 68
Iron (Fe^{56}) 69
Copper (Cu^{63}) 69
Zinc (Zn^{66}) 70
Strontium (Sr^{88}) 70
Antimony (Sb^{121}) 71
Lanthanum (La^{139}) 71
Lead (Pb^{208}) 71
Uranium (U^{238}) 72
Individual IIT 160-02 72
Second molar 72
Carbon (C13) 72
Magnesium (Mg^{24}) 72
Phosphorus (P^{31}) 73
Sulfur (S^{32}) 73
Calcium (Ca^{44}) 73
Iron (Fe^{56}) 74
Copper (Cu^{63}) 74
Zinc (Zn^{66}) 75
Strontium (Sr^{88}) 76
Antimony (Sb^{121}) 76
Lanthanum (La^{139}) 77
Lead (Pb^{208}) 77
Uranium (U^{238}) 78
Third Molar 78
Carbon (C^{13}) 78
Magnesium (Mg^{24}) 78
Phosphorus (P^{31}) 79

Sulfur (S^{32}) 79
Calcium (Ca^{44}) 79
Iron (Fe^{56}) 80
Copper (Cu^{63}) 80
Zinc (Zn^{66}) 81
Strontium (Sr^{88}) 81
Antimony (Sb^{121}) 82
Lanthanum (La^{139}) 82
Lead (Pb^{208}) 83
Uranium (U^{238}) 83
Individual IIT 178-01 83
First molar 83
Carbon (C^{13}) 83
Magnesium (Mg^{24}) 84
Phosphorus (P^{31}) 84
Sulfur (S^{32}) 84
Calcium (Ca^{44}) 85
Iron (Fe^{56}) 85
Copper (Cu^{63}) 85
Zinc (Zn^{66}) 86
Strontium (Sr^{88}) 86
Antimony (Sb^{121}) 87
Lanthanum (La^{139}) 87
Lead (Pb^{208}) 87
Uranium (U^{238}) 88
Second Molar 88
Carbon (C^{13}) 88
Magnesium (Mg^{24}) 89
Phosphorus (P^{31}) 89
Sulfur (S^{32}) 89
Calcium (Ca^{44}) 90

Iron (Fe^{56})..... 90
Copper (Cu^{63})..... 90
Zinc (Zn^{66}) 91
Strontium (Sr^{88})..... 91
Antimony (Sb^{121}) 92
Lanthanum (La^{139}) 92
Lead (Pb^{208})..... 92
Uranium (U^{238})..... 93
Third Molar..... 93
Carbon (C^{13})..... 93
Magnesium (Mg^{24})..... 94
Phosphorus (P^{31}) 94
Sulfur (S^{32})..... 94
Calcium (Ca^{44}) 94
Iron (Fe^{56})..... 95
Copper (Cu^{63})..... 95
Zinc (Zn^{66}) 95
Strontium (Sr^{88})..... 96
Antimony (Sb^{121}) 96
Lanthanum (La^{139}) 96
Lead (Pb^{208})..... 97
Uranium (U^{238})..... 97
Individual IIT 190-01..... 97
First molar..... 97
Carbon (C^{13})..... 97
Magnesium (Mg^{24})..... 98
Phosphorus (P^{31}) 98
Sulfur (S^{32})..... 98
Calcium (Ca^{44}) 99
Iron (Fe^{56})..... 99
Copper (Cu^{63})..... 99

Zinc (Zn^{66}) 100
Strontium (Sr^{88}) 100
Antimony (Sb^{121}) 101
Lanthanum (La^{139}) 101
Lead (Pb^{208}) 101
Uranium (U^{238}) 102
Individual IIT 197-01 102
First molar 102
Carbon (C^{13}) 102
Magnesium (Mg^{24}) 103
Phosphorus (P^{31}) 103
Sulfur (S^{32}) 104
Calcium (Ca^{44}) 105
Iron (Fe^{56}) 105
Copper (Cu^{63}) 106
Zinc (Zn^{66}) 107
Strontium (Sr^{88}) 108
Antimony (Sb^{121}) 109
Lanthanum (La^{139}) 109
Lead (Pb^{208}) 109
Uranium (U^{238}) 110
Second molar 111
Carbon (C^{13}) 111
Magnesium (Mg^{24}) 111
Phosphorus (P^{31}) 112
Sulfur (S^{32}) 112
Calcium (Ca^{44}) 112
Iron (Fe^{56}) 112
Copper (Cu^{63}) 113
Zinc (Zn^{66}) 113
Strontium (Sr^{88}) 114

Antimony (Sb^{121}) 114
Lanthanum (La^{139}) 115
Lead (Pb^{208}) 115
Uranium (U^{238}) 115
Individual IIT 213-01 116
First molar 116
Carbon (C^{13}) 116
Magnesium (Mg^{24}) 116
Phosphorus (P^{31}) 116
Sulfur (S^{32}) 117
Calcium (Ca^{44}) 117
Iron (Fe^{56}) 117
Copper (Cu^{63}) 118
Zinc (Zn^{66}) 118
Strontium (Sr^{88}) 119
Antimony (Sb^{121}) 119
Lanthanum (La^{139}) 119
Lead (Pb^{208}) 120
Uranium (U^{238}) 120
Individual IIT 217-01 121
First molar 121
Carbon (C^{13}) 121
Magnesium (Mg^{24}) 121
Phosphorus (P^{31}) 122
Sulfur (S^{32}) 122
Calcium (Ca^{44}) 122
Iron (Fe^{56}) 123
Copper (Cu^{63}) 123
Zinc (Zn^{66}) 124
Strontium (Sr^{88}) 124
Antimony (Sb^{121}) 125

Lanthanum (La^{139}) 125
Lead (Pb^{208}) 125
Uranium (U^{238}) 126
Individual IIT 220-01 126
First molar 126
Carbon (C^{13}) 126
Magnesium (Mg^{24}) 126
Phosphorus (P^{31}) 127
Sulfur (S^{32}) 127
Calcium (Ca^{44}) 128
Iron (Fe^{56}) 128
Copper (Cu^{63}) 129
Zinc (Zn^{66}) 129
Strontium (Sr^{88}) 130
Antimony (Sb^{121}) 130
Lanthanum (La^{139}) 131
Lead (Pb^{208}) 131
Uranium (U^{238}) 132
Second molar 132
Carbon (C^{13}) 132
Magnesium (Mg^{24}) 132
Phosphorus (P^{31}) 133
Sulfur (S^{32}) 133
Calcium (Ca^{44}) 133
Iron (Fe^{56}) 134
Copper (Cu^{63}) 134
Zinc (Zn^{66}) 135
Strontium (Sr^{88}) 135
Antimony (Sb^{121}) 136
Lanthanum (La^{139}) 136
Lead (Pb^{208}) 137

Uranium (U^{238}) 137
Third molar 138
Carbon (C^{13}) 138
Magnesium (Mg^{24}) 138
Phosphorus (P^{31}) 138
Sulfur (S^{32}) 139
Calcium (Ca^{44}) 139
Iron (Fe^{56}) 139
Copper (Cu^{63}) 140
Zinc (Zn^{66}) 140
Strontium (Sr^{88}) 141
Antimony (Sb^{121}) 141
Lanthanum (La^{139}) 141
Lead (Pb^{208}) 142
Uranium (U^{238}) 142
Individual IIT 236-01 143
First molar 143
Carbon (C^{13}) 143
Magnesium (Mg^{24}) 143
Phosphorus (P^{31}) 144
Sulfur (S^{32}) 144
Calcium (Ca^{44}) 144
Iron (Fe^{56}) 145
Copper (Cu^{63}) 145
Zinc (Zn^{66}) 145
Strontium (Sr^{88}) 146
Antimony (Sb^{121}) 147
Lanthanum (La^{139}) 147
Lead (Pb^{208}) 147
Uranium (U^{238}) 148
Individual IIT 263-01 148

First molar 148
Carbon (C^{13}) 148
Magnesium (Mg^{24}) 149
Phosphorus (P^{31}) 149
Sulfur (S^{32}) 150
Calcium (Ca^{44}) 150
Iron (Fe^{56}) 150
Copper (Cu^{63}) 151
Zinc (Zn^{66}) 151
Strontium (Sr^{88}) 152
Antimony (Sb^{121}) 153
Lanthanum (La^{139}) 153
Lead (Pb^{208}) 153
Uranium (U^{238}) 154
Individual IIT 312-01 154
First molar 154
Carbon (C^{13}) 154
Magnesium (Mg^{24}) 155
Phosphorus (P^{31}) 155
Sulfur (S^{32}) 156
Calcium (Ca^{44}) 156
Iron (Fe^{56}) 156
Copper (Cu^{63}) 156
Zinc (Zn^{66}) 157
Strontium (Sr^{88}) 158
Antimony (Sb^{121}) 158
Lanthanum (La^{139}) 158
Lead (Pb^{208}) 159
Uranium (U^{238}) 159
Third molar 159
Carbon (C^{13}) 159

Magnesium (Mg^{24}) 160
Phosphorus (P^{31}) 160
Sulfur (S^{32}) 160
Calcium (Ca^{44}) 160
Iron (Fe^{56}) 161
Copper (Cu^{63}) 161
Zinc (Zn^{66}) 161
Strontium (Sr^{88}) 162
Antimony (Sb^{121}) 162
Lanthanum (La^{139}) 163
Lead (Pb^{208}) 163
Uranium (U^{238}) 163
Individual IIT 315-01 164
First molar 164
Carbon (C^{13}) 164
Magnesium (Mg^{24}) 164
Phosphorus (P^{31}) 164
Sulfur (S^{32}) 165
Calcium (Ca^{44}) 165
Iron (Fe^{56}) 165
Copper (Cu^{63}) 165
Zinc (Zn^{66}) 166
Strontium (Sr^{88}) 166
Antimony (Sb^{121}) 167
Lanthanum (La^{139}) 167
Lead (Pb^{208}) 167
Uranium (U^{238}) 168
Second molar 168
Carbon (C^{13}) 168
Magnesium (Mg^{24}) 169
Phosphorus (P^{31}) 169

Sulfur (S^{32}) 169
Calcium (Ca^{44}) 169
Iron (Fe^{56}) 170
Copper (Cu^{63}) 170
Zinc (Zn^{66}) 170
Strontium (Sr^{88}) 171
Antimony (Sb^{121}) 171
Lanthanum (La^{139}) 172
Lead (Pb^{208}) 172
Uranium (U^{238}) 172
Individual IIT 316-01 173
Second molar 173
Carbon (C^{13}) 173
Magnesium (Mg^{24}) 173
Phosphorus (P^{31}) 174
Sulfur (S^{32}) 174
Calcium (Ca^{44}) 174
Iron (Fe^{56}) 175
Copper (Cu^{63}) 175
Zinc (Zn^{66}) 176
Strontium (Sr^{88}) 176
Antimony (Sb^{121}) 177
Lanthanum (La^{139}) 177
Lead (Pb^{208}) 177
Uranium (U^{238}) 178
Comparative Concentration Analysis 179
Inter-Individual Analysis 179
Copper (Cu^{63}) 180
First Molar Comparison 180
Second Molar Comparison 181
Third Molar Comparison 182

Strontium (Sr^{88}) 183
First Molar Comparison 183
Second Molar Comparison 184
Third Molar Comparison 185
Zinc (Zn^{66}) 186
First Molar Comparison 186
Second Molar Comparison 187
Third Molar Comparison 188
Antimony ($Sb^{121)}$ 189
First Molar Comparison 189
Second Molar Comparison 190
Third Molar Comparison 191
Lead (Pb^{208}) 192
First Molar Comparison 192
Second Molar Comparison 193
Third Molar Comparison 194
Intra-Individual Analysis 195
Copper 195
Strontium 197
Zinc 198
Antimony 199
Lead 200
CHAPTER SIX: DISCUSSION 202
Inter-Individual Analysis 202
Copper (Cu^{63}) 202
First Molar Comparison 203
Second Molar Comparison 204
Third Molar Comparison 204
Strontium (Sr^{88}) 205
First Molar Comparison 206
Second Molar Comparison 206

Third Molar Comparison 207
Zinc (Zn^{66}) 208
First Molar Comparison 208
Second Molar Comparison 209
Third Molar Comparison 209
Antimony (Sb^{121}) 210
First Molar Comparison 210
Second Molar Comparison 210
Third Molar Comparison 211
Lead (Pb^{208}) 211
First Molar Comparison 212
Second Molar Comparison 212
Third Molar Comparison 213
Intra-Individual Analysis 213
Copper 213
Strontium 215
Zinc 216
Antimony 217
Lead 219
CHAPTER SEVEN: CONCLUSION 221
Limitations 224
Future Research 225
APPENDIX A: ELEMENT MAPS 227
APPENDIX B: INTER- AND INTRA- INDIVIDUAL ELEMENT COMPARISONS BASED ON LITERATURE 284
REFERENCES 289

LIST OF FIGURES

Figure 1 Geographical location of the archaeological site of Sedeinga located in Northeastern Africa within modern day Sudan. Map adapted from National Geographic Map. 6
Figure 2 Topographical map of Sedeinga with area of sample extraction highlighted (adapted from Rilly and Francigny, 2010). 7
Figure 3 Map of funerary clusters in Sector II (adapted from Rilly and Francigny, 2011). 9
Figure 4 Sample IIT 160-01_M1 as received for analysis. 41
Figure 5 Left: Sample IIT 160-02_M2 as received for analysis. Right: Sample IIT160-2_M3 as received for analysis. 42
Figure 6 Left: Sample IIT 178-01_M1 as received for analysis. Center: Sample IIT 178-01_M2 as received for analysis. Right: Sample IIT 178-01_M3 as received for analysis. 43
Figure 7 Sample IIT 190-01_M1 as received for analysis. 43
Figure 8 Left: Sample IIT 197-01_M1 as received for analysis. Right: Sample IIT 197-01_M2 as received for analysis. 44
Figure 9 Sample IIT 213-01_M1 as received for analysis. 45
Figure 10 Sample IIT 217-01_M1 as received for analysis. 46
Figure 11 Left: Sample IIT 220-01_M1 as received for analysis. Center: Sample IIT 220-01_M2 as received for analysis. Right: Sample IIT 220-01_M3 as received for analysis. 47
Figure 12 Sample IIT 236-01_M1 as received for analysis. 48
Figure 13 Sample IIT 263-01_M1 as received for analysis. 48
Figure 14 Left: Sample IIT 312-01_M1 as received for analysis. Right: Sample IIT 312-01_M3 as received for analysis. 49
Figure 15 Left: Sample IIT 315-01_M1 as received for analysis. Right: Sample IIT 315-01_M2 as received for analysis. 50
Figure 16 Sample IIT 316-01_M2 as received for analysis 50
Figure 17 Process overview. Step-by-step procedure for preparing samples for data analysis... 51
Figure 18 Sample IIT 197-01_M2. Left: Sample as received for analysis. Right: Sample following cleaning and reconstruction. 52
Figure 19. Materials: epoxy hardener and epoxy resin, used to embed samples. 53
Figure 20 Embedding process. Left: Sample placement in silicone mold prior to resin added. Center: Labelling system used (sample IIT 315-01_M2). Right: Sample placement inside the de-pressurizer chamber. 53
Figure 21 Left: Locked de-pressurizer with samples placed inside. Right: Gage set at ~20psi for ~24 hours. 53
Figure 22 Samples embedded in resin with labels that correspond with samples. 54
Figure 23 Left: Buehler™ IsoMet Speed Saw and saw speed at ~8. Center: sample placed in the chuck for thin-sectioning. Right: thin-sectioned sample mounted on adhesive on a black disk. . 55
Figure 24 Left: Materials used for creating standard solutions. Right: Pictured from left to right: Synthetic hydroxyapatite, multi-element, sulfur, magnesium. 57

Figure 25 Measurement of synthetic hydroxyapatite used as the base material in standard solution mixture. 59
Figure 26 Left: Four standard solutions prior to hand-pressing. Right: Materials used to hand-press standard solution tablets. From left to right: ceramic mortar and pestle, final standard solution tablet, and handheld pill press. 60
Figure 27 Image of standard solutions taken by the macro-camera feature in Axiom-LA®. 61
Figure 28 Screenshot of computer code with lines 3, 9, 10, 11 which require adjustment according to sample. 64
Figure 29 Screenshot of computer code for each element with axis parameters (line 72) needing adjustment to create contrast in two-dimensional map. 65
Figure 30. Scale of determined detection and concentration values for two-dimensional mapping of each element. 67
Figure 31 Graphed concentration values of copper (Cu^{63}) for all first molar (M1) dental samples to evaluate inter-individual analysis. 181
Figure 32 Graphed concentration values of copper (Cu^{63}) for all second molar (M2) dental samples to evaluate inter-individual analysis. 182
Figure 33 Graphed concentration values of copper (Cu^{63}) for all third molar (M3) dental samples to evaluate inter-individual analysis. 183
Figure 34 Documented concentration values of strontium (Sr^{88}) for all first molar (M1) dental samples to evaluate inter-individual analysis. 184
Figure 35 Documented concentration values of strontium (Sr^{88}) for all second molar (M2) dental samples to evaluate inter-individual analysis. 185
Figure 36 Documented concentration values of strontium (Sr^{88}) for all third molar (M3) dental samples to evaluate inter-individual analysis. 186
Figure 37 Graphed concentration values of zinc (Zn^{66}) for all first molar (M1) dental samples to evaluate inter-individual analysis. 187
Figure 38 Graphed concentration values of zinc (Zn^{66}) for all first molar (M1) dental samples to evaluate inter-individual analysis. 188
Figure 39 Graphed concentration values of zinc (Zn^{66}) for all third molar (M3) dental samples to evaluate inter-individual analysis. 189
Figure 40 Graphed concentration values of antimony (Sb^{121}) for all first molar (M1) dental samples to evaluate inter-individual analysis. 190
Figure 41 Graphed concentration values of antimony (Sb^{121}) for all second molar (M2) dental samples to evaluate inter-individual analysis. 191
Figure 42 Graphed concentration values of antimony (Sb^{121}) for all third molar (M3) dental samples to evaluate inter-individual analysis. 192
Figure 43 Graphed concentration values of lead (Pb^{208}) for all first molar (M1) dental samples to evaluate inter-individual analysis. 193
Figure 44 Graphed concentration values of lead (Pb^{208}) for all second molar (M2) dental samples to evaluate inter-individual analysis. 194

Figure 45 Graphed concentration values of lead (Pb^{208}) for all third molar (M3) dental samples to evaluate inter-individual analysis. 195
Figure 46 Outlined graphed concentration values of copper (Cu^{63}) for dental samples to evaluate intra-individual analysis. 196
Figure 47 Outlined graphed concentration values of strontium (Sr^{88}) for dental samples to evaluate intra-individual analysis. 198
Figure 48 Outlined graphed concentration values of zinc (Zn^{66}) for dental samples to evaluate intra-individual analysis. 199
Figure 49 Outlined graphed concentration values of antimony (Sb^{121}) for dental samples to evaluate intra-individual analysis. 200
Figure 50 Outlined graphed concentration values of lead (Pb^{208}) for dental samples to evaluate intra-individual analysis. 201

LIST OF TABLES

Table 1. Artifacts found concealed in tombs in Sector II (Rilly & Francigny 2010; 2011). 11
Table 2. Element overview. Element information including category, physiological role, with deficiency and toxicity effects. 24
Table 3. Sample inventory including first, second, or third permanent molars present for analysis per individual. 38
Table 4 Root completion stages (Moorrees et al., 1963). 40
Table 5 Individual age assessment based on Moorrees et al. (1963) and Smith (1991). 40
Table 6 Four standard solution used for standard reference material to determine concentration values of trace elements. 58
Table 7 Element concentration values (N/A- not available; L- low; I- intermediate; H- high).. 178
Table 8. Inter- and intra- individual comparison of copper, zinc, and strontium to determine breastfeeding habits in M1 samples. 285
Table 9 Inter- and intra- individual variation of strontium and zinc to determine dietary consumption in M2 and M3. 286
Table 10. Inter- and intra- individual variation of exposure levels to antimony in M1, M2, and M3. 287
Table 11 Inter- and intra- individual variation of exposure levels of lead in M1, M2, and M3. 288

LIST OF ABBREVIATIONS

A1/2	Apex ½ Closed
Ac	Apex Closure Completed
AD	Anno Domini
Ca	Calcium
cm	centimeter
Cu	Copper
DEJ	Dentin Enamel Junction
Fe	Iron
g	gram
H	High
I	Intermediate
L	Low
La	Lanthanum
LA-ICP-MS	Laser Ablation- Inductively Coupled Plasma-Mass Spectrometry
M	Molar
M1	First Molar
M2	Second Molar
M3	Third Molar
Mg	Magnesium
µm	micrometer
mg	milligram
mm	millimeter
MNI	Minimum Number of Individuals
N/A	Not Available
P	Phosphorus
Pb	Lead

ppb	parts per billion
ppm	parts per million
ppt	parts per trillion
psi	pounds per square inch
R1/4	Root Length ¼
R1/2	Root Length ½
R3/4	Root Length ¾
Rc	Root Completion
Ri	Initial Root Formation
S	Sulfur
Sb	Antimony
SEDAU	Sedeinga Archaeological Unit
Sr	Strontium
U	Uranium
UL	Upper Limit
Zn	Zinc

CHAPTER ONE: INTRODUCTION

Two anthropological sub-disciplines, biological anthropology and archaeology, often combine methodologies to further understand the behaviors of past populations. Human remains contain information that can aid in identifying various aspects of their daily activities. Due to the development cycle and static nature of human dentition, analytical methods can be applied to reconstruct an individual's life history spanning across approximately 20 years of infancy, childhood, and adolescent life. Further examination of intra-tooth incremental growth in human dentition allows for greater resolution of an individual's life history, such as dietary habits, migration patterns, or cultural activities.

Extraction of trace elements from calcified tissue using laser ablation- inductively coupled plasma- mass spectrometry (LA-ICP-MS) is a relatively young technique. This method has been utilized for reconstructing life histories through two-dimensional mapping of trace elements for analysis of calcified tissues, such as teeth (Hare et al., 2011). Teeth are preferred because unlike bone, they are not subject to remodeling, have set chronological stages of development (Cox et al., 1996), and are resistant to diagenesis after burial (Cox et al., 1996; Budd et al., 1998; 2000). All of these factors create a chronological time capsule that can be deciphered by researchers through examination of trace elements throughout the tooth. By comprehending each stage of tooth development, researchers are more apt to create a more accurate timeline based on evidence provided by trace elements. Trace element analysis has been applied to the reconstruction of dietary habits (Gibson, 1994; Lee-Thorp et al., 2003; Eriksson, 2013; Humphrey, 2014), determining residency and mobility (Eriksson, 2013), as well

as creating further comprehension of cultural activities (Gulson, 1996; Al-Ashban et al., 2004; Al-Kaff et al., 1993).

Research Questions

The purpose of this study is to document the life history of individuals interred in a Meroitic elite necropolis located at the site of Sedeinga in northern Sudan. The site is dated to approximately the 1st century AD to the beginning of the 4th century AD (Rilly & Francigny, 2012). The sample consists of 13 adult and juvenile individuals, with a total tooth sample of 21 permanent molars that includes first, second, and third molars. The number of teeth per individual varies, with two individuals having all three molars represented, four individuals with only two molars present, and seven individuals with one molar present for analysis. For the six individuals that have multiple molars, intra-individual variation and life history will be reconstructed. All individuals will be used to determine inter-individual variation.

The following questions will be examined in this thesis:

1) Was intra- individual variation present in dietary consumption or cultural behaviors based on elements found within an individual's multiple molars after analysis?

2) Was an inter-individual variation apparent, based on developmental age through permanent molars, which indicated a distinction between dietary consumption against all individuals?

3) Based on known medicinal and cosmetic use of kohl in neighboring societies, as well as archaeological evidence found at Sedeinga, if individuals will have used kohl based on observed increased levels of lead or antimony?

These questions will be answered through the examination of trace elements within human dental samples. The dentin and enamel section of each tooth sample will be subjected to laser ablation-inductively coupled plasma-mass spectrometry (LA-ICP-MS) to determine detection and concentrations of specified elements. For the purposes of this study, the following elements were chosen for their ability to aid in the interpretation of dietary intake and environmental exposure: major elements calcium (Ca^{44}) and phosphorus (P^{31}); minor elements magnesium (Mg^{24}), sulfur (S^{32}), carbon (C^{13}), and strontium (Sr^{88}); and metals iron (Fe^{56}), copper (Cu^{63}), zinc (Zn^{66}), and antimony (Sb^{121}). The examination of these elements allow a window into the past to better comprehend diet, migration, and cultural traditions of the Nubians at the site of Sedeinga. Further, lanthanum (La^{139}), lead (Pb^{208}), and uranium (U^{238}) were examined as indicators of diagenesis. Following mapping of these elements, the concentration of Cu^{63}, Zn^{66}, $Sr^{88,}$ Sb^{121}, and Pb^{208} were measured to evaluate dietary trends and cultural behaviors.

Intra-individual variation will be examined in individuals with more than one tooth type (e.g. M1, M2, and M3) present for analysis. Inter-individual comparisons will assist in determining possible differences linked to developmental age. Lastly, the analysis of lead and antimony may verify the cultural use of cosmetics, particularly kohl, based on concentration levels mapped in each individual.

Chapter Two will provide a literature review that provides background information for the site of Sedeinga and highlight documented cultural use of kohl among the Nubian culture. Chapter Three will provide background information on dental composition, including characteristics associated with enamel and dentin; the formation of incremental lines within dentition; a chronological time frame in which first, second, and third molars develop; the process of elemental absorption into the tooth structure; and a descriptive overview of the elements used in this study that includes their physiological role. Chapter Four provides the detailed list of materials and methodologies used in this study to perform elemental analysis. Chapter Five includes a description for each elements' detection levels and concentration values based on their two-dimensional mapping. This section focuses on the location of high, moderate, and low values; highlighting observed inclusions, such as striations; and noting the presence of visible fracture lines within the element map. Chapter Six discusses inter- and intra- individual analysis based on comparative graphed concentration values based on tooth type and what each element can implicate for that individual's life history. Chapter Seven reexamines the research questions and what concentration values determined for the general population and for each individual. Limitations and future research will be further considered in this section.

CHAPTER TWO: ARCHAEOLOGICAL SAMPLE BACKGROUND

Minimal information regarding a Nubian population, exhumed at the site of Sedeinga in modern-day Sudan, is readily available. Recent archaeological excavations conducted at Sedeinga have initiated the need for further research to be implemented into a group of elite individuals exhumed from the Meroitic cemetery of Sedeinga. This chapter provides a background on previous archaeological excavations under the direction of Rilly and Francigny, from excavation season 2010 through 2014, and constructs a chronological timeline of the site of Sedeinga based on structural composition and presence of materials in these structures.

Sedeinga

Archaeological efforts of the previous director Berger el-Naggar, were continued under the direction of Claude Rilly and co-director Vincent Francigny in 2009. The Sedeinga Archaeological Unit (SEDAU) recommenced excavations following seven years of inactivity at the Meroitic cemetery located in northern Sudan (Rilly and Francigny, 2010). Sedeinga is positioned on the western bank of the Nile River, approximately 30 km south of the contemporaneous neighboring community of Sai Island and 160 km north of Dongola (Rilly and Francigny, 2013) (Figure 1).

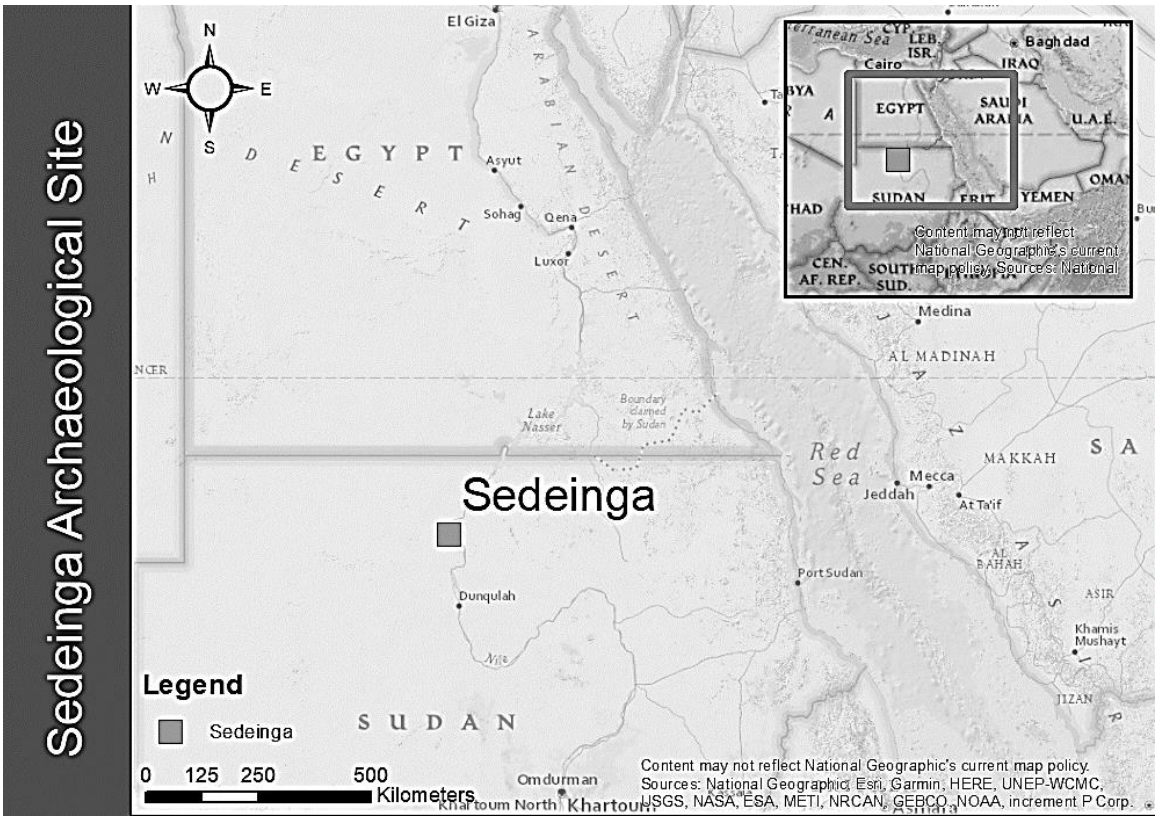

Figure 1 Geographical location of the archaeological site of Sedeinga located in Northeastern Africa within modern day Sudan. Map adapted from National Geographic Map.

There were two objectives for the 2009 excavation season, the first was to produce a detailed topographical map of the cemetery, which included monument and burial locations (Figure 2). The map documented a total of 570,000 m^2 of Sedeinga landscape, including Sector I and II, in relation to the Temple of Tiyi (Rilly and Francigny, 2010). The focus was centered on excavating Sector II, because of minimal excavation efforts previously conducted in this area, as well as the need for further documentation by researchers (Francigny et al., 2014). The location of Sector II, from which the samples for this study are derived, lies west of the Temple of Tiyi and its western border is a contemporary camel track used for transport between Darfur and Egypt (Rilly and Francigny, 2011). Further excavations in 2010 revealed two arid stream beds,

or wadis, that bordered the north and south perimeter of Sector II and divided the cemetery into three sections (Sectors I, II, and III), with Sector II lying central between the two (Rilly and Francigny, 2011).

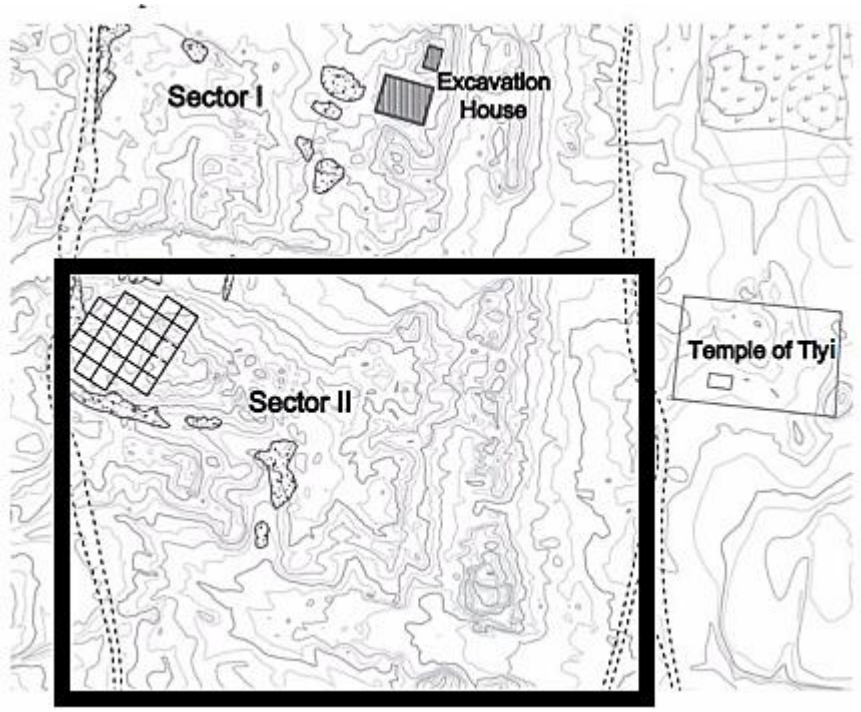

Figure 2 Topographical map of Sedeinga with area of sample extraction highlighted (adapted from Rilly and Francigny, 2010).

The second focus of the 2009 excavation season was to gain a better understanding of the chronological order of burials at Sedeinga, and a further understanding of the development of the Meroitic necropolis within Sector II (Rilly and Francigny, 2013). A brief description of Sector II (Rilly and Francigny, 2010) notes a pyramidal superstructure that extended eastward from the contemporary camel track and two perpendicular 'L-shaped' previously excavated trenches, one extending in a north-south direction, while the second trench was perpendicular to this first

trench and extended in an east-west direction. In 2009, the excavation of Sector II was centered parallel to the east-west trench and continued westward.

Following the 2009 excavation, the 2010 field season focused on Sector III as well as Sector West (Rilly and Francigny, 2011). Although excavations in Sector II were halted for a field season, the information recovered in other areas revealed chronological order of the burials, along with further understanding of the types of structures that would be expected to be recovered based on construction techniques. A general interpretation of the development of the necropolis was based on a cluster system with one or two "patron pyramids" that represent familial burials and divide the burial clusters (Rilly and Francigny, 2011). Rows of satellite monuments thought to be of lower status surrounded the clusters. The interpretation of the development of the Meroitic necropolis is the basis for understanding social hierarchy during the Early and Classic Meroitic periods (Rilly and Francigny, 2010).

It was during the 2011 season, that researchers were able to identify and classify four stages of Meroitic funerary customs based on their chronological order (Rilly & Francigny 2012). Figure 3 is an illustrated layout of the funerary clusters mapped in Sector II. Each of the observed funerary burial clusters were dated chronologically according to context, with the first stage occurring before the 1st century AD and was associated with patron pyramids that had been constructed of pink or grey colored mud bricks (Rilly and Francigny, 2011). The second stage begins around the 1st century AD and was associated with monuments constructed from grey-colored mud bricks. The third stage occurred during the 2nd and 3rd century AD and is dominated by newer tombs that had been built in open, unoccupied areas, as well as the reuse of tombs in other areas. The fourth stage, at the end of the 3rd century to the beginning of the 4th century AD,

showed the continual reuse of tombs, as well as the construction of superstructures that had been built on top of earlier monuments (Rilly and Francigny, 2011).

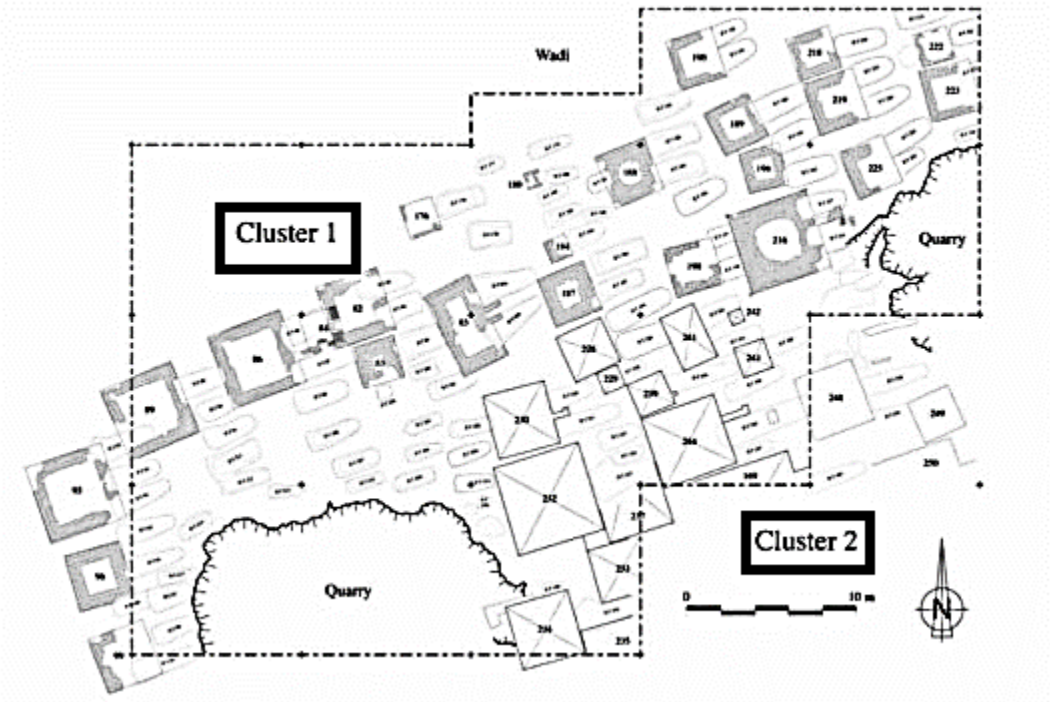

Figure 3 Map of funerary clusters in Sector II (adapted from Rilly and Francigny, 2011).

Tomb Structure

As of 2012, over 400 tombs associated with pyramids have been excavated at Sedeinga (Fisher, 2012). During the Napatan period (900-270 BC), pyramids were built in the Sector West and the eastern region of Sector I, and were found to contain the tombs of not only the wealthiest individuals, but Sedeinga's rulers as well. During this period, lower status individuals were buried in the western section of Sector III (Rilly and Francigny, 2011). During the Meroitic period (270 BC- 470 CE), local princes were buried in the Sector West beneath smaller pyramids located east of the Napatan superstructures, while second rank officials were located beneath

monuments, or simplified structures, in Sector II (Rilly and Francigny, 2011). Simple tombs lacking superstructures, were also located in this section.

During the Late Meroitic Period, mid-2nd century AD, a "democratization" of burials based on status occurs in the cemetery (Rilly and Francigny, 2011). This meant that superstructures were no longer reserved for only the wealthy and juveniles were also included in the cemetery within their own tombs and in some cases, with smaller superstructures of their own (Rilly and Francigny, 2011). Prior to democratization, juvenile burials consisted of small intrusive pits beneath superstructures.

Following the democratization, an inverse relationship occurred between the quantity and quality of the burial superstructures. While the greatest number of superstructures were constructed during the Late Period, it was apparent that the quality of the materials used to build these structures diminished. Many superstructures were erected beside or on top of former pyramids, using recycled materials to construct portions of the tombs (Rilly and Francigny, 2010).

Since most of the tombs had been plundered by robbers prior to archaeological efforts leaving only a mere 2% still intact, the presence of artifacts associated with elite individuals used to determine status were rare and made the identification of individual's social status challenging (Francigny et al., 2014). Archaeologists, however, were able to identify the wealthier individuals through other pieces of evidence left behind by looters. The wealthiest individuals were identified through the presence of stelae within the burial that could have only been produced by a handful of specialists (Rilly and Francigny, 2011). Identification of the items found within the

excavated tombs of Sector II associated with the samples utilized for this study are highlighted in Table 1.

Table 1. Artifacts found concealed in tombs in Sector II (Rilly & Francigny 2010; 2011).

Tomb no.	Artifacts
IIT160	None
IIT178	Decayed wood coffin; Small Bes amulet- blue and green glazed faience
IIT190	None
IIT197	None
IIT213	Surface- large stone artifacts
IIT217	Fragment of a pot; Coffin and cover- carved from Dom palm tree and tied together w/ rope Wood replaced with termite dung
IIT220	Copper-alloy bowl *in situ*
IIT236	None
IIT263	None
IIT312	None
IIT315	None
IIT316	None

Diet

The Nile River provides seasonal flooding that creates a nutrient-enriched environment ideal for agricultural production. The Nubian people were highly dependent on crop production as their main source of food, with meat consumption being limited (Shinnie, 1996). The Nubian people utilized the Nile River as their water supply to produce crops. Noted crops produced during the Meroitic period include sorghum and date palms (Shinnie, 1996; Török et al., 1997). Sorghum was used as a main ingredient for *kisra*, a staple bread consumed in the region. Dates were known to be dried and consumed when long journeys across the desert took place (Shinnie, 1996). *Kisra* was typically consumed with vegetables including cow peas, okra, cress, purslane,

lettuce, onions, and garlic, and occasionally with meats including beef, mutton and goat (Shinnie, 1996). In Meroe, cattle were domesticated in large numbers due to the available grasslands used for grazing (Shinnie, 1996). This allowed for increased beef consumption during the Meroitic period and the availability of cow's milk, while sheep and goat were only consumed on special occasions.

Kohl

The use of antimony- and lead- based kohl in Nubian societies has been documented in areas of the Middle East. Kohl is widely used as a traditional medicine (Al-Kaff et al., 1993; Lekouch et al., 2001; Al-Ashban et al., 2004) as well as for beautification purposes (Al-Kaff et al., 1993; Al-Ashban et al., 2004; Hardy et al., 2004; Al-Qutob et al., 2013; Gondal et al., 2015) in contemporary areas such as the Indian subcontinent, the Arabian Peninsula, and northern Africa (Gondal et al., 2015). Pure kohl originally consisted of antimony sulfide and trisulfide in the form of stibnite, but as these materials became scarcer, galena (lead sulfide [PbS]) became a common substitute in kohl eye cosmetics (Al-Kaff et al., 1993; Gondal et al., 2015). Other compounds that were included in kohl are zincite (ZnO), minium (Pb_3O_4), magnetite (Fe_3O_4), goethite (FeO(OH)), and cuprite (Cu_2O) (Al-Qutob et al., 2013).

An estimated 40% of children in contemporary Middle Eastern cultures are expected to have kohl applied to their eyes within the first postnatal month for either cosmetic or medicinal reasons (Al-Kaff et al., 1993:26). It is also very common for women and children to apply kohl for cosmetic purposes (Lekouch et al., 2001; Hardy et al., 2004; Gondal et al., 2015). Kohl is applied daily to an infant's palpebral conjunctiva daily, and while use is discontinued on males

beyond the first year, females continue to use kohl for beautification throughout their adolescence (Nir et al., 1992). According to Al-Ashban et al. (2004:292), a "fine kohl powder is applied to the conjunctive surface of the eyelid" and is comparable to the use of eyeliner for beautification purposes.

Medicinally, kohl is applied to the eyes of children for multiple reasons. It is thought to prevent or treat ocular diseases (Al-Kaff et al., 1993), such as conjunctivitis, eye soreness, and light sensitivity (Hardy et al., 2004; Gondal et al., 2015). It is also applied to the umbilical cords of newborns (Al-Kaff et al., 1993) or applied after circumcision procedures to halt excessive bleeding (Al-Ashban et al., 2004). Adult males may also use kohl to improve vision. When applied to the lid surface, it helps to reflect sunlight, thereby reducing glare (Al-Kaff et al., 1993). Unfortunately, when kohl is lead-based galena, it may have an adverse effect on health and can result in lead poisoning.

CHAPTER THREE: LITERATURE REVIEW

The most recent use of laser ablation- inductively coupled plasma- mass spectrometry (LA-ICP-MS) is a methodology that permits access into the daily lives of past peoples. Utilization of this methodology increases our potential understanding of social, political, and agricultural systems through detection of trace elements within calcified tissues, such as teeth. This chapter will discuss the various sections of permanent molars, including the enamel and dentin regions; provide a chronological time frame of human dental development; discuss the process of trace element absorption into human dentition; provide a descriptive overview of trace elements used to reconstruct past populations; and the sequential process exhibited with LA-ICP-MS, and the advantages associated with its use.

Dentition

Dental Composition

Each tooth consists of three distinct layers, the cementum, dentin, and enamel, which develop to form the hard-mineralized tissue of the tooth. The pulp cavity remains active throughout life and contains nerve and blood tissue (Webb et al., 2005). The cementum is a thin layer of calcified tissue (Webb et al., 2005) that encompasses the outer surface of the root (Kang et al., 2004). The enamel and dentin layers both contain inorganic material, known as hydroxyapatite, with enamel covering the crown of the tooth, and the dentin, consisting of dense bony tissue that is enclosed within the enamel, comprises most of the inner tooth and root (Eerkens and Bartelink, 2013).

During the developmental secretory stage, the organic matrix of the tooth is formed (Humphrey et al., 2007). Dentin and enamel of first molars begin to develop around the sixth week in utero (Webb et al., 2005; Asaduzzman et al., 2017). Dentin is required for enamel formation in a process called reciprocal induction (Ten Cate, 1998). Dentin and enamel grows in thin layers, each of which takes weeks or even months to form (Eerkens et al., 2016). Each of these layers are formed utilizing biomolecules extracted from digested foods. During initial formation, enamel and dentin are deposited at the dentin-enamel junction (DEJ), with each successive layer being deposited upon the previous, creating a coating that seals the layer and prevents remodeling. Expansion of the dentin and enamel layers continues away from the DEJ creating horizontal layers in the crown of the tooth and ring-like layers as it continues to grow toward the apex of the root (Kang et al., 2004). It is during this stage of formation that elements are deposited into the dentin portion of the tooth (Asaduzzman et al., 2017). Distinctions can be observed between the dentin and enamel layers, including growth trajectory, density, and chemical composition. Dentin and enamel contain both inorganic hydroxyapatite crystals and an organic collagen matrix protein, but composition differs between the two (Asaduzzman et al., 2017).

Enamel

Enamel makes up the crown of the tooth and is classified as the hardest mineralized tissue in the body (Reitznerová et al., 2000). Enamel is comprised of inorganic materials, or hydroxyapatite crystals, with organic lipids and proteins, and water condensed between the apatite crystals of the matrix (Kang et al. 2004). As the tooth reaches maturation, these organic

materials are almost completely displaced from between the crystals and are replaced with inorganic material (Ten Cate, 1998). Enamel formation is completed before the tooth reaches maturation, at which point eruption occurs (Kang et al., 2004).

Enamel formation takes place in two stages, the secretory stage and the maturation phase. The secretory stage of the organic matrix is known as amelogenesis (Ten Cate, 1998). First, hydroxyapatite crystals and ameloblasts cells are secreted directly onto the surface layer of dentin. These enamel forming cells move in an outward direction from the dentin, forming conical projections known as Tomes processes. These processes close during the maturation stage and are then filled with apatite crystals that replace water and inorganic material. The crystals observed in the hydroxyapatite are observed to form in an organized structure (Shellis and Dibdin, 2000). After formation has completed, enamel is unable to remodel or repair itself due to the lack of blood vessels within the enamel layer (Uryu et al., 2003). The tooth then enters the protective stage, with the main purpose of preserving enamel until eruption occurs (Ten Cate, 1998). Although, teeth do not exhibit remodeling after formation, enamel is still susceptible to alterations from environmental exposure.

Dentin

Most of the tooth is composed of dentin, with approximately 72% consisting of inorganic material, or hydroxyapatite, 20% consisting of organic material, and another 10% composed of water (Dean, 2017). Dentin is more active than enamel, is composed of smaller apatite crystals that are not as densely packed as those observed in enamel, and further exhibits an increased amount of organic material compared to enamel (Eerkens et al., 2016). The extracellular matrix

of dentin has been compared to bone matrix (Ruch and Lesot, 2000) having increased compressive and tensile strength, making it both rigid and elastic, attributing to a high resistance toward cracking (Dean, 2017).

Dentin is a hard, mineralized tissue that is encapsulated and preserved between the enamel layers and cementum, reducing exposure to the surrounding environment (Kumagai et al., 2012) as well as the oral environment (Asaduzzman et al., 2017). Dentin, however, is at an increased risk of diagenesis due to its increased permeability and microstructure (Dean, 2017). Secondary dentin, as a response to dental trauma, can be deposited after dental growth has completed. Further, dentin tubules found within the fluid in the layer of dentin just beneath the crown ensures a consistent source of hydration that is needed for the tooth to stay alive. Postmortem, dentin tubules no longer provide the tooth with hydration and the tubules draw up any fluid within proximity and contributes to the occurrence of diagenesis taking place.

Incremental lines

Trace elements can also accumulate in the tooth when it is subject to demineralization as a reaction to physiological stressors, such as malnutrition, infection, or any other type of disturbance in the tooth's nutrient supply (Dean, 2017). These events interrupt the regular formation of incremental lines that occur during normal growth periods. Stress events can be detected through the appearance of Harris lines, linear enamel hypoplasia (Schurr, 1998), and irregular Retzius lines (Dean, 2010). These accentuated lines are non-incremental and are not representative of normal secretion. Of these stress markers, the neonatal line is the most well-known.

The neonatal line is an accentuated line that reflects physiological disturbances associated with the birthing process (Humphrey et al., 2007). In teeth whose crowns are developing at the time of birth, the neonatal line separates dental development that occurs before and after birth, allowing the postnatal diet to be detected in the enamel within two weeks after birth (Humphrey et al., 2007). Because the neonatal line is present in most individuals and has a direct correlation with the period of birth, it is therefore widely used as a marker of chronological order of events known to occur during dental development (Dolphin et al., 2005).

Both regular and irregular incremental layers in dental tissue act as a natural biomonitor that becomes an archival, permanent record of the past (Webb et al., 2005). Microspatial isotopic and trace element analysis of dentition can provide information on dietary habits linked to the process of weaning and the introduction of supplementary foods, social status, sex, and age (Eerkens et al., 2014). Dentition also provides insight into pollution levels present in the environment, the geographic residence and mobility of the individual (Dolphin et al., 2005), and instances of exposure to metal during adolescence (Hare et al., 2011). Because of the developmental period of first permanent molars, early dietary change, such as weaning can be documented. Second permanent molars exhibit change in dietary habits following the weaning period. Third molars form during the years of transition from adolescence to adulthood, providing information for a different period of development (Eerkens et al., 2016).

Chronology of Tooth Formation

Tooth formation is a definitive process that is chronologically set to a known time that spans throughout the juvenile growth period. In juveniles, the dental age of individuals can be

predicted within a range of two-month period, with a standard deviation of $\pm$ 0.56 year of age when only a single tooth is present during assessment, or $\pm$ 0.09 years of age when five or more teeth are available for analysis (Smith, 1991). Dental formation has proven to be a better indicator for determining age for juveniles than skeletal developmental due to the minimal amount of variance that is known to occur within developmental stages. This acquired dental age is used to assess physiological age through stages of skeletal development (Smith, 1991).

According to Smith (1991), there are two stages of dental development, the first is the formation of the crown and the second is observed in the formation of the roots. Dental age can be approximated through known formation and emergence where the formation period is superior to emergence with emergence being influenced by environmental factors, loss of deciduous teeth, and space availability in the dental arch (Moorrees et al., 1963:1490). Teeth are observed to erupt after formation of the crown has occurred and as formation of the roots is almost complete (Smith, 1991).

On average, the permanent first molar is initiated in utero and formation commences within the first year of postnatal development (Budd et al., 1998). The second and third molars are initiated approximately 3-4 months postnatal, with the second molar crown beginning to form between 2-4 years of age, while the third molar crown begins to develop at approximately 5-6 years of age (Smith, 1991). Emergence of the permanent dentition occurs relatively later in life, with the first molar emerging between 6 and 8 years of age, the second molar emerging between 10-12 years of age, and the third molar erupting at the age of maturation, or ~18 years of age. Tooth development is usually complete by 20 years of age.

Formation rates between males and females are variable. Female root development is noted to take approximately 0.14 years less than in males, and female root maturation takes approximately 0.5 years less. If the sex of the individual is unknown, juvenile age prediction can vary and will most likely have introduced error (Smith, 1991).

Element absorption

Following eruption, permeability of the tooth increases from the outer surface of the enamel inward to the DEJ. It is observed along weakened areas, such as the laminar pores in prism junctions where apatite crystals from different regions meet, and a change in the orientation of the crystals is observed (Shellis and Dibdin, 2000). The increased porosity of the enamel plays a significant role in the presence of trace elements within the dental matrix (Reynard and Balter, 2014). Trace elements accumulate within these large, open channels of the vascularized tissue, or within the channels observed between differing tissues, such as the enamel dentin junction (Reynard and Balter, 2014) and are then substituted into the apatite lattice (Losee and Ludwig, 1970), or the hydroxyapatite structure of the inorganic layer of enamel.

Both essential and nonessential elements are taken up in the dentition and are found to be preserved within the incremental lines of the inorganic aspect of the tooth, while the organic component contains stable isotopes as well as DNA (Dean, 2017). During development, elements attach to the collagen fibers (Kumagai et al., 2012) present within the layer of predentin (Dean, 2017) and are known to accumulate until approximately 50 years of age (Kumagai et al., 2012). Based on the accumulation of trace elements, an individual's life history can be recreated through analytical mapping and analysis of elements within dentition.

Trace Elements

Common elements found in dentition include both essential and non-essential elements. Essential elements are present in all healthy, living tissue (Bodnar & Dimitriu, 2012), and are necessary for growth and development (Friese and Markert, 2000). A deficiency in nutritional intake of essential elements can result in physiological or structural disorders, while an overabundance can result in toxic levels and possibly lead to death (Friese and Markert, 2000). Non-essential elements are not necessary for life but are still commonly found in the dental dentin and enamel regions and can accumulate throughout an individual's lifetime. Trace elements can accumulate in hard tissues, such as dentin and enamel, through ingestion (Kumagai et al., 2012), inhalation from the atmosphere, as well as absorption through the skin (Losee & Ludwig, 1970). The presence and intensity of trace elements are most notably derived from an individual's source of food, with water consumption being a secondary source, and variance of trace elements is observed based on region (Losee & Ludwig, 1970).

Trace elements that are reliable indicators of dietary habits or environmental exposures include calcium, phosphorus, sulfur, strontium, and carbon (Kang et al., 2004; Asaduzzman et al., 2017). Calcium and phosphorus are used as reference to verify the sample consists of calcium hydroxyapatite, the main elemental constituents that make up dental structure. Sulfur is utilized as a dietary indicator and is present in a variety of foods. Strontium and carbon are also indicators of dietary habits and are utilized to determine different levels of trophic fractionation that differ according to increased trophic levels as well as environmental factors. Carbon exhibits an inverse relationship with strontium, with carbon levels observed to increase as trophic levels increase, while strontium levels exhibit an inverse relationship to trophic levels,

decreasing as trophic levels increase (Lee-Thorp & Sponheimer, 2006). Strontium permits similar insight into dietary trophic fractionation, as well as an individual's weaning period, with strontium values exhibiting an influx in elemental detection and concentration to occur alongside the introduction of supplementary foods into the diet (Eerkens et al., 2011), while carbon levels have been observed to decrease during this period (Eerkens & Bartelink, 2013).

Trace metals also commonly found in dentition can enter the body through ingestion, along with inhalation or exposure and absorption through the skin (Gondal et al., 2015). Trace metals commonly detected in dentition include copper, zinc, antimony, and lead. Concentration and presence of copper and zinc are observed to have an inverse relationship during the body's absorption of the two elements. Since copper is noted to have unpaired electrons, it is more readily available to assist in redox reactions necessary for physiological functions to occur within the body. Zinc, however, does not have unpaired electrons, inhibiting redox reactions from occurring, interfering with physiological functions (Fraga, 2005). Lead and antimony are both markers of cultural behavior, as there is no known biological role in the body and if observed in dentition indicate environmental exposure. Both metals have been noted to be toxic in miniscule quantities (Brown et al., 2004) and are observed to replace calcium in the hydroxyapatite structure of teeth as they accumulate within the hard tissues of the body (Lane and Duffy, 1996).

Archaeological samples can be altered by the postmortem environment through diagenesis (Williams and Siegele, 2014), providing false representation of the individual during life. In this study, teeth have been chosen for more precise calculations based on their decreased susceptibility to diagenesis comparable to bone (Lee-Thorp et al., 2003). It is possible, however, for elements to diagenetically exchange in the tooth. By conducting an analysis on uranium and

lanthanum, a rare earth element, contamination of the samples postmortem can be determined. Table 2 provides an overview of the trace elements that will be mapped during elemental analysis for this research.

Table 2. Element overview. Element information including category, physiological role, with deficiency and toxicity effects.

Element	Category	Physiological Role	Deficiency	Toxicity
Calcium	Reference	Bone and tooth structure, nerve transmission, muscle contraction, blood clotting, blood pressure, regulation, hormone secretion (Grosvenor & Smolin 2010)	Increased risk of osteoporosis (Grosvenor & Smolin 2010)	Elevated blood calcium, kidney stones (Grosvenor & Smolin 2010)
Phosphorus	Reference	Structure of bones and teeth, membranes, ATP, and DNA; acid-base balance (Grosvenor & Smolin 2010)	Bone loss, weakness, lack of appetite (Grosvenor & Smolin 2010)	Calcium resorption from bone (Grosvenor & Smolin 2010)
Sulfur	Migration	Part of amino acids, vitamins, acid-base balance (Grosvenor & Smolin 2010)	None	None
Strontium	Diet	Promotes growth	None	None
Carbon	Diet	Form proteins, carbohydrates, and fats; regulate body physiology; gives insight in to later years of childhood (Lee-Thorp et al. 2003)	Low levels-suggest high intake of C^3 foods	High levels-suggest high intake of C^4 foods
Copper	Diet	Transports iron from intestinal cells; connective tissue synthesis, lipid metabolism, maintenance of heart muscle, function of immune function and central nervous system (Grosvenor & Smolin 2010)	Iron deficiency anemia; elevated blood cholesterol, impaired growth (Grosvenor & Smolin 2010)	Iron deficiency anemia (Grosvenor & Smolin 2010)

Element	Category	Physiological Role	Deficiency	Toxicity
Zinc	Diet	Growth and development; increased immunocompetence; (Grosvenor & Smolin 2010)	Decreased immune system function (Failla 2003); failure to grow (Papa et al. 2012)	Decrease immune function, hinder Cu absorption (Grosvenor & Smolin 2010)
Lead	Behavior	None	None	Toxic
Antimony	Behavior	None	None	None
Lanthanum	Diagenesis	None	None	High levels-suggest contamination post-mortem
Uranium	Diagenesis	None	None	High levels-suggest contamination post-mortem

Major Elements

Calcium

Calcium is categorized as a major element within dentition and is a critical element for survival. As a necessary component, calcium is known to play a significant role in various physiological functions such as the structuring of bone and teeth. Calcium also enables nerve transmission, muscle contraction, proper blood clotting, as well as regulating blood pressure and hormone secretion (Grosvenor and Smolin, 2010). With 99% of calcium in the body found within the skeletal structure (Picciano, 2000), it is one of the main components in hydroxyapatite (Sharp, 2005), attributing approximately 1.5% to the total body weight (Grosvenor and Smolin, 2010). Calcium also plays a major role in the inorganic component of the enamel structure within the tooth (Bodnar and Dimitriu, 2012). Due to its consistency within mineralized tissue,

calcium is commonly used as a standard reference in calibrating data retrieved from calcified tissues (Dolphin et al., 2005).

According to Chandra (1985), calcium aids in trace element absorption, such as iron and zinc, and with the efficient utilization of trace elements within the body. Calcium absorption rates are reliant on Vitamin D values, and when a sufficient supply of Vitamin D is present, approximately 25% of bioavailable calcium is absorbed into the body, whereas if the body is deficient in Vitamin D, only 10% can be absorbed (Grosvenor and Smolin, 2010). Decreased bioavailability of calcium prompts bone resorption to support other physiological functions. When a decreased supply of calcium continues for extended periods, the hydroxyapatite in hard tissue is not replaced and loss of bone mass may result in osteoporosis.

Alternately, excessive consumption of calcium can also have adverse effects on health. Excess calcium results in the release of calcitonin, which impedes the release of calcium into the bloodstream, resulting in symptoms such as nausea, vomiting, constipation, abdominal pain, thirst, frequent urination, and loss of appetite (Grosvenor and Smolin, 2010). Long-term exposure to high intake of calcium can result in the formation of kidney stones (Grosvenor and Smolin, 2010). The recommended Upper Limit (UL) of consumption for adults between the ages of 19 and 50 is 1000 mg/day, but growing juveniles and older adults require higher daily intake (Grosvenor and Smolin, 2010).

Phosphorus

Phosphorus has a direct association with calcium in the makeup of hydroxyapatite, the major constituent of enamel (Bodnar and Dimitriu, 2012). Because of its known relationship

with calcium, it can also be used as a reference for other elements (Grosvenor and Smolin, 2010). Phosphorus plays a significant role in skeletal development in which 85% of total phosphorus consumed can be found inside the hard tissues, such as bone and teeth (Metkovic et al., 2000).

An inverse relationship has been observed between phosphorus intake and the density of bone mineral, decreasing calcium bioavailability and resulting in symptoms of calcium deficiency (Sharp, 2005). Increased phosphorus consumption, in conjunction with observed decreased bioavailability of calcium, has been shown to contribute to the reduced absorption of iron and zinc (Chandra, 1985). The impaired absorption rate for trace elements iron and zinc, whose physiological functions actively regulate other elements within the body, is associated with increased phosphorus intake.

Decreased bioavailability of phosphorus has been attributed to a multitude of physiological issues, including weakness and loss of appetite, and is implicated in skeletal issues such as bone loss (Grosvenor and Smolin, 2010). Bone loss, however, can also be associated with excessive intake of phosphorus. The recommended UL for adults is 4000 mg/day (Grosvenor and Smolin, 2010).

Minor elements

Magnesium

Magnesium is found in lesser abundance than calcium or phosphorus and is thus considered a minor element. Contained within the mineral of the bone, it is an essential element

necessary for maintaining bone structure. Approximately 50-60% of total magnesium intake is contained within the skeletal structure (Friese and Markert, 2000). This minor element is involved in multiple physiological functions and is important in numerous biogeochemical processes (Anon, 1996).

Magnesium has been shown to be a necessary element for maintaining proper function of cell division and growth and is also utilized in energy metabolism to release energy from carbohydrates, fats, and proteins (Friese and Markert, 2000). Magnesium contributes to the structural formation of teeth and bones by regulating calcium levels (Friese and Markert, 2000). Magnesium is also responsible for nerve transmission and the contraction of muscle tissue (Grosvenor and Smolin, 2010). Further, it contributes to the process of blood clotting and the regulation of blood pressure, while also playing a role in hormone secretion, and maintaining cardiovascular health (Friese and Markert, 2000).

Magnesium intake has a positive correlation with bone mineral density (Geissler and Powers, 2005). Decreased magnesium intake directly affects the cells required for bone remodeling (Bogden and Klevay, 2010). Reduced magnesium intake can disturb homeostasis values of calcium, resulting in hypocalcemia, or decreased calcium absorption (Anon, 1996), which can lead to iron-deficiency anemia (Bogden and Klevay, 2010) and osteoporosis (Friese and Markert, 2000). Health effects associated with high magnesium intake are far less severe, with only lowered blood pressure as a known effect (Friese and Markert, 2000), and is typically only associated with supplements, not dietary intake (Grosvenor and Smolin, 2010). Magnesium concentrations are similar in adults and juveniles over 5 months old, while newborns exhibit

slightly lower levels (Bogden and Klevay, 2010). The recommended UL for adults from supplements is 350 mg/day (Grosvenor and Smolin, 2010).

Sulfur

The concentration values of sulfur in body tissues are approximately 100 times lower than those of carbon and nitrogen. Recent technological advances now allow for the detection of sulfur values (Eriksson, 2013). Sulfur is another essential element normally provided through dietary consumption. Sulfur has various responsibilities in physiological function including an active role in regulating body acidity levels, balancing amino-acids and vitamins within the body, and bone protein formation (Grosvenor and Smolin, 2010). There is no recommended daily intake for this element, and according to Grosvenor and Smolin (2010), there are no adverse health effects associated with increased or decreased levels of sulfur in the diet.

Detected sulfur levels can provide information on migration patterns, and permit researchers to trace individual mobility using local faunal as reference (Eriksson, 2013). Through comparison of concentration values across a population, similar sulfur values are indicative of individuals from the same region, but if values differ, then a change in location at the time of tissue development is apparent. Eriksson (2013) recommended analyzing carbon and nitrogen stable isotope values to rule out dietary change as the main cause of altered sulfur values when conducting an intra-individual analysis. Sulfur concentration values may also differ based on the proximity and type of water sources (Eriksson, 2013). For example, if an individual resided in a marine community, their sulfur values would be elevated compared to those residing

in terrestrial communities. Further, sulfur values of terrestrial residents vary according to geographic region and whether a freshwater source is present.

Carbon

Carbon is a minor element that is essential for all living things with concentration values derived from dietary habits as well as climate variance (Eerkens et al., 2016). The use of carbon in the body is essential for the regulation of body physiology. It is utilized in protein formation and regulates dietary carbohydrates and fat consumption (Schurr 1998). 72% of carbon found in collagen is attributed to dietary protein intake, while the other 28% is attributed to carbohydrates and fats (Eerkens et al., 2016). There are no known adverse health effects associated with increased or decreased carbon intake.

Carbon values are dependent on local C_3 and C_4 vegetation. During photosynthesis, plants variably discriminate against carbon resulting in differences observed between C_3 and C_4 plants (O'Leary, 1998). C_3 plants have lower carbon values (Schurr, 1998) associated with terrestrial plants, which suggests high consumption of trees shrubs, tubers, root crops, rice, cereals, soybean, fruits, and nuts (Eriksson, 2013). C_4 plants have higher values (Schurr, 1998) associated with hot, arid environments, such as grassy savannahs, and suggests a diet consisting of grasses and sedges, and crops such as maize, sugar cane, millet, and sorghum (Eriksson, 2013). Eerkens et al. (2016), observed freshwater terrestrial C_3 plant values overlapping with C_4 plant values making confirmation of diet more difficult to understand through analysis of carbon values only. High carbon values have also been attributed to a diet rich in marine life. Determining diet from carbon values has proven to be difficult due to the inability to

discriminate between direct (plants) and indirect (animals) carbon consumption (Lee-Thorp et al., 2003).

After dietary variation has been accounted for, peaks in carbon values can be attributed to other variables. Shifting values of carbon, used in association with other elements, can expose other possibilities, such as change in diet linked to relocation, lack of resources (Eerkens et al., 2016), or the introduction of supplementary foods observed during infant weaning (Dupras et al., 2001). Carbon values, however, are not uniform and must be configured to the region and period being studied (Eriksson, 2013).

Trace Metals

Iron

Iron is classified as a trace metal and is also an essential micronutrient used as a resource to infer dietary habits (Pais and Jones, 1997). Bioavailability of the element depends on other metals such as copper, zinc, and titanium (Pais and Jones, 1997). Iron absorption can also be inhibited by increased calcium levels (Chandra, 1985), which can affect the formation of healthy bones (Bogden and Klevay, 2010). Iron can be found in hemoglobin and is essential in removing carbon dioxide from the body as well as transporting oxygen throughout the body. It is further utilized in myoglobin which assists in muscle contraction (Grosvenor and Smolin, 2010).

In excess amounts, iron has been found to be toxic to tissues and cells (Geissler and Powers, 2005). Acute iron toxicity is common in children under the age of 6, but toxicity can occur over a gradual period, ultimately causing organ damage (Grosvenor and Smolin, 2010).

Toxic levels occur at approximately 200 mg and can be lethal between 7-35 grams (Pais and Jones, 1997). Iron deficiency a noted problem among adolescence because more iron is needed during growth, and can ultimately result in anemia (Chandra, 1986). Iron is necessary in the synthesis of hemoglobin to increase blood volume necessary for menstruating girls, while higher intake is required for boys whose blood volume expands at a faster rate than girls (Grosvenor and Smolin, 2010). Further, its function in myoglobin is necessary for increasing muscle mass, in younger boys. The recommended daily dietary intake is between 6-40 mg (Pais and Jones, 1997) with adolescence requiring ~ 3-5g of iron necessary during growth periods (Bogden and Klevay, 2010).

Copper

Copper is an essential trace metal present in all living things (Bodnar and Dimitriu, 2012). Its properties are required for the oxidation and reduction process that occurs in enzymes (Papa et al., 2012), or redox reactions that occur because of unpaired electrons (Fraga, 2005). Copper is typically the electron donor when unpaired electrons are present (Kern and Mathiason, 2012). Copper binds to the enzymatic proteins that contribute to structural and storage functions (Fraga, 2005). Further, copper has been linked to the fusion of iron into hemoglobin (Chandra, 1985).

Copper exhibits an inverse relationship with zinc when considering the absorption rates of the two elements. Excess copper can hinder zinc absorption, but with only a minimal effect (Chandra, 1985). If the absorption of copper becomes inhibited by increased zinc intake, however, it can result in copper deficiency (Bogden and Klevay, 2000), hindering or preventing

the transport of iron resulting in iron deficiency anemia (Grosvenor and Smolin, 2010). Although copper deficiency is rare, it can be found in children with poor nutritional status and results in disturbed growth (Bogden and Klevay, 2000). The recommended daily intake is between 2-5 mg day (Pais and Jones, 1997), with the UL determined to be 10mg/ day (Grosvenor and Smolin, 2010).

Zinc

Zinc is an essential nutrient that is necessary for a multitude of physiological functions involved in growth and development. The mineral is utilized in various enzyme functions involved in growth (Grosvenor and Smolin, 2010). Zinc is associated with the development and maintenance of hard tissues involved in skeletal growth and plays a fundamental role in bone mineralization of the bone and remodeling (Moller, 1967; Geissler and Powers, 2005). It is also known to influence hormones that regulate cell division associated with the growth and repair of tissues, the immune system, and development of sex organs (Grosvenor and Smolin, 2010).

Endogenous zinc is obtained through secretions from the pancreas and gallbladder, and retained within mucosal cells of the small intestine, while exogenous zinc is obtained through diet with excess zinc excreted through defecation (Geissler and Powers, 2005). Dietary intake replaces zinc lost through excretion at a rate of approximately 20 to 40% through intestinal absorption (Reilly, 2004). When insufficient zinc is observed, the body increases the rate of dietary zinc absorption through the jejunum (Grosvenor and Smolin, 2010), necessitating daily intake of zinc to prevent health effects related to zinc deficiency (Pais and Jones, 1997).

Although a minimal amount of zinc is required for proper body functioning, an intake of 5-40mg/ day is still necessary (Pais and Jones, 1997). Zinc deficiency can affect growth and development, as well as interfere with proper immune system functioning, and can also cause skin rashes and diarrhea (Grosvenor and Smolin, 2010). Zinc is also utilized in the proper functioning and use of vitamins A and D (Grosvenor and Smolin, 2010). Individuals in which new tissue synthesis is known to occur, such as adolescence still in developmental stages and pregnant women, are also at a higher risk for zinc deficiency (Bogden and Klevay, 2000).

An inverse relationship between zinc and other elements, such as copper and iron, can contribute to nutritionally related deficiencies (Grosvenor and Smolin, 2010). A high influx of zinc can cause nutritional deficiencies due to inhibition of element absorption (Geissler and Powers, 2005). The UL for zinc is set at 40mg/ day, with levels exceeding 40mg released from the body through excretion of feces (Grosvenor and Smolin, 2010). Infant intake values are much lower than those of an adult male, measuring at 6.4mg daily and 15.5 mg daily, respectively (Bogden and Klevay, 2000). Toxic intake has been noted to be at 150-600 mg/ day with lethal values at 6 g (Pais and Jones, 1997).

Strontium

Strontium is a trace metal that is considered non-essential to biological processes. Strontium values are used to detect dietary changes from infancy to childhood (Humphrey et al., 2007) with low strontium values observed in the neonate, followed by increased values in infants during the weaning period (Schurr, 1998). Strontium values permit insight into dietary behavior based on known trophic levels following the introduction of supplementary foods into the diet

(Lee-Thorp & Sponheimer, 2006). Higher strontium levels are attributed to plant-based diets since plants have increased values of strontium (Webb et al., 2005). Since strontium is a non-essential element, no reported health effects are associated with increased or decreased consumption.

Laser Ablation-Inductively Coupled Plasma-Mass Spectrometry (LA-ICP-MS)

There are a variety of methods used by researchers that enable detection of chemical composition within hard tissues, such as teeth. Laser Ablation-Inductively Coupled Plasma-Mass Spectrometry (LA-ICP-MS) has proven to be the most promising method used in stable isotope and trace element analysis (Hare et al., 2011), with utilization of this method first being documented in 1996 (Cox et al., 1996). Before this method was used, a process equivalent to "total digestion" (i.e. completely destroyed) of the sample was utilized, but it was both destructive and inaccurate. The Mass Spectrometer (MS) improved qualitative data retrieval of multi-element profile deposition present in dental samples.

Laser Ablation-Inductively Coupled Plasma-Mass Spectrometry (LA-ICP-MS) is used to detect the presence of multiple trace elements and document their profile over space and time (Dolphin et al., 2005). This method can create two-dimensional maps of trace elements present within the sample, displaying the various elements based on the samples structural and developmental features (Hare et al., 2011). In the tooth, this type of mapping allows for detection and concentration analysis of the pre-and post-natal enamel, the neonatal line, the dentin enamel junction, dentin, as well as the dentin-pulp junction (Kang et al., 2004). By investigating these specific areas of a tooth, inter- and intra-individual variations can be determined. Further, these

differences can be interpreted in light of cultural factors such as dietary behaviors or status related activities.

Advantages of LA-ICP-MS

There are many advantages associated with using LA-ICP-MS on tooth samples. This method has allowed researchers to compare large datasets in a visual manner with increased scanning speeds and lowered detection limits of elements (Neufeld, 2004) and detection of more than 90% of elements (Friese and Markert, 2000). Further, entire tooth sections are now able to be mapped, which was not able to be done prior to LA-ICP-MS (Hare et al., 2011). This methodology allows researchers a more accurate data retrieval process, giving the results higher precision and more reliability in outcome.

The use of LA-ICP-MS also includes an increased sensitivity to elemental detection. The extreme level of sensitivity allows for the detection of multiple elements at the parts per million (ppm) level (Neufeld, 2004) creating "elemental fingerprints" or unique patterns, within each sample (Cox et al. 1996:254). These trace element signatures allow for an accurate evaluation of differences to be documented and cross compared to other samples (Neufeld, 2004), with precision of element data at 0.1-2% (Friese and Markert, 2000:154). Elemental deposition in mineralized tissue provides a unique map for each individual due to age, and variability in uptake availability due to factors such as dietary intake and environment.

Further, because LA-ICP-MS has the ability to produce elemental maps with a higher detailed resolution of data, detailed microanalysis of dental inclusions can be performed. Another benefit of this technique is the ability to detect a time axis that becomes a basis for

chronological studies (Lochner et al., 1999). Various types of samples, such as hair, teeth, and bone, can be analyzed by this technique, giving researchers a retrospective timeline to perform a comparative analysis of intra-individual variation.

A final known benefit of LA-ICP-MS is that the method is minimally destructive to samples, allowing the integrity of the sample to remain for multiple measurements to take place. The total volume ablated on the sample surface irradiated by the UV laser is less than 1µg (Neufeld, 2004). Since only a minimal amount of the sample is needed for analysis, LA-ICP-MS gives researchers the ability to investigate small fragments and also reduces the amount of sample preparation needed before ablation can be performed (Neufeld, 2004).

CHAPTER FOUR: METHODS AND MATERIALS

This chapter provides a step-by-step overview of the methodology used to extract data from each sample.

Documentation

A trace element analysis was performed on a total of 21 tooth samples obtained from 13 adult and juvenile individuals. Samples were selected based on the availability of first, second, and third permanent molars, and the number of each varied between individuals (Table 3). Intra-individual variation was examined for six individuals with more than one permanent molar available for sampling, while samples from all 13 individuals were used to interpret elemental data in order to determine dietary habits, lifestyle changes, and/or physiological stressors.

Table 3. Sample inventory including first, second, or third permanent molars present for analysis per individual.

Tomb no.	**MNI**	**Individual no.**	**M1**	**M2**	**M3**
IIT160	2	01	X		
IIT160	2	02		X	X
IIT178	7	01	X	X	X
IIT190	Not available	01	X		
IIT197	Not available	01	X	X	
IIT213	5	01	X		
IIT217	1	01	X		
IIT220	Not available	01	X	X	X
IIT236	Not available	01	X		
IIT263	Not available	01	X		
IIT312	Not available	01	X		X
IIT315	Not available	01	X	X	
IIT316	Not available	01		X	

Visual disturbances, including discoloring, fracturing of the tooth, and location of caries, were documented to provide clarification for any anomalies that might be observed in the two-dimensional maps of each sample. Each sample was photographed in its original form before the fractured teeth were reconstructed using organic adhesive and prior to removing any external debris from the surface of the samples.

Individual Dental Age Assessment

For tooth samples that were not fully developed, dental age was assessed based on Moorrees et al. (1963) and Smith's (1991) stages of development. Root development for each tooth was scored (Table 4) using Moorrees et al.'s (1963) standards. Smith's (1991) aging method was then applied to each root development score to determine an age range (Table 5). For individuals whose sex cannot be determined, an age range that includes development rates for both males and females is included.

Root development (of completely formed third molars) indicates that only two of the individuals included in this sample were determined to be over the age of 20 years old, IIT 160-02 and IIT 312-01. Sex of these two individuals was undetermined due to the commingled nature of the remains found within the tombs.

Table 4 Root completion stages (Moorrees et al., 1963).

Stage	Description
Ri	Initial root formation
R1/4	Root length ¼
R1/2	Root length ½
R3/4	Root length ¾
Rc	Root complete
A1/2	Apex ½ closed
Ac	Apex closure complete

Table 5 Individual age assessment based on Moorrees et al. (1963) and Smith (1991).

Sample #	Tomb no.	Individual no.	Tooth Type	Stage (Moorrees et al., 1963)	Age of Attainment (F-M) (Smith, 1991)	Estimated Age Range of Individual (years)
1	IIT160	01	M1	R1/4	8.7-9.4	8.7-9.4
2	IIT160	02	M2	Ac	14.6-14.9	
3	IIT160	02	M3	Ac	20.7-20.0	> 20 years (adult)
4	IIT178	01	M1	Ac	8.7-9.4	
5	IIT178	01	M2	R3/4	10.7-11.1	
6	IIT178	01	M3	Ri	12.9-12.8	10.7-12.9
7	IIT190	01	M1	R3/4	5.7-5.9	5.7-5.9
8	IIT197	01	M1	R3/4	5.7-5.9	
9	IIT197	01	M2	R1/4	4.5-4.6	4.5-5.9
10	IIT213	01	M1	R1/2-3/4	5.2-5.9	5.2-5.9
11	IIT217	01	M1	R1/2	5.1-5.2	5.1-5.2
12	IIT220	01	M1	Ac	8.7-9.4	
13	IIT220	01	M2	Rc-Ac	12.9-14.9	
14	IIT220	01	M3	A1/2	18.3-18.2	18.2-18.3
15	IIT236	01	M1	R3/4-Rc	5.9-6.3	5.9-6.3
16	IIT263	01	M1	R1/2-R3/4	5.2-5.9	5.2-5.9
17	IIT312	01	M1	Ac	8.7-9.4	
18	IIT312	01	M3	Ac	20.7-20.0	> 20 years (adult)
19	IIT315	01	M1	Ac	8.7-9.4	
20	IIT315	01	M2	Ac	14.6-14.9	> 14.9 years
21	IIT316	01	M2	R1/2	9.8-10.1	9.8-10.1

IIT 160-01

Available information associated with the individual from Tomb IIT 160-01 was minimal. A fragmented first molar was present for analysis and required reconstruction before proceeding (Figure 4). Utilizing Moorrees et al.'s (1963) methodology of dental stage development, this first molar exhibited 25% root completion and is estimated to be 8.7 to 9.4 years of age (Smith, 1991).

Figure 4 Sample IIT 160-01_M1 as received for analysis.

IIT 160-02

The remains available for analysis from the second individual exhumed from Tomb IIT 160 (i.e. IIT 160-02) included both the second and third molar (Figure 5). The second molar was fragmented and required reconstruction. Based on root development, this individual is an adult. The second molar was classified with completed closure of the apex (Ac), and Smith's (1991) method classifies the age of attainment for this stage at approximately 14.6 to 14.9 years. The third molar was also classified as having a completed closure of the apex (Ac) with an estimated age of attainment at approximately 20.0 to 20.7 years. The root development of both teeth indicate this individual is older than 20 years of age.

Figure 5 Left: Sample IIT 160-02_M2 as received for analysis. Right: Sample IIT160-2_M3 as received for analysis.

IIT 178-01

This tomb was excavated in the 2010 field season and was found plundered and looted by robbers prior to excavation, with none of its original contents present (Rilly and Francigny, 2011). Within the tomb, a decayed wood coffin was observed and a small blue and green glazed faience amulet featuring the god of childbirth, was found. The commingled remains of multiple individuals were discovered in the tomb. The minimum number of individuals is seven with three adults and four juveniles estimated between the ages of 1 and 14 years. One juvenile from this tomb was included within the sample of this study and was later estimated to be 8.7 to 12.9 years of age.

The remains available for the individual from Tomb IIT 178-01 included the first, second, and third molar (Figure 6). Both the first and third molar were fragmented and required reconstruction. The first molar root apex was completed (Ac) with an age of attainment at approximately 8.7 to 9.4 years. The second molar root is 75% completed (R3/4) and the age of attainment was determined to be approximately 10.7 to 11.1 years. The third molar root had

initiated formation and was classified as Ri, with the age of attainment estimate at approximately 12.8 to 12.9 years of age. This individual is estimated to be approximately 10.7 to 12.9 years.

Figure 6 Left: Sample IIT 178-01_M1 as received for analysis. Center: Sample IIT 178-01_M2 as received for analysis. Right: Sample IIT 178-01_M3 as received for analysis.

IIT 190-01

A partial fragmented first molar represents the individual from Tomb IIT 190 (Figure 7). The root is approximately 75% completed and was classified as R3/4. The age of attainment is estimated to be approximately 5.7 to 5.9 years of age. Since this was the only tooth available for analysis, the age of this individual is estimated to be approximately 5.7 to 5.9 years.

Figure 7 Sample IIT 190-01_M1 as received for analysis.

IIT 197-01

One individual represented by the first and second molars was sampled from tomb IIT 197 (Figure 8). Both teeth were fragmented and required reconstructed. The first molar had approximately 75% root formation (R3/4), and the estimated age of attainment is approximately 5.7 to 5.9 years. The second molar had approximately 25% of the root formed (R1/4), with an age of attainment of approximately 4.5 to 4.6 years of age. Individual IIT 197-01 dental age is estimated to be approximately 4.5 to 5.9 years.

Figure 8 Left: Sample IIT 197-01_M1 as received for analysis. Right: Sample IIT 197-01_M2 as received for analysis.

IIT 213-01

Excavated during the 2010 season, Tomb IIT 213 was previously looted. No artifacts were discovered in this tomb, but a minimum number of individuals were documented at five (Rilly and Francigny, 2011). One juvenile from this tomb was included within the sample of this study and was estimated to be 5.2 to 5.9 years of age.

The individual sampled from this tomb is represented by a first molar (Figure 9). The root formation is observed to be 50-75% complete (R1/2-3/4). This stage of development occurs between the ages of 5.2 and 5.9 years.

Figure 9 Sample IIT 213-01_M1 as received for analysis.

IIT 217-01

Excavated during the 2009 season, this tomb is located in the west section of the trench excavated along the north-south row. This undisturbed tomb was found to contain the remains of a one 7-year-old juvenile *in situ* (Rilly and Francigny, 2010). Based on the lack of soft tissue, the sex of this individual was not determined. The juvenile was located inside a coffin carved from the trunk of a dom palm tree. Remains of a rope used to tie the coffin together, a shroud, and a hide garment were also present. A pottery fragment was also found within the tomb (Rilly and Francigny, 2011). This juvenile was included within the sample of this study and was estimated to be 6 to 7.5 years old (Rilly and Francigny, 2010). Bone necrosis was noted on the entire cranium, in addition to pathological striae on the frontal and occipital bones. The etiology of these observed pathologies is unknown (Rilly and Fancigny, 2010).

The first molar (Figure 10) represents the individual from tomb IIT 217. The root is 50% complete (R1/2), and the estimated age for this juvenile is approximately 5.2 to 5.9 years of age. It should be noted, however, that original age determination made in the field estimated the individual to be 6.5 to 7 years of age (Rilly and Francigny, 2010).

Figure 10 Sample IIT 217-01_M1 as received for analysis.

IIT 220-01

During the 2010 excavations, Tomb IIT 220 was discovered to be connected to a neighboring tomb, IIT 219 (Rilly and Francigny, 2011). Within the tomb, a copper alloy bowl was found *in situ* within proximity of human remains recovered from the tomb. One juvenile from this tomb was included within the sample of this study, and estimated to be 8.7 to 18.3 years of age.

The first, second molar, and third molars were extracted from Tomb IIT 220 for analysis (Figure 11). Although the first molar root was fragmented, reconstruction was not necessary since one root was intact for analytical purposes. The second molar was also fragmented, and reconstruction was required. The first molar was observed to have complete closure of the root

apex (Ac), and age of attainment for this stage is observed to occur between approximately 8.7 to 9.4 years. The stage of development for the second molar was determined to be between root completion and complete closure of the root apex (Rc-Ac). According to Smith (1991), these stages are typically observed at approximately 12.9 to 14.9 years of age. The estimated age of this individual is 18.2 to 18.3 years based on the development of the third molar.

Figure 11 Left: Sample IIT 220-01_M1 as received for analysis. Center: Sample IIT 220-01_M2 as received for analysis. Right: Sample IIT 220-01_M3 as received for analysis.

IIT 236-01

The individual from Tomb IIT 236 is represented by a first molar (Figure 12). The root is assessed to be approximately 75% to fully developed (R3/4-Rc). This stage of attainment is observed at approximately 5.9 to 6.3 years of age.

Figure 12 Sample IIT 236-01_M1 as received for analysis.

IIT 263-01

The individual from Tomb IIT 263 is represented by a first molar (Figure 13). The first molar was fragmented and required reconstruction. The root is between 50-75% developed (R1/2-3/4). The estimated age of attainment for this stage of dental development occurs at approximately 5.7 to 5.9 years of age, and thus this individual's age is estimated to be 5.7 to 5.9 years.

Figure 13 Sample IIT 263-01_M1 as received for analysis.

IIT 312-01

The individual from Tomb IIT 312 is represented by the first and third molars (Figure 14). The first molar was observed to be fragmented and required reconstruction. Both the first and third molar roots appear to have completed formation and were classified as having completed apex closure (Ac). Complete apex closure of the first molar typically begins at the age of 8.7 years and is completed in the third molar at the age of 20.7 years. Due to the completed development of the third molars, this individual is estimated to be greater than 20 years old and is therefore categorized as an adult.

Figure 14 Left: Sample IIT 312-01_M1 as received for analysis. Right: Sample IIT 312-01_M3 as received for analysis.

IIT 315-01

The individual from Tomb IIT 315 is represented by the first and second molars (Figure 15). The second molar was observed to be fragmented and required reconstruction. The roots of both the first and third molars appear to be completely formed and were classified as having complete apex closure (Ac). Age of complete development of the first molar typically occurs at the age of 8.7 years and 14.9 years for the second molar. Since the third molar is unavailable for

analysis, and there is no further information available, the age for this individual can only be estimated at greater than 14.9 years.

Figure 15 Left: Sample IIT 315-01_M1 as received for analysis. Right: Sample IIT 315-01_M2 as received for analysis.

IIT 316-01

The individual from Tomb IIT 316 is represented by a second molar (Figure 16). The root is approximately 50% developed (R1/2). The estimated age range for this stage of development is approximately 9.8 to 10.1 years. This individual is estimated to be 9.8 to 10.1 years of age.

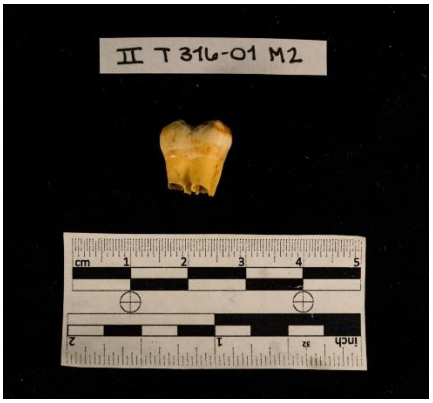

Figure 16 Sample IIT 316-01_M2 as received for analysis

Sample Preparation

Preparation of the samples followed the method outlined by Crowder et al. (2012). The step-by-step process used for preparing the dental samples for laser ablation is outlined in Figure 17.

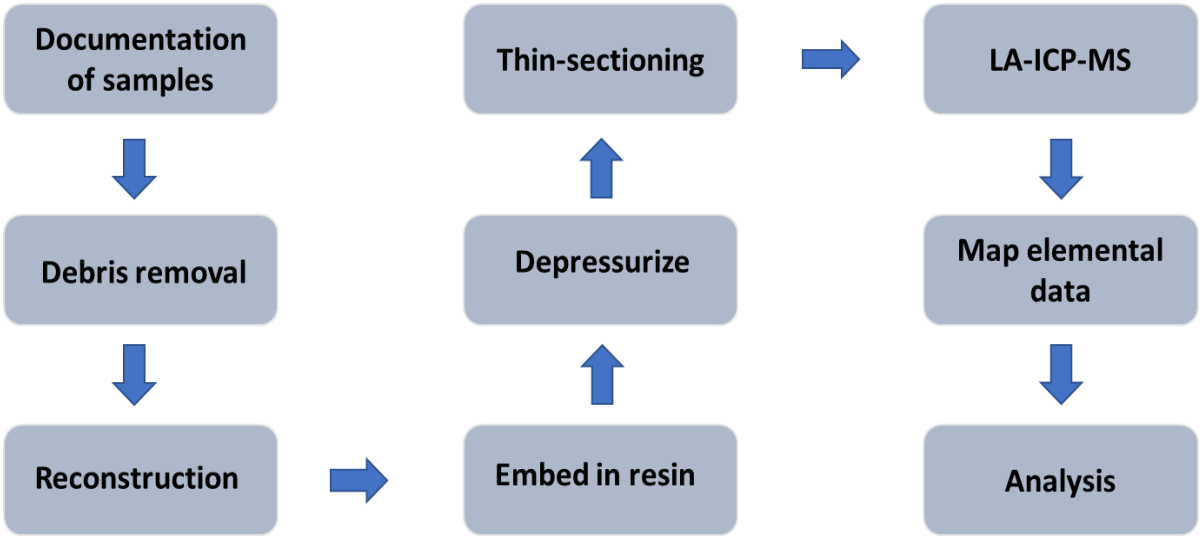

Figure 17 Process overview. Step-by-step procedure for preparing samples for data analysis.

To begin preparations, all samples were cleaned using distilled water and a soft-bristled toothbrush to remove loose debris. Dental tools were used to scrape off any calculus that was not removable by the toothbrush. Each sample was then given a final rinse to guarantee the removal of all debris before each sample was dried for approximately 24 hrs. to ensure it was completely void of all moisture. After drying of the sample was complete, fragmentary teeth were reconstructed using an organic adhesive (Elmer's School Glue®) applied by a cotton swab

(Q-tip®). The reconstructed samples were placed on paper towels for approximately 24 hrs. to allow the adhesive to dry completely. Figure 18 show an example of a fragmented tooth before and after reconstruction.

Figure 18 Sample IIT 197-01_M2. Left: Sample as received for analysis. Right: Sample following cleaning and reconstruction.

After drying of the adhesive was complete, each sample was embedded in resin. The resin consisted of 25 g of epoxy resin vigorously mixed with 3 g of epoxy hardener (Figure 19). Two samples were placed in each plastic mold, and then completely submerged in a liquid resin (Figure 20). Each sample was positioned to allow adequate spacing between the teeth and the wall of the mold. The molds were then placed in a pressure chamber at 20 psi for 24 hrs, which allowed the resin mixture to permeate crevices within the teeth as well as minimizing air bubbles that may be present in the resin (Figure 21). Figure 20 shows the embedded tooth after completed drying and removed from the plastic mold.

Figure 19. Materials: epoxy hardener and epoxy resin, used to embed samples.

Figure 20 Embedding process. Left: Sample placement in silicone mold prior to resin added. Center: Labelling system used (sample IIT 315-01_M2). Right: Sample placement inside the de-pressurizer chamber.

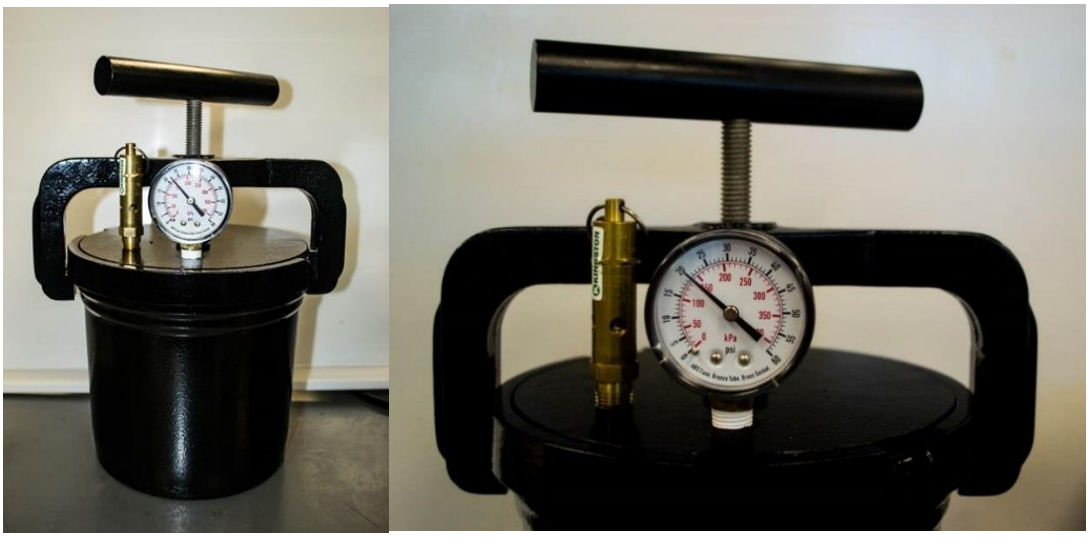

Figure 21 Left: Locked de-pressurizer with samples placed inside. Right: Gage set at ~20psi for ~24 hours.

Figure 22 Samples embedded in resin with labels that correspond with samples.

Thin-sectioning of the samples was achieved using a Beuhler IsoMet^{TM} slow-speed saw with a 3 in. diamond blade. The blade was first prepared by performing several cuts through a dressing stick. The dressing stick was reused after the cutting of every tooth to ensure minimal contamination between samples. Once the blade had passed through the dressing stick twice, a new sample was placed in the chuck for cutting. Since the teeth were paired in one mold during the embedding process, a single-cut was made to separate the two samples before thin-sectioning of each sample commenced. Teeth were then cut on a vertical plane from cusp to root, so the cross-section could reveal the developmental regions of each tooth with each thin-section measuring between approximately 0.5-1.0 mm in width (Figure 23). Following the thin-sectioning of each sample, they were individually mounted on a black disk using adhesive (as seen in Figure 21) and placed in the ablation chamber for analysis with the LA-ICP-MS.

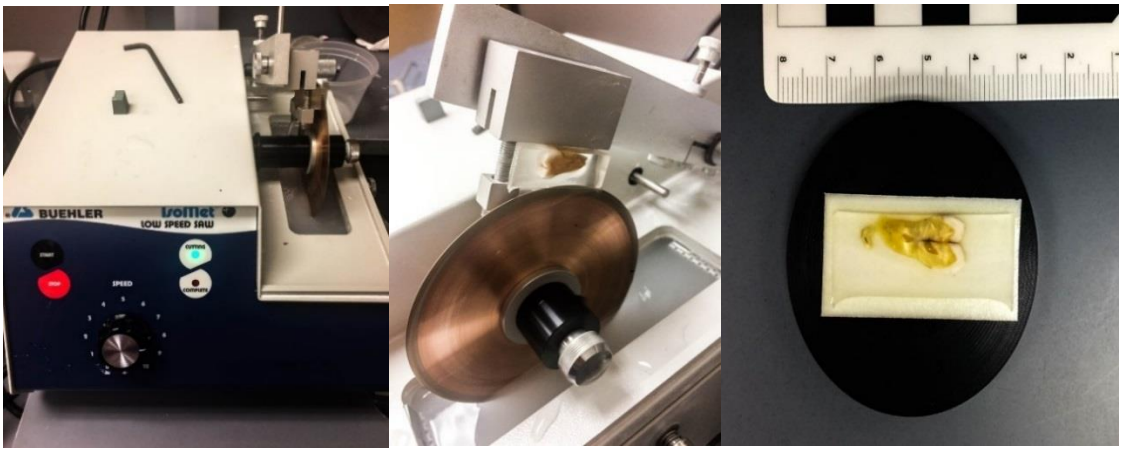

Figure 23 Left: Buehler™ IsoMet Speed Saw and saw speed at ~8. Center: sample placed in the chuck for thin-sectioning. Right: thin-sectioned sample mounted on adhesive on a black disk.

LA-ICP-MS Analysis

Trace elemental analysis was performed using LA-ICP-MS. Setup of the machine requires purging as a preventative measure to expel elements from the chambers and eliminate possible contamination. After configuration of the machine has completed, the ablation chamber is opened, and the surface glass must be cleaned with ethyl alcohol applied to a sterile tissue to remove residue, before placing the mounted sample inside. After the sample has been loaded, the machine must be purged again with argon gas to ensure limited sample contamination. While waiting for the machine to purge out all gases and contaminants, the parameters of the sample can be setup through the Axiom-LA® software.

To setup the parameters of the surface sample, an image of the sample must be configured through image stitching. Image stitching creates a grid-like image and a perimeter on the surface area of the sample that will serve as the border around which the laser will ablate the surface. When the stitched image is completed, it will appear in the lower right-hand corner of the screen and the borders of the map will then become a fixed point. By clicking once on the

top left border of the tooth, and then clicking on the bottom right border of the tooth and changing the setting to have consecutively ablated lines for the laser to follow. The number of horizontal lines will vary as the horizontal and vertical dimensions of the map change to ensure the entire tooth is inside the area intended for laser ablation. After the dimensions have been set, the perimeter of the tooth is reviewed through the micro-camera setting to ensure the entire tooth is within the mapping boundaries.

Before starting laser ablation, the channels for proper gas flow are confirmed open and that the velocity and delay are both set to 11 sec. The pattern time is input into the worksheet by converting the total time to minutes by multiplying that time by 60 and then adding 500 minutes to allow the gas flow sufficient time to not only cover the surface area mapped, but to further account for any lag in the detection of elements as it is transported throughout the chambers. Gas 1, or helium (He), is set to 0.6 and Gas 2, argon (Ar), is set to 0.58. After all settings were properly configured and the gas flow chart appeared unobstructed, the machine was ready to record the specified elements present within the sample.

LA-ICP-MS is meant to discriminate elemental differences at the parts per million (ppm) level (Neufeld, 2004). For the documentation that will appear in the analysis section, the elements were mapped based on ppm. First, an increase in energy input provides an increase in the pulsed laser beam (Kang et al., 2004), creating "spot sizes" that are approximately 5µm-300 µm (Neufeld, 2004). Following ablation, it is converted into a vapor phase and this micro sample is transported by argon gas into the plasma region where temperatures are increased and produced slightly charged ions that are then separated based on mass-to-charge ions (Arora et al., 2011). The trace elements are then converted into stable isotopes and recorded in the sample file

with this information later being extracted and utilized as the dataset for element analysis. The data is logged in a folder labelled with the date and sample number for future use in mapping the "elemental fingerprint" of each sample (Cox et al., 1996).

Standard Solutions

Synthetic hydroxyapatite was used as the standard reference to normalize the elemental signal and served as a baseline for comparison. Desired elements for analysis were added to the synthetic hydroxyapatite to create four additional standard solutions. Figure 24 depicts the materials required to complete this process. Individual tablets were prepared to use as a standard reference. Table 6 provides a detailed account of the approximate measurements for each of the four standard solutions that were added to synthetic hydroxyapatite. The documented weight is in grams (g) and the concentration of the liquid elements is under the final concentration column. These standard solutions were utilized for calibrating the trace elements presence in each sample based on their concentration values.

Figure 24 Left: Materials used for creating standard solutions. Right: Pictured from left to right: Synthetic hydroxyapatite, multi-element, sulfur, magnesium.

Table 6 Four standard solution used for standard reference material to determine concentration values of trace elements.

	1st Standard Solution		2nd Standard Solution		3rd Standard Solution		4th Standard Solution	
Element	Mass (g)	Final concentration (µl)	Mass (g)	Final concentration (µl)	Mass (g)	Final concentration (µl)	Mass (g)	Final concentration (µl)
Synthetic Hydroxyapatite	1.0009	1000	1.0025	1000	1.0038	1000	1.0004	1000
Mg	1.7341	500	2.293	100	3.2428	1750	1.1447	100
Al, Ti, V, Cr, Mn, Ni, Cu, Zn, Sr, Pb	1.7962	20	2.3764	100	3.4998	200	1.7414	400
S	2.2613	250	2.6935	100	4.4691	750	2.4645	500
Sb	2.3244	20	2.8374	100	4.7150	200	3.1013	400

Approximately 1 g of synthetic hydroxyapatite was used as the solid base to insert the liquid trace elements utilized in analysis (Figure 25). After measuring out the synthetic hydroxyapatite powder, 500 µl of Magnesium was added to the powder, followed by 20 µl of Al, Ti, V, Cr, Mn, Ni, Cu, Zn, Sr, and Pb, 250 µl of S, and lastly 20 µl of Sb. This mixture was used as the first standard solution used in calibrating trace elements within the sample. The second standard solution consisted of 100 µl of each element to be added to the synthetic hydroxyapatite. The third standard solution consisted of 1750 µl of Mg, 200 µl of Al, Ti, V, Cr, Mn, Ni, Cu, Zn, Sr, and Pb, 750 µl of S, and 200 µl of Sb. The fourth standard solution measurement of elements added to the synthetic hydroxyapatite was 100 µl, 400 µl, 500 µl, 400 µl respectively. A minimal amount of water was added to the mixture to homogenize the solution.

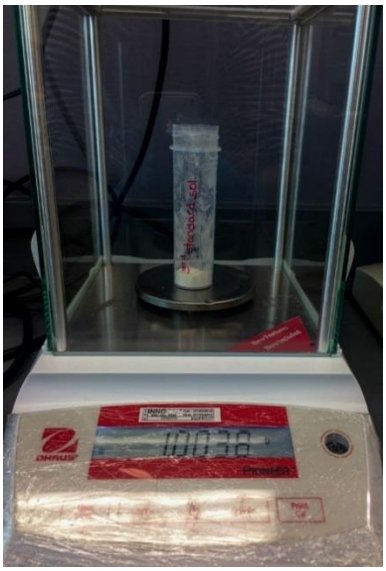

Figure 25 Measurement of synthetic hydroxyapatite used as the base material in standard solution mixture.

After the elements were added to the synthetic hydroxyapatite, each vial was thoroughly shaken to ensure homogeneity across the mixture and was then placed inside a glass beaker within a heating chamber that was set to approximately 65° F, to dry while avoiding the possibility of contamination. After allowing the mixture to dry inside the chamber for 24 hrs, the final product was removed from the heat chamber and crushed into a fine powder using a ceramic mortar and pestle (Figure 26). This powder was then pressed into a round tablet approximately 1 cm in diameter, using a handheld pill press. Two discs were created for each standard solution reference material and these were placed inside plastic bags to prevent contamination.

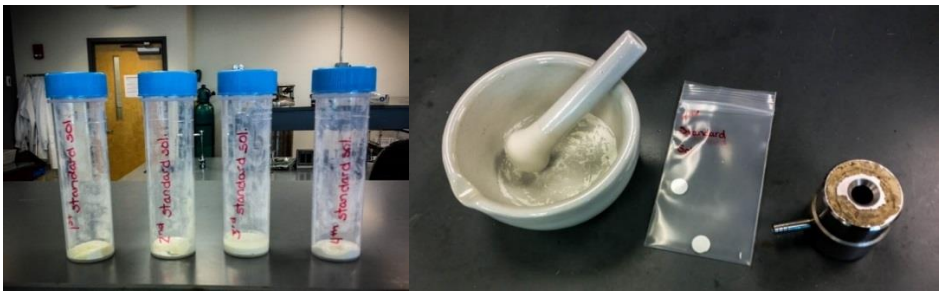

Figure 26 Left: Four standard solutions prior to hand-pressing. Right: Materials used to hand-press standard solution tablets. From left to right: ceramic mortar and pestle, final standard solution tablet, and handheld pill press.

Each of these discs were run through LA-ICP-MS when samples were laser ablated to ensure proper calibration for analysis of element concentrations. The standard solutions were placed on a blue disk (Figure 27) in a T-form with standard solution 1-2-3 placed in a straight line and standard solution 4 placed beneath standard solution 2. This was done to prevent confusion of the samples during placement in the ablation chamber and the transfer back to their labelled storage bags. The standard solution tablets were placed into the ablation chamber, the system was purged for approximately 5 mins.

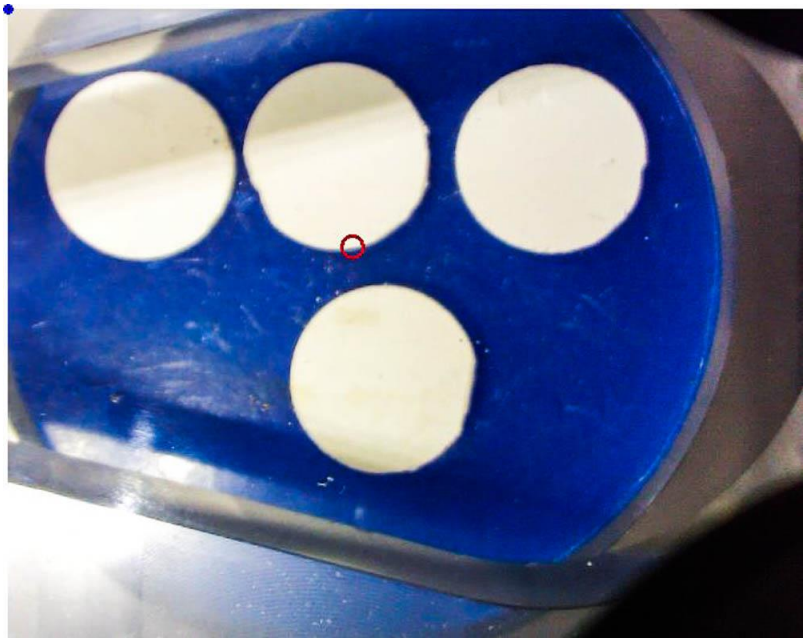

Figure 27 Image of standard solutions taken by the macro-camera feature in Axiom-LA®.

While waiting for the machine to purge, the designated ablation time was changed to a total of 530 secs and saved in to the method section of the software to record the data. Under the operations "general" tab, using the macro camera, a snapshot of the tablets as viewed on the screen was taken to be used for reference when navigating between the standard solutions. This image appeared in the lower right-hand screen under the "general" tab. Next, the number of lines desired for ablation was altered to ten with the continual horizontal line ablation process selected.

After purging of the machine, was completed, the projected area for ablation was determined by clicking on the 1st standard solution in the image on the lower right-hand corner of the screen. This switched the camera from macro- to micro-, zooming in on the area intended for laser ablation. Clicking on any area of the standard solution, ten lines appeared on the surface area of the first solution tablet. To create a perimeter for measurement, the horizontal

measurement was set to 3 mm and the vertical measurement was set to -1.5 mm for all standard solution measurements. The perimeter of the grid was reviewed to ensure there was not an overlap with any previous ablation processes on the surface of the standard solution. If there was overlap observed between ablation patterns, the grid was reset elsewhere on the surface area. If no overlap in ablation patterns was observed, the sample was run.

On the second screen, "run" was selected to allow for the machine to start the flow of gases through the chambers. After waiting approximately 30 seconds to ensure the system was running properly and the laser was turned on by selecting the image that appeared to have the laser. Further, "log" had been activated on the second screen to ensure the data would be stored. This process was repeated for all four standard solutions, using the image in the lower right-hand part of the screen to navigate between samples.

Mapping

After the dental sample had been through the laser ablation process, analysis of the elements in each sample was conducted by mapping elemental data with MATLAB® software. The presence of the following elements was mapped using MATLAB®: Major elements Ca^{44} and P^{31}; Minor elements Mg^{24}, S^{32}, C^{13}, and Sr^{88}; Metals Fe^{56}, Cu^{63}, Zn^{66}, Sb^{121}, and Pb^{208}; and La^{139} and U^{238} to determine if diagenesis had occurred. These were then compared to the following elements that were mapped using MATLAB® to determine the concentration levels of elements that were detected during laser ablation: Mg^{24}, P^{31}, S^{32}, Fe^{56}, Cu^{63}, Zn^{66}, Sr^{88}, Sb^{121}, and Pb^{208}.

The calibration curve used to determine concentration values of each element was also a determinant in which elements would be utilized for analysis in determining dietary consumption and cultural use of lead- or antimony-based kohl. The calibration curve was determined using known concentration values in the four standard solutions which were compared to baseline data for each element. After graphing the concentration values of each element, if a positive linear relationship was observed (Cu^{63}, Zn^{66}, Sr^{88}, Pb^{208}, Sb^{121}), the data was observed to portray more accurate measurements. Elements that were not observed to have a positive linear relationship were not included in the concentration value analysis (Mg^{24}, P^{31}, S^{32}, Fe^{56}). These limitations were attributed to the presence of a large concentration range, error within the matrix, and interference from the presence of atmospheric elements.

To map the elements out for analytical purposes, a coding system was setup in MATLAB®. Along with the coding file, the data retrieved from the LA-ICP-MS file was opened in MATLAB® and maps were created for concentration levels of each element. To begin, the standard solution data analyzed that day was separated into four sets of data and labelled "Standard solution" with the corresponding number (1-4). After the data had been reorganized into separate files, a calibration curve was produced using MATLAB® and the generated code. Calibration curves were produced for each element to determine the intensity of elements present within each sample.

The calibration curve was then incorporated into the mapping system to create a two-dimensional visual of the data obtained during LA-ICP-MS. Mapping of the concentration intensities of the five chosen elements, Cu^{63}, Zn^{66}, Sr^{88}, Sb^{121}, and Pb^{208}, was conducted in the same way as documenting and mapping of the detection of the fourteen elements Ca^{44} and P^{31};

Minor elements Mg^{24}, S^{32}, C^{13}, and Sr^{88}; Metals Fe^{56}, Cu^{63}, Zn^{66}, Sb^{121}, Pb^{208}; and La^{139} and U^{238}. Figure 28 is an overview of the computer code screen containing lines 3, 9, 10, and 11 that need to be adjusted for each sample.

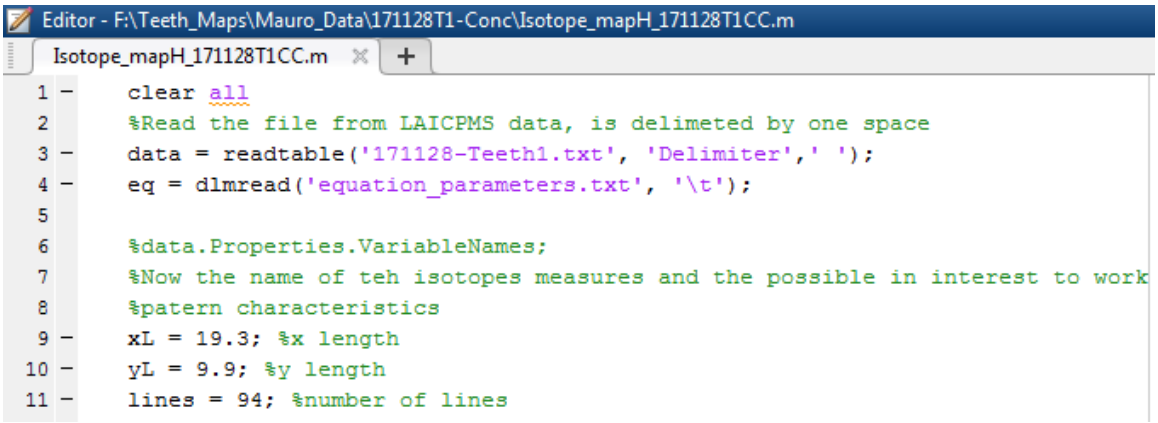

Figure 28 Screenshot of computer code with lines 3, 9, 10, 11 which require adjustment according to sample.

After all images were produced, the color scheme was manually altered for an accurate presentation of the detection levels for each element. To correct the color contrast in each image the range was individually altered per element by increasing and decreasing the minimum and maximum range (Figure 29). When the two-dimensional image of the surface area displayed the correct detection of each element, the sample was reconfigured, and the new images were auto saved to each file. This procedure was conducted to record both element detection and concentration levels in each sample that was used in further analysis.

Editor - F:\Teeth_Maps\Mauro_Data\171128T1-Conc\Isotope_mapH_171128T1CC.m

Isotope_mapH_171128T1CC.m

```
61
62 -    figure
63 -    smth_MIsotope3 = smooth(data.M31,10,'sgolay',2); %smooth process for the sample
64 -    Isotope3 = smth_MIsotope3 (a:b);
65 -    Matrix_Iso3Ca = (reshape (Isotope3,[],lines).')./Matrix_Iso5;
66 -    Matrix_Iso3 = (Matrix_Iso3Ca - eq(2,2))/eq(2,1);
67 -    image(x,y,Matrix_Iso3,'CDataMapping','scaled');
68 -    title('Isotopic distribution');
69 -    xlabel('length (mm)')
70 -    ylabel('width (mm)')
71 -    colormap (jet)
72 -    caxis([0,5000]) %change color scale (using caxis)
73 -    colorbar('FontSize', 8)
74 -    truesize
75 -    print('31P', '-dpng')
76 -    hold on
77
```

Figure 29 Screenshot of computer code for each element with axis parameters (line 72) needing adjustment to create contrast in two-dimensional map.

CHAPTER FIVE: RESULTS

The results of this study consist of two-dimensional maps that are representative of element detection in each tooth and the concentration values for the following elements: Cu^{63}, Zn^{66}, Sr^{88}, Pb^{208}, and Sb^{238} (Appendix A). The concentration values for each element are then graphed for inter-individual analysis based on first, second, and third molars across the population. This chapter will conclude with graphed concentration values for intra-individual analysis based on individuals that have more than one permanent molar, determining change of dietary habits across a lifespan and the cultural use of kohl.

Two-dimensional Maps

For each element, the location of elemental detection will be designated to the following regions: enamel, dentin, dentin-enamel junction, and border. Further, any observations of increased detection or concentration values within each map, such as the presence of striations or fracture lines, will be identified. Detection and concentration values will be scored low, intermediate, or high (Figure 30).

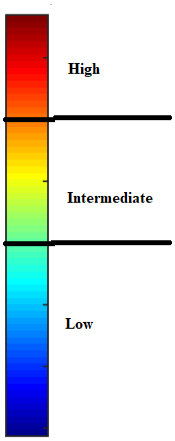

Figure 30. Scale of determined detection and concentration values for two-dimensional mapping of each element.

Individual IIT 160-01

First molar

Carbon (C13)

The two-dimensional map for detection values of carbon (C^{13}) exhibits increased detection values in the dentin region. No inclusions of carbon are present in this tooth. Postmortem fracture lines are observed in the dentin and enamel region and the high intensity observed in the fracture lines corresponds with elemental reading of the resin base.

Magnesium (Mg^{24})

The two-dimensional map for detection values of magnesium (Mg^{24}) exhibits increased detection values in the dentin region. An inclusion of magnesium is present in the dentin region on the lingual aspect. High detection values are observed around the inclusion, dissipating in

intensity as distance increases from the inclusion. A postmortem fracture line is observed in the dentin region, with smaller radiating fracture lines moving toward the lingual aspect.

Phosphorus (P^{31})

The two-dimensional map for detection values of phosphorus (P^{31}) exhibits increased detection values in the enamel region. High and intermediate detection values are present at the dentin-enamel junction (DEJ) as well as along the enamel border of the lingual cusp. Intermediate detection values are apparent in the lingual aspect of the dentin region. A postmortem fracture line with lingually radiating fractures lines are observed in the buccal aspect of the dentin.

Sulfur (S^{32})

The two-dimensional map for detection values of sulfur (S^{32}) exhibits increased detection values in the dentin region. Intermediate detection values are observed in the lingual aspect of the tooth, with higher concentrations present around the DEJ and root tip, as well as along the lingual aspect of the border in the lingual aspect of the enamel. An inclusion of sulfur is present in the lingual aspect of the dentin region of this tooth. A postmortem fracture line is observed in the buccal aspect of the dentin.

Calcium (Ca^{44})

The two-dimensional map for detection values of calcium (Ca^{44}) exhibits increased detection values in the enamel region. Intermediate detection values are apparent in the enamel as well as the lingual aspect of the dentin region. High detection values are present at the dentin-

enamel junction (DEJ), as well as along the enamel border of the lingual cusp. A postmortem fracture line with lingually radiating fracture lines is observed in the buccal aspect of the dentin.

Iron (Fe^{56})

The two-dimensional map for detection values of iron (Fe^{56}) exhibits low detection values in the overall dentin and enamel regions. High detection levels indicate the inclusion of iron in the enamel region near the fissure of the cusps. Intermediate values are observed on the buccal cusp border as well as the lower lingual cusp border. A postmortem fracture line is observed in the dentin region of the lingual root tip and radiates perpendicular to the root border.

Copper (Cu^{63})

The two-dimensional map for detection values of copper (Cu^{63}) exhibits low detection values in the overall dentin and enamel regions. High detection values are present in the enamel region from the buccal cusp radiating toward the lingual root tip. No elemental detection is present in the fracture lines. The sporadic red dots on the lingual side of the tooth are consistent with a delayed read by the Mass Spectrometer.

The two-dimensional map for concentration values of copper (Cu^{63}) exhibits low detection values in the buccal aspect of the tooth. High detection values of copper are present in the enamel region from the buccal cusp radiating toward the lingual root tip. A postmortem fracture line is observed in the buccal aspect of the dentin with intermediate element values.

Zinc (Zn^{66})

The two-dimensional map for detection values of zinc (Zn^{66}) exhibits low detection values present throughout the dentin region of the tooth. The enamel border exhibits intermediate levels of detection with high detection values present in the lingual aspect of the enamel border. Intermediate to high detection values are observed in the fissure of the cusp. A fracture line is observed in the buccal aspect of the dentin and radiates toward the lingual aspect. Low elemental detection was observed within the fracture line.

The two-dimensional map for concentration values of zinc (Zn^{66}) exhibits an absence of detection values in the overall dentin and enamel regions with low intensity values observed in the buccal aspect of the tooth. High detection values are present in the enamel region from the buccal cusp radiating toward the lingual root tip. A postmortem fracture line is observed in the buccal aspect of the dentin with intermediate element values.

Strontium (Sr^{88})

The two-dimensional map for detection values of strontium (Sr^{88}) exhibits increased detection values in the enamel and dentin regions. Intermediate detection values are apparent in both the dentin and enamel regions with a decrease in detection values observed at the DEJ. Several inclusions of strontium are present in this tooth, with high detection values present near the fissure line in the enamel and in the lingual aspect of the dentin, as well as along the enamel border of the lingual cusp. Slightly increased intermediate values are present in the enamel along the DEJ. A postmortem fracture line is observed in the buccal aspect of the dentin and radiates toward the cusp, halting at the DEJ.

The two-dimensional map for concentration values of strontium (Sr^{88}) exhibits low detection values in the overall dentin and enamel regions. Although striations are apparent, they are at negative values and will not be considered for analysis.

Antimony (Sb^{121})

The two-dimensional map for detection values of antimony (Sb^{121}) exhibits low detection values in the lingual aspect of the enamel border. No inclusions of antimony were observed.

The two-dimensional map for concentration values of antimony (Sb^{121}) exhibits an absence of detection values in the overall tooth. No inclusions of antimony were observed.

Lanthanum (La^{139})

The two-dimensional map for detection values of lanthanum (La^{139}) exhibits low detection values observed in the dentin as well as around the border encompassing the tooth. High detection values are observed in the enamel near the DEJ, as well as in the enamel border of the fissure line of the cusps. The sporadic red dots on the lingual side of the tooth are consistent with a delayed read by the Mass Spectrometer.

Lead (Pb^{208})

The two-dimensional map for detection values of lead (Pb^{208}) exhibits low detection values in the overall enamel and dentin regions. The enamel border and DEJ exhibit an intermediate level of detection with high detection values present in the lingual aspect of the DEJ. Striations with a low level of detection are observed in the buccal aspect of the enamel as well as in the dentin.

The two-dimensional map for concentration values of lead (Pb^{208}) exhibits low detection values in the overall dentin and enamel regions with intermediate values observed in the DEJ and along the border of the tooth. High detection values are present in the enamel region near the DEJ exhibiting high detection values. A postmortem fracture line is observed in the buccal aspect of the dentin with intermediate element values.

Uranium (U^{238})

The two-dimensional map for detection values of uranium (U^{238}) exhibits low detection values in the dentin region tooth. No inclusions of uranium were observed.

Individual IIT 160-02

Second molar

Carbon (C13)

The two-dimensional map for detection values of carbon (C^{13}) exhibits low detection values in the dentin and enamel region. No inclusions of carbon are present in this tooth. Postmortem fracture lines are observed in the dentin and enamel region. The high intensity observed in the fracture lines corresponds with elemental reading of the resin base.

Magnesium (Mg^{24})

The two-dimensional map for detection values of magnesium (Mg^{24}) exhibits increased detection values in the dentin region. Low detection values are observed in the dentin with intermediate detection values around the inner root border. High detection values are present in

the dentin region near the DEJ, dissipating in intensity as distance increases from the inclusion. A postmortem fracture line with low detection values is present in the dentin region of the lingual aspect near the enamel border.

Phosphorus (P^{31})

The two-dimensional map for detection values of phosphorus (P^{31}) exhibits intermediate detection values in the buccal aspect of the enamel region and high detection values observed in the buccal aspect of the DEJ. Intermediate detection values are apparent in the lingual aspect of the root. High detection values present in the dentin region near the dentin-enamel junction (DEJ) as well as at the superior aspect of the inner root border. Striations with intermediate values are apparent in the inferior aspect of the dentin region. A postmortem fracture line is observed in the dentin region of the lingual aspect near the enamel border.

Sulfur (S^{32})

The two-dimensional map for detection values of sulfur (S^{32}) exhibits increased detection values in the buccal aspect of the dentin region. Intermediate detection values are observed in the buccal aspect of the tooth, with higher detection values present in the superior dentin region, as well as along the buccal aspect of the border, and along the superior aspect of the root border.

Calcium (Ca^{44})

The two-dimensional map for detection values of calcium (Ca^{44}) exhibits overall low detection values across the tooth with increased detection values in the superior aspect as well as along the inner root border. Intermediate detection values are exhibited in the buccal cusp of the

enamel region as well as the buccal aspect of the dentin region. The inner root border is observed to have intermediate values. No inclusions of calcium are present in this tooth. A postmortem fracture line is observed in the buccal aspect of the dentin and radiates toward the lingual aspect.

Iron (Fe^{56})

The two-dimensional map for detection values of iron (Fe^{56}) exhibits an absence of detection values in the overall dentin and enamel regions. Low detection values are present around the inner root border, and a slight detection of iron is present at the DEJ. High detection values are observed on the buccal cusp of the enamel border. Intermediate detection values are present in the superior dentin region. Postmortem fracture lines are observed in the superior aspect of this sample that and separate the cusp of the tooth into three sections. Intermediate elemental detection values of iron are observed at these fracture lines.

Copper (Cu^{63})

The two-dimensional map for detection values of copper (Cu^{63}) exhibits low detection value in the dentin region. The high intensity detection observed in the lingual inferior aspect of the tooth are consistent with a delay in the element reading attributed to the utilization of the LA-ICP-MS. No inclusions of copper are present in this sample. Postmortem fracture lines in the superior aspect of this sample are observed to separate the cusp of the tooth into three sections. Two radiate inferiorly from the buccal cusp and the third radiates from the lingual aspect of the enamel border. Intermediate elemental detection values of copper are present in the fracture lines.

The two-dimensional map for concentration values of copper (Cu^{63}) exhibits low detection values in the overall dentin and enamel regions. No inclusions of copper are present. Postmortem fracture lines are observed within the superior aspect of this sample. Two radiate inferiorly from the buccal cusp and the third radiates from the lingual aspect of the enamel border. Low concentration values are mapped in these fracture lines.

Zinc (Zn^{66})

The two-dimensional map for detection values of zinc (Zn^{66}) exhibits low detection values in the overall enamel and dentin region. The tooth border exhibits intermediate values of detection with high detection values present in the buccal aspect of the enamel border. Intermediate values are also observed around the inner root border with detection values dissipating as distance from border increases. Low to intermediate detection values are present in the buccal aspect of the dentin region. Further, high detection values are present in the fissure line of the cusps. A postmortem fracture line is observed in the fissure line of the enamel and radiates toward the inferior aspect of the sample.

The two-dimensional map for concentration values of zinc (Zn^{66}) exhibits low concentration values in the enamel region and a low concentration value throughout the dentin region. Low to intermediate concentration values of zinc are observed in the inner root border. Low to intermediate concentration values are present in the buccal aspect of the dentin region. Further, low detection values are present in the fissure line of the cusps. A postmortem fracture line is observed in the buccal aspect of the dentin with intermediate concentration values.

Strontium (Sr^{88})

The two-dimensional map for detection values of strontium (Sr^{88}) exhibits overall low detection values in the enamel and the dentin regions. Intermediate detection values are apparent in the superior aspect of both the dentin and enamel regions with a decrease in detection values observed along the lingual aspect of the DEJ. Intermediate detection values are also observed at along the inner root border of the dentin and near the fissure line in the enamel. A postmortem fracture line is observed in the lingual aspect of the dentin.

The two-dimensional map for concentration values of strontium (Sr^{88}) exhibits striations within the dentin region. Low concentration values are present within these striations. Further, the enamel border exhibits high concentration values on the superior aspects of the cusps. No inclusions of strontium are present.

Antimony (Sb^{121})

The two-dimensional map for detection values of antimony (Sb^{121}) exhibits low detection values in the overall tooth. No inclusions of antimony were observed. A postmortem fracture line with intermediate detection values was observed in the dentin region of the buccal aspect and at the fissure line of the cusps within the dentin region.

The two-dimensional map for concentration values of antimony (Sb^{121}) exhibits low concentration values. No inclusions of antimony were observed. A postmortem fracture line with intermediate detection values was observed in the dentin region of the buccal aspect as well as one at the fissure line of the cusps within the dentin region.

Lanthanum (La^{139})

The two-dimensional map for detection values of lanthanum (La^{139}) exhibits low detection values in the dentin located near the inner root border as well as around the border encompassing the tooth. High detection values are observed on the buccal and lingual aspect of the border and in the superior region of the dentin. A postmortem fracture line with low detection values was observed in the dentin region of the buccal aspect as well as one at the fissure line of the cusps.

Lead (Pb^{208})

The two-dimensional map for detection values of lead (Pb^{208}) exhibits low detection values in the overall enamel and dentin regions. The border and DEJ exhibit an intermediate level of detection. High detection values present in the superior aspect of the inner root border as well as in the buccal aspect of the dentin border and in the buccal cusp of the enamel border. High detection values were observed in the superior region of the dentin. A postmortem fracture line with low detection value was observed in the dentin region of the buccal aspect as well as a second at the fissure line of the cusps within the dentin region.

The two-dimensional map for concentration values of lead (Pb^{208}) exhibits low concentration values in the overall dentin and enamel regions with intermediate values observed in the DEJ and along the border of the roots. High concentration values were observed in the superior region of the dentin with lowered concentration values as distance from superior region increases. A postmortem fracture line with low detection values was observed in the dentin region of the buccal aspect as well as a second at the fissure line of the cusps within the dentin

region, and a third fracture line is perpendicular to the first two and located within the buccal aspect of the dentin region.

Uranium (U^{238})

The two-dimensional map for detection values of uranium (U^{238}) exhibits low detection values throughout the tooth. No inclusions of uranium were observed.

Third Molar

Carbon (C^{13})

The two-dimensional map for detection values of carbon (C^{13}) exhibits low detection values in the dentin and enamel region. Low detection values are present in the lingual aspect of the dentin near the DEJ. Postmortem fracture lines are observed in the dentin and enamel region with low detection values. The first fracture line is observed at the fissure line and radiates toward the inferior aspect of the tooth. A second fracture line is observed at the lingual aspect of the dentin perpendicular to the first fracture.

Magnesium (Mg^{24})

The two-dimensional map for detection values of magnesium (Mg^{24}) exhibits low detection values in the lingual aspect of the dentin region. Intermediate detection values are observed in the lingual aspect of the dentin border as well as near the inferior area in which an absence of tooth material is observed in the tooth. High detection values are present in the dentin region along the superior aspect of the inferior exclusion of tooth material in the dentin.

Postmortem fracture lines are observed in the dentin and enamel region with low elemental detection. The first fracture line is observed at the fissure line and radiates toward the inferior aspect of the tooth. A second fracture line is observed at the lingual aspect of the dentin perpendicular to the first fracture.

Phosphorus (P^{31})

The two-dimensional map for detection values of phosphorus (P^{31}) exhibits increased detection values in the enamel region. The lingual aspect of the enamel cusp exhibits intermediate detection values. High detection values are present in the lingual aspect of the enamel border. Postmortem fracture lines with low element detection are observed in the dentin and enamel region as well. The first fracture line is observed at the fissure line and radiates toward the inferior aspect of the tooth. A second fracture line is observed at the lingual aspect of the dentin perpendicular to the first fracture.

Sulfur (S^{32})

The two-dimensional map for detection values of sulfur (S^{32}) exhibits high detection values in the lingual aspect of the tooth. Detection values decrease as distance from the lingual border increases. No inclusions of sulfur are present in this tooth.

Calcium (Ca^{44})

The two-dimensional map for detection values of calcium (Ca^{44}) exhibits intermediate detection values in the lingual cusp of the enamel region as well as the lingual aspect of the dentin region. Low detection values are observed near the superior and inferior regions in which

an absence of tooth material is observed in the tooth. No inclusions of calcium are present in this tooth. Postmortem fracture lines with low element detection are observed in the dentin and enamel region. The first fracture line is observed at the fissure line and radiates toward the inferior aspect of the tooth. A second fracture line is observed at the lingual aspect of the dentin perpendicular to the first fracture.

Iron (Fe^{56})

The two-dimensional map for detection values of iron (Fe^{56}) exhibits low detection values around the border, and a slight detection of iron is present around the superior region of absent material observed in the sample. Intermediate detection values are observed on the inferior aspect of the superior absence of material in the dentin region. A postmortem fracture line with high element detection is observed at the fissure line and radiates toward the inferior aspect of the tooth.

Copper (Cu^{63})

The two-dimensional map for detection values of copper (Cu^{63}) exhibits low detection values. Low to high detection value are documented to occur at the lingual aspect of the border in the dentin region projecting toward the buccal aspect. High concentration values are present at the inferior region of absent material in this sample.

The two-dimensional map for concentration values of copper (Cu^{63}) exhibits low concentration values in the lingual aspect of the dentin region. No inclusions of copper are

present. A postmortem fracture line with high elemental detection is observed at the fissure line and radiates toward the inferior aspect of the tooth.

Zinc (Zn^{66})

The two-dimensional map for detection values of zinc (Zn^{66}) exhibits low detection values in the border region as well as surrounding the areas of absent material. No inclusions of zinc are present in this sample. A postmortem fracture line with low detection values is observed at the fissure line and radiates toward the inferior aspect of the tooth.

The two-dimensional map for concentration values of zinc (Zn^{66}) exhibits low concentration values throughout the dentin region. High concentration values of zinc are observed surrounding the superior region of which material is absent and intermediate concentration values surrounding the inferior region of absent material in the sample. Concentration values decrease as distance from absent material increases. No inclusions of zinc are present in this sample. A postmortem fracture line with intermediate concentration values is observed at the fissure line and radiates toward the inferior aspect of the tooth.

Strontium (Sr^{88})

The two-dimensional map for detection values of strontium (Sr^{88}) exhibits low detection values in the superior, lingual aspect of both the dentin and enamel regions. Low detection values are also observed in the superior region of absent material. No inclusions of strontium are present in this tooth. Striations of low detection are observed in the lingual aspect of the dentin

region. A postmortem fracture line with low elemental detection is observed in the lingual aspect of the dentin.

The two-dimensional map for concentration values of strontium (Sr^{88}) exhibits the presence of striations within the dentin and enamel region, although these striations are at a negative concentration value and will not be further examined because of this value. High concentration values are observed on the superior aspects of the cusps of the enamel border. Intermediate values are observed in the dentin region near the fissure line of the cusps.

Antimony (Sb^{121})

The two-dimensional map for detection values of antimony (Sb^{121}) exhibits low detection values in the overall tooth. Increased detection values of antimony are documented as part of a delay that occurs within the LA-ICP-MS during data reading. No inclusions of antimony were observed.

The two-dimensional map for concentration values of antimony (Sb^{121}) exhibits low concentration values in the overall tooth. No inclusions of antimony were observed.

Lanthanum (La^{139})

The two-dimensional map for detection values of lanthanum (La^{139}) exhibits low detection values in the dentin region of the tooth. Intermediate detection values are observed superior to the absence of material as well as around the border encompassing the tooth. High detection values are observed on the superior aspect of the superior region of absent material.

Lead (Pb^{208})

The two-dimensional map for detection values of lead (Pb^{208}) exhibits low detection values in the overall enamel and dentin regions. The encompassing border as well as the surrounding border of the inferior region of absent material exhibit low levels of detection. Intermediate to high detection values are observed on the superior region of absent material in the dentin.

The two-dimensional map for concentration values of lead (Pb^{208}) exhibits low concentration values in the superior region of absent material. No inclusions of lead were observed.

Uranium (U^{238})

The two-dimensional map for detection values of uranium (U^{238}) exhibits low detection values throughout the tooth. No inclusions of uranium were observed.

Individual IIT 178-01

First molar

Carbon (C^{13})

The two-dimensional map for detection values of carbon (C^{13}) exhibits intermediate values in the dentin border and along the DEJ as well as the surrounding the region of absent material in the inferior aspect of the tooth. No inclusions of carbon are present in this tooth. Postmortem fracture lines with high detection values are observed in the lingual aspect of the dentin and enamel region.

Magnesium (Mg^{24})

The two-dimensional map for detection values of magnesium (Mg^{24}) exhibits low detection values in the dentin region. Intermediate detection values are observed around the inferior aspect of the root border. High detection values are observed in the dentin region surrounding the region of absent material decreasing as distance from the region of absent material increases. Postmortem fracture lines with low elemental detection are observed in the superior, lingual aspect of the dentin region.

Phosphorus (P^{31})

The two-dimensional map for detection values of phosphorus (P^{31}) exhibits intermediate detection values along the DEJ and lingual aspect of the root. High detection values are present in the dentin near the region of absent material in the inferior aspect of the tooth. A postmortem fracture line with low elemental detection is observed in the dentin region of the lingual aspect near the enamel border.

Sulfur (S^{32})

The two-dimensional map for detection values of sulfur (S^{32}) exhibits intermediate detection values in the lingual aspect of the tooth, with high detection values present in the inferior aspect of the tooth along the lingual aspect of the root border. High detection values are observed around the perimeter of the region of absent material with detection values decreasing as distance from this region increases.

Calcium (Ca^{44})

The two-dimensional map for detection values of calcium (Ca^{44}) exhibits intermediate detection values in the superior aspect of the enamel, the fissure line, and along the inferior, lingual aspect of the root border. High detection values are present around the region of absent material with decreasing values observed as distance from region increases. A postmortem fracture line with low detection values is observed in the lingual aspect of the dentin and radiates from the DEJ.

Iron (Fe^{56})

The two-dimensional map for detection values of iron (Fe^{56}) exhibits low detection values around the tooth border, and a detection of iron is present around the region of absent material. High detection values are present in the buccal and lingual aspect of the dentin tooth border. A postmortem fracture line with high elemental detection is observed in the middle of the dentin region and radiates from the area of absent material in a superior direction.

Copper (Cu^{63})

The two-dimensional map for detection values of copper (Cu^{63}) exhibits low detection values for the dentin region. Intermediate detection values are observed surrounding the region of absent material in the inferior aspect of the root. Intermediate detection values are observed in the buccal aspect near the dentin border.

The two-dimensional map for concentration values of copper (Cu^{63}) exhibits low concentration values in the overall dentin and enamel regions. The DEJ exhibits intermediate values. Intermediate concentration values are present in the buccal aspect of the dentin region

along the tooth border as well as in the buccal cusp border in the enamel region. A postmortem fracture line with high concentration values is observed at the lingual aspect of the DEJ.

Zinc (Zn^{66})

The two-dimensional map for detection values of zinc (Zn^{66}) exhibits low detection values throughout the dentin region. The border exhibits intermediate values of detection with high detection values present in the region observed to have an absence of material which decreases as distance from region increases. A postmortem fracture line with low detection values is observed in the lingual aspect of the dentin near the DEJ.

The two-dimensional map for concentration values of zinc (Zn^{66}) exhibits low concentration values in the enamel and dentin regions. Low concentration values are observed surrounding the region of absent material in the inferior aspect of the root border. High detection values are observed around the enamel border of the cusps. Striations with low concentration values are evident in the buccal aspect within the dentin region

Strontium (Sr^{88})

The two-dimensional map for detection values of strontium (Sr^{88}) exhibits overall low detection values in the enamel region with intermediate detection values observed in the dentin region. Intermediate detection values are apparent in the inferior aspect of the dentin, the root border, and in the lingual aspect of the DEJ. Intermediate detection values are also observed surrounding the absence of material in the inferior aspect of the tooth. High detection values are present near the DEJ along the lingual aspect of the dentin border. A postmortem fracture line with low elemental detection is observed in the lingual aspect of the dentin near the DEJ.

The two-dimensional map for concentration values of strontium (Sr^{88}) exhibits low concentration values within the dentin and buccal aspect of the enamel region. Intermediate concentration values are present across the dentin region stretching from the lingual to dental aspect. High concentration values are present in the buccal aspect of the dental border with observed high concentration values.

Antimony (Sb^{121})

The two-dimensional map for detection values of antimony (Sb^{121}) exhibits inconsistent low detection values in the overall tooth. No inclusions of antimony were observed.

The two-dimensional map for concentration values of antimony (Sb^{121}) exhibits overall intermediate concentration values in the tooth. No inclusions of antimony were observed.

Lanthanum (La^{139})

The two-dimensional map for detection values of lanthanum (La^{139}) exhibits low detection values in the border encompassing the tooth. High detection values are observed on the buccal and lingual aspect of the border. No inclusions of lanthanum were observed.

Lead (Pb^{208})

The two-dimensional map for detection values of lead (Pb^{208}) exhibits low detection values in the overall enamel and dentin regions. The border and DEJ exhibit an intermediate detection values. Intermediate detection values are also present surrounding the region of absent material in the inferior aspect of the root. No inclusions of lead were observed.

The two-dimensional map for concentration values of lead (Pb^{208}) exhibits low concentration values in the superior aspect of dentin as well as the buccal aspect of the enamel region. Intermediate values are observed in the buccal aspect of the DEJ. No inclusions of lead were observed.

Uranium (U^{238})

The two-dimensional map for detection values of uranium (U^{238}) exhibits low detection values in the superior aspect of the dentin region and along the enamel border. Several inclusions of high detection were observed in the dentin region of the crown and radiate toward the inferior aspect, one on the dentin border of the buccal aspect, the second on the lingual dentin border, and the third on the inner aspect of the dentin parallel to the second inclusion.

Second Molar

Carbon (C^{13})

The two-dimensional map for detection values of carbon (C^{13}) exhibits low detection values in the lingual aspect of the dentin and enamel regions and intermediate values are observed in the buccal aspect of the dentin region. Intermediate values are observed in the superior aspect of the dentin. No inclusions of carbon are present. A postmortem fracture line with intermediate detection values is observed radiating toward the inferior aspect of the tooth from the enamel border.

Magnesium (Mg^{24})

The two-dimensional map for detection values of magnesium (Mg^{24}) exhibits increased detection values in the lingual aspect of the dentin region. Low detection values are observed in the dentin. Intermediate detection values are observed in the superior aspect of the dentin. A postmortem fracture line is observed in the dentin region that radiates toward the inferior aspect of the tooth from the DEJ. The low intensity observed in the fracture lines corresponds with elemental reading of the resin base.

Phosphorus (P^{31})

The two-dimensional map for detection values of phosphorus (P^{31}) exhibits intermediate detection values in the lingual aspect of the tooth with increased detection values at the DEJ. A postmortem fracture line is observed radiating from the enamel border toward the inferior aspect of the tooth. The low intensity observed in the fracture lines corresponds with elemental reading of the resin base.

Sulfur (S^{32})

The two-dimensional map for detection values of sulfur (S^{32}) exhibits high detection values in the lingual aspect of the tooth that decrease to intermediate values and low detection values as distance from the lingual border increases. No inclusions of sulfur are present in this tooth.

Calcium (Ca^{44})

The two-dimensional map for detection values of calcium (Ca^{44}) exhibits intermediate detection values across the tooth with increased detection values in the lingual aspect. Intermediate detection values are exhibited in the lingual aspect of the DEJ. No inclusions of calcium are present in this tooth. A postmortem fracture line is observed radiating from the enamel border toward the inferior aspect of the tooth. The low intensity observed in the fracture lines corresponds with elemental reading of the resin base.

Iron (Fe^{56})

The two-dimensional map for detection values of iron (Fe^{56}) exhibits low detection values in the overall dentin and enamel regions. Low detection values are present around the border, and intermediate detection values are present around the region of absent material. An inclusion of iron is present in the lingual aspect of the dentin border. A postmortem fracture line with high detection values is observed at the enamel border and radiates toward the inferior aspect of the tooth.

Copper (Cu^{63})

The two-dimensional map for detection values of copper (Cu^{63}) exhibits low detection values. An inclusion of copper with intermediate values is present in the lingual aspect of the dentin region. A postmortem fracture line with intermediate detection is observed at the enamel border and radiates toward the inferior aspect of the tooth.

The two-dimensional map for concentration values of copper (Cu^{63}) exhibits low concentration values in the dentin region and on the lingual cusp in the enamel region.

Inclusions of intermediate concentration values are present along the lingual and buccal aspects of the dentin near the border of the root. A postmortem fracture line with high elemental concentration values is observed in the enamel region of the cusp and radiates toward the inferior aspect of the tooth.

Zinc (Zn^{66})

The two-dimensional map for detection values of zinc (Zn^{66}) exhibits intermediate detection values present in the border and low detection values in the dentin region. Intermediate detection values are present in the superior aspect of the region of absent material. A postmortem fracture line is observed at the enamel border and radiates toward the inferior aspect of the tooth.

The two-dimensional map for concentration values of zinc (Zn^{66}) exhibits low concentration value throughout the dentin region and intermediate concentration values in the enamel border of the cusp. No inclusions of zinc are present in this sample.

Strontium (Sr^{88})

The two-dimensional map for detection values of strontium (Sr^{88}) exhibits low detection values in the dentin region and along the DEJ. Intermediate detection values are observed in the buccal aspect of the dentin. Striations of low detection are observed in the superior aspect of the dentin region. A postmortem fracture line is observed at the enamel border and radiates toward the inferior aspect of the tooth.

The two-dimensional map for concentration values of strontium (Sr^{88}) exhibits low concentration values in the lingual aspect of the dentin as well as the surrounding the region of absent material in the inferior aspect of the root. Inclusions of intermediate concentration values are present in the lingual and buccal aspect of the dentin border.

Antimony (Sb^{121})

The two-dimensional map for detection values of antimony (Sb^{121}) exhibits low detection values. No inclusions of antimony were observed.

The two-dimensional map for concentration values of antimony (Sb^{121}) exhibits low concentration values. No inclusions of antimony were observed.

Lanthanum (La^{139})

The two-dimensional map for detection values of lanthanum (La^{139}) exhibits intermediate detection values around the region of absent material as well as around the border encompassing the tooth. An inclusion of high detection values was observed on the lingual and buccal aspect of the dentin border. Intermediate detection values are present on the buccal cusp of the enamel. A postmortem fracture line of intermediate concentration values is present at the superior aspect of the region of absent material.

Lead (Pb^{208})

The two-dimensional map for detection values of lead (Pb^{208}) exhibits low detection values in the overall encompassing border as well as the surrounding border of the inferior

region of absent material. An inclusion of high detection values was observed in the lingual aspect of the dentin border region. Striations of low detection values were observed in the dentin.

The two-dimensional map for concentration values of lead (Pb^{208}) exhibits intermediate values in the encompassing border of the tooth as well as around the region of absent material in the inferior aspect of the tooth. A striation of low concentration values is present in the superior aspect of the dentin

Uranium (U^{238})

The two-dimensional map for detection values of uranium (U^{238}) exhibits inclusions of high detection values uranium in the enamel as well as in the buccal and lingual aspect of the dentin border. A postmortem fracture line with low detection values is present at the superior aspect of the tooth and radiates towards the region of absent material.

Third Molar

Carbon (C^{13})

The two-dimensional map for detection values of carbon (C^{13}) exhibits low detection values in the dentin and enamel regions. Intermediate values are observed in the DEJ. Several postmortem fracture lines of intermediate detection values are observed to radiate from the enamel border to the DEJ and from the DEJ toward the inferior aspect of the tooth.

Magnesium (Mg^{24})

The two-dimensional map for detection values of magnesium (Mg^{24}) exhibits intermediate values along the buccal aspect of the DEJ. Inclusions of magnesium are present at the buccal and lingual root tips and exhibit intermediate values. Postmortem fracture lines are observed in the dentin region radiating toward the inferior aspect of the tooth from the DEJ.

Phosphorus (P^{31})

The two-dimensional map for detection values of phosphorus (P^{31}) exhibits intermediate detection values along the enamel border as well as at the DEJ. No inclusions of phosphorus are present in this tooth. A postmortem fracture line is observed radiating from the lingual aspect of the DEJ in the dentin and radiates toward the inferior aspect of the tooth.

Sulfur (S^{32})

The two-dimensional map for detection values of sulfur (S^{32}) exhibits high detection values in the dentin region of the tooth as well as the buccal aspect of the enamel region. An inclusion of sulfur is present in the buccal root tip and exhibits high detection values.

Calcium (Ca^{44})

The two-dimensional map for detection values of calcium (Ca^{44}) exhibits intermediate detection values in the enamel border as well as the DEJ. No inclusions of calcium are present in this tooth. A postmortem fracture line is observed to radiate from the lingual aspect of the DEJ toward the inferior aspect of the tooth.

Iron (Fe^{56})

The two-dimensional map for detection values of iron (Fe^{56}) exhibits low detection values are present around the border. Inclusions with high detection values are present in the dentin border of the tooth and exhibit high detection values.

Copper (Cu^{63})

The two-dimensional map for detection values of copper (Cu^{63}) exhibits intermediate detection values along the DEJ as well as in the buccal aspect of the enamel border. No inclusions of copper are present in this sample.

The two-dimensional map for concentration values of copper (Cu^{63}) exhibits low concentration values in the dentin region. Intermediate concentration values are observed along the DEJ and along the border encompassing the tooth. No inclusions of copper are present.

Zinc (Zn^{66})

The two-dimensional map for detection values of zinc (Zn^{66}) exhibits intermediate detection values present in the border region and low detection values in the dentin region. An inclusion of high detection value is present in buccal aspect of the enamel border. Postmortem fracture lines with intermediate values are observed in the dentin and radiate from the DEJ toward the inferior aspect.

The two-dimensional map for concentration values of zinc (Zn^{66}) exhibits low concentration value throughout the dentin region and intermediate concentration values in the enamel border of the cusp. No inclusions of zinc are present in this sample.

Strontium (Sr^{88})

The two-dimensional map for detection values of strontium (Sr^{88}) exhibits low detection values in the dentin region and intermediate values along the DEJ. An inclusion with high detection values is present in the lingual root tip. A postmortem fracture line is observed to radiate from the lingual aspect of the DEJ toward the inferior aspect of the tooth.

The two-dimensional map for concentration values of strontium (Sr^{88}) exhibits low concentration in the dentin region. High concentration values are observed in the enamel border as well as the lingual aspect of the dentin. No inclusions of strontium are present.

Antimony (Sb^{121})

The two-dimensional map for detection values of antimony (Sb^{121}) exhibits low detection values. No inclusions of antimony were observed.

The two-dimensional map for concentration values of antimony (Sb^{121}) exhibits low concentration values. No inclusions of antimony were observed.

Lanthanum (La^{139})

The two-dimensional map for detection values of lanthanum (La^{139}) exhibits intermediate detection values around the border encompassing the tooth. An inclusion of high detection values was observed on the lingual aspect of the dentin border near the root tip.

Lead (Pb^{208})

The two-dimensional map for detection values of lead (Pb^{208}) exhibits low detection values in the dentin region with the presence of striations. Intermediate values were observed in the encompassing border of the tooth.

The two-dimensional map for concentration values of lead (Pb^{208}) exhibits low concentration values in the dentin region as well as the enamel border.

Uranium (U^{238})

The two-dimensional map for detection values of uranium (U^{238}) exhibits low detection values observed in the encompassing tooth border. An inclusion with high detection values is observed in the lingual root tip.

Individual IIT 190-01

First molar

Carbon (C^{13})

The two-dimensional map for detection values of carbon (C^{13}) exhibits low detection values in the dentin region. No inclusions of carbon are present in this tooth. Several postmortem fracture lines are observed. The first starts at the peak of the DEJ and radiates towards the area of absent material, while the second begins at the fissure line between the cusps and radiates toward the region of absent material. Intermediate intensity is observed in these fracture lines. The third fracture line exhibits high detection values and is observed to start at the peak of the lingual cusp and radiates to the root tip.

Magnesium (Mg^{24})

The two-dimensional map for detection values of magnesium (Mg^{24}) exhibits low detection values in the dentin and enamel regions. An inclusion of high detection is present in the buccal aspect of the dentin region, decreasing in intensity as distance from the inclusion increases. A postmortem fracture line is observed to start at the peak of the lingual cusp and radiates to the root tip.

Phosphorus (P^{31})

The two-dimensional map for detection values of phosphorus (P^{31}) exhibits intermediate detection values in the enamel and dentin regions. High detection values are present in the superior, buccal aspect of the tooth. A postmortem fracture line is observed to start at the peak of the lingual cusp and radiates to the root tip.

Sulfur (S^{32})

The two-dimensional map for detection values of sulfur (S^{32}) exhibits intermediate detection values in the buccal aspect of the dentin region. An inclusion of high detection values are present in the buccal aspect of the dentin region decreasing in intensity as distance increases from the inclusion. A postmortem fracture line is observed to start at the peak of the lingual cusp and radiates to the root tip.

Calcium (Ca^{44})

The two-dimensional map for detection values of calcium (Ca^{44}) exhibits intermediate detection values. An inclusion of high detection values is present in the buccal aspect of the dentin region and decreases in intensity as distance increases from the inclusion. A postmortem fracture line is observed to start at the peak of the lingual cusp and radiates to the root tip.

Iron (Fe^{56})

The two-dimensional map for detection values of iron (Fe^{56}) exhibits low detection values around the tooth border. No inclusions of iron are present. A postmortem fracture line of high elemental detection is observed to start at the peak of the lingual cusp and radiates to the root tip.

Copper (Cu^{63})

The two-dimensional map for detection values of copper (Cu^{63}) exhibits low detection values in the dentin region. Intermediate detection values are observed in the border encompassing the tooth. Inclusions of high detection values are present in the crown fissure line of the enamel. Intermediate detection values are present in the buccal cusp of the enamel border. A postmortem fracture line of low elemental detection is observed to start at the peak of the lingual cusp and radiates to the root tip.

The two-dimensional map for concentration values of copper (Cu^{63}) exhibits low concentration values in the overall dentin and enamel regions. Inclusions of high concentrations are present in the crown fissure line of the enamel and the buccal cusp of the enamel border. An inclusion of intermediate values is present in the lingual aspect of the dentin border. A

postmortem fracture line with high concentration values is observed to start at the peak of the lingual cusp and radiates to the root tip.

Zinc (Zn^{66})

The two-dimensional map for detection values of zinc (Zn^{66}) exhibits low detection values in the dentin region. The enamel border exhibits intermediate values of detection with high detection values present in the buccal cusp. A postmortem fracture line is observed to start at the peak of the lingual cusp and radiates to the root tip.

The two-dimensional map for concentration values of zinc (Zn^{66}) exhibits low concentration values throughout the dentin region. High detection values are observed around the enamel border of the cusps. An inclusion of low concentration values is present in the fissure line of the enamel. Striations of low concentration are evident in the superior aspect within the dentin region.

Strontium (Sr^{88})

The two-dimensional map for detection values of strontium (Sr^{88}) exhibits intermediate detection values at the center of the tooth which decreases in value as distance increases from the center. Low detection values are observed in the enamel region. An inclusion of high detection values is present in the lingual root tip. A postmortem fracture line is observed to start at the peak of the lingual cusp and radiates to the root tip.

The two-dimensional map for concentration values of strontium (Sr^{88}) exhibits low concentration values within the dentin. Inclusions of high concentration values are present on

the buccal and lingual aspect of the dentin border decreasing as distance from the inclusion increases.

Antimony (Sb^{121})

The two-dimensional map for detection values of antimony (Sb^{121}) exhibits low detection values in the overall tooth. No inclusions of antimony were observed.

The two-dimensional map for concentration values of antimony (Sb^{121}) exhibits intermediate concentration values in the tooth. No inclusions of antimony were observed.

Lanthanum (La^{139})

The two-dimensional map for detection values of lanthanum (La^{139}) exhibits intermediate detection values in the border encompassing the tooth. No inclusions of lanthanum were observed in this sample. A postmortem fracture line with intermediate detection values is observed to start at the peak of the lingual cusp and radiates to the root tip.

Lead (Pb^{208})

The two-dimensional map for detection values of lead (Pb^{208}) exhibits low detection values in the inferior aspect of the dentin and the superior aspect of the enamel. Intermediate detection values are present in the DEJ and surround the absence of material in the inferior aspect of the root as well as in the buccal root tip. Striations of low intensity are observed in the dentin region. A postmortem fracture line is observed to start at the peak of the lingual cusp and radiates to the root tip.

The two-dimensional map for concentration values of lead (Pb^{208}) exhibits low concentration values in the superior aspect of dentin and high concentration values in the cusps of the enamel border. Intermediate values are observed in the DEJ and striations of low intensity are observed in the dentin region. Inclusions of lead were observed in the region of absent material in the inferior aspect of the tooth. A postmortem fracture line with high element concentration values is observed to start at the peak of the lingual cusp and radiates to the root tip.

Uranium (U^{238})

The two-dimensional map for detection values of uranium (U^{238}) exhibits low detection values in the inferior aspect and along the border surrounding the tooth. Inclusions of high detection values are observed at the fissure line of the cusps in the enamel region as well as on the buccal aspect of the enamel border. A postmortem fracture line of low detection is observed to start at the peak of the lingual cusp and radiates to the root tip.

Individual IIT 197-01

First molar

Carbon (C^{13})

The two-dimensional map for detection values of carbon (C^{13}) exhibits low detection values in the dentin region. No inclusions of carbon are present in this tooth. Several postmortem fracture lines of intermediate detection are present. The first radiates from the lingual aspect of the buccal cusp toward the buccal aspect of the dentin border. The second

fracture line is observed to radiate from the fissure line toward the inferior aspect of the buccal dentin border. The third fracture line also radiates from the fissure line but extends toward the inferior aspect and terminates at the superior aspect of the inner root border. The final fracture line is observed to radiate from the inferior aspect of the region of absent material and radiates toward the superior aspect of the inner root border.

Magnesium (Mg^{24})

The two-dimensional map for detection values of magnesium (Mg^{24}) exhibits low detection values in the dentin region. Intermediated detection vales are present in the buccal aspect of the dentin. An inclusion of high detection is present in the inferior buccal aspect of the dentin border that decreases in detection values as distance from the inclusion increases.

Several postmortem fracture lines are observed within this sample. The first radiates from the lingual aspect of the buccal cusp toward the buccal aspect of the dentin border. The second fracture line is observed to radiate from the fissure line toward the inferior aspect of the buccal dentin border. The third fracture line also radiates from the fissure line but extends toward the inferior aspect and terminates at the superior aspect of the inner root border. The final fracture line is observed to radiate from the inferior aspect of the region of absent material and radiates toward the superior aspect of the inner root border.

Phosphorus (P^{31})

The two-dimensional map for detection values of phosphorus (P^{31}) exhibits low detection values in the enamel and dentin regions. Intermediate detection values are present in the buccal

aspect of the tooth. Inclusions of high detection values are present in the inferior, buccal aspect of the dentin region within the root tip and decreases detection values as distance from the inclusion increases. A second inclusion is present in the lingual aspect of the inferior dentin region within the root tip and is observed to have intermediate values.

Several postmortem fracture lines are present. The first radiates from the lingual aspect of the buccal cusp toward the buccal aspect of the dentin border. The second fracture line is observed to radiate from the fissure line toward the inferior aspect of the buccal dentin border. The third fracture line also radiates from the fissure line but extends toward the inferior aspect and terminates at the superior aspect of the inner root border. The final fracture line is observed to radiate from the inferior aspect of the region of absent material and radiates toward the superior aspect of the inner root border.

Sulfur (S^{32})

The two-dimensional map for detection values of sulfur (S^{32}) exhibits low detection values in the dentin region. An inclusion of high detection value is present in the inferior, buccal aspect of the dentin region and decreases in intensity as distance from the inclusion increases.

Several postmortem fracture lines are present. The first radiates from the lingual aspect of the buccal cusp toward the buccal aspect of the dentin border. The second fracture line is observed to radiate from the fissure line toward the inferior aspect of the buccal dentin border. The third fracture line also radiates from the fissure line but extends toward the inferior aspect and terminates at the superior aspect of the inner root border. The final fracture line is observed

to radiate from the inferior aspect of the region of absent material and radiates toward the superior aspect of the inner root border.

Calcium (Ca^{44})

The two-dimensional map for detection values of calcium (Ca^{44}) exhibits intermediate detection values across the tooth. An inclusion of high detection values is present in the inferior buccal and lingual aspects of the dentin border along the root tips. High detection values are observed around the buccal inclusion, dissipating in intensity as distance increases from the inclusion. Intermediate detection values are observed in the lingual inclusion.

Several postmortem fracture lines are observed within this sample. The first radiates from the lingual aspect of the buccal cusp toward the buccal aspect of the dentin border. The second fracture line is observed to radiate from the fissure line toward the inferior aspect of the buccal dentin border. The third fracture line also radiates from the fissure line but extends toward the inferior aspect and terminates at the superior aspect of the inner root border. The final fracture line is observed to radiate from the inferior aspect of the region of absent material and radiates toward the superior aspect of the inner root border.

Iron (Fe^{56})

The two-dimensional map for detection values of iron (Fe^{56}) exhibits low detection values in the inferior and buccal regions of the tooth. Intermediate detection values are present in the border of the root tips. Low detection values are present in the DEJ.

Several postmortem fracture lines of high detection values are observed within this sample. The first radiates from the lingual aspect of the buccal cusp toward the buccal aspect of the dentin border. The second fracture line is observed to radiate from the fissure line toward the inferior aspect of the buccal dentin border. The third fracture line also radiates from the fissure line but extends toward the inferior aspect and terminates at the superior aspect of the inner root border. The final fracture line is observed to radiate from the inferior aspect of the region of absent material and radiates toward the superior aspect of the inner root border.

Copper (Cu^{63})

The two-dimensional map for detection values of copper (Cu^{63}) exhibits low detection values in the dentin region and enamel border. Intermediate detection values are observed in the root tips.

Several postmortem fracture lines of high element detection are observed within this sample. The first radiates from the lingual aspect of the buccal cusp toward the buccal aspect of the dentin border. The second fracture line is observed to radiate from the fissure line toward the inferior aspect of the buccal dentin border. The third fracture line also radiates from the fissure line but extends toward the inferior aspect and terminates at the superior aspect of the inner root border. The final fracture line is observed to radiate from the inferior aspect of the region of absent material and radiates toward the superior aspect of the inner root border.

The two-dimensional map for concentration values of copper (Cu^{63}) exhibits low concentration values in the border encompassing the tooth. No inclusions of copper are present in this sample.

Several postmortem fracture lines are apparent, with the first fracture line observed to radiate from the fissure line toward the inferior aspect of the buccal dentin border with low concentration values detected. The second fracture line also radiates from the fissure line but extends toward the inferior aspect and terminates at the superior aspect of the inner root border with high concentration values detected. The final fracture line is observed to radiate from the inferior aspect of the region of absent material and radiates toward the superior aspect of the inner root border and exhibits high concentration values.

Zinc (Zn^{66})

The two-dimensional map for detection values of zinc (Zn^{66}) exhibits low detection values in the dentin region. The enamel border exhibits intermediate values of detection with high detection values present in the buccal cusp. Inclusions of intermediate detection values are present in the buccal superior aspect of the region in which material is, and in the root tips along the border. Several postmortem fracture lines are apparent, with the first fracture line observed to radiate from the fissure line toward the inferior aspect of the buccal dentin border. The second fracture line also radiates from the fissure line but extends toward the inferior aspect and terminates at the superior aspect of the inner root border. The final fracture line is observed to radiate from the inferior aspect of the region of absent material and radiates toward the superior aspect of the inner root border.

The two-dimensional map for concentration values of zinc (Zn^{66}) exhibits low concentration value throughout the dentin region and at the DEJ. High detection values are observed around the enamel border of the cusps. No inclusions of zinc are present. Several

postmortem fracture lines of low concentrations are observed. The first radiates from the lingual aspect of the buccal cusp toward the buccal aspect of the dentin border. The second fracture line also radiates from the fissure line but extends toward the inferior aspect and terminates at the superior aspect of the inner root border.

Strontium (Sr^{88})

The two-dimensional map for detection values of strontium (Sr^{88}) exhibits intermediate detection values in the dentin with high detection observed in the buccal and lingual dentin border toward the inferior aspect of the tooth. Low detection values are observed in the enamel region. Several postmortem fracture lines of low detection are observed within this sample. The first radiates from the lingual aspect of the buccal cusp toward the buccal aspect of the dentin border. The second fracture line is observed to radiate from the fissure line toward the inferior aspect of the buccal dentin border. The third fracture line also radiates from the fissure line but extends toward the inferior aspect and terminates at the superior aspect of the inner root border. The final fracture line is observed to radiate from the inferior aspect of the region of absent material and radiates toward the superior aspect of the inner root border.

The two-dimensional map for concentration values of strontium (Sr^{88}) exhibits intermediate concentration values within the dentin with high concentrations are observed in the enamel border. No inclusions are present in this sample.

Antimony (Sb^{121})

The two-dimensional map for detection values of antimony (Sb^{121}) exhibits low detection values. No inclusions of antimony were observed.

The two-dimensional map for concentration values of antimony (Sb^{121}) exhibits intermediate concentration values. No inclusions of antimony were observed. Postmortem fracture lines were observed with values that coincide with the elemental reading of the resin base.

Lanthanum (La^{139})

The two-dimensional map for detection values of lanthanum (La^{139}) exhibits intermediate detection values in the border encompassing the tooth. Inclusions of intermediate detection values were observed in the enamel border of the buccal cusp, the lingual dentin border in the inferior aspect of the tooth, and the superior aspect of the region of absent material. Several postmortem fracture lines of low detection values were observed on the buccal and lingual aspect of the region of absent material.

Lead (Pb^{208})

The two-dimensional map for detection values of lead (Pb^{208}) exhibits high detection values at the DEJ with values decreasing as distance from the DEJ increases. Low detection values are present throughout the tooth with intermediate values in the buccal and lingual aspect of the dentin border located in the roots. Striations are present in the dentin region and exhibit low detection values. An inclusion of high detection values is observed around the superior

aspect of the region in which material is absent. Postmortem fracture lines were observed on the buccal and lingual aspect of the region of absent material.

The two-dimensional map for concentration values of lead (Pb^{208}) exhibits low concentration values in the superior aspect of dentin and high concentration values in the cusps of the enamel border. Intermediate values are observed in the DEJ and striations of low intensity are observed in the dentin region. Inclusions of intermediate concentration values were observed at the region of absent material in the superior aspect of the tooth. Several postmortem fracture lines of low concentration values are present. The first radiates from the lingual aspect of the buccal cusp toward the buccal aspect of the dentin border. The second fracture line is observed to radiate from the fissure line toward the inferior aspect of the buccal dentin border. The third fracture line also radiates from the fissure line but extends toward the inferior aspect and terminates at the superior aspect of the inner root border. The final fracture line is observed to radiate from the inferior aspect of the region of absent material and radiates toward the superior aspect of the inner root border.

Uranium (U^{238})

The two-dimensional map for detection values of uranium (U^{238}) exhibits low detection values. An inclusion of high detection values is observed at the buccal cusp in the enamel border. A postmortem fracture line of low detection values is observed in the lingual aspect of the dentin region.

Second molar

Carbon (C^{13})

The two-dimensional map for detection values of carbon (C^{13}) exhibits low detection values in the dentin region. High detection values are present in the lingual aspect of the DEJ. Several postmortem fracture lines of intermediate detection are observed within this sample. The first radiates from the buccal aspect of the DEJ toward the inferior aspect of the tooth. The second fracture line is observed to radiate from the first fracture toward the inferior aspect of the buccal dentin region. The third fracture line radiates from the lingual cusp in the enamel and extends toward the inferior aspect and terminates at the inferior aspect of the tooth. The final fracture line is observed to radiate from the inferior aspect of the sample and radiates toward the superior aspect within the dentin.

Magnesium (Mg^{24})

The two-dimensional map for detection values of magnesium (Mg^{24}) exhibits low detection values in the dentin and enamel regions. No inclusions of magnesium are present. Several postmortem fracture lines are observed within this sample. The first radiates from the buccal aspect of the DEJ toward the inferior aspect of the tooth. The second fracture line is observed to radiate from the first fracture toward the inferior aspect of the buccal dentin region. The third fracture line radiates from the lingual cusp in the enamel and extends toward the inferior aspect and terminates at the inferior aspect of the tooth. The final fracture line is observed to radiate from the inferior aspect of the sample and radiates toward the superior aspect within the dentin.

Phosphorus (P^{31})

The two-dimensional map for detection values of phosphorus (P^{31}) exhibits intermediate detection values in the dentin region, with low detection values in the enamel. Intermediate detection values are present in the buccal aspect of the enamel border. A postmortem fracture line shows significant elemental difference in the buccal aspect of the dentin radiating from the DEJ toward the inferior aspect of the tooth.

Sulfur (S^{32})

The two-dimensional map for detection values of sulfur (S^{32}) exhibits intermediate detection values within the dentin region and enamel border. Low detection values are observed in the enamel region. No inclusions of sulfur are present. A postmortem fracture line is present in the buccal aspect of the dentin radiating from the DEJ toward the inferior aspect of the tooth.

Calcium (Ca^{44})

The two-dimensional map for detection values of calcium (Ca^{44}) exhibits intermediate detection values across the dentin region and enamel border with low detection present in the enamel. No inclusions of calcium are present. A postmortem fracture line is detected and shows significant elemental difference in the buccal aspect of the dentin radiating from the DEJ toward the inferior aspect of the tooth.

Iron (Fe^{56})

The two-dimensional map for detection values of iron (Fe^{56}) exhibits inconsistent low detection values in the DEJ and enamel border. Inclusions of high detection values are present in

the fissure of the cusps. A postmortem fracture line with high detection values is detected in the buccal aspect of the dentin radiating from the DEJ toward the inferior aspect of the tooth and low detection values throughout the inferior aspect of the fracture.

Copper (Cu^{63})

The two-dimensional map for detection values of copper (Cu^{63}) exhibits low detection values in the dentin region as well as in the enamel border. No inclusions of copper are present within this sample.

The two-dimensional map for concentration values of copper (Cu^{63}) exhibits low concentration values in the border encompassing the tooth and in the buccal aspect of the DEJ. No inclusions of copper are present in this sample. A postmortem fracture line with low concentration value is present in the buccal aspect of the dentin radiating from the DEJ toward the inferior aspect of the tooth.

Zinc (Zn^{66})

The two-dimensional map for detection values of zinc (Zn^{66}) exhibits low detection values in the dentin region. The enamel border exhibits intermediate values of detection with high detection values present in the buccal cusp. No inclusions are present in this sample. Several postmortem fracture lines of low detection values are apparent, with the first fracture line radiating from the DEJ toward the inferior aspect of the tooth. The second fracture line also radiates from the lingual aspect of the DEJ and radiates toward the inferior aspect of the tooth.

The two-dimensional map for concentration values of zinc (Zn^{66}) exhibits low concentration value throughout the dentin region as well as at the DEJ. High detection values are observed around the enamel border of the cusps. No inclusions of zinc are present.

Strontium (Sr^{88})

The two-dimensional map for detection values of strontium (Sr^{88}) exhibits intermediate detection values in the dentin region and low values observed within the enamel. An inclusion of intermediate detection is present in the enamel border of the buccal cusp. A postmortem fracture line is present in the buccal aspect of the dentin and extends toward the inferior aspect of the tooth.

The two-dimensional map for concentration values of strontium (Sr^{88}) exhibits negative concentration values and will not be considered for analytical purposes.

Antimony (Sb^{121})

The two-dimensional map for detection values of antimony (Sb^{121}) exhibits low detection values in the overall tooth. An inclusion of intermediate detection values was observed in the enamel border of the buccal cusp. A postmortem fracture line of high intensity is present in the superior buccal aspect of the dentin.

The two-dimensional map for concentration values of antimony (Sb^{121}) exhibits low concentration values in the tooth. No inclusions of antimony were observed.

Lanthanum (La^{139})

The two-dimensional map for detection values of lanthanum (La^{139}) exhibits low detection values in the dentin region and enamel border. Inconsistent inclusions of lanthanum were observed in this sample on the enamel border as well as the along the DEJ.

Lead (Pb^{208})

The two-dimensional map for detection values of lead (Pb^{208}) exhibits intermediate detection values at the DEJ and the enamel border. Low detection values are present in the enamel region. Striations of intermediate detection values are present in the dentin region. A postmortem fracture line is observed on the buccal aspect of the dentin region radiating from the DEJ toward the inferior aspect of the tooth.

The two-dimensional map for concentration values of lead (Pb^{208}) exhibits low concentration values in the dentin and enamel border. Striations of low concentration values are apparent in the dentin region. No inclusions of lead were observed. A postmortem fracture line of low elemental concentrations is observed on the buccal aspect of the dentin region radiating form the DEJ toward the inferior aspect of the tooth.

Uranium (U^{238})

The two-dimensional map for detection values of uranium (U^{238}) exhibits low detection values throughout the dentin region of the tooth. The enamel border exhibits inconsistent high detection values in the buccal cusp. No inclusions of uranium are observed.

Individual IIT 213-01

First molar

Carbon (C^{13})

The two-dimensional map for detection values of carbon (C^{13}) exhibits low detection values in the dentin region. No inclusions of carbon are present in this tooth. A postmortem fracture line is observed at the fissure line between the cusps and extends toward the inferior aspect of the dentin. The intermediate detection values of the fracture line is indicative of elemental reading within the resin base.

Magnesium (Mg^{24})

The two-dimensional map for detection values of magnesium (Mg^{24}) exhibits intermediate values in the dentin region with high detection values present near the pulp cavity. Low detection values are present in the enamel region. No inclusions of magnesium are present. A postmortem fracture line is observed at the fissure line and projects toward the inferior aspect of the dentin region.

Phosphorus (P^{31})

The two-dimensional map for detection values of phosphorus (P^{31}) exhibits intermediate detection values in the enamel region, and in the dentin root tips. The remaining dentin exhibits low detection values. No inclusions of phosphorus are present in this tooth. A postmortem fracture line is observed at the fissure line of the cusps and projects toward the pulp cavity.

Sulfur (S^{32})

The two-dimensional map for detection values of sulfur (S^{32}) exhibits intermediate detection values in the dentin region and low detection values within the enamel region. High detection values are observed near the pulp cavity of the dentin and intensity decreases as distance increases. No inclusions of sulfur are present in this sample. A postmortem fracture line is observed in the fissure line of the cusps and extends toward the pulp cavity.

Calcium (Ca^{44})

The two-dimensional map for detection values of calcium (Ca^{44}) exhibits intermediate detection values in the enamel region and low detection within the dentin region. Intermediate detection values are apparent along the pulp cavity as well as in the roots of the sample. A postmortem fracture line is observed in the fissure line between the cusps and projecting toward the pulp cavity at the inferior aspect of the dentin.

Iron (Fe^{56})

The two-dimensional map for detection values of iron (Fe^{56}) exhibits low detection values in the overall dentin and enamel regions, and in the DEJ. An inclusion of high detection value is present in the dentin region near the pulp cavity. A postmortem fracture line with low detection values is observed in the fissure of the cusps and projects toward the inferior aspect of the dentin toward the pulp cavity.

Copper (Cu^{63})

The two-dimensional map for detection values of copper (Cu^{63}) exhibits several inclusions within the dentin region. The first inclusion presents intermediate detection values in the lingual aspect of the dentin region. The second inclusion presents high detection values in the inferior aspect of the dentin region near the pulp cavity.

The two-dimensional map for concentration values of copper (Cu^{63}) exhibits low concentration values in the overall dentin and enamel regions. Several inclusions of intermediate concentration values are present. The first inclusion is present in the lingual aspect of the dentin and the second inclusion is in the center of the dentin region. A postmortem fracture line of high concentration is observed radiating from the fissure line toward the inferior aspect of the dentin. High concentration values within this fracture line indicate element reading associated with the resin base.

Zinc (Zn^{66})

The two-dimensional map for detection values of zinc (Zn^{66}) exhibits low detection values in the enamel region with intermediate detection values presenting in the enamel border. The inferior aspect of the dentin near the pulp cavity also exhibits intermediate detection values. A postmortem fracture line is observed at the fissure line and radiates toward the inferior aspect of the tooth.

The two-dimensional map for concentration values of copper (Cu^{63}) exhibits low concentration values in the dentin region. Intermediate concentration values are observed in the enamel border. No inclusions of copper are present in this sample.

Strontium (Sr^{88})

The two-dimensional map for detection values of strontium (Sr^{88}) exhibits intermediate detection values in the enamel and dentin region with low detection values observed at the DEJ. Intermediate to high detection values are apparent near the pulp cavity within the inferior aspect of the dentin and continues into the root tips. A postmortem fracture line is observed in the fissure line between the cusps and extends toward the inferior aspect of the dentin region terminating at the pulp cavity.

The two-dimensional map for concentration values of strontium (Sr^{88}) exhibits low concentration values in the inferior aspect of the dentin region. No inclusions of strontium are present.

Antimony (Sb^{121})

The two-dimensional map for detection values of antimony (Sb^{121}) exhibits low detection values observed in the lingual aspect of the enamel border. No inclusions of antimony were observed.

The two-dimensional map for concentration values of antimony (Sb^{121}) exhibits low detection values in the overall tooth. No inclusions of antimony were observed.

Lanthanum (La^{139})

The two-dimensional map for detection values of lanthanum (La^{139}) exhibits low detection values observed around the border encompassing the tooth. An inclusion of high detection values is present in the inferior aspect of the dentin near the pulp. A second inclusion

of high detection is present on the inferior buccal aspect of the dentin border. A postmortem fracture line with low element detection is observed projecting from the fissure line towards the inferior aspect of the dentin region.

Lead (Pb^{208})

The two-dimensional map for detection values of lead (Pb^{208}) exhibits low detection values in the dentin region. Intermediate detection values are present in the enamel border and DEJ exhibit an intermediate level of detection. Several inclusions are observed. The first is observed with high detection values in the inferior aspect of the dentin region near the pulp cavity. The second inclusion presents intermediate detection values in the buccal root tip. Striations of a low level of detection are observed throughout the tooth.

The two-dimensional map for concentration values of lead (Pb^{208}) exhibits low concentration values in the dentin and enamel regions. Intermediate concentration values are observed along the border of the tooth. A postmortem fracture line of low concentration value is observed at the fissure line and radiates toward the inferior aspect of the dentin terminating at the pulp cavity.

Uranium (U^{238})

The two-dimensional map for detection values of uranium (U^{238}) exhibits low detection values in the dentin region tooth. An inclusion of high detection value is observed in the inferior aspect of the dentin bordering the pulp cavity, with detection values decreasing as distance from the pulp cavity increases. A postmortem fracture line of intermediate detection values is present

at the fissure line and projects toward the inferior aspect of the dentin terminating at the pulp cavity.

Individual IIT 217-01

First molar

Carbon (C^{13})

The two-dimensional map for detection values of carbon (C^{13}) exhibits low detection values in the dentin region. Inclusions of intermediate detection values are present in the superior buccal and lingual aspects of the dentin. Several postmortem fracture lines of intermediate detection values are observed within this sample. Two radiate from the fissure line between the cusps and extend toward the inferior aspect of the dentin. The intermediate detection observed in the fracture lines is comparable to the elemental reading within the resin base.

Magnesium (Mg^{24})

The two-dimensional map for detection values of magnesium (Mg^{24}) exhibits low detection values in the dentin and enamel regions. Intermediate detection values are present near the pulp cavity. Inclusions of intermediate detection values are present in the superior buccal and lingual aspects of the dentin. Several postmortem fracture lines are observed within this sample. Two radiate from the fissure line between the cusps and extend toward the inferior aspect of the dentin. A third fracture line is observed to project from the buccal aspect of the DEJ toward the inferior aspect of the dentin. The fourth fracture line is observed at the lingual aspect of the dentin following the DEJ.

Phosphorus (P^{31})

The two-dimensional map for detection values of phosphorus (P^{31}) exhibits intermediate detection values in the superior aspect of the tooth with inconsistent high detection values present in the DEJ. The superior aspect of the tooth exhibits low detection values. Inclusions of high detection values are present in the inferior aspect of the dentin near the pulp cavity, and in the lingual aspect of the dentin near the peak of the DEJ. Several postmortem fracture lines are observed within this sample. Two fractures radiate from the fissure line between the cusps and extend toward the inferior aspect of the dentin. A third fracture line is observed at the lingual aspect of the dentin following the DEJ.

Sulfur (S^{32})

The two-dimensional map for detection values of sulfur (S^{32}) exhibits low detection values in the dentin region and the lingual aspect of the enamel border. Intermediate detection values are observed near the pulp cavity in the dentin. No inclusions of sulfur are present in this sample. Two postmortem fracture lines radiate from the fissure line between the cusps and extend toward the inferior aspect of the dentin. A third fracture line is observed at the lingual aspect of the dentin following the DEJ.

Calcium (Ca^{44})

The two-dimensional map for detection values of calcium (Ca^{44}) exhibits intermediate detection values in the enamel region and low detection within the dentin region. Intermediate detection values are present along the pulp cavity as well as in the superior lingual aspect of the dentin. roots of the sample. Two postmortem fracture lines radiate from the fissure line between

the cusps and extend toward the inferior aspect of the. A third fracture line is observed at the lingual aspect of the dentin following the DEJ.

Iron (Fe^{56})

The two-dimensional map for detection values of iron (Fe^{56}) exhibits low detection values in the border encompassing the tooth and around the pulp cavity. An inclusion of high detection value is present in the inferior aspect of the dentin region near the pulp cavity.

Copper (Cu^{63})

The two-dimensional map for detection values of copper (Cu^{63}) exhibits low detection values in the lingual aspect of the dentin. An inclusion of high detection is present in the lingual aspect of the dentin region with high values observed near the pulp cavity.

The two-dimensional map for concentration values of copper (Cu^{63}) exhibits low concentration values in the overall dentin and enamel regions. Intermediate detection values are observed in the lingual aspect of the dentin and along the lingual aspect of the DEJ. An inclusion of intermediate concentration is present in the inferior aspect of the dentin region. A postmortem fracture line with high concentration values is observed projecting from the fissure line toward the inferior aspect of the dentin. High concentration values are observed within this fracture line and are consistent with the resin base.

Zinc (Zn^{66})

The two-dimensional map for detection values of zinc (Zn^{66}) exhibits intermediate detection values in the enamel border and the inferior aspect of the dentin near the pulp cavity. Inclusions of intermediate detection values are present in the enamel border near the fissure line as well as at the enamel border in the lingual cusp. Two postmortem fracture lines project from the fissure line between the cusps and extend toward the inferior aspect of the dentin. A third fracture line is observed at the lingual aspect of the dentin following the DEJ.

The two-dimensional map for concentration values of zinc (Zn^{66}) exhibits low concentration values in the dentin. Intermediate and high concentration values are observed in the enamel border. No inclusions of copper are present in this sample. A postmortem fracture line with low concentration values is observed projecting from the fissure line and terminating at the DEJ.

Strontium (Sr^{88})

The two-dimensional map for detection values of strontium (Sr^{88}) exhibits low detection values observed at the DEJ. Intermediate to high detection values are present near the pulp cavity within the inferior aspect of the dentin as well as along the inferior aspect of the dentin region. Two postmortem fracture lines project from the fissure line between the cusps and extend toward the inferior aspect of the dentin. A third fracture line is observed at the lingual aspect of the dentin following the DEJ.

The two-dimensional map for concentration values of strontium (Sr^{88}) exhibits negative concentration values within this sample and will not be considered in further analysis.

Antimony (Sb^{121})

The two-dimensional map for detection values of antimony (Sb^{121}) exhibits low detection values in the overall tooth. No inclusions of antimony were observed.

The two-dimensional map for concentration values of antimony (Sb^{121}) exhibits low detection values. No inclusions of antimony were observed.

Lanthanum (La^{139})

The two-dimensional map for detection values of lanthanum (La^{139}) exhibits low detection values observed around the border encompassing the tooth. An inclusion of intermediate detection was observed in the inferior lingual aspect of the dentin near the pulp cavity.

Lead (Pb^{208})

The two-dimensional map for detection values of lead (Pb^{208}) exhibits low detection values in the DEJ and in the border encompassing the tooth. Several inclusions of high detection values are observed at the inferior aspect of the dentin region near the pulp cavity. Striations with low levels of detection are observed throughout the tooth. Two postmortem fracture lines radiate from the fissure line between the cusps and extend toward the inferior aspect of the dentin

The two-dimensional map for concentration values of lead (Pb^{208}) exhibits intermediate concentration values in the DEJ and border encompassing the tooth. Striations with a low level of detection are observed throughout the tooth. A postmortem fracture line of low elemental

detection is observed at the fissure line and projects toward the inferior aspect of the dentin terminating at the pulp cavity.

Uranium (U^{238})

The two-dimensional map for detection values of uranium (U^{238}) exhibits low detection values throughout the tooth. An inclusion of low detection values is observed in the inferior aspect of the dentin bordering the pulp cavity.

Individual IIT 220-01

First molar

Carbon (C^{13})

The two-dimensional map for detection values of carbon (C^{13}) exhibits low detection values in the dentin region. No inclusions of carbon are present. Several postmortem fracture lines of low detection values are observed within this sample. The first projects from the lingual aspect of the DEJ toward the inferior aspect of the dentin border, while the second fracture line radiates from the fissure line toward the inferior buccal aspect of the dentin. The low intensity observed in the fracture lines is comparable to the elemental reading within the resin base.

Magnesium (Mg^{24})

The two-dimensional map for detection values of magnesium (Mg^{24}) exhibits low detection values in the dentin. Inclusions of intermediate detection values are present in the inferior aspect of the dentin within the root tip as well as in the superior aspect of the dentin.

Several postmortem fracture lines are observed within this sample. The first radiates from the lingual aspect of the DEJ toward the inferior aspect of the dentin border, while the second fracture line radiates from the fissure line toward the inferior buccal aspect of the dentin.

Phosphorus (P^{31})

The two-dimensional map for detection values of phosphorus (P^{31}) exhibits intermediate detection values in the superior aspect of the dentin. High detection values are present in the buccal aspect of the root dentin. Low detection values are present in the enamel region. No inclusions are present within this sample. Two postmortem fracture lines are present in the superior aspect of the tooth. The first fracture line projects from the lingual aspect of the DEJ toward the inferior aspect of the dentin border, while the second fracture line radiates from the fissure line toward the inferior buccal aspect of the dentin.

Sulfur (S^{32})

The two-dimensional map for detection values of sulfur (S^{32}) exhibits high detection values in the buccal aspect of the dentin in the root. Intermediate detection values are observed in the superior aspect of the dentin and in the enamel border. No inclusions of sulfur are present in this sample. Several postmortem fracture lines are present in the superior aspect of the tooth and exhibit. The first fracture line projects from the lingual aspect of the DEJ toward the inferior aspect of the dentin border, while the second fracture line radiates from the fissure line toward the inferior buccal aspect of the dentin.

Calcium (Ca^{44})

The two-dimensional map for detection values of calcium (Ca^{44}) exhibits intermediate detection values throughout the dentin region. High detection is observed in the lingual aspect of the inferior aspect of the dentin. Low detection values are observed in the enamel region. No inclusions of calcium are observed in this sample. Several postmortem fracture lines are present in the superior aspect of the tooth. The first fracture line projects from the lingual aspect of the DEJ toward the inferior aspect of the dentin border, while the second fracture line radiates from the fissure line toward the inferior buccal aspect of the dentin.

Iron (Fe^{56})

The two-dimensional map for detection values of iron (Fe^{56}) exhibits low detection values in the border encompassing the tooth. Several inclusions are observed within the sample. An inclusion of intermediate detection is present in the buccal aspect of the dentin border. A second inclusion of high detection is present in the superior aspect of the enamel border with high detection values observed. Several postmortem fracture lines with low detection values are present in the superior aspect of the tooth. The first fracture line projects from the lingual aspect of the DEJ toward the inferior aspect of the dentin border, while the second fracture line radiates from the fissure line toward the inferior buccal aspect of the dentin.

Copper (Cu^{63})

The two-dimensional map for detection values of copper (Cu^{63}) exhibits inconsistent low detection values in the border encompassing the tooth and in the superior aspect of the dentin region. No inclusions of copper are present in this sample.

The two-dimensional map for concentration values of copper (Cu^{63}) exhibits low concentration values in the dentin. Intermediate concentration values are observed in the lingual aspect of the enamel and along the lingual aspect of the DEJ. A postmortem fracture line with low concentration value is observed projecting from the fissure line toward the inferior lingual aspect of the dentin border.

Zinc (Zn^{66})

The two-dimensional map for detection values of zinc (Zn^{66}) exhibits intermediate detection values in the buccal and lingual enamel border as well as at the fissure line. Low detection values are observed in the dentin. Inclusions of zinc are present in the root tip of the dentin as well as in the center of the inferior aspect of the dentin and present with high detection values that dissipate as distance from inclusion center increases. Several postmortem fracture lines are present in the superior aspect of the tooth. The first fracture line projects from the lingual aspect of the DEJ toward the inferior aspect of the dentin border, while the second fracture line radiates from the fissure line toward the inferior buccal aspect of the dentin.

The two-dimensional map for concentration values of zinc (Zn^{66}) exhibits low concentration values in the dentin and enamel. Inclusions of intermediate concentration values are present in the root tip as well as the inferior aspect of the dentin. Several postmortem

fracture lines of low concentration values are present in the superior aspect of the. The first fracture line projects from the lingual aspect of the DEJ toward the inferior aspect of the dentin border, while the second fracture line radiates from the fissure line toward the inferior buccal aspect of the dentin.

Strontium (Sr^{88})

The two-dimensional map for detection values of strontium (Sr^{88}) exhibits intermediate detection values in the dentin region. High detection values are observed in the inferior aspect of the tooth, along the buccal aspect of the root and the superior aspect of the dentin between fracture lines along the DEJ. Several postmortem fracture lines are present in the superior aspect of the tooth. The first fracture line projects from the lingual aspect of the DEJ toward the inferior aspect of the dentin border, while the second fracture line radiates from the fissure line toward the inferior buccal aspect of the dentin.

The two-dimensional map for concentration values of strontium (Sr^{88}) exhibits low concentration values within the dentin. Inclusions of high concentration values are present in the superior aspect of the enamel border.

Antimony (Sb^{121})

The two-dimensional map for detection values of antimony (Sb^{121}) exhibits inconsistency of elemental detection in the overall tooth and is attributed to debris within the LA-ICP-MS during ablation. No inclusions of antimony were observed.

The two-dimensional map for concentration values of antimony (Sb^{121}) exhibits an absence of detection values in the overall tooth. No inclusions of antimony were observed. Further, no fracture lines were observed.

Lanthanum (La^{139})

The two-dimensional map for detection values of lanthanum (La^{139}) exhibits low detection values observed around the border encompassing the tooth. Inclusions of high detection values are present in the superior aspect of the enamel border, and the superior lingual aspect of the dentin border. A postmortem fracture line of low elemental detection is observed in the lingual aspect of the enamel, radiating from the enamel border to the lingual dentin border.

Lead (Pb^{208})

The two-dimensional map for detection values of lead (Pb^{208}) exhibits low detection values in the border encompassing the tooth and intermediate values along the DEJ. An inclusion of high detection is observed in the lingual aspect of the DEJ. Striations with a low level of detection are observed in the superior aspect of the dentin.

The two-dimensional map for concentration values of lead (Pb^{208}) exhibits low values in the border encompassing the tooth and intermediate values along the DEJ. An inclusion of high concentration values is observed in the lingual aspect of the DEJ. A second inclusion of intermediate concentration is observed in the inferior aspect of the tooth. Striations with a low level of detection are observed in the superior aspect of the dentin.

Uranium (U^{238})

The two-dimensional map for detection values of uranium (U^{238}) exhibits low detection values throughout the tooth. An inclusion of high detection value is observed in the superior aspect of the enamel border. A postmortem fracture line of intermediate concentration is observed in the lingual cusp, projecting from the enamel border and terminating at the superior aspect of the dentin border. Intermediate values are observed in the superior aspect of the fracture line with low concentration in the inferior aspect.

Second molar

Carbon (C^{13})

The two-dimensional map for detection values of carbon (C^{13}) exhibits low detection values in the dentin region. Intermediate detection values of carbon are present in the dentin pulp cavity and along the lingual aspect of the DEJ. A postmortem fracture line is observed radiating from the fissure line in the enamel toward the inferior aspect of the tooth. The intermediate intensity observed in the fracture line is comparable to the elemental reading within the resin base.

Magnesium (Mg^{24})

The two-dimensional map for detection values of magnesium (Mg^{24}) exhibits low detection values in the dentin. No inclusions of magnesium are in this sample. Several postmortem fracture lines are observed within this sample. The first fracture line radiates from

the buccal aspect of the DEJ toward the pulp cavity, while the second fracture line radiates from the fissure line toward the pulp cavity.

Phosphorus (P^{31})

The two-dimensional map for detection values of phosphorus (P^{31}) exhibits intermediate detection values within the dentin. High detection values are present at the superior aspect of the pulp cavity as well as in the lingual aspect of the root. Low detection values are observed in the enamel region. A postmortem fracture line is present at the fissure line terminating at the pulp cavity.

Sulfur (S^{32})

The two-dimensional map for detection values of sulfur (S^{32}) exhibits high detection values in the lingual aspect of the dentin. Intermediate values are observed in the lingual aspect of the enamel and buccal aspect of the dentin. Low detection values are present in the buccal aspect of the enamel. No inclusions of sulfur are present in this sample. A postmortem fracture line with intermediate detection values is present in the buccal aspect of the DEJ and at the fissure area of the DEJ, both of which terminate at the pulp cavity.

Calcium (Ca^{44})

The two-dimensional map for detection values of calcium (Ca^{44}) exhibits high detection values observed in the lingual aspect of the inferior aspect of the dentin. Intermediate detection values are observed around the pulp cavity exhibits. Low detection values are observed in the

enamel region. A postmortem fracture line is present in the fissure line projecting toward pulp cavity.

Iron (Fe^{56})

The two-dimensional map for detection values of iron (Fe^{56}) exhibits intermediate detection values in the border encompassing the tooth. An inclusion of high detection values is present in the superior lingual aspect of the dentin border. Striations of low detection are observed in the lingual aspect of the tooth projecting from the pulp cavity and are also observed in the root. A postmortem fracture line of intermediate detection is apparent starting at the fissure line and projecting toward the pulp cavity.

Copper (Cu^{63})

The two-dimensional map for detection values of copper (Cu^{63}) exhibits low detection values in the dentin and tooth border. High detection values are observed in the lingual aspect of the dentin bordering the pulp cavity. An inclusion of intermediate detection value is present in the lingual root of the inferior dentin region. A postmortem fracture line of intermediate detection is observed radiating from the fissure line toward the pulp cavity.

The two-dimensional map for concentration values of copper (Cu^{63}) exhibits low concentration values in the dentin. Intermediate detection values are observed in the enamel region. Intermediate concentrations are present along the lingual aspect of the DEJ and in the roots. Inclusions of intermediate concentrations are present in both roots. A postmortem

fracture line of high concentration value is observed radiating from the fissure line toward the pulp cavity.

Zinc (Zn^{66})

The two-dimensional map for detection values of zinc (Zn^{66}) exhibits intermediate detection values in the dentin region surrounding the pulp cavity with intensity decreasing as distance from the pulp cavity increases. The enamel border exhibits high detection in the lingual aspect and intermediate values in the buccal aspect. An inclusion of intermediate detection values is present at the superior aspect of the roots. Striations of low detection are observed in the roots. A postmortem fracture line is present at the fissure line as well as the buccal aspect of the DEJ and projects toward the pulp cavity.

The two-dimensional map for concentration values of zinc (Zn^{66}) exhibits low concentration values in the dentin and enamel. An inclusion of intermediate concentration values is present in the buccal root tip.

Strontium (Sr^{88})

The two-dimensional map for detection values of strontium (Sr^{88}) exhibits intermediate detection values in the dentin region with low values observed within the enamel. High detection values are present in the inferior lingual aspect of the tooth and in the lingual aspect along the DEJ. The superior aspect of the pulp cavity exhibits high detection values in the dentin region with values decreasing as distance from the pulp cavity increases. Inclusions of high detection are present in the superior buccal root and in the root tip of the buccal root. Two

postmortem fracture lines are present within the dentin of the tooth projecting from the DEJ toward the pulp cavity.

The two-dimensional map for concentration values of strontium (Sr^{88}) exhibits low concentration values within the dentin region. Inclusions of high concentration are present in the superior aspect of the enamel border and along the superior aspect of the pulp cavity. A third inclusion is observed in the buccal aspect of the superior dentin border and is observed to have intermediate values.

Antimony (Sb^{121})

The two-dimensional map for detection values of antimony (Sb^{121}) exhibits inconsistent low elemental detection in the overall tooth and is attributed to debris within the LA-ICP-MS during ablation. An inclusion of antimony is observed within the lingual root border.

The two-dimensional map for concentration values of antimony (Sb^{121}) exhibits low concentrations. No inclusions of antimony were observed.

Lanthanum (La^{139})

The two-dimensional map for detection values of lanthanum (La^{139}) exhibits high detection values observed around the border encompassing the tooth and border the pulp cavity. No inclusions of lanthanum were observed. A postmortem fracture line with inconsistent high elemental detection is observed projecting from the fissure line and radiating toward the pulp cavity.

Lead (Pb^{208})

The two-dimensional map for detection values of lead (Pb^{208}) exhibits inconsistent intermediate detection values observed in the border encompassing the tooth and surrounds the pulp cavity. Inclusions of intermediate detection values are observed in the dentin of the roots. Striations with a low level of detection are present within the dentin and enamel regions. A postmortem fracture line with intermediate detection values is observed at the fissure line in the enamel and radiates toward the inferior aspect.

The two-dimensional map for concentration values of lead (Pb^{208}) exhibits low values in the dentin and intermediate values observed in the enamel. Inclusions of intermediate concentrations are observed in the inferior aspect of both roots as well as along the inferior aspect of the pulp cavity within the dentin region. Striations with intermediate levels of detection are observed throughout the tooth. A postmortem fracture line of intermediate concentration values is present at the fissure line in the enamel and projects toward the pulp cavity.

Uranium (U^{238})

The two-dimensional map for detection values of uranium (U^{238}) exhibits low detection values in the enamel and dentin regions. An inclusion of intermediate detection values is observed in the superior aspect of the lingual dentin border. A second inclusion of high detection is observed at the fissure line of the enamel border.

Third molar

Carbon (C^{13})

The two-dimensional map for detection values of carbon (C^{13}) exhibits intermediate detection values in the dentin region near the pulp cavity and along the lingual aspect of the DEJ. A postmortem fracture line is observed radiating from the buccal cusp in the enamel toward the pulp cavity. A second fracture line is observed to radiate from the mid-section of the DEJ and radiate toward the lingual aspect of the dentin. The intermediate intensity observed in the fracture lines is comparable to the elemental reading within the resin base.

Magnesium (Mg^{24})

The two-dimensional map for detection values of magnesium (Mg^{24}) exhibits low detection values in the dentin. An inclusion with intermediate detection values is present at the superior aspect of the pulp cavity that decreases in detection as distance from the pulp cavity increases. Several postmortem fracture lines are observed within this sample. The first fracture line is observed radiating from the buccal cusp in the enamel toward the pulp cavity. A second fracture line is observed to radiate from the mid-section of the DEJ and radiate toward the lingual aspect of the dentin.

Phosphorus (P^{31})

The two-dimensional map for detection values of phosphorus (P^{31}) exhibits low detection values within the dentin and enamel regions. High detection values are present in the superior lingual aspect of the pulp cavity and dentin border, and in the buccal aspect of the roots. A

postmortem fracture line is present radiating from the buccal aspect of the dentin and radiating toward the pulp cavity.

Sulfur (S^{32})

The two-dimensional map for detection values of sulfur (S^{32}) exhibits intermediate detection values in the lingual aspect of the dentin, and low values observed in the buccal aspect of the dentin. No inclusions of sulfur are present in this sample. A postmortem fracture line is present in the at the buccal aspect of the DEJ in the dentin radiating toward the pulp cavity.

Calcium (Ca^{44})

The two-dimensional map for detection values of calcium (Ca^{44}) exhibits low detection values in the superior aspect of the dentin. Intermediate detection values are present in the inferior aspect of the dentin region and in the superior dentin region surrounding the pulp cavity. Low detection values are present in the enamel region. A postmortem fracture line is present in the buccal aspect of the DEJ and radiates toward the pulp cavity.

Iron (Fe^{56})

The two-dimensional map for detection values of iron (Fe^{56}) exhibits intermediate detection values in the border encompassing the tooth. No inclusions of iron are present within this sample. A postmortem fracture line with intermediate detection values is observed to radiate toward the superior aspect of the root tip.

Copper (Cu^{63})

The two-dimensional map for detection values of copper (Cu^{63}) exhibits low detection values in the lingual aspect of the tooth and in the border encompassing the tooth. Intermediate detection values are observed in the lingual aspect of the enamel. An inclusion of intermediate detection is present in the lingual cusp of the enamel.

The two-dimensional map for concentration values of copper (Cu^{63}) exhibits low concentration values. Intermediate concentration values observed in the border encompassing the tooth and along the superior border of the pulp cavity within the dentin. An inclusion of intermediate concentration is present in the lingual cusp within the enamel region.

Zinc (Zn^{66})

The two-dimensional map for detection values of zinc (Zn^{66}) exhibits low detection values in the dentin region. Intermediate detection values are present in the surrounding pulp cavity with detection values decreasing as distance from the pulp cavity increases. The enamel border also exhibits intermediate detection values. A postmortem fracture line is present at the buccal aspect of the DEJ and radiates toward the pulp cavity. A second fracture line is observed near the superior lingual aspect of the pulp cavity within the dentin region.

The two-dimensional map for concentration values of zinc (Zn^{66}) exhibits low concentration values in the dentin and enamel regions. High concentrations are observed in the enamel border. Striations of low concentration are present and project from the dentin pulp cavity, decreasing in concentration as distance from the pulp cavity increases.

Strontium (Sr^{88})

The two-dimensional map for detection values of strontium (Sr^{88}) exhibits intermediate detection values in the dentin region and low values observed within the enamel region. The inferior buccal aspect of the tooth exhibits high detection values along the dentin border. The superior aspect of the pulp cavity exhibits intermediate detection values in the dentin region with values decreasing as distance from the pulp cavity increases. Inclusions of high detection are observed in the inferior lingual root tip. A postmortem fracture line is present at the buccal aspect of the DEJ in the dentin radiating toward the pulp cavity.

The two-dimensional map for concentration values of strontium (Sr^{88}) exhibits overall low concentration values within the dentin and enamel border. No inclusions of strontium are present within this sample.

Antimony (Sb^{121})

The two-dimensional map for detection values of antimony (Sb^{121}) exhibits inconsistent low elemental detection in the overall tooth and is attributed to debris within the LA-ICP-MS during ablation. No inclusions of antimony are observed within this sample.

The two-dimensional map for concentration values of antimony (Sb^{121}) exhibits overall low concentration values in the tooth. No inclusions of antimony were observed.

Lanthanum (La^{139})

The two-dimensional map for detection values of lanthanum (La^{139}) high detection values observed around the enamel border. Intermediate detection values are present along the dentin

border and superior pulp cavity. A postmortem fracture line with low element detection is observed to radiate from the root tip toward the pulp cavity.

Lead (Pb^{208})

The two-dimensional map for detection values of lead (Pb^{208}) exhibits intermediate detection values in the border and in the region surrounding the pulp cavity. Striations with a low level of detection are observed in the inferior aspect of the tooth within the dentin. A postmortem fracture line is observed to radiate from the buccal superior aspect of the pulp cavity.

The two-dimensional map for concentration values of lead (Pb^{208}) exhibits low values in the dentin. High concentration values are observed in the enamel border and the superior aspect of the pulp cavity. Intermediate concentration values are observed in the dentin border and the inferior aspect of the pulp cavity. Striations with low concentration values are observed within the dentin.

Uranium (U^{238})

The two-dimensional map for detection values of uranium (U^{238}) low detection values throughout the tooth with inconsistent intermediate to high detection values observed in the border encompassing the tooth. No inclusions of uranium are observed within this sample.

Individual IIT 236-01

First molar

Carbon (C^{13})

The two-dimensional map for detection values of carbon (C^{13}) exhibits low detection values in the dentin region. An inclusion of intermediate detection values is present in the buccal root tip. Several postmortem fracture lines are observed within this sample. The first projects from the lingual aspect of the enamel border and radiates toward the inferior aspect of the dentin. The second is observed to radiate from the fissure line toward the inferior buccal aspect of the dentin border. Multiple perpendicular lines are observed in the dentin region of the tooth. All fracture lines are consistent with intermediate detection values observed that indicate elemental reading of the resin base.

Magnesium (Mg^{24})

The two-dimensional map for detection values of magnesium (Mg^{24}) exhibits low detection values in the dentin. Inclusions of intermediate detection values are present in the inferior aspect of the dentin within the lingual root tip, and in the superior buccal aspect of the dentin. Several postmortem fracture lines are observed within this sample. The first projects from the lingual aspect of the enamel border and radiates toward the inferior aspect of the dentin. The second is observed to radiate from the fissure line toward the inferior buccal aspect of the dentin border. Multiple perpendicular lines are observed in the dentin region of the tooth.

Phosphorus (P^{31})

The two-dimensional map for detection values of phosphorus (P^{31}) exhibits intermediate detection values in the superior aspect of the dentin. High detection values are present in the mesial aspect of the root dentin. Low detection values are present in the enamel and intermediate detection values are observed along the DEJ. Two postmortem fracture lines are present and radiate from the lingual aspect of the enamel border and radiates toward the inferior aspect of the dentin. The second is observed to radiate from the fissure line toward the inferior buccal aspect of the dentin border. Multiple perpendicular fracture lines are observed in the superior aspect of the dentin region and exhibit intermediate detection values.

Sulfur (S^{32})

The two-dimensional map for detection values of sulfur (S^{32}) exhibits low detection values in the dentin region and in the mesial aspect of the enamel region. Intermediate values are observed in the buccal root and the buccal aspect of the lingual root. A postmortem fracture line is present in the superior lingual aspect of the dentin radiating toward the inferior aspect of the tooth.

Calcium (Ca^{44})

The two-dimensional map for detection values of calcium (Ca^{44}) exhibits low detection values in the dentin. Intermediate detection values are observed in the DEJ, as well as the buccal root and the buccal aspect of the lingual root. Low detection values are observed in the enamel region. A postmortem fracture line is present in the superior lingual aspect of the dentin radiating toward the inferior aspect of the tooth.

Iron (Fe^{56})

The two-dimensional map for detection values of iron (Fe^{56}) exhibits low detection values in the border encompassing the tooth. An inclusion of intermediate detection is present in the lingual cusp within the enamel. A postmortem fracture line with intermediate detection values is observed at the fissure line and radiates toward the inferior aspect of the buccal dentin border

Copper (Cu^{63})

The two-dimensional map for detection values of copper (Cu^{63}) low detection values. No inclusions of copper are present in this sample.

The two-dimensional map for concentration values of copper (Cu^{63}) exhibits low concentration values in the dentin and enamel regions. Inconsistent intermediate inclusions of copper are present in the buccal aspect of the tooth. A postmortem fracture line with intermediate concentration values is observed projecting from the fissure line toward the inferior aspect of the tooth.

Zinc (Zn^{66})

The two-dimensional map for detection values of zinc (Zn^{66}) exhibits low detection values in the dentin region. The buccal and lingual aspects of the enamel border are observed to have intermediate detection values as well as the inner root border. An inclusion of high detection is present in the enamel border at the fissure line. A postmortem fracture line is

observed in the lingual aspect of the dentin and radiates from the DEJ toward the inferior aspect of the tooth.

The two-dimensional map for concentration values of zinc (Zn^{66}) exhibits low concentration values in the dentin region. Inclusions of intermediate concentration are present in the lingual and buccal aspect of the enamel border and in the fissure line. Striations o flow concentration values are observed within the dentin.

Strontium (Sr^{88})

The two-dimensional map for detection values of strontium (Sr^{88}) exhibits intermediate detection values in the dentin region with low detection within the enamel. The inferior aspect of the tooth exhibits high detection values in the buccal aspect of the root and along the border of the lingual root. Inclusions of intermediate detection are present in enamel region near the fissure line and on the buccal dentin border. Several postmortem fracture lines are present in the superior aspect of the tooth. The first fracture line projects from the lingual aspect of the DEJ toward the inferior aspect of the dentin, while the second fracture line radiates from the fissure line toward the inferior buccal aspect of the dentin.

The two-dimensional map for concentration values of strontium (Sr^{88}) exhibits low concentration values within the dentin region. Inclusions of high concentration values are present in the superior buccal and lingual aspects of the enamel border. Striations of low concentration values are present in the dentin region as well. A postmortem fracture line of intermediate concentrations is apparent at the fissure line and radiates toward the inferior aspect of the dentin.

Antimony (Sb^{121})

The two-dimensional map for detection values of antimony (Sb^{121}) exhibits inconsistency of elemental detection in the overall tooth and is attributed to debris within the LA-ICP-MS during ablation. No inclusions of antimony were observed.

The two-dimensional map for concentration values of antimony (Sb^{121}) exhibits low detection values. No inclusions of antimony were observed.

Lanthanum (La^{139})

The two-dimensional map for detection values of lanthanum (La^{139}) exhibits low detection values around the border encompassing the tooth. Inclusions of high detection values lanthanum were observed in the superior buccal and lingual aspects of the dentin border. A postmortem fracture line is observed radiating from the fissure line toward the inferior aspect of the tooth. The superior aspect of the fracture line exhibits high concentration values, while the inferior aspect is observed to have low concentration values.

Lead (Pb^{208})

The two-dimensional map for detection values of lead (Pb^{208}) exhibits low detection values in the dentin and enamel regions. Intermediate detection values are present in the border encompassing the tooth and along the DEJ. An inclusion of high detection is observed in the buccal aspect of the DEJ. A second inclusion of intermediate detection is observed at the fissure line within the enamel. Striations with a low level of detection are observed in the superior aspect of the dentin.

The two-dimensional map for concentration values of lead (Pb^{208}) exhibits low values in the dentin and enamel regions and intermediate values along the DEJ. An inclusion of high concentration is observed in the lingual aspect of the DEJ. A second inclusion of high concentration is observed in the fissure line of the tooth. Striations with low concentration values are observed in the superior aspect of the dentin.

Uranium (U^{238})

The two-dimensional map for detection values of uranium (U^{238}) exhibits low detection values throughout the tooth. An inclusion of intermediate detection values is observed in the superior buccal and lingual aspects of the dentin border. A postmortem fracture line exhibiting intermediate detection is observed at the fissure line of the cusps and radiates toward the inferior aspect of the dentin.

Individual IIT 263-01

First molar

Carbon (C^{13})

The two-dimensional map for detection values of carbon (C^{13}) exhibits low detection values in the dentin region. An inclusion of intermediate detection is present within the dentin region along the lingual aspect of the DEJ. Several postmortem fracture lines are observed within this sample. The first projects from the buccal aspect of the enamel border and radiates toward the inferior aspect of the dentin. The second is observed to radiate from the fissure line toward the inferior lingual aspect of the dentin border. Multiple fracture lines are observed in the

dentin region of the tooth, including two that radiate from the lingual aspect of the DEJ. The first radiates towards the dentin pulp cavity, while the second radiates toward the dentin border. Several fracture lines are observed in the lingual root and run perpendicular to the root. All fracture lines are consistent with intermediate detection values observed that indicate elemental reading of the resin base.

Magnesium (Mg^{24})

The two-dimensional map for detection values of magnesium (Mg^{24}) exhibits low detection values in the dentin and enamel region. Intermediate detection values are observed along the DEJ and in the dentin region superior to the pulp cavity. An inclusion of intermediate detection is present in the buccal aspect of the DEJ. Several postmortem fracture lines are observed within this sample. The first projects from the buccal aspect of the DEJ and radiates toward the inferior aspect of the dentin. The second is observed to radiate from the mesial aspect of the DEJ toward the pulp cavity. Perpendicular fracture lines are observed in the dentin region of the lingual root.

Phosphorus (P^{31})

The two-dimensional map for detection values of phosphorus (P^{31}) exhibits intermediate and high detection values along the superior aspect of the dentin pulp cavity in the dentin region. No inclusions are present within this sample. Several postmortem fracture lines are observed within this sample. The first projects from the buccal aspect of the DEJ and radiates toward the inferior aspect of the dentin. The second is observed to radiate from the mesial aspect of the DEJ

toward the pulp cavity. Perpendicular fracture lines are observed in the dentin region of the lingual root.

Sulfur (S^{32})

The two-dimensional map for detection values of sulfur (S^{32}) exhibits low detection values in the dentin region. Intermediate values are observed in the inferior aspect of the roots and along the border of the pulp cavity. A postmortem fracture line is present at the buccal aspect of the DEJ and radiates toward the pulp cavity. A second fracture line is observed to radiate from the lingual aspect of the pulp cavity toward the superior aspect of the dentin region. A third fracture line is observed to be perpendicular to the root.

Calcium (Ca^{44})

The two-dimensional map for detection values of calcium (Ca^{44}) exhibits intermediate and high detection values along the superior aspect of the dentin pulp cavity in the dentin region. No inclusions are present within this sample. Several postmortem fracture lines are observed within this sample. The first projects from the buccal aspect of the DEJ and radiates toward the inferior aspect of the dentin. The second is observed to radiate from the mesial aspect of the DEJ toward the pulp cavity. Perpendicular fracture lines are observed in the dentin region of the lingual root.

Iron (Fe^{56})

The two-dimensional map for detection values of iron (Fe^{56}) exhibits low detection values in the superior aspect of the border encompassing the tooth. High detection values are

observed in the inferior aspect of the tooth along the root borders of the dentin. An inclusion of high detection is present in the superior aspect of the lingual cusp within the enamel border. Several postmortem fracture lines with low detection values are present. The first fracture line is present at the buccal cusp and radiates toward the pulp cavity. A second fracture line is observed to radiate from the lingual aspect of the pulp cavity toward the superior aspect of the dentin region. A third fracture line is observed to be perpendicular to the root.

Copper (Cu^{63})

The two-dimensional map for detection values of copper (Cu^{63}) exhibits low elemental detection. No inclusions of copper are present in this sample.

The two-dimensional map for concentration values of copper (Cu^{63}) exhibits low concentration values in the dentin and enamel regions. Inconsistent intermediate inclusions of copper are present in the lingual aspect of the tooth. Several postmortem fracture lines of high element detection are present. The first is present at the buccal cusp and radiates toward the pulp cavity. A second fracture line is observed to radiate from the lingual aspect of the pulp cavity toward the superior aspect of the dentin region. A third fracture line is observed to be perpendicular to the root. All fracture lines high elemental detection values indicate elemental reading of the resin base.

Zinc (Zn^{66})

The two-dimensional map for detection values of zinc (Zn^{66}) exhibits low detection values in the dentin region and superior aspect of the pulp cavity. Intermediate detection values

are observed in the enamel border. Several postmortem fracture lines of high element detection are present. A fracture line is present at the buccal cusp and radiates toward the pulp cavity. A second fracture line is observed to radiate from the lingual aspect of the pulp cavity toward the superior aspect of the dentin region. A third fracture line is observed to be perpendicular to the root. The high elemental detection values of the fracture lines indicate element reading of the resin base.

The two-dimensional map for concentration values of zinc (Zn^{66}) exhibits low concentration values in the dentin region. High concentration values are observed in the enamel border. No inclusions of copper are present within this sample. Several postmortem fracture lines are present. The first is observed at the buccal cusp and radiates toward the pulp cavity. The second fracture line is observed to radiate from the lingual aspect of the pulp cavity toward the superior aspect of the dentin region.

Strontium (Sr^{88})

The two-dimensional map for detection values of strontium (Sr^{88}) exhibits low detection values in the enamel region. Intermediate detection values are present in the inferior aspect of the dentin, along the dentin pulp cavity and in the inferior aspect of the lingual root tip. Several postmortem fracture lines are present. The first is observed at the buccal cusp and radiates toward the pulp cavity. The second fracture line is observed to radiate from the lingual aspect of the pulp cavity toward the superior aspect of the dentin region.

The two-dimensional map for concentration values of strontium (Sr^{88}) exhibits low concentration values within the enamel. Intermediate to high concentration values are present

within the dentin region. No inclusions of strontium are present within this sample. Several postmortem fracture lines of intermediate concentration are present. The first is observed at the buccal cusp at the DEJ and radiates toward the pulp cavity. The second fracture line is observed to radiate from the lingual aspect of the pulp cavity toward the superior aspect of the dentin region.

Antimony (Sb^{121})

The two-dimensional map for detection values of antimony (Sb^{121}) exhibits inconsistency of elemental detection in the overall tooth and is attributed to debris within the LA-ICP-MS during ablation. No inclusions of antimony were observed.

The two-dimensional map for concentration values of antimony (Sb^{121}) exhibits low detection values in the overall tooth. No inclusions of antimony were observed.

Lanthanum (La^{139})

The two-dimensional map for detection values of lanthanum (La^{139}) exhibits low to high detection values around the border encompassing the tooth. No inclusions of lanthanum were observed within this sample.

Lead (Pb^{208})

The two-dimensional map for detection values of lead (Pb^{208}) exhibits low detection values in the dentin and enamel regions. Intermediate detection values are present at the border encompassing the tooth and along the DEJ. An inclusion of high detection is observed in the

buccal and lingual aspect of the DEJ. Striations with a low level of detection are observed in the superior aspect of the dentin. A postmortem fracture line is present in the buccal cusp at the DEJ and radiates toward the pulp cavity. A second postmortem fracture line is observed to radiate from the lingual aspect of the pulp cavity toward the superior aspect of the dentin region.

The two-dimensional map for concentration values of lead (Pb^{208}) exhibits low values in the dentin and enamel regions and intermediate values along the DEJ. An inclusion of high concentration is observed in the buccal aspect of the DEJ. Several postmortem fracture lines of intermediate concentration values were present. The first is observed at the buccal cusp at the DEJ and radiates toward the pulp cavity. The second fracture line is observed to radiate from the lingual aspect of the pulp cavity toward the superior aspect of the dentin region.

Uranium (U^{238})

The two-dimensional map for detection values of uranium (U^{238}) exhibits low detection values in the superior aspect of the enamel border and the inferior aspect of the encompassing border. The buccal and lingual aspect of the roots borders exhibit high detection values. No inclusions of uranium are observed within this sample.

Individual IIT 312-01

First molar

Carbon (C^{13})

The two-dimensional map for detection values of carbon (C^{13}) exhibits low detection values in the superior aspect of the dentin region. An inclusion of intermediate detection values

is present within the lingual aspect of the dentin region. Several postmortem fracture lines with intermediate detection are observed within this sample. The first projects from the buccal aspect of the dentin and radiates toward the lingual dentin border. The second and third fracture lines are observed in the superior aspect of the lingual and buccal roots. The intermediate detection values observed in these postmortem fractures indicate elemental reading of the resin base.

Magnesium (Mg^{24})

The two-dimensional map for detection values of magnesium (Mg^{24}) exhibits low detection values in the dentin region. Intermediate detection values are observed in the superior aspect of the tooth. Inclusions of intermediate detection are present in the lingual aspect of the dentin, and the buccal and lingual dentin borders.

Phosphorus (P^{31})

The two-dimensional map for detection values of phosphorus (P^{31}) exhibits intermediate detection values in the superior aspect of the dentin region and along the root borders. Low detection values are observed along the inferior aspect of the tooth and in the enamel region. Inclusions are present within the buccal aspect of the dentin border and exhibit high detection values, as well as in the lingual dentin with intermediate detection values. Postmortem fracture lines are observed within the superior aspect of the roots.

Sulfur (S^{32})

The two-dimensional map for detection values of sulfur (S^{32}) exhibits low detection values in the dentin region. An inclusion of high detection values is present in the buccal aspect of the dentin border. Inclusions of intermediate detection are observed in the lingual aspect of the dentin border and in the inferior lingual aspect of the dentin region. A postmortem fracture line is present in the inferior aspect of the buccal root.

Calcium (Ca^{44})

The two-dimensional map for detection values of calcium (Ca^{44}) exhibits intermediate detection values in the superior aspect of the dentin region pulp cavity and in the lingual root tip. An inclusion of high detection values is observed in the buccal dentin border. Inclusions of intermediate detection values are observed in the lingual dentin border and the inferior aspect of the lingual dentin region. Several postmortem fracture lines are present in the buccal and lingual root.

Iron (Fe^{56})

The two-dimensional map for detection values of iron (Fe^{56}) exhibits low detection values in the dentin region of the tooth. The enamel border exhibits high detection values on the buccal aspect and intermediate values are observed in the lingual aspect.

Copper (Cu^{63})

The two-dimensional map for detection values of copper (Cu^{63}) exhibits low significant elemental detection. No inclusions of copper are present in this sample. Further, no fracture

lines were observed. High detection values are consistent with residue buildup from prior ablation procedures.

The two-dimensional map for concentration values of copper (Cu^{63}) exhibits low concentration values in the buccal superior aspect of the dentin and enamel regions. Intermediate concentration values are present in the buccal root border. Inconsistent intermediate inclusions of copper are present in the lingual aspect of the tooth. High concentration values are observed in the superior lingual aspect of the dentin region. A postmortem fracture line is present in the superior and lingual buccal roots with high values of concentration, which indicate element reading of the resin base.

Zinc (Zn^{66})

The two-dimensional map for detection values of zinc (Zn^{66}) exhibits intermediate detection values in the buccal and lingual aspect of the enamel border as well as in the superior buccal and lingual aspect of the dentin border. An inclusion of intermediate detection is present in the inferior lingual aspect of the dentin region.

The two-dimensional map for concentration values of zinc (Zn^{66}) exhibits low concentration values in the inferior aspect of the dentin. No inclusions of copper are present within this sample. Postmortem fracture lines are present in the superior lingual and buccal roots.

Strontium (Sr^{88})

The two-dimensional map for detection values of strontium (Sr^{88}) exhibits intermediate detection values in the inferior aspect of the tooth with inconsistent intermediate values observed in the superior aspect. Low elemental detection values are observed in the enamel region of the tooth. No inclusions of strontium are present within this sample.

The two-dimensional map for concentration values of strontium (Sr^{88}) exhibits intermediate detection values in the inferior aspect of the tooth. The superior aspect of the enamel border is observed to have high element concentrations. No inclusions of strontium are present within this sample.

Antimony (Sb^{121})

The two-dimensional map for detection values of antimony (Sb^{121}) exhibits inconsistent elemental detection in the overall tooth which is attributed to debris within the LA-ICP-MS during ablation. No inclusions of antimony were observed.

The two-dimensional map for concentration values of antimony (Sb^{121}) exhibits low detection values in the overall tooth. No inclusions of antimony were observed.

Lanthanum (La^{139})

The two-dimensional map for detection values of lanthanum (La^{139}) exhibits high detection values observed around the superior aspect of the border encompassing the tooth. No inclusions of lanthanum were observed within this sample.

Lead (Pb^{208})

The two-dimensional map for detection values of lead (Pb^{208}) exhibits low detection values in the inferior aspect of the dentin region. High detection values are observed along the DEJ with values decreasing toward the inferior aspect of the dentin. No inclusions of lead are observed within this sample.

The two-dimensional map for concentration values of lead (Pb^{208}) exhibits low values in the superior aspect of the dentin region. High concentrations are observed in the DEJ. No inclusions are observed within this sample.

Uranium (U^{238})

The two-dimensional map for detection values of uranium (U^{238}) exhibits inconsistent low levels of detection values throughout the tooth. Intermediate detection values are observed in the superior aspect of the enamel border. An inclusion of high element detection values is observed in the superior buccal aspect of the dentin border.

Third molar

Carbon (C^{13})

The two-dimensional map for detection values of carbon (C^{13}) exhibits low detection values throughout the tooth. An inclusion of intermediate detection value is present within the lingual aspect of the dentin border.

Magnesium (Mg^{24})

The two-dimensional map for detection values of magnesium (Mg^{24}) exhibits intermediate detection values in the dentin superior to the pulp cavity. An inclusion of high detection value is present in the lingual aspect of the dentin border. Inconsistent intermediate elemental detection is observed within the dentin border of the tooth.

Phosphorus (P^{31})

The two-dimensional map for detection values of phosphorus (P^{31}) exhibits intermediate detection values in the dentin superior to the pulp cavity. An inclusion of high detection values is present in the lingual aspect of the dentin border. Inconsistent intermediate detection values are observed in the dentin border of the tooth as well.

Sulfur (S^{32})

The two-dimensional map for detection values of sulfur (S^{32}) exhibits intermediate values in the dentin superior to the pulp cavity. Inclusions of high detection values are present in the lingual aspect of the dentin border with inconsistent intermediate values observed along the buccal aspect of the dentin border.

Calcium (Ca^{44})

The two-dimensional map for detection values of calcium (Ca^{44}) exhibits low detection values in the overall tooth with intermediate detection values observed in the dentin superior to

the pulp cavity. Inclusions of high detection are present in the lingual dentin border. Inclusions of inconsistent intermediate detection values are observed in the buccal dentin border.

Iron (Fe^{56})

The two-dimensional map for detection values of iron (Fe^{56}) exhibits low detection values within the tooth. An inclusion of high detection is present in the superior lingual aspect of the dentin border.

Copper (Cu^{63})

The two-dimensional map for detection values of copper (Cu^{63}) exhibits low elemental detection. No inclusions of copper are present in this sample. Intermediate detection values are consistent with residue buildup from prior ablation procedures.

The two-dimensional map for concentration values of copper (Cu^{63}) exhibits low concentration values throughout the tooth with inconsistent intermediate concentrations observed within the buccal aspect. The superior lingual aspect of the dentin border exhibits lowered concentration values at the site of inclusion.

Zinc (Zn^{66})

The two-dimensional map for detection values of zinc (Zn^{66}) exhibits intermediate detection values in the dentin region superior to the pulp cavity. An inclusion of intermediate detection is present in the superior lingual aspect of the dentin border. Further, inconsistent intermediate detection values are observed throughout the buccal aspect of the dentin border.

The two-dimensional map for concentration values of zinc (Zn^{66}) exhibits low concentration values throughout the sample. An inclusion of intermediate concentration values is observed in the dentin region superior to the pulp cavity.

Strontium (Sr^{88})

The two-dimensional map for detection values of strontium (Sr^{88}) exhibits intermediate detection values within the borders of the tooth. Low detection values are observed in the dentin border. No inclusions of strontium are present within this sample.

The two-dimensional map for concentration values of strontium (Sr^{88}) exhibits intermediate detection values in the buccal and lingual aspect of the tooth. Low elemental detection is observed along the border of the tooth as well as at the site of inclusion. The dental pulp cavity exhibits high concentration values of strontium.

Antimony (Sb^{121})

The two-dimensional map for detection values of antimony (Sb^{121}) exhibits low elemental detection in the border. An inclusion of intermediate detection is observed within the superior lingual aspect of the dentin border.

The two-dimensional map for concentration values of antimony (Sb^{121}) exhibits low detection values in the overall tooth. No inclusions of antimony were observed.

Lanthanum (La^{139})

The two-dimensional map for detection values of lanthanum (La^{139}) exhibits high detection values around the border encompassing the tooth and along the dentin bordering the pulp cavity. No inclusions of lanthanum were observed within this sample.

Lead (Pb^{208})

The two-dimensional map for detection values of lead (Pb^{208}) exhibits intermediate detection values observed around the dentin bordering the pulp cavity. Inclusions of intermediate detection values are observed at the superior aspect of the lingual dentin border and in the buccal aspect of the dentin superior to the pulp cavity.

The two-dimensional map for concentration values of lead (Pb^{208}) exhibits low values along the border of the tooth. An inclusion of low detection is observed within the buccal aspect of the dentin superior to the pulp cavity.

Uranium (U^{238})

The two-dimensional map for detection values of uranium (U^{238}) exhibits inconsistent low levels of detection values throughout the tooth. Intermediate detection values are observed in the inferior aspect of the dentin border. An inclusion of intermediate element detection is observed in the superior lingual aspect of the dentin border.

Individual IIT 315-01

First molar

Carbon (C^{13})

The two-dimensional map for detection values of carbon (C^{13}) exhibits intermediate detection values in the lingual aspect of the dentin. An inclusion of intermediate detection value is present along the mesial aspect of the dentin. An inclusion of high detection is present in the inferior aspect of the root. Several postmortem fracture lines of intermediate detection are observed radiating form the superior aspect of the tooth toward the inferior aspect within this sample. The intermediate detection values indicate element reading of the resin base.

Magnesium (Mg^{24})

The two-dimensional map for detection values of magnesium (Mg^{24}) exhibits low detection values in the dentin region. Inclusions of intermediate detection are present in the inferior lingual aspect of the dentin and the inferior mesial aspect. A postmortem fracture line is observed at the mesial aspect of the enamel border and radiates toward the inferior aspect.

Phosphorus (P^{31})

The two-dimensional map for detection values of phosphorus (P^{31}) exhibits intermediate values along the lingual aspect of the dentin border and along the DEJ. Inclusions of intermediate detection values are present in the inferior lingual aspect of the dentin and the inferior mesial aspect. A postmortem fracture line is observed at the mesial aspect of the enamel border and radiates toward the inferior aspect.

Sulfur (S^{32})

The two-dimensional map for detection values of sulfur (S^{32}) exhibits detection values that were not properly configured prior to mapping and will not be used in further analysis.

Calcium (Ca^{44})

The two-dimensional map for detection values of calcium (Ca^{44}) exhibits intermediate detection values in the lingual aspect of the dentin border and along the border of the pulp cavity. Inclusions of high detection are present superior to the pulp cavity. An inclusion of intermediate value is present in the superior mesial aspect of the dentin region. A postmortem fracture line is observed at the superior aspect of the tooth and radiates toward the inferior aspect.

Iron (Fe^{56})

The two-dimensional map for detection values of iron (Fe^{56}) exhibits low elemental detection within the overall sample. An inclusion of intermediate detection is present along the lingual border.

Copper (Cu^{63})

The two-dimensional map for detection values of copper (Cu^{63}) exhibits low element detection. No inclusions of copper are present.

The two-dimensional map for concentration values of copper (Cu^{63}) exhibits low concentration values in the overall tooth. An inclusion of intermediate concentration is present in the superior lingual aspect of the dentin. A postmortem fracture line of high concentration

reading is present at the superior aspect of the tooth and radiates toward the inferior aspect. The high concentration values indicates elemental reading of the resin base.

Zinc (Zn^{66})

The two-dimensional map for detection values of zinc (Zn^{66}) exhibits low detection in the dentin border. Intermediate detection values are observed in the dentin superior to the pulp cavity. An inclusion of intermediate detection is present in the superior mesial aspect of the dentin. Striations of zinc are observed within the dentin region of the tooth and exhibit intermediate detection values. A postmortem fracture line is present within the superior mesial aspect of the tooth and radiates toward the inferior aspect.

The two-dimensional map for concentration values of zinc (Zn^{66}) exhibits intermediate concentration values within the dentin. High concentrations are observed in the pulp cavity with intermediate concentration observed superior to the pulp cavity within the dentin region. An inclusion of intermediate concentration is observed in the superior mesial aspect of the dentin.

Strontium (Sr^{88})

The two-dimensional map for detection values of strontium (Sr^{88}) exhibits intermediate values in the inferior aspect of the tooth. An inclusion of high detection is present superior to the pulp cavity within the dentin region. Also, along the inferior aspect of the dentin is an inclusion that exhibits intermediate values. A third inclusion of intermediate detection is present in the superior mesial aspect of the dentin. Striations of intermediate detection are observed within the dentin region. A postmortem fracture line is observed at the superior mesial aspect of the tooth.

The two-dimensional map for concentration values of strontium (Sr^{88}) exhibits intermediate concentration values in the inferior aspect of the tooth and low elemental detection in the superior aspect. The superior aspect of the enamel border is observed to have high element concentrations. Striations of intermediate concentrations are observed within the inferior aspect of the dentin.

Antimony (Sb^{121})

The two-dimensional map for detection values of antimony (Sb^{121}) exhibits inconsistent elemental detection in the overall tooth which is attributed to debris within the LA-ICP-MS during ablation. No inclusions of antimony were observed.

The two-dimensional map for concentration values of antimony (Sb^{121}) low detection values in the overall tooth. No inclusions of antimony were observed.

Lanthanum (La^{139})

The two-dimensional map for detection values of lanthanum (La^{139}) exhibits low detection values around the border encompassing the tooth. An inclusion of intermediate detection is observed within the pulp cavity. A second inclusion of low detection values is observed within the superior aspect of the dentin.

Lead (Pb^{208})

The two-dimensional map for detection values of lead (Pb^{208}) exhibits low detection values along the dentin border of the tooth and along the superior aspect of the tooth.

Intermediate detection values are observed within the pulp cavity. An inclusion of intermediate detection is observed within the superior mesial aspect of the tooth. A postmortem fracture line is observed within the superior aspect of the tooth and radiates toward the inferior aspect.

The two-dimensional map for concentration values of lead (Pb^{208}) exhibits low values within the dentin region. Intermediate concentration values are observed along the DEJ and in the pulp cavity. An inclusion of intermediate concentration is present in the superior mesial aspect of the dentin.

Uranium (U^{238})

The two-dimensional map for detection values of uranium (U^{238}) exhibits low detection throughout the tooth with inconsistent low levels observed within the lingual aspect of the dentin. No inclusions of uranium are present within this sample.

Second molar

Carbon (C^{13})

The two-dimensional map for detection values of carbon (C^{13}) exhibits low detection values in the dentin region. Intermediate detection values are observed in the inferior aspect of the dentin and in the pulp cavity. Several postmortem fracture lines with intermediate detection values radiate from the superior aspect of the tooth toward the inferior aspect. The intermediate detection values indicate elemental reading of the resin base.

Magnesium (Mg^{24})

The two-dimensional map for detection values of magnesium (Mg^{24}) exhibits intermediate detection values around the pulp cavity as well as the inner root border. Several postmortem fracture lines are observed at the superior mesial aspect of the DEJ and radiate toward the pulp cavity.

Phosphorus (P^{31})

The two-dimensional map for detection values of phosphorus (P^{31}) exhibits intermediate values in the dentin surrounding the pulp cavity, the buccal and lingual roots, and the buccal cusp of the enamel. Postmortem fracture lines are observed at the superior mesial aspect of the DEJ and radiate toward the pulp cavity.

Sulfur (S^{32})

The two-dimensional map for detection values of sulfur (S^{32}) exhibits low detection values within the dentin region of the sample. No inclusions are observed. Postmortem fracture lines are observed at the superior mesial aspect of the DEJ and radiate toward the pulp cavity.

Calcium (Ca^{44})

The two-dimensional map for detection values of calcium (Ca^{44}) exhibits intermediate values in the dentin surrounding the pulp cavity, the buccal and lingual roots, and the buccal cusp of the enamel. Postmortem fracture lines are observed at the superior mesial aspect of the DEJ and radiate toward the pulp cavity.

Iron (Fe^{56})

The two-dimensional map for detection values of iron (Fe^{56}) exhibits low detection at the inner root border and the inferior aspect of the pulp cavity. An inclusion of intermediate detection is present along the lingual dentin border.

Copper (Cu^{63})

The two-dimensional map for detection values of copper (Cu^{63}) exhibits intermediate detection at the lingual border of the tooth. Inclusions of intermediate detection values are present in the enamel border of the buccal cusp as well as the inferior aspect of the pulp cavity.

The two-dimensional map for concentration values of copper (Cu^{63}) exhibits low concentration values in the overall tooth. No inclusions of copper are present within this sample. Postmortem fracture lines of low concentration are observed at the superior mesial aspect of the DEJ and radiate toward the pulp cavity. These low concentration values that indicate element reading of the resin base.

Zinc (Zn^{66})

The two-dimensional map for detection values of zinc (Zn^{66}) exhibits intermediate detection in the border encompassing the tooth, the dentin surrounding the pulp cavity, and the inner root border. An inclusion of intermediate detection is present in the superior lingual aspect of the dentin border. Postmortem fracture lines with low concentration values are observed at the superior mesial aspect of the DEJ and radiate toward the pulp cavity. The low concentration values indicate element reading of the resin base.

The two-dimensional map for concentration values of zinc (Zn^{66}) exhibits low concentration values within the dentin region. Intermediate concentrations are observed in the dentin surrounding the pulp cavity and the inner root borders. No inclusions of zinc are observed within this sample.

Strontium (Sr^{88})

The two-dimensional map for detection values of strontium (Sr^{88}) exhibits intermediate values in the overall tooth with increased detection observed in the buccal cusp of the enamel. Intermediate detection values are observed in the lingual and buccal aspect of the dentin region surrounding the inner root border and, in the dentin, surrounding the pulp cavity. Striations of intermediate detection values are observed within the dentin region. A postmortem fracture line is observed at the superior mesial aspect of the DEJ and radiates toward the pulp cavity.

The two-dimensional map for concentration values of strontium (Sr^{88}) exhibits intermediate concentration values in the overall tooth with higher concentrations in the superior lingual aspect. Striations of intermediate concentration values are observed within the dentin.

Antimony (Sb^{121})

The two-dimensional map for detection values of antimony (Sb^{121}) exhibits inconsistent elemental detection in the overall tooth which is attributed to debris within the LA-ICP-MS during ablation (Figure 382). No inclusions of antimony were observed.

The two-dimensional map for concentration values of antimony (Sb^{121}) exhibits low concentration values in the overall tooth. No inclusions of antimony were observed.

Lanthanum (La^{139})

The two-dimensional map for detection values of lanthanum (La^{139}) exhibits low detection values observed around the inferior dentin border encompassing the tooth. Intermediate detection values of lanthanum are observed in the dentin regions surrounding the pulp cavity and the inner root border.

Lead (Pb^{208})

The two-dimensional map for detection values of lead (Pb^{208}) exhibits low detection values along the dentin border of the tooth. Intermediate detection values are observed along the inner root border and in the dentin surrounding the pulp cavity. Inclusions of intermediate detection are observed within the superior aspect of the tooth.

The two-dimensional map for concentration values of lead (Pb^{208}) exhibits low values within the dentin with intermediate concentration values observed along the pulp cavity and inner root border. Inclusions of high concentrations are present in the superior aspect of the dentin.

Uranium (U^{238})

The two-dimensional map for detection values of uranium (U^{238}) exhibits low element detection throughout the tooth. No inclusions of uranium are present within this sample.

Individual IIT 316-01

Second molar

Carbon (C^{13})

The two-dimensional map for detection values of carbon (C^{13}) exhibits low detection values in the dentin region. Intermediate detection values are observed along the pulp cavity. No inclusions of carbon are present. Several postmortem fracture lines with intermediate detection values are observed within the superior aspect of the tooth. The first is observed to radiate from the fissure line terminating at the pulp cavity. The second is observed to radiate perpendicular to the first and terminates in the lingual aspect of the DEJ. While the third appears at the buccal aspect of the DEJ and radiates toward the pulp cavity. The intermediate detection values indicate element reading of the resin base.

Magnesium (Mg^{24})

The two-dimensional map for detection values of magnesium (Mg^{24}) exhibits low detection in the superior aspect of the tooth. Intermediate values are observed at the pulp cavity and decrease as distance from the pulp cavity increases. Several postmortem fracture lines are observed within the superior aspect of the tooth. The first is observed to radiate from the fissure line terminating at the pulp cavity. The second is observed to radiate perpendicular to the first and terminates in the lingual aspect of the DEJ. While the third appears at the buccal aspect of the DEJ and radiates toward the pulp cavity.

Phosphorus (P^{31})

The two-dimensional map for detection values of phosphorus (P^{31}) exhibits low detection values within the superior aspect of the dentin region. Intermediate detection values are observed in the buccal aspect of the enamel and the lingual aspect of the DEJ. The dentin region superior to the pulp cavity is observed to have high detection values that decrease as distance from the pulp cavity increases. Several postmortem fracture lines are observed within the superior aspect of the tooth. The first is observed to radiate from the fissure line terminating at the pulp cavity. The second is observed to radiate perpendicular to the first and terminates in the lingual aspect of the DEJ. While the third appears at the buccal aspect of the DEJ and radiates toward the pulp cavity.

Sulfur (S^{32})

The two-dimensional map for detection values of sulfur (S^{32}) exhibits low elemental detection values within the enamel region and intermediate detection values within the dentin region. High detection values are observed in the buccal and lingual root tips

Calcium (Ca^{44})

The two-dimensional map for detection values of calcium (Ca^{44}) exhibits intermediate detection values within the superior aspect of the dentin region, the buccal aspect of the enamel, and the lingual aspect of the DEJ. The dentin region superior to the pulp cavity is observed to have high detection values that decrease as distance from the pulp cavity increases. Several postmortem fracture lines are observed within the superior aspect of the tooth. The first is observed to radiate from the fissure line terminating at the pulp cavity. The second is observed

to radiate perpendicular to the first and terminates in the lingual aspect of the DEJ. While the third appears at the buccal aspect of the DEJ and radiates toward the pulp cavity.

Iron (Fe^{56})

The two-dimensional map for detection values of iron (Fe^{56}) exhibits low detection in the enamel border and inconsistent high detection is observed along the inferior border of the tooth. Inclusions of high detection are present in the inferior aspect of the dentin and exhibit high detection values. A postmortem fracture line of low element detection is observed to radiate from the fissure line between the cusps toward the inferior aspect of the tooth.

Copper (Cu^{63})

The two-dimensional map for detection values of copper (Cu^{63}) exhibits low element detection. Inclusions of high detection values are present in the buccal aspect of this sample.

The two-dimensional map for concentration values of copper (Cu^{63}) exhibits low concentration values in the overall tooth. Inclusions of intermediate concentrations are present in the superior buccal aspect of the tooth. A postmortem fracture line is present at the superior aspect of the dentin and radiates toward the pulp cavity. A second fracture line radiate perpendicular to the first. Both fracture lines exhibit low detection values that are consistent with the elemental reading of the resin base.

Zinc (Zn^{66})

The two-dimensional map for detection values of zinc (Zn^{66}) exhibits low detection within the inferior aspect of the enamel. Intermediate detection values are observed in the enamel border and in the dentin region. The dentin shows intermediate detection values that increase along the superior aspect of the pulp cavity. Inclusions of high detection are present in the fissure line of the enamel as well as along the buccal cusp. A postmortem fracture line is present at the superior aspect of the dentin and radiates toward the pulp cavity. A second postmortem fracture line radiates perpendicular to the first. A third postmortem fracture line is observed in the buccal dentin region superior to the pulp cavity.

The two-dimensional map for concentration values of zinc (Zn^{66}) exhibits low concentration values within the dentin region. High concentrations are observed in the enamel border. No inclusions of zinc are present.

Strontium (Sr^{88})

The two-dimensional map for detection values of strontium (Sr^{88}) exhibits low values in the superior aspect of the tooth. Intermediate values are observed in the lingual and buccal root tips, along the DEJ, and in the dentin surrounding the pulp cavity. A postmortem fracture line is present at the superior aspect of the dentin and radiates toward the pulp cavity. A second postmortem fracture line radiates perpendicular to the first.

The two-dimensional map for concentration values of strontium (Sr^{88}) exhibits low concentration values in the superior aspect of the dentin. Intermediate concentration values are present in the lingual and buccal roots.

Antimony (Sb^{121})

The two-dimensional map for detection values of antimony (Sb^{121}) exhibits low element detection in the overall tooth. No inclusions of antimony were observed.

The two-dimensional map for concentration values of antimony (Sb^{121}) exhibits low element concentrations in the overall tooth. No inclusions of antimony were observed.

Lanthanum (La^{139})

The two-dimensional map for detection values of lanthanum (La^{139}) exhibits low detection values in the inferior aspect of the dentin. High detection values are present in the dentin border surrounding the pulp cavity. No inclusions of lanthanum are observed within this sample.

Lead (Pb^{208})

The two-dimensional map for detection values of lead (Pb^{208}) exhibits low detection values in the dentin and along the enamel border. Intermediate detection values are present superior to the pulp cavity. Inclusions of high detection values are observed within the superior buccal aspect of the tooth.

The two-dimensional map for concentration values of lead (Pb^{208}) exhibits low elemental detection within the overall sample. No inclusions are present.

Uranium (U^{238})

The two-dimensional map for detection values of uranium (U^{238}) exhibits low elemental detection throughout the tooth. The dentin surrounding the pulp cavity exhibits inconsistent intermediate detection values. An inclusion of high detection is present superior to the lingual aspect of the pulp cavity.

Element concentration values for each individual sample were analyzed and labelled as not available (N/A), low (L), intermediate (I), or high (H) as seen in Table 7.

Table 7 Element concentration values (N/A- not available; L- low; I- intermediate; H- high).

Individual Tooth	Copper	Strontium	Zinc	Antimony	Lead
IIT 160-01_M1	H	I	I	N/A	L
IIT 160-02_M2	I	H	L	L	L
IIT 160-02_M3	L	L	L	N/A	N/A
IIT 178-01_M1	I	L	H	H	L
IIT 178-01_M2	L	L	H	N/A	L
IIT 178-01_M3	L	L	H	H	N/A
IIT 190-01_M1	L	L	H	H	H
IIT 197-01_M1	I	H	H	L	L
IIT 197-01_M2	L	I	H	L	L
IIT 213-01_M1	L	L	H	L	L
IIT 217-01_M1	L	L	H	H	L
IIT 220-01_M1	L	L	L	N/A	L
IIT 220-01_M2	L	L	H	L	L
IIT 220-01_M3	L	L	I	L	L
IIT 236-01_M1	L	L	I	N/A	L
IIT 263-01_M1	L	L	I	L	L
IIT 312-01_M1	L	I	L	L	I
IIT 312-01_M3	L	I	I	L	L
IIT 315-01_M1	L	L	L	I	H
IIT 315-01_M2	H	L	I	I	H
IIT 316-01_M2	I	L	I	I	L

Comparative Concentration Analysis

In order to interpret intra- and inter- individual variations in element detection and concentration, comparisons were made. These comparisons aided in the understanding of dietary habits and cultural exposure. A comparative concentration analysis was performed following the two-dimensional mapping of trace elements, on elements copper (Cu^{56}), zinc (Zn^{66}), and strontium (Sr^{88}) to evaluate dietary habits. A comparative analysis on antimony (Sb^{121}), and lead (Pb^{208}) was performed to determine if cultural use of kohl in this population occurred. Values were graphed using concentration range values per element and to understand any possible differences within the population.

Inter-Individual Analysis

Inter-individual analysis was performed on thirteen individuals across the sample. According to the assessed age of the individuals, only two individuals (160-02 and 312-01) were identified to be of adult status, ten individuals were determined to be of juvenile status (160-01, 178-01, 190-01, 197-01, 213-01, 217-01, 220-01, 236-01, 263-01, 316-01), and one individual (315-01) is of unknown maturity status. A total of 11 first molars were present to perform a comparative element concentration analysis, of which one (312-01) was of known mature status, one individual's maturity status was unknown (315-01), and nine individuals were determined to be juveniles (160-01, 178-01, 190-01, 197-01, 213-01, 217-01, 220-01, 236-01, and 263-01). A total of six second molars were available for concentration comparisons with one individual of adult status (160-02), one of unknown maturity status (315-01), along with four juveniles (178-01, 197-01, 220-01, and 316-01). Lastly, four third molars were present for comparative

concentration analysis with two individuals of known mature status (160-02 and 312-01) and two juveniles (178-01 and 220-01).

Copper (Cu^{63})

First Molar Comparison

Upon analysis of the first molars, concentration values in individuals 160-01 (300 ppm), 178-01 (200 ppm), and 197-01 (150 ppm) exhibit elevated levels of copper compared to the other individuals (Figure 31). High concentration values for copper were present in individual 160-01 (300 ppm). Intermediate concentration values were observed in individuals 178-01 (200 ppm) and 197-01 (150 ppm). The remaining first molars exhibited low (< 100 ppm) copper concentration values.

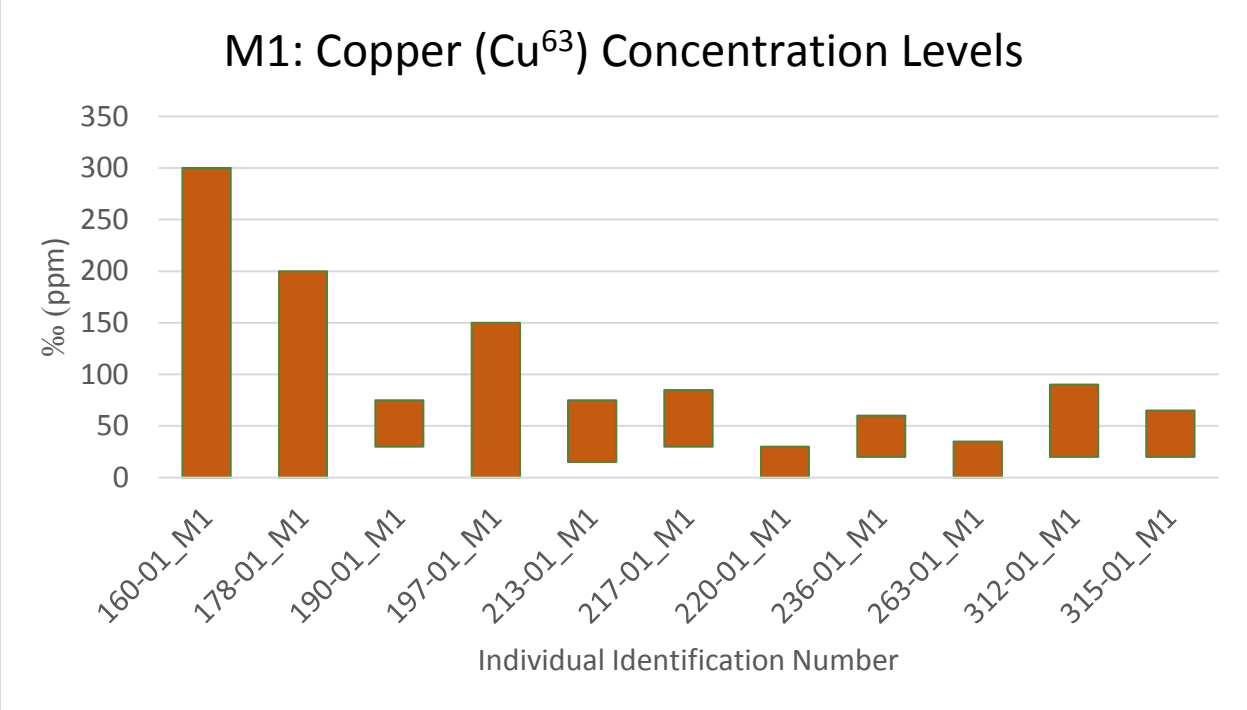

Figure 31 Graphed concentration values of copper (Cu^{63}) for all first molar (M1) dental samples to evaluate inter-individual analysis.

Second Molar Comparison

Upon analysis of the second molars individuals 160-02, 315-01, and 316-01 exhibit elevated concentration levels for copper (Figure 32). Toxic concentration values were observed for individual 315-01 (300 ppm). High concentration values were observed for individuals 160-02 (200 ppm) and 316-01 (200 ppm). Optimal copper requirements were observed for individual 197-01. The remaining second molars (178-01 and 220-01) were observed to have deficient concentration values of copper (< 100 ppm).

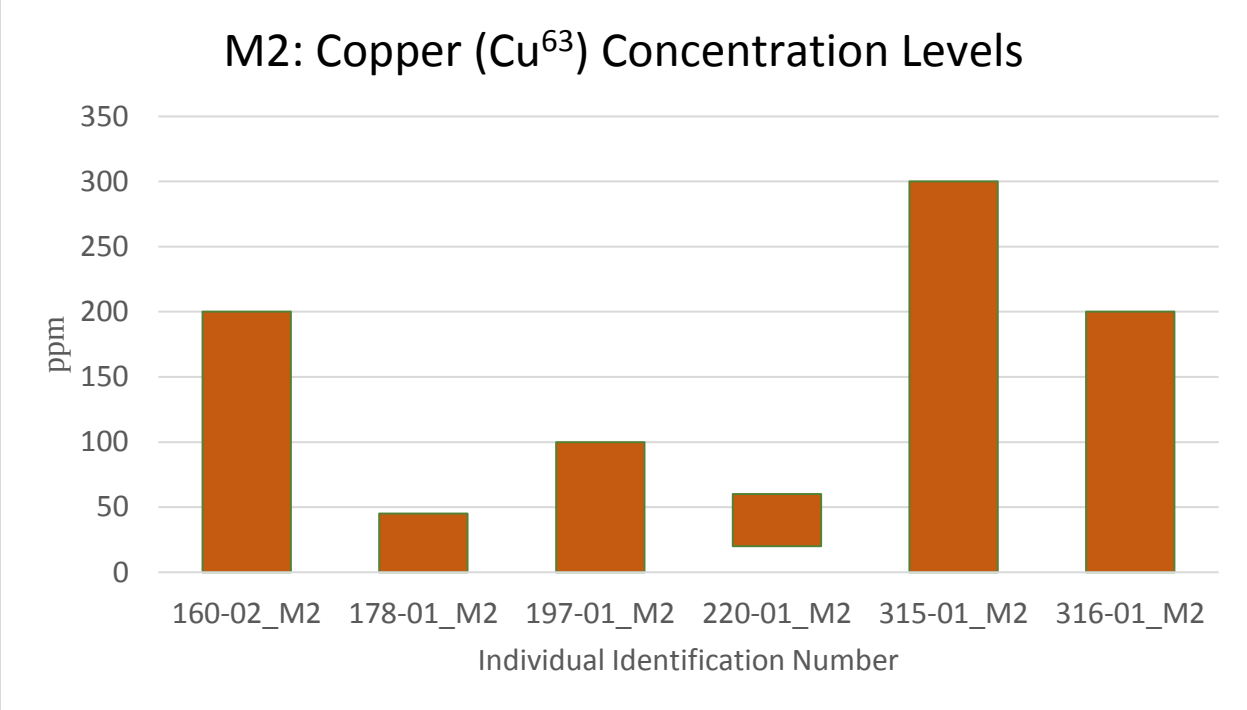

Figure 32 Graphed concentration values of copper (Cu^{63}) for all second molar (M2) dental samples to evaluate inter-individual analysis.

Third Molar Comparison

Concentration values for copper in all third molars were observed to be low with values of less than 100 ppm (Figure 33). Individuals 178-01 (70 ppm), and 312-01 (90 ppm) have optimal copper concentrations compared to individuals 160-02 an 220-01 whose concentration values are considered deficient (e.g. 30 ppm).

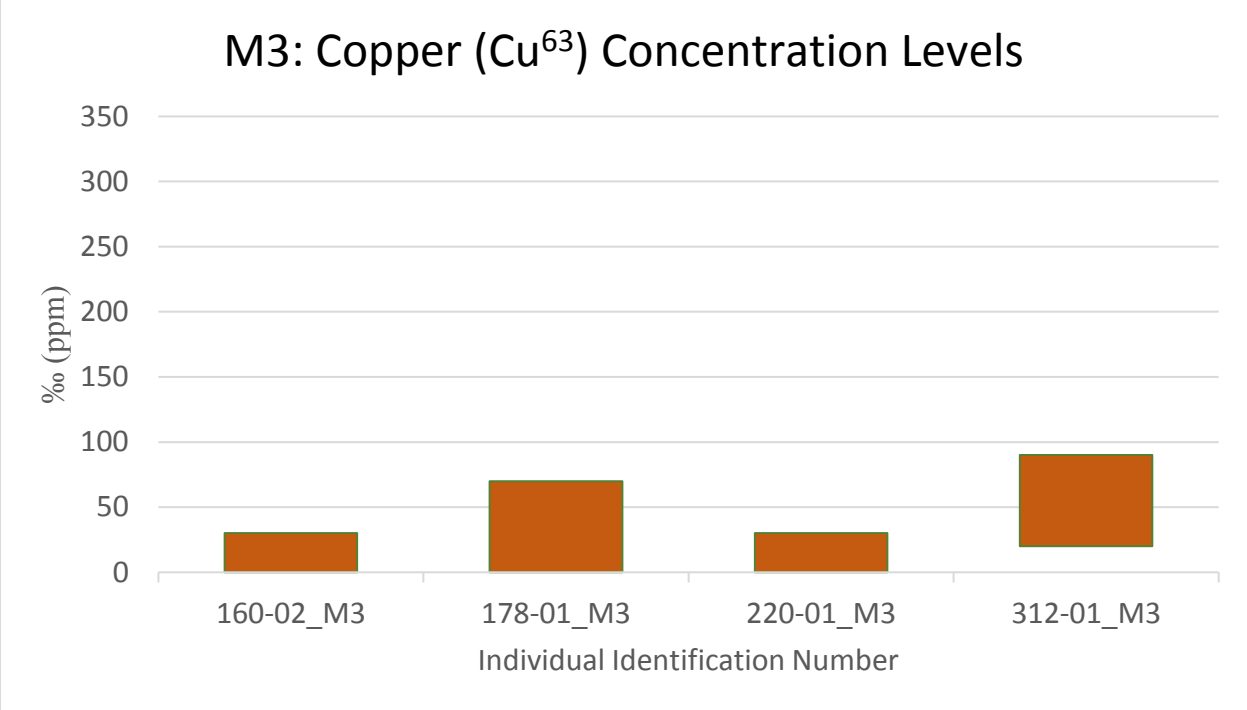

Figure 33 Graphed concentration values of copper (Cu^{63}) for all third molar (M3) dental samples to evaluate inter-individual analysis.

Strontium (Sr^{88})

First Molar Comparison

First molar strontium concentration values are elevated in individuals 160-01, 197-01, and 312-01 (Figure 34). The highest concentration is observed in individual 197-01 (8000 ppm). Intermediate concentration values are observed in individuals 160-01 (3000 ppm) and 312-01 (3000 ppm). The remaining first molars are observed to have lower strontium concentration values (< 900 ppm).

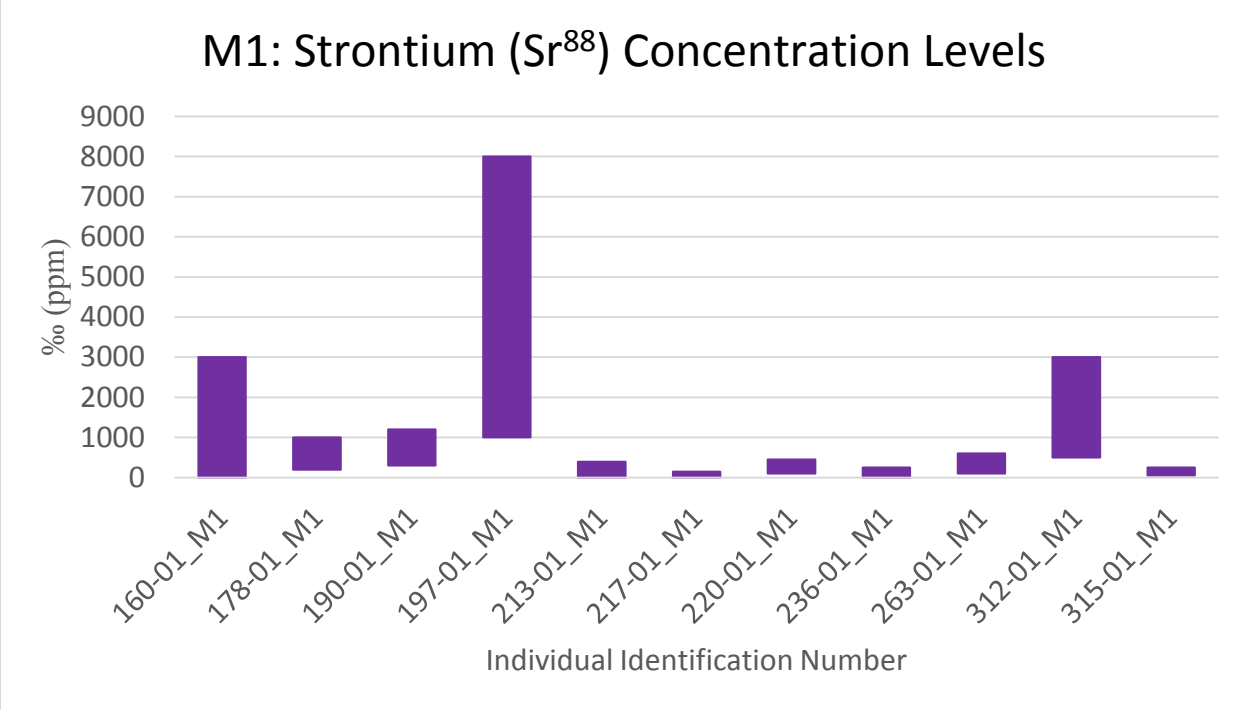

Figure 34 Documented concentration values of strontium (Sr^{88}) for all first molar (M1) dental samples to evaluate inter-individual analysis.

Second Molar Comparison

Second molar concentration values for strontium showed elevated levels in individuals 160-02 and 197-01 (Figure 35). The highest concentration values were observed in individual 160-02 (4000 ppm). Intermediate concentration values were observed in individual 197-01 (2000 ppm). The remaining second molars were observed to have low strontium concentration values (< 450 ppm).

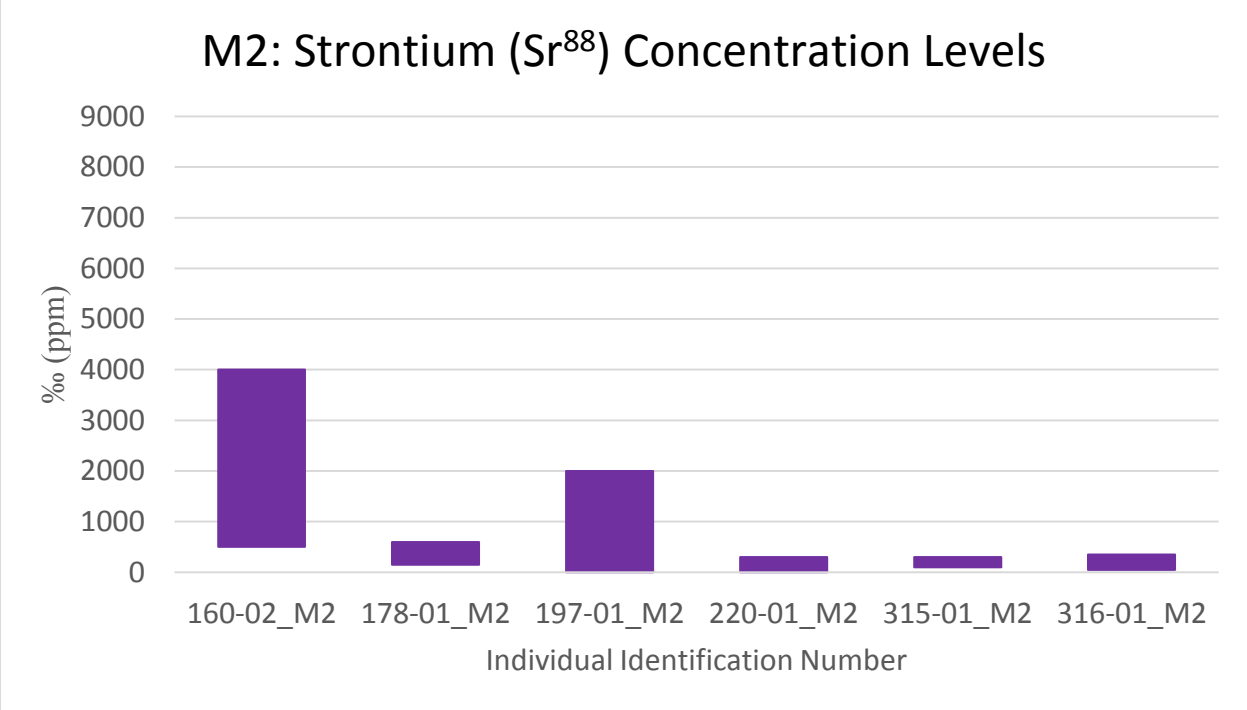

Figure 35 Documented concentration values of strontium (Sr^{88}) for all second molar (M2) dental samples to evaluate inter-individual analysis.

Third Molar Comparison

Strontium concentration values for the third molar sample indicate the highest levels in individual 312-01 (3000 ppm) (Figure 36). The remaining third molars were observed to have low strontium concentration values (< 500 ppm). The increased concentration values observed in 312-01 can be indicative of a plant-enriched diet when compared to other third molars whose concentration values of strontium are consistently low.

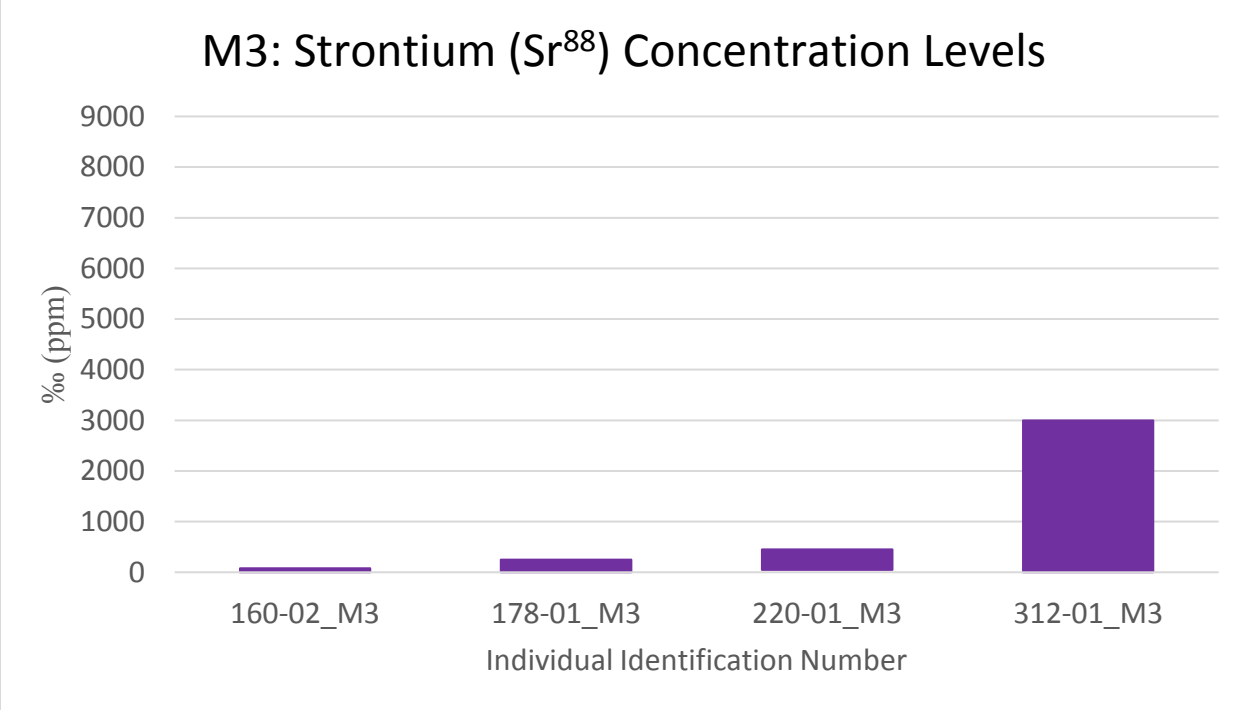

Figure 36 Documented concentration values of strontium (Sr^{88}) for all third molar (M3) dental samples to evaluate inter-individual analysis.

Zinc (Zn^{66})

First Molar Comparison

First molar concentration values for zinc revealed that individuals 178-01, 190-01, 197-01, 213-01 and 217-01 exhibited elevated levels (Figure 37). The highest concentration values for zinc were observed in individuals 178-01 (700 ppm), 190-01 (800 ppm), 197-01 (900 ppm), 213-01 (700 ppm), and 217-01 (700 ppm). Intermediate concentration values were observed in individuals 160-01 (600 ppm), 236-01 (500 ppm), and 263-01 (600 ppm). The remaining first molars were observed to have low zinc concentration values (< 400 ppm).

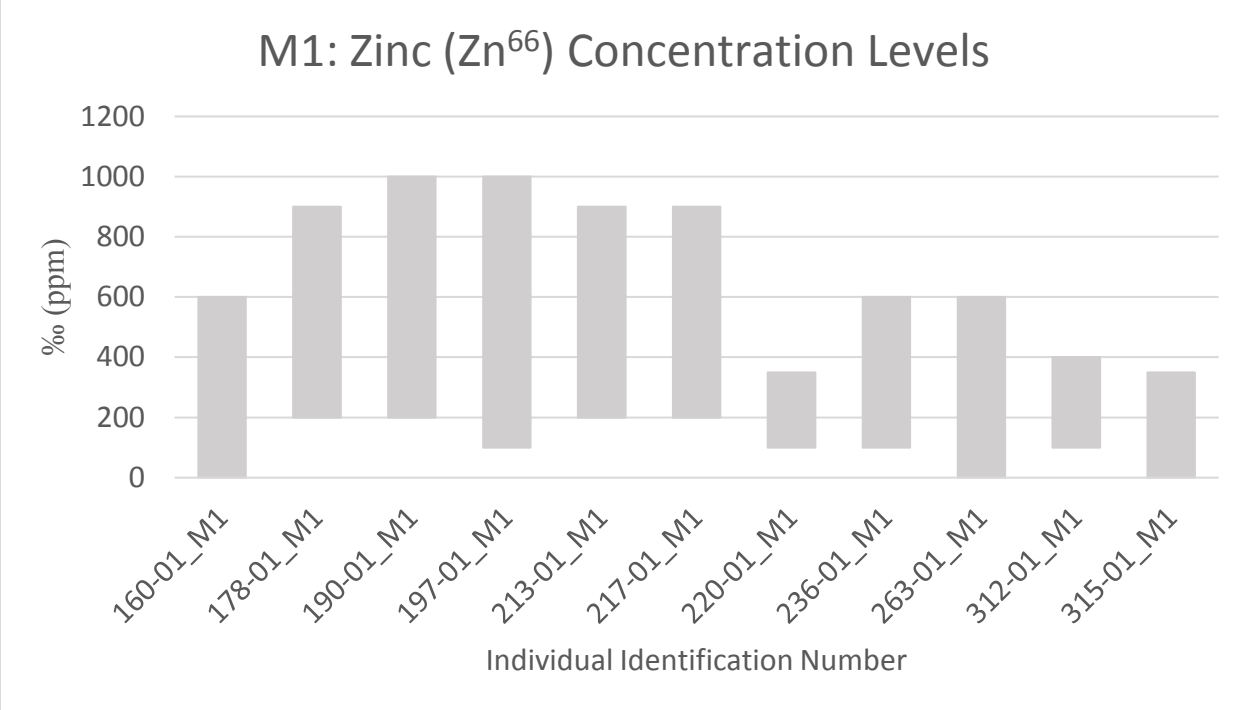

Figure 37 Graphed concentration values of zinc (Zn^{66}) for all first molar (M1) dental samples to evaluate inter-individual analysis.

Second Molar Comparison

Figure 38 shows high concentration values for zinc were observed in individuals 178-01 (900 ppm) and 197-01 (1000 ppm). Intermediate concentration values were observed in individual 220-01 (700 ppm), 315-01 (600 ppm), and 316-01 (600 ppm). The remaining second molar was observed to have copper concentration values measured to be less than 500 ppm.

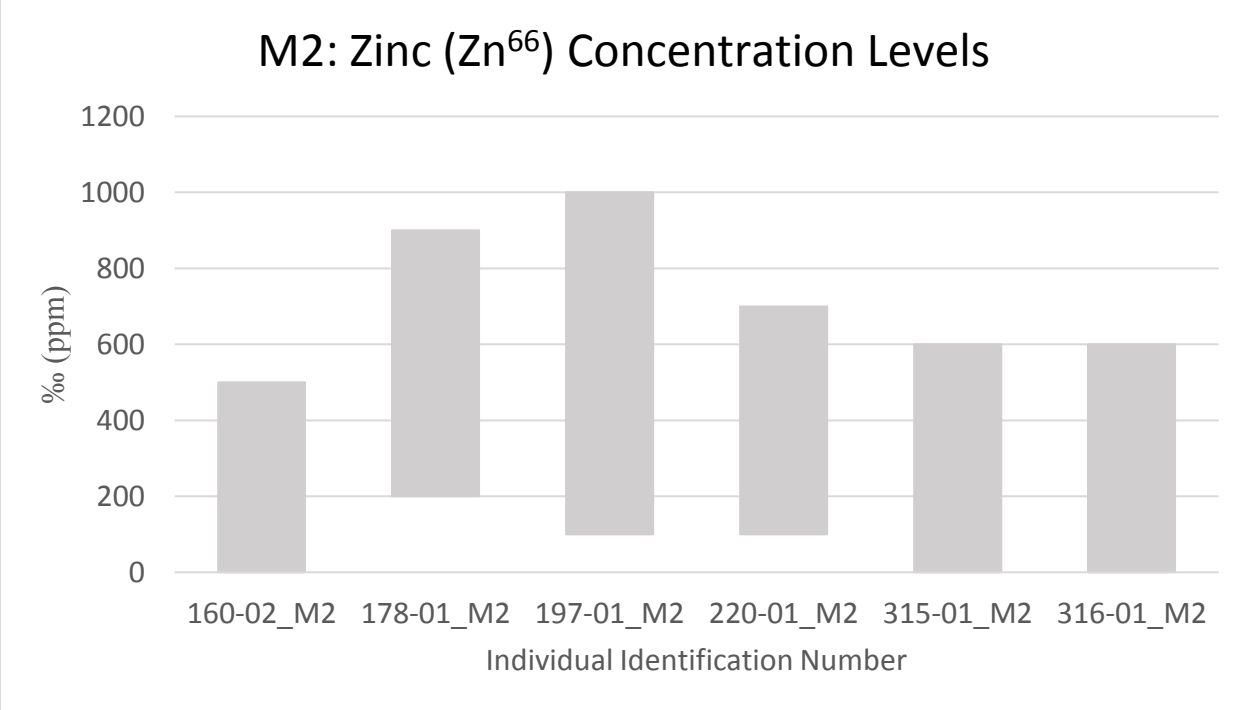

Figure 38 Graphed concentration values of zinc (Zn^{66}) for all first molar (M1) dental samples to evaluate inter-individual analysis.

Third Molar Comparison

The highest concentration values for zinc were observed in individual 178-01 (800 ppm) (Figure 39). Intermediate concentration values were observed in individuals 220-01 (700 ppm) and 312-01 (700 ppm). The remaining first molars were observed to have low copper concentration values (< 400 ppm).

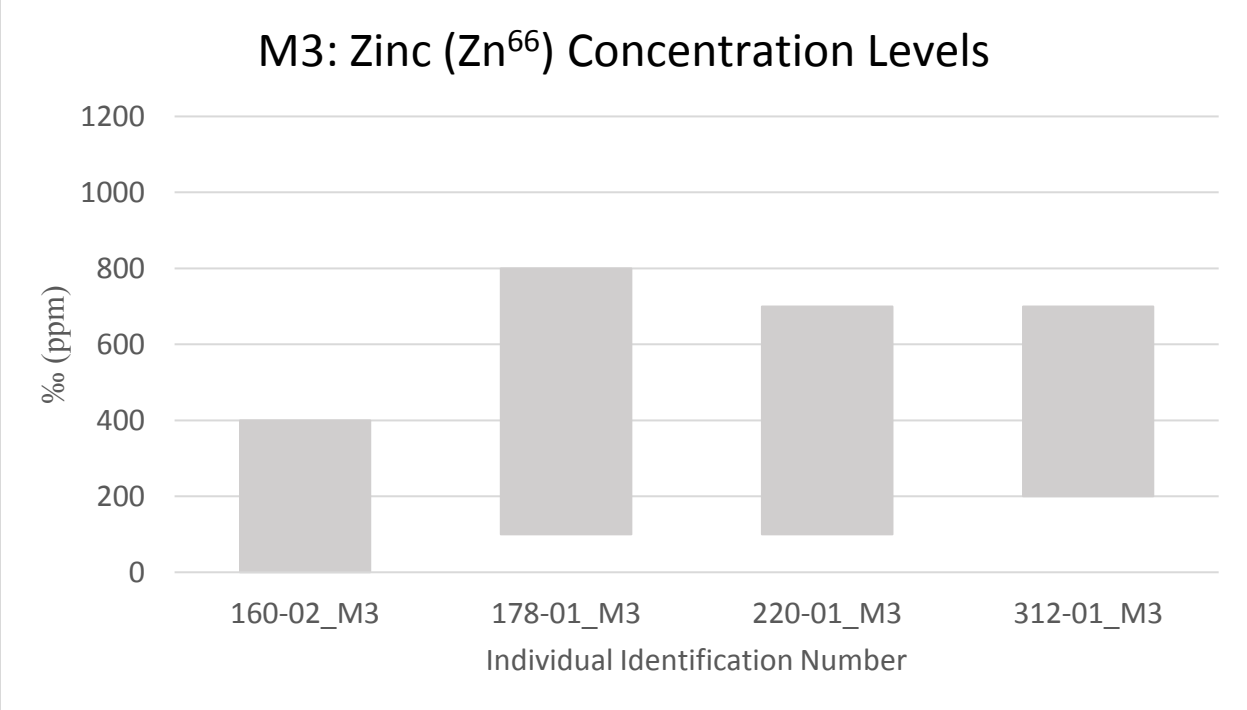

Figure 39 Graphed concentration values of zinc (Zn^{66}) for all third molar (M3) dental samples to evaluate inter-individual analysis.

Antimony ($Sb^{121)}$

First Molar Comparison

Individuals 178-01 (40 ppm), 190-01 (45 ppm), and 217-01 (50 ppm) exhibit the highest levels of antimony (Figure 40). Intermediate concentration values were observed in individuals 315-01 (35 ppm). The remaining first molars were observed to have low antimony concentration values (< 20 ppm).

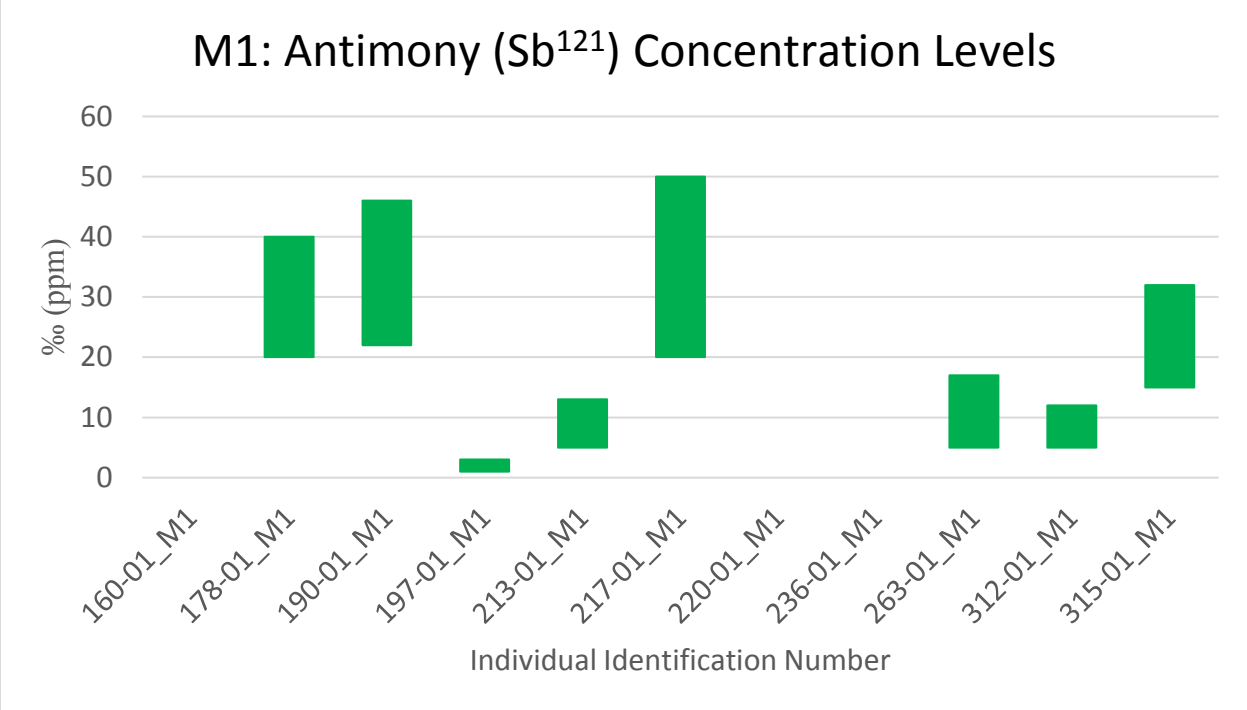

Figure 40 Graphed concentration values of antimony (Sb^{121}) for all first molar (M1) dental samples to evaluate inter-individual analysis.

Second Molar Comparison

In the second molar sample, the highest, although intermediate, concentration values for antimony were found in individuals 315-01 (32 ppm), and 316-01 (30 ppm) (Figure 41). Low concentration values for antimony were observed in individuals 160-02 (2 ppm) and 197-01 (3 ppm). The remaining first molars showed no concentration of antimony.

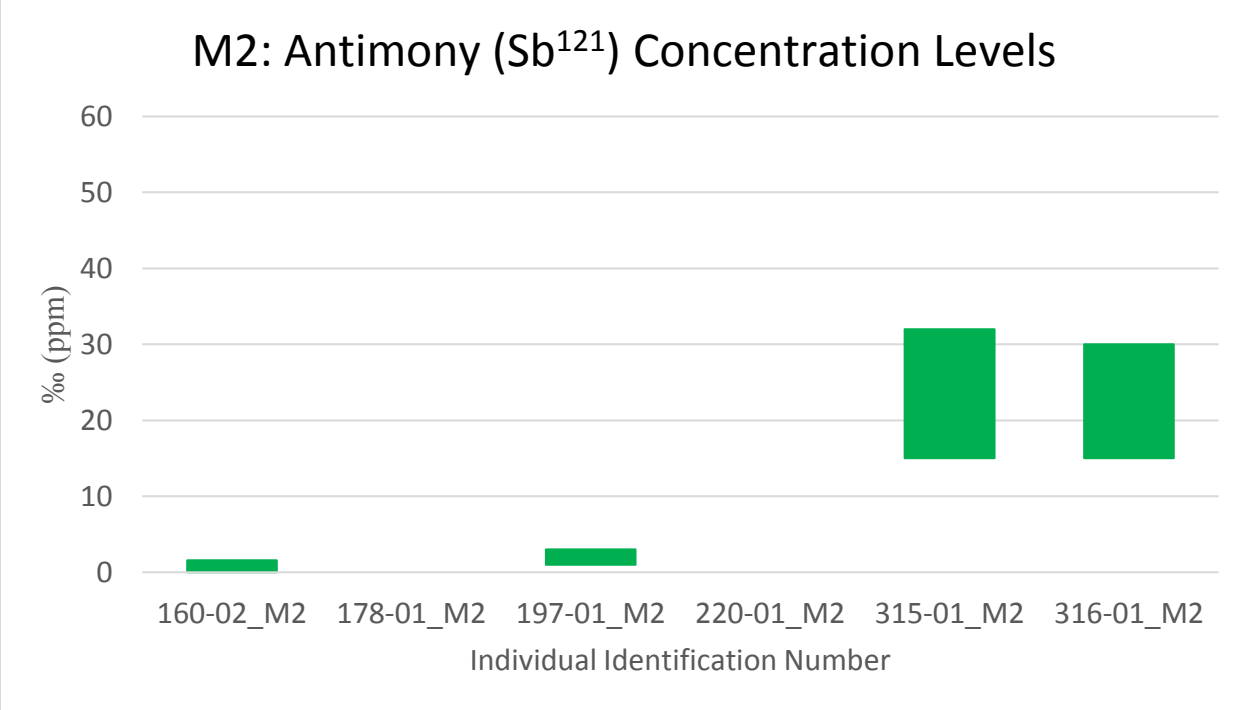

Figure 41 Graphed concentration values of antimony (Sb^{121}) for all second molar (M2) dental samples to evaluate inter-individual analysis.

Third Molar Comparison

The highest concentration values for antimony in the third molar sample are found in individual 178-01 (50 ppm) (Figure 42). Low concentration values were observed in individuals 220-01 (15 ppm) and 312-01 (13 ppm). The remaining third molar (160-02) no concentration of antimony.

Upon analysis of the graphed concentration values of antimony in third molars, it can be determined that 178-01 was exposed to high levels of antimony during early childhood, while concentration values of antimony for 160-02 suggests no exposure.

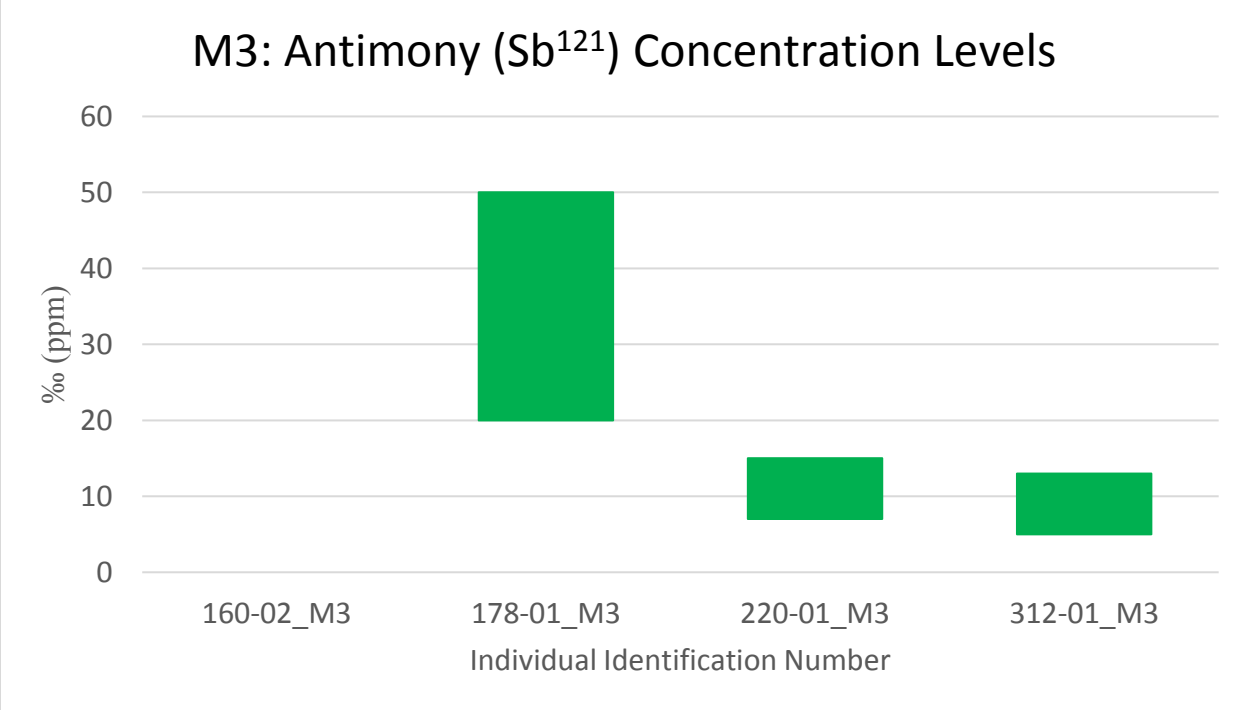

Figure 42 Graphed concentration values of antimony (Sb^{121}) for all third molar (M3) dental samples to evaluate inter-individual analysis.

Lead (Pb^{208})

First Molar Comparison

The highest concentration values for lead in the first molar sample are found in individuals 190-01 (30 ppm) and 315-01 (35 ppm) (Figure 43). Intermediate concentration was observed in individual 312-01 (10 ppm). The remaining first molars were observed to have lead concentration values measured to be less than 10 ppm.

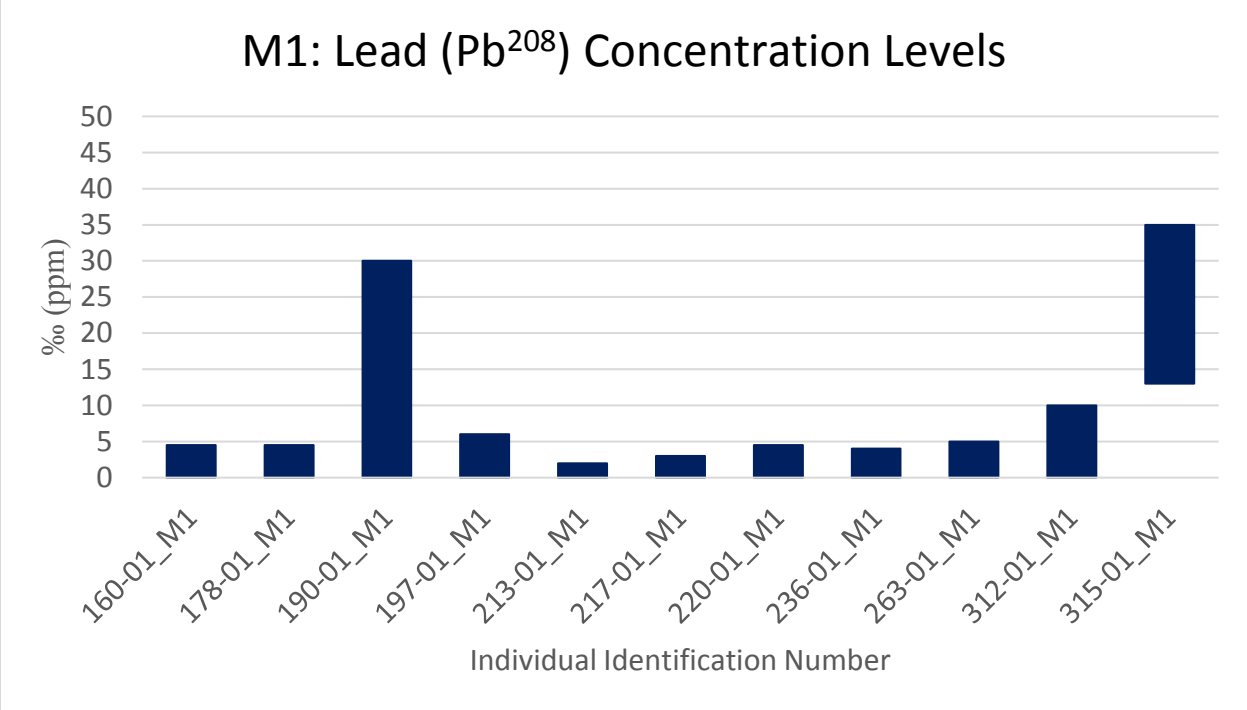

Figure 43 Graphed concentration values of lead (Pb^{208}) for all first molar (M1) dental samples to evaluate inter-individual analysis.

Second Molar Comparison

The highest concentration values for lead in the second molar sample are found in individual 315-01 (43 ppm) (Figure 44). The remaining second molars of the sample were observed to have low lead concentration values (< 10 ppm).

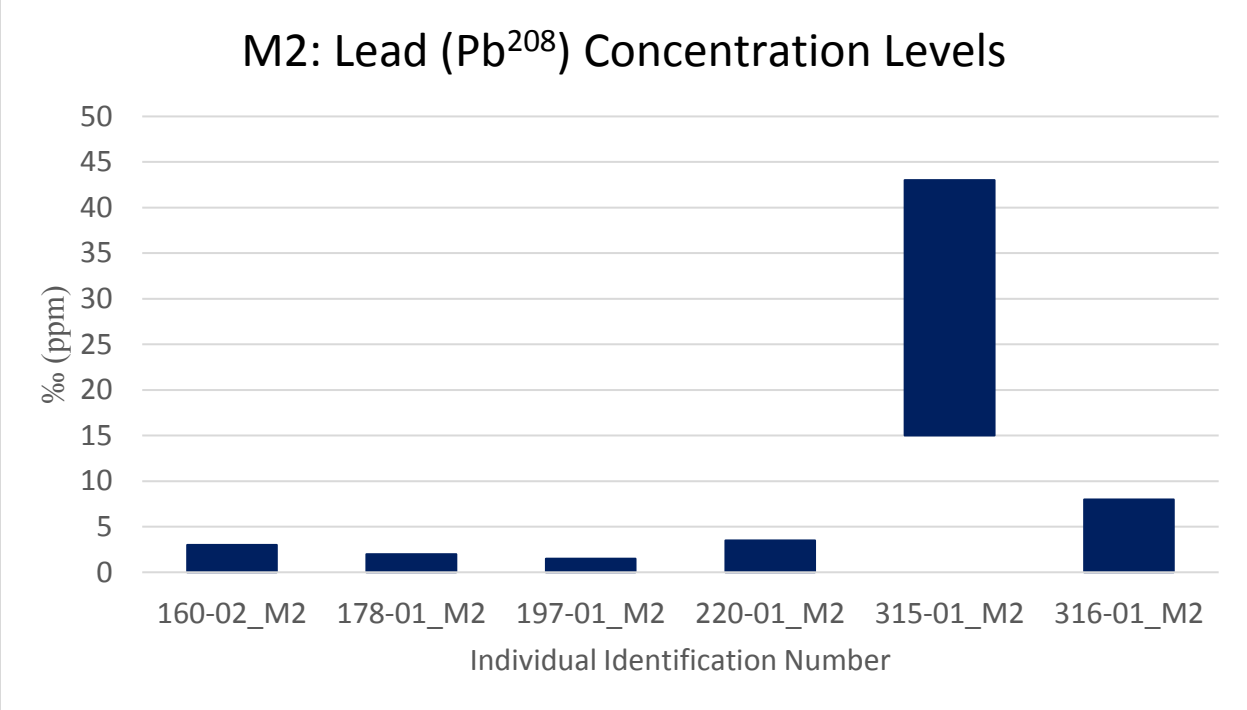

Figure 44 Graphed concentration values of lead (Pb^{208}) for all second molar (M2) dental samples to evaluate inter-individual analysis.

Third Molar Comparison

The highest concentration values for lead in the third molar sample are found in individuals 220-01 (5 ppm) and 312-01 (2 ppm) (Figure 45). The remaining third molars (160-02 and 178-01) exhibited no concentration of lead.

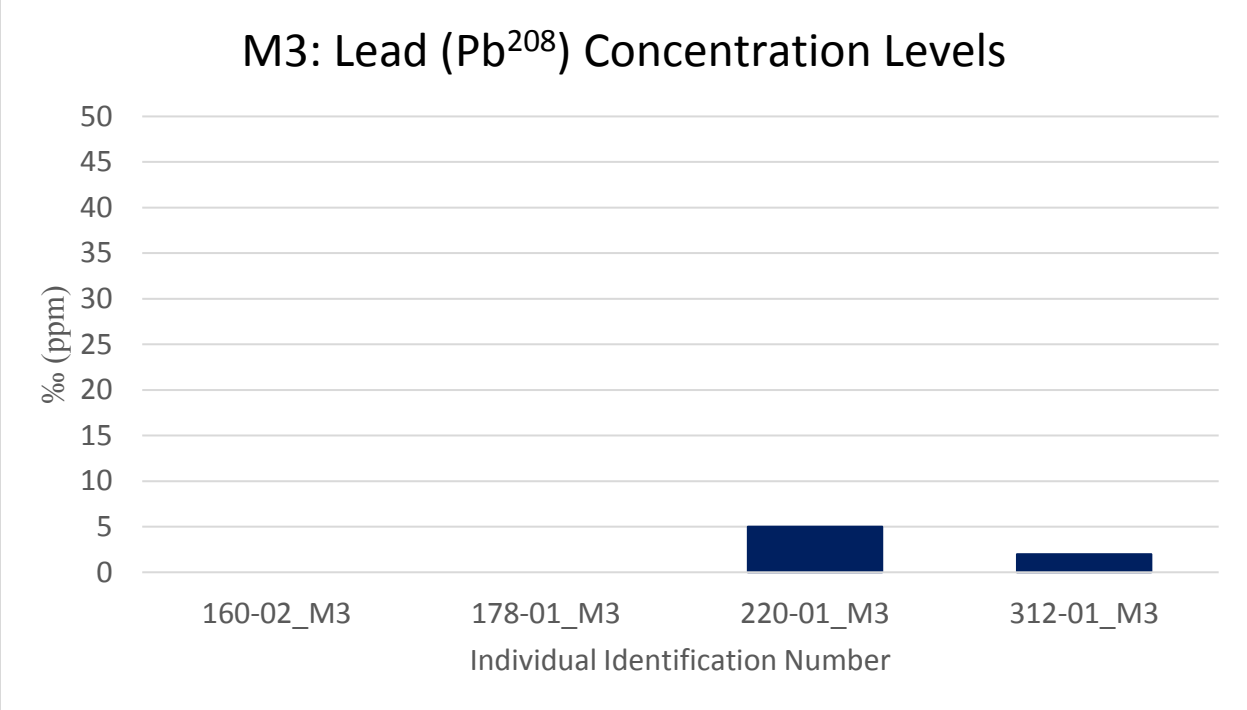

Figure 45 Graphed concentration values of lead (Pb^{208}) for all third molar (M3) dental samples to evaluate inter-individual analysis.

Intra-Individual Analysis

Intra-individual analysis was performed on the six individuals that had more than one molar available for comparison. Individuals 197-01 and 315-01 had the first and second molars available for elemental analysis. Individual 160-02 had second and third molars available, while individual 312-01 had the first and third molar available for analysis. Two individuals (178-01 and 220-01) had the first, second, and third molars available for analysis.

Copper

Copper values in 160-02 are observed to decrease from mid-childhood (M2) to late adolescence (M3). Individual 178-01 was observed to exhibit high concentration values of

copper within the first molar, during early childhood, with a decrease observed in the second molar, during mid-childhood, before slightly increasing concentrations in the third molar, during late adolescence. Individual 197-01 exhibits decreased copper concentration values as time progressed, from early childhood (M1), to mid-childhood (M2). The copper concentration in individual 220-01 exhibits similar values in early childhood (M1) and late adolescence (M3), with elevated concentrations observed during mid-childhood (M2). Concentration values in 312-01 of copper remain at the same values between early childhood (M1) and late adolescence (M3). An increase of copper in individual 315-01 is observed between early childhood (M1) and mid-childhood (M2).

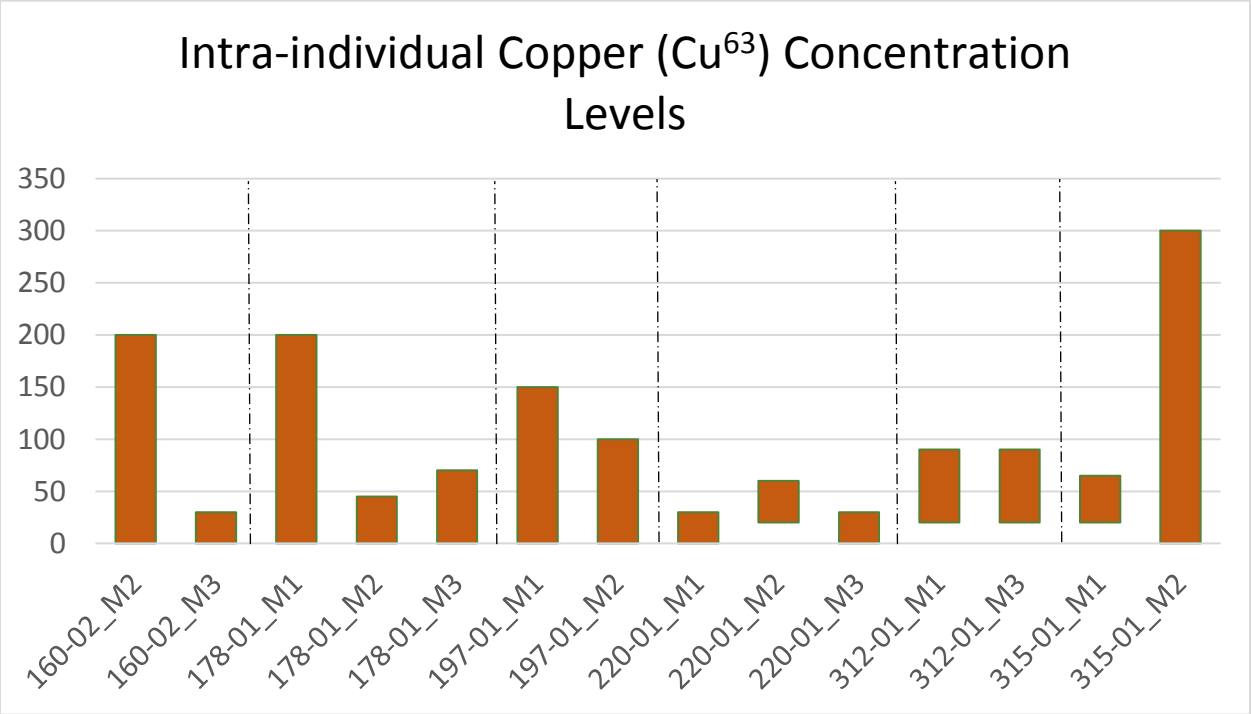

Figure 46 Outlined graphed concentration values of copper (Cu^{63}) for dental samples to evaluate intra-individual analysis.

Strontium

Strontium values in 160-02 are observed to decrease from mid-childhood (M2) to late adolescence (M3). Individual 178-01 also exhibited a decrease in strontium concentrations from early childhood (M1), throughout mid-childhood (M2), and into late adolescence (M3). Individual 197-01 exhibits decreased strontium concentration values as time progressed, from early childhood (M1), to mid-childhood (M2). The strontium concentration in individual 220-01 exhibits similar values in early childhood (M1) and late adolescence (M3), with decreased concentrations observed during mid-childhood (M2). Concentration values of strontium remain at the same values between early childhood (M1) and late adolescence (M3) for individual 312-01. Individual 315-01 exhibits consistent concentrations of strontium between early childhood (M1) and mid-childhood (M2).

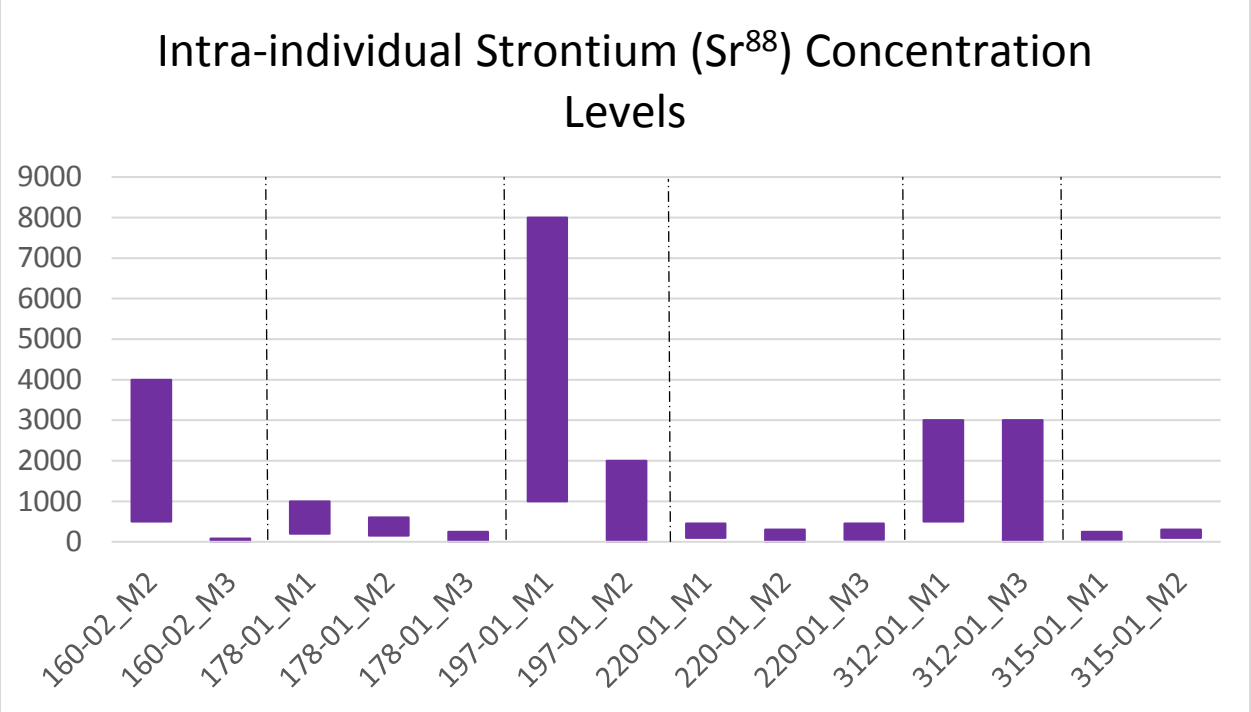

Figure 47 Outlined graphed concentration values of strontium (Sr^{88}) for dental samples to evaluate intra-individual analysis.

Zinc

Zinc values in 160-02 are observed to decrease from mid-childhood (M2) to late adolescence (M3). Individual 178-01 exhibits consistent zinc concentrations from early childhood (M1) throughout mid-childhood (M2), and a decrease in zinc into late adolescence (M3). Individual 197-01 exhibits consistent zinc concentration values as time progressed, from early childhood (M1), to mid-childhood (M2). The zinc values observed in individual 220-01 exhibits lower concentrations in early childhood (M1) and mid-childhood (M2), with increased concentrations observed during late adolescence (M3). Concentration values of zinc increase from early childhood (M1) to late adolescence (M3) for individual 312-01. Individual 315-01

also exhibits increased concentrations of zinc between early childhood (M1) and mid-childhood (M2).

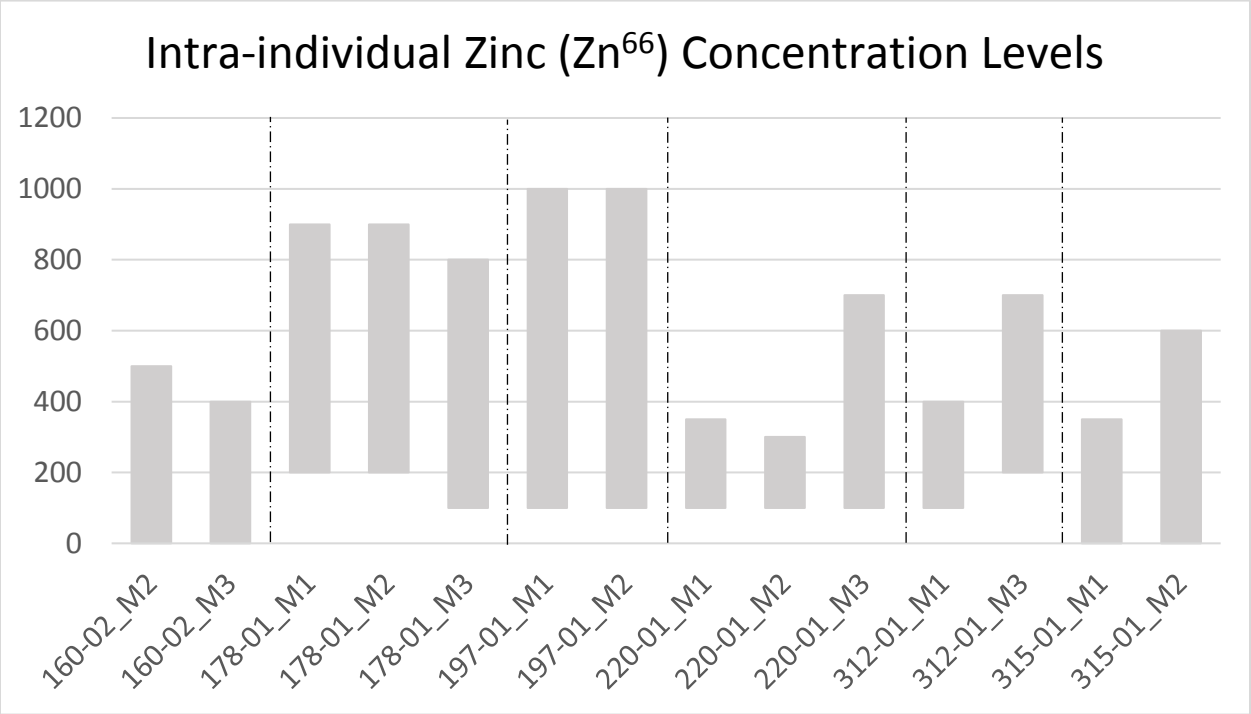

Figure 48 Outlined graphed concentration values of zinc (Zn^{66}) for dental samples to evaluate intra-individual analysis.

Antimony

Antimony values in 160-02 are observed to decrease from mid-childhood (M2) to late adolescence (M3). Individual 178-01 exhibits increased concentrations from early childhood (M1) to late adolescence (M3) and no concentration values of antimony are observed in mid-childhood (M2). Individual 197-01 exhibits consistent antimony concentration values as time progressed, from early childhood (M1) to mid-childhood (M2). The antimony values observed in individual 220-01 exhibit no concentration values in early childhood (M1) and mid-childhood

(M2), with increased concentrations observed during late adolescence (M3). Concentrations of antimony for individual 312-01 exhibit slightly increased values from early childhood (M1) to late adolescence (M3). Individual 315-01 also exhibits consistent concentrations of antimony between early childhood (M1) and mid-childhood (M2).

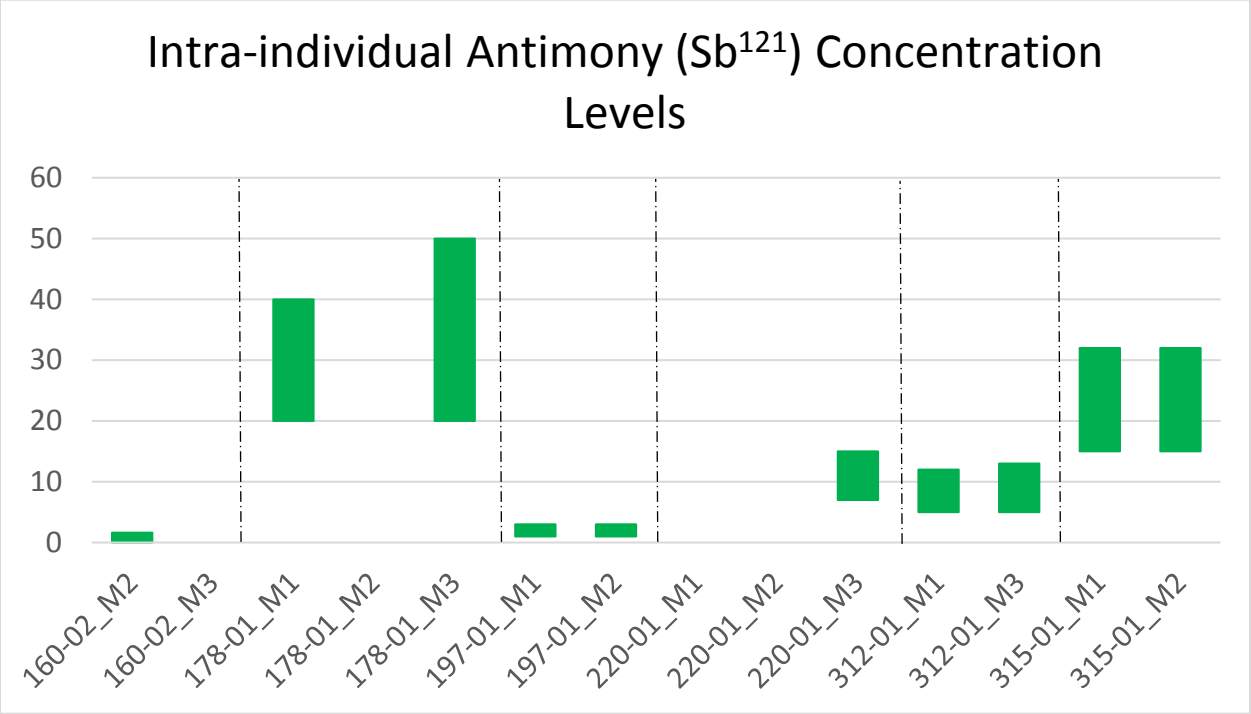

Figure 49 Outlined graphed concentration values of antimony (Sb^{121}) for dental samples to evaluate intra-individual analysis.

Lead

Lead values in 160-02 are observed to decrease from mid-childhood (M2) to late adolescence (M3). Individual 178-01 exhibits decreased lead concentrations from early childhood (M1) to mid-childhood (M2) and no concentration values of lead are observed in late adolescence (M3). Individual 197-01 exhibits decreased lead concentration values as time progressed, from early childhood (M1) to mid-childhood (M2). The lead values observed in

individual 220-01 fluctuate concentration values from early childhood (M1) and decrease in mid-childhood (M2), and increasing concentrations observed during late adolescence (M3). Concentrations of lead for individual 312-01 exhibit decreased values from early childhood (M1) to late adolescence (M3). Individual 315-01 increased concentrations of lead between early childhood (M1) and mid-childhood (M2).

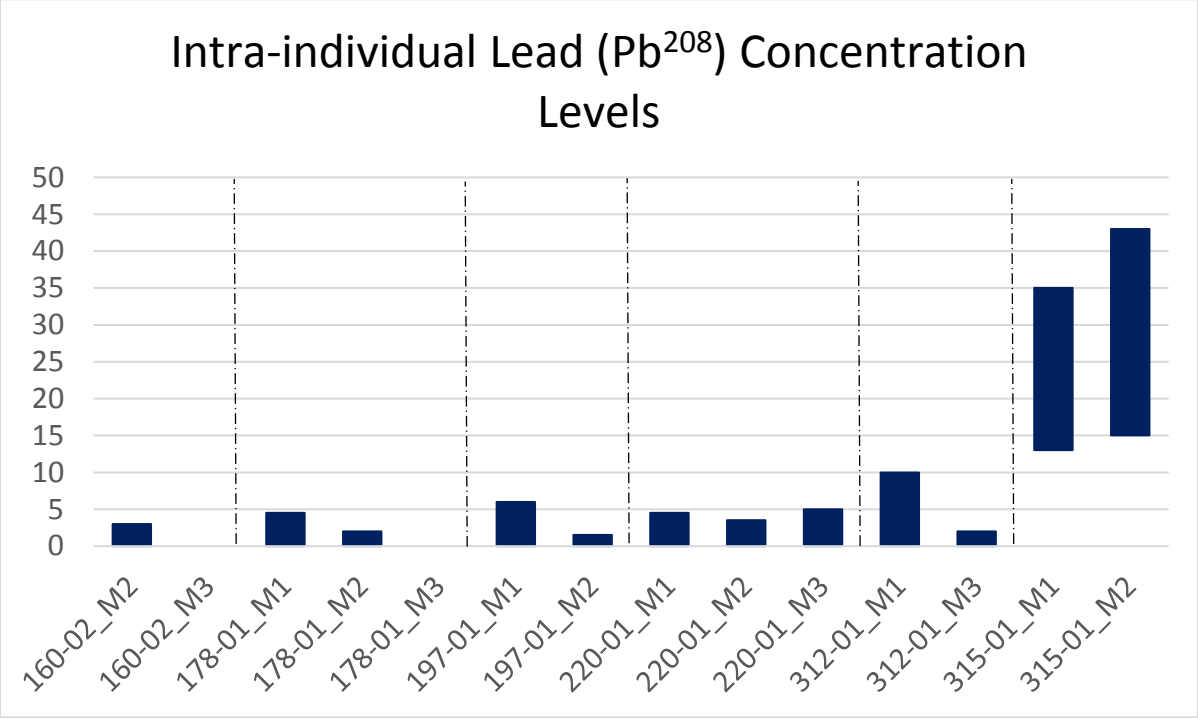

Figure 50 Outlined graphed concentration values of lead (Pb^{208}) for dental samples to evaluate intra-individual analysis.

CHAPTER SIX: DISCUSSION

Inter- individual comparisons of dietary consumption and cultural use of kohl will be evaluated based on concentration values of trace elements. Copper, zinc, strontium, antimony, and lead values will be compared within three developmental stages (first, second, and third molars). First molars begin developing while *in utero* and continue until approximately 9 years of age (Smith, 1991). Second molars typically develop from 4 to 15 years of age, while third molars are seen to develop later in adolescence between 9 and 20 years of age.

After inter-individual variation of dietary consumption and cultural use of kohl, intra-individual comparisons will be analyzed to determine if the presence of dietary variation is present and if the cultural use of kohl changes as the individual ages. An overview of element implications based on the literature can be observed in Appendix B.

Inter-Individual Analysis

A total of thirteen individuals were assessed for inter-individual variation of element concentration based on tooth sample. Analysis will be conducted based on first, second, and third molars for each of the five elements (copper, zinc, strontium, antimony, and lead). First molars will indicate diet and cultural use of kohl in early childhood, second molars will indicate diet and cultural habits for mid-childhood, and third molars will represent late adolescence.

Copper (Cu^{63})

Bioavailability of copper in the first molar is attributed to dietary habits during early childhood. Approximately 75 to 100 mg/day are considered optimal intake levels of copper for

physiological function. Excess amounts of copper can inhibit zinc absorption but is suggested to have minimal effects on physiological function (Chandra, 1985). Toxicity is observed to occur in individuals whose consumption is greater than 250 mg (Pais and Jones, 1997). Optimal sources of copper include unprocessed grains, nuts, legumes, organ meat, and seafood (Losee and Ludwig, 1970).

Although copper deficiency is rare, it has been observed in malnourished children (Bogden and Klevay, 2000). Since copper is a necessary component for the transport of iron, copper deficiency can decrease the necessary supply of iron and present as iron-deficiency anemia (Grosvenor and Smolin, 2010). Copper deficiency has been associated with anemia, neutropenia, and bone demineralization (Chandra, 1985). Dairy products, fruits, berries, and tubers are poor dietary sources of copper (Losee and Ludwig, 1970).

First Molar Comparison

Upon analysis of the graphed concentration values for copper, during early childhood, one individual (160-01) shows toxic values of copper (Pais and Jones, 1997). Two individuals exhibit concentration values consistent with copper deficiency (220-01, 263-01), suggesting malnourishment (Bogden and Klevay, 2000).

Individuals 178-01 (200 ppm) and 197-01 (150 ppm) exceed the recommended amount of copper intake, but not at toxic levels. Individual 160-01 (300 ppm) presents with toxic levels of copper concentrations. Individuals 190-01, 213-01, 217-01, 236-01, 312-01, and 315-01 present with concentration values that are optimal daily nutritional requirements. Individuals 220-01 and 263-01 exhibit concentration values of less than 50 mg within the first molar sample.

Second Molar Comparison

Analysis of copper values in second molars indicate dietary habits associated to mid-childhood. Individual 315-01 (300 ppm) was observed to have toxic concentration values of copper. Individuals 160-02 (200 ppm) and 316-01 (200 ppm) exceeded recommended copper values but were below toxic levels. Individual 197-01 (100 ppm) was observed to be within range of the recommended copper requirements. The remaining second molars (178-01 and 220-01) exhibited low concentration values of copper (< 100 ppm) that may result in copper deficiency if malnourishment throughout growth continues.

Third Molar Comparison

Individuals 178-01 (70 ppm) and 312-01 (90 ppm) were observed to meet dietary copper requirements. Individuals 160-02 and 220-01 had concentration values that would indicate malnourishment in these individuals during late adolescence (e.g. 30 ppm).

The general population appears to meet the copper requirements. During early childhood, one individual is observed to have toxic values, with one individual in mid-childhood exhibiting toxic values as well. Toxic values are not observed in late childhood. Copper deficiency is observed in two individuals for each compared age group of early childhood, mid-childhood, and late adolescence.

Full-term infants have an adequate supply of copper when born (Reilly, 2004). Dietary intake following birth determines the concentration values observed in permanent teeth. Infants that are exclusively breastfed exhibit higher copper concentrations than infants that are introduced to other sources of milk following birth (Chandra, 1985). Based on these graphs, we

can see that as individuals go through the aging process, copper concentration values decrease from the values observed in first molars to those observed in third molars. This change in concentration can be attributed to a shift in dietary habits as individuals mature. Newborn infants start out at optimal copper concentration values and infants that are breastfed exhibit have higher copper concentrations. When weaning commences and supplementary foods are introduced, copper values will begin to decrease. Decreased copper values can also be associated with a diet that contains poor sources of copper. Copper deficiency in the diet can result in impaired growth, increased risk to infection (Grosvenor and Smolin, 2010), and is associated with osteoporosis (Bogden and Klevay, 2000).

Strontium (Sr^{88})

Bioavailability of strontium in the first molar is indicative of residency and dietary habits during early childhood. Strontium values of plants vary according to their geographical region (Webb et al., 2005) and can, therefore, be utilized in determining migration patterns and residency. Bodnar and Dimitriu (2005) have determined average strontium concentrations of populations from various geographic regions to range between 100 and 1000 ppm. Strontium intake that exceeds these values can decrease calcium concentrations in bone (Asaduzzman, 2017).

Dietary change can be observed in the transition from infancy to childhood based on strontium values. Breastfed infants exhibit lower values of strontium, while infants that are weaned using cow milk exhibit higher values of strontium (Humphrey et al., 2007). Following the weaning period, dietary habits based on trophic behavior can further be determined as

strontium is observed to have an inverse relationship to protein in the diet (Dolphin et al., 2005). Since plants are a better source of strontium than meat, herbivores exhibit higher strontium concentration values than omnivores or carnivores (Webb et al., 2005). Further, diets high in legume consumption have increased strontium concentrations, while diets rich in cereal grains contain lower strontium values (Pais and Jones, 1997).

First Molar Comparison

During early childhood, high concentration values are observed in individual 197-01 and may indicate migration from place of birth. Intermediate concentration values are observed in individuals 160-01 (3000 ppm) and 312-01 (3000 ppm), which can indicate infants who may have relied on cow's milk instead of being breastfed. Intermediate detection values can be attributed to infants that were breastfed but were also supplemented by cow milk. The remaining first molars are observed to have lower strontium concentration values (< 900 ppm) that are consistent with individuals who were breastfed as infants.

Second Molar Comparison

During mid-childhood, high concentration values were observed in individual 160-02 (4000 ppm), this is however still within the estimated concentration range. Intermediate concentrations of strontium were observed in individual 197-01 (2000 ppm) and also suggests adequate intake of strontium. The remaining second molars exhibited low strontium concentration values (< 450 ppm) but are still consistent with recommended strontium intake. The increased concentration values observed in 160-02 and 197-01 can be indicative of a plant-

enriched diet when compared to other second molars whose concentration values of strontium are consistently low.

Third Molar Comparison

Analysis of strontium concentration values in late adolescence, as indicated by the third molar sample indicate optimal intake. High concentration values observed in individual 312-01 can be indicative of a plant-enriched diet when compared to other third molars whose concentration values of strontium are consistently low. Individual 160-02 exhibits strontium deficiency in the diet suggesting a diet that is rich in animal proteins.

Based on concentration values for strontium across the population, we can see that individual 197-01 may have migrated after birth due to the extreme difference in concentration values observed during early childhood (Webb et al., 2005). It can also be hypothesized that individual 160-01 and 312-01 were weaned using cow's milk based on the elevated concentration values (Humphrey et al., 2007). While all other individuals were most likely exclusively breastfed due to the low concentration values observed across the population during early childhood. During mid-childhood, individuals 160-02 and 197-01 exhibit increased strontium values compared to the rest of the second molar sample, which may indicate a plant-based diet. During late childhood, 312-01 exhibits higher strontium concentrations that may be consistent with a plant-based diet. Individual 160-02 is observed to have strontium deficiency, which may indicate a diet rich in animal proteins. According to Dolphin et al. (2005), a decrease in strontium values postnatal is associated with consumption of a higher quality diet, and increased consumption of animal protein.

Zinc (Zn^{66})

Bioavailability of zinc observed in the first, second, and third molars is attributed to dietary habits during childhood. Recommended dietary zinc intake varies by age (Reilly, 2004). Although excess dietary zinc is not toxic and is excreted from the body, high intake can interfere with copper absorption rates (Grosvenor and Smolin, 2010). High sources of zinc content are observed in human milk (Chandra, 1985), red meats, whole grains, and shellfish (Bogden and Klevay, 2000; Geissler and Powers, 2005).

Because of its physiological role in growth and development (Dolphin et al., 2005), juveniles and prenatal women are at a higher risk for zinc deficiency (Bogden and Klevay, 2000). Zinc deficiency has been associated with an impaired immune system and improper development of bone (Grosvenor and Smolin, 2010). Zinc absorption is inhibited by diets high in phytic acid that are found in cereals, legumes, and vegetables (Geissler and Powers, 2005), putting vegetarians at a higher risk for zinc deficiency than carnivores.

First Molar Comparison

Early childhood zinc concentration values were observed to have elevated concentration values in individuals 178-01, 190-01, 197-01, 213-01 and 217-01. These values may indicate individuals who were exclusively breastfed. Intermediate concentration values in individuals 160-01, 236-01, and 263-01 can indicate individuals that were weaned using cow's milk during breastfeeding. The low zinc concentration values observed in 220-01, 312-01, and 315-01 may indicate individuals that were not breastfed and instead fed with cow's milk.

Second Molar Comparison

The increased concentration of zinc observed in 178-01 and 197-01 during mid-childhood may indicate a diet rich in animal meat. The rest of the population is observed to have lower zinc values that can indicate an omnivorous diet. While individual 160-02 exhibits low zinc values that may be attributed to a plant-based diet.

Third Molar Comparison

During late adolescence, the population is observed to consume an omnivorous diet, with the exception of individual 160-02 whose zinc concentrations values appear low. This can indicate a diet that is rich in plant-life and may be attributed to a vegetarian diet.

Based on the graphed values of zinc, breastfed infants may be determined through high values exhibited during early childhood. With low values being consistent with individuals that may have been weaned at an early age using cow milk. During mid-childhood and late adolescence, high zinc concentrations have been associated with increased consumption of a high protein diet (Kern and Mathiason, 2012). Based on this finding, individuals 178-01 and 197-01, who both exhibit high concentration values for zinc, can be determined to have a protein-enhanced diet. Individual 160-02, however, was observed to have low concentration values for zinc during mid-childhood and late adolescence, which can be attributed to a vegetarian diet.

Antimony (Sb^{121})

As the availability of antimony decreased, lead sulfide became the main constituent for the eye cosmetic, kohl, which is traditionally used in Middle East cultures (Al-Ashban et al., 2004). There is no data for when lead increasingly become the main component in kohl. Analysis of concentration values would indicate if the individuals at Sedeinga applied kohl comprised of antimony.

First Molar Comparison

During early childhood, exposure to antimony is observed in individuals 178-01, 190-01, 217-01, and 315-01. Individuals 197-01, 213-01, 263-01, and 312-01 were observed to have minimal exposure during early childhood with low concentration values of antimony present. While other individuals (160-01, 220-01, 236-01) were not exposed to antimony at all during early childhood.

Second Molar Comparison

During mid-childhood, intermediate concentration values for antimony were found in individuals 315-01 and 316-01, which is consistent with exposure to antimony. Minimal exposure to antimony is observed in individuals 160-02 and 197-01. The remaining second molars (178-01, 220-01) showed no concentration of antimony and were, therefore, not exposed to the metal.

Third Molar Comparison

During late adolescence, one individual (178-01) was exposed to antimony in high concentrations. The low concentration values observed in individuals 220-01 and 312-01 indicate exposure to antimony occurred during late adolescence. The remaining third molar (160-02) suggests no exposure to antimony.

Upon analysis of the graphed concentration values of antimony in first molars, it can be determined that some individuals were exposed to high levels of antimony during early childhood (178-01, 190-01, and 217-01), while others had no exposure to antimony (160-01, 220-01, and 236-01). Exposure to antimony is observed to decrease across the population from early childhood to late adolescence. This can indicate use of antimony-based kohl products during early childhood on some individuals, while others were not exposed to this type of kohl at all during childhood. Children with minimal exposure to lead may have had contact with antimony through mother's use of antimony-based kohl, through contact with the mother, followed by "mouthing" by the child, antimony may have been ingested and not directly applied to the infant's skin. Individuals with zero concentration values were not exposed to antimony-based kohl products.

Lead (Pb^{208})

In a case study of infants from the Middle East, kohl, as a source of lead poisoning, was examined by Nir et al. (1992). Individuals were categorized into two categories of infants "kohled" and "non-kohled." Kohled infants were known to have direct contact with kohl through daily application of the cosmetic to their palpebral conjunctive. Non-kohled infants

were categorized as infants that were exposed to lead-based products through the mother's use. Kohled infants exhibited infants with lead levels greater than 20 ppm, while non-kohled infants exhibit an increase in lead levels. This can be compared to a study of prehistoric Nubian populations whose mean lead values were measured to be approximately 2 ppm (Budd et al., 2000). Concentration values of lead detected in contemporary kohl was determined to be between 8 and 15 ppm (Gondal et al., 2015). Further, individuals with low lead concentrations of 0.4 to 3.5 ppm were determined to be exposed to lead *in utero* in a contemporary population of lead miner families in Australia (Gulson, 1996).

First Molar Comparison

During early childhood, individuals 190-01 and 315-01 exhibit high concentrations of lead, suggesting application of lead-based kohl in infants within the first year of life. Intermediate concentrations were observed in individual 312-01 and is consistent with exposure to lead during early childhood, which is consistent with contemporary lead levels of contemporary kohl (Gondal et al., 2015). The remaining first molars (160-01, 178-01, 197-01, 213-01, 217-01, 220-01, 236-01, 263-01) were observed to have lead concentration values measured to be less than 10 ppm, which would suggest minimal exposure to lead. This can be attributed to the mother's use of kohl and absorption of lead that occurs *in utero* (Gulson, 1996).

Second Molar Comparison

During mid-childhood, high concentration values for lead are observed in individual 315-01. These values indicate direct use of lead-based kohl in this individual. The remaining second molars of the sample (160-02, 178-01, 197-01, 220-01, 316-01) were observed to have low lead

concentration values (< 10 ppm), and is consistent with values that suggest indirect exposure to lead.

Third Molar Comparison

During late adolescence, Individuals 220-01 and 312-01 exhibit low concentration values and is consistent with indirect exposure to lead. The remaining third molars (160-02 and 178-01) exhibited no concentration of lead. The lack of lead observed in 160-02 and 178-01 may suggest that these individuals did not use lead-based kohl products.

Lead concentrations are observed to decrease from early childhood (first molars) to late adolescence (third molars). Traditionally kohl is not applied to children's eyes following the first year. Females may continue use, but males do not apply again until maturity has been reached. The decrease in lead across the projected stages indicates the individuals in the sample discontinued their use of lead, or had limited exposure to lead-based kohl as they aged.

Intra-Individual Analysis

Six individuals, with more than one molar, were analyzed to determine intra-individual analysis.

Copper

Individual 160-02 exhibits a decrease in copper concentrations from the second molar to the third molar. This can be attributed to a dietary shift to sources with decreased copper values.

The insufficient copper values observed during late adolescence is consistent with malnourishment.

Individual 178-01 was observed to exhibit high concentration values of copper within the first molar with a dramatic decrease in the second molar before slightly increasing concentrations in the third molar. A loss of copper during mid-childhood may have resulted from a diet low in animal proteins but was altered during late adolescence with optimal values for copper observed.

Individual 197-01 exhibited high copper intake during early childhood, but concentration values of copper were not considered toxic. This was followed by intermediate values observed during mid-childhood that is attributed to proper intake of copper throughout childhood.

Individual 220-01 exhibits low initial values of copper in the first molar before a slight increase in the second molar was observed, with decreased concentration values exhibited in the third molar, returning to similarly observed values as the first molar. This can be attributed to a dietary change during mid-childhood that consisted of foods high in animal protein.

No change in copper concentration values was observed in individual 312-01 with diet remaining consistent between early childhood and late adolescence.

Further, individual 315-01 exhibited a significant increase in copper concentration values between the development of the first and second molar. This increase in copper values is consistent with a dietary shift from early childhood to mid-childhood, such as an increased consumption of animal proteins within the diet.

Strontium

Individual 160-02 exhibits a decrease in strontium concentrations from the second molar to the third molar. This can be attributed to a dietary shift to sources with decreased strontium values. The high concentration values observed during mid-childhood is consistent with a plant-based diet, while the decrease observed during late adolescence can be associated with the introduction of foods high in animal protein.

Individual 178-01 was observed to exhibit consistently decreasing concentrations of strontium from early childhood to late adolescence. The loss of strontium may have resulted from a diet that became more dependent on animal proteins, decreasing consumption of plants that are high in strontium.

Individual 197-01 exhibited high strontium intake during early childhood that may be associated with residency consistent of a different geographical location during early childhood. The intermediate values observed during mid-childhood are consistent with a plant-based diet.

Individual 220-01 exhibits consistently low values of strontium from early childhood to late adolescence. This can be attributed to an individual who was breastfed during early childhood and transitioned to a diet high in animal protein from mid-childhood to late adolescence.

No change in strontium concentration values was observed in individual 312-01 with diet remaining consistent between early childhood and late adolescence. This can be attributed to an infant that was weaned using cow's milk and strontium values that are consistent with a plant-based diet during late adolescence.

Further, individual 315-01 exhibited no change in strontium concentration values in diet, remaining consistent between early to mid-childhood. This is consistent with an individual who was not breastfed and whose diet during mid-childhood was animal-based.

Zinc

Individual 160-02 exhibits a decrease in zinc concentrations from the second molar to the third molar. This can be attributed to a dietary shift to sources with decreased zinc values. The high concentration values observed during mid-childhood is consistent with a diet high in animal proteins, while the decrease observed during late adolescence can be associated with a diet more enriched in plant-based food sources.

Individual 178-01 exhibits consistent zinc concentrations from early to mid-childhood with slightly decreasing values observed into late adolescence. The consistently high zinc values are consistent with breastfeeding during infancy with a diet high in animal proteins being introduced following the weaning period.

Individual 197-01 exhibited high zinc intake during early childhood that is associated with infants who are breastfed. The increased values observed during mid-childhood are consistent with a diet high in animal proteins.

Individual 220-01 exhibits low values of zinc from early to mid-childhood. The low values observed in 220-01 during early childhood are associated with an infant who was weaned using cow's milk. Consistently low zinc values observed during mid-childhood indicate a diet that is low in animal protein. A shift in dietary habits is observed during late adolescence when

zinc values are observed to increase and are consistent with an increase in animal proteins to the diet.

Individual 312-01 exhibits an increase in zinc values from early childhood to late adolescence. The low zinc values observed during early childhood can be attributed to an infant that was weaned using cow's milk. The increased concentration values observed during late adolescence are consistent with an omnivorous diet.

Further, individual 315-01 exhibited no change in strontium concentration values in diet, remaining consistent between early to mid-childhood. This is consistent with an individual who was not breastfed and whose diet during mid-childhood was animal-based.

Antimony

Individual 160-02 exhibits a decrease in antimony concentrations from the second molar to the third molar. This can be attributed to decreased exposure from mid-childhood to late adolescence. The values observed in mid-childhood are consistent with minimal exposure of antimony. No exposure to antimony is observed during late adolescence.

Individual 178-01 exhibits high antimony concentrations during early childhood with no exposure to antimony observed in mid-childhood. This individual was exposed to high concentrations of antimony during late adolescence. The values observed during early childhood and late adolescence are consistent with direct exposure to an antimony-based kohl product.

Individual 197-01 exhibited low antimony values across this individual's life span from early to mid-childhood. Concentration values observed during early childhood suggest indirect

exposure *in utero.* The antimony values observed during mid-childhood are consistent with indirect exposure.

Individual 220-01 exhibits antimony values consistent with no exposure during early to mid-childhood. The antimony values are observed to increase during late adolescence and suggest exposure.

Individual 312-01 exhibits consistent antimony concentrations from early childhood to late adolescence. The intermediate values observed during early childhood are consistent with direct exposure. Further, values observed during late adolescence suggest indirect exposure.

Individual 315-01 exhibits intermediate antimony values from early to mid-childhood. These values suggest direct exposure and use of antimony-based kohl products during childhood.

Antimony concentration values of this sample indicate that high levels of antimony were found in some individuals included in this sample. It was also observed that individuals with concentration values of antimony were consistent across molar samples presented from one individual. Individuals with high antimony values exhibited consistency of concentration values for antimony. Likewise, individuals who had low antimony values in the first molar, also exhibited low antimony values in the second molar or third molar. This would indicate consistent environmental exposure or use of antimony products across lifespan. Although 178-01 exhibits inconsistent concentration values for antimony across lifespan

Lead

Individual 160-02 exhibits a decrease in lead concentrations from the second molar to the third molar. This can be attributed to a decrease in exposure from mid-childhood to late adolescence. The values observed in mid-childhood are consistent with minimal exposure to lead. No exposure to antimony is observed during late adolescence.

Individual 178-01 exhibits low lead concentrations during early to mid-childhood. This can be attributed to a decrease in exposure, with the highest amount of exposure observed while *in utero*, from mother's use of lead-based kohl during pregnancy. No exposure to lead is observed during late adolescence.

Individual 197-01 exhibited low antimony values from early to mid-childhood. Concentration values observed during early childhood suggest indirect exposure *in utero.* The lead values observed during mid-childhood are consistent with indirect exposure.

Individual 220-01 exhibits lead values that are consistently low across childhood. Concentration values observed during early childhood suggest indirect exposure *in utero.* The lead values observed during mid-childhood and late adolescence are consistent with indirect exposure.

Individual 312-01 exhibits increased lead concentrations from early childhood that suggests indirect exposure while *in utero.* Concentration values observed during late adolescence suggest minimal indirect exposure to lead-based kohl products.

Individual 315-01 exhibits increased lead values from early to mid-childhood. These values suggest direct exposure and use of lead-based kohl products during childhood.

With the exception of individual 315-01, we can see the overall concentration values of lead decrease as individuals go through the aging process. This can be attributed to female use of lead-based kohl products that enter into the tooth during development while the individual is *in utero*. The decrease in lead observed in individuals is consistent with the discontinued use of kohl beyond the first year of age. Concentrations of lead are still observed during mid-childhood likely because of continued indirect contact with the mother. The low concentrations observed during late adolescence are consistent with the lack of contact to lead-based products, as contact with the mother is minimalized.

These values could also suggest that all individuals are male, with individual 315-01 being female. This can be determined as the concentration of lead increases with age. Since females typically continue application of kohl beyond the first year of life, the high concentration values would be typical for an individual who applies kohl daily.

CHAPTER SEVEN: CONCLUSION

This research aimed to answer the following research questions based on the trace element analysis of 21 dental samples from 13 individuals excavated from the elite Nubian Meroitic Cemetery of Sedeinga, located in northern Sudan for the period between the 1st c. AD to the 4th c. AD. The focus of this study was to answer the following questions: 1) Was intra-individual variation present in dietary habits or cultural behaviors based on elements found within an individual's multiple molars after analysis; 2) Was an inter-individual variation apparent, based on developmental age, that indicated a distinction between dietary habits against all individuals; and 3) Based on known medicinal and cosmetic use of kohl in neighboring societies, as well as archaeological evidence found at Sedeinga, if individuals will have used kohl based on observed increased levels of lead or antimony?

Mapped concentration values of trace elements were used to determine inter- and intra-individual variation in a Nubian population from Sedeinga has given a chronological insight into dietary habits and cultural use of kohl. Detected dietary habits based on inter-individual analysis exhibits variation in diet across the population. Cultural use of antimony or lead based kohl was observed within the population. Elevated concentration values are observed during early childhood and decreases as individuals enter mid-childhood and into late adolescence. Detected dietary habits observed during intra-individual analysis exhibit steady diet throughout childhood. The cultural use of kohl or antimony observed within the individuals of this sample are observed to have decreased exposure to lead- or antimony- based products as concentration values

decrease as they age from early childhood to mid-childhood with minimal to no exposure observed during late adolescence.

By conducting trace element analysis across the sample based on first molar (early childhood), second molar (mid-childhood), and third molar (late adolescence), trends in dietary habits and cultural habits were revealed. Information revealed about first molars provided dietary and cultural habits that were attributed to the mother. Trace element values observed in second and third molars are exclusive to the individual's dietary habits.

Cultural use of antimony or lead based kohl was observed to decrease as the individual aged. This was attributed to increased exposure while *in utero* and use of the cosmetic by the mother during pregnancy. The decreased values observed during mid-childhood can be attributed to minimal exposure to kohl by the individual. Further, little to no concentration values of antimony and kohl are associated with no exposure to any kohl products during late adolescence.

Trace element analysis of dietary and cultural habits were then examined in individuals that had more than one molar analyzed in this sample.

Individual 160-02 had the second and third molar available for analysis. Element concentrations used to determine dietary habits of individual 160-02 indicate malnourishment with decreased copper and zinc values. Low zinc concentrations suggest a diet that is plant-based during mid-childhood, but the low strontium values observed in late adolescence indicate the introduction of animal proteins to the diet. Further, antimony and lead values decreased from minimal to no exposure.

Individual 178-01 had the first, second, and third molar available for analysis. Element concentrations used to determine dietary habits indicate breastfeeding with high zinc values observed during early childhood. Decreasing strontium values, consistently high zinc values, and indicate a diet that became more dependent on animal proteins than plant-life as the individual matured. Further, antimony values suggest direct exposure during early childhood and late adolescence, with no exposure observed during mid-childhood. Lead values suggest exposure while *in utero*, as a result of mother's use during pregnancy and exposure during mid-childhood. No exposure to lead was observed during late adolescence.

Individual 197-01 had the first and second molar available for analysis. The high strontium concentrations observed in this individual indicate migration from a different geographical region. Element concentrations used to determine dietary habits indicate breastfeeding with high zinc values and high copper values observed during early childhood. Intermediate strontium values and high zinc values indicate an omnivorous diet. Further, antimony and lead values suggest exposure while *in utero*, as a result of mother's use during pregnancy and indirect exposure during mid-childhood.

Individual 220-01 had the first, second, and third molar available for analysis. Element concentrations used to determine dietary habits indicate an individual who was weaned using cow's milk with low zinc values observed during early childhood. Copper, strontium, and zinc values indicate a diet that was enriched in animal protein during late adolescence. Further, antimony values suggest no exposure during early to mid-childhood, while values in late adolescence suggest indirect exposure. Lead values suggest exposure while *in utero*, as a result

of mother's use during pregnancy and indirect exposure during mid-childhood to late adolescence.

Individual 312-01 had the first and third molar available for analysis. Element concentrations used to determine dietary habits indicate an individual who was weaned using cow's milk with low zinc values observed during early childhood. Copper, strontium, and zinc values indicate an omnivorous diet. Further, antimony and lead values suggest exposure while *in utero*, as a result of mother's use during pregnancy and indirect exposure during late adolescence.

Individual 315-01 had the first and second molar available for analysis. Element concentrations used to determine dietary habits indicate an individual who was weaned using cow's milk with low zinc values observed during early childhood. Copper, strontium, and zinc values indicates a diet high in animal proteins. Further, antimony and lead values suggest direct exposure while *in utero*, as a result of mother's use during pregnancy, and use of lead and antimony based kohl products during mid-childhood.

Limitations

One of the limitations of this study involves the small sample size available for analysis. The sample size consisted of 13 individuals present for inter-individual analysis and only six individuals available for intra-individual analysis. It was further noted that the sample available for analysis belonged to a specific group of elite individuals. The literature on the excavations of Sedeinga notes that this cemetery, based on mortuary structures, contained burials of the elite.

To gather full perspective and comprehension of a society or culture, retrieving information from all individuals is necessary, otherwise only partial representation of the population is observed.

Another limitation includes the inability to further map other elements' concentration values to gain better insight into the Nubian diet. This has been attributed to errors observed in the calibration curve that prevented two-dimensional mapping of these elements. The issues of calibration for elements Mg^{24}, P^{31}, S^{32}, and Fe^{56} have been noted and will be corrected for in future research.

Future Research

Further research can be conducted using the data obtained during the initial ablation process. Since this research focused on permanent molars only, further analysis and extension of individual life histories can be achieved by adding tissues, such as bone, hair samples, and deciduous teeth if available. Data retrieved from bone can help to interpret dietary habits within the last ten years prior to death. Depending on length, hair samples can provide element information for up to several years preceding death. Lastly, other teeth such as deciduous teeth can provide information from the *in utero* period reflecting material intake, allowing researchers to study multiple generations.

Approximating age of element deposition could also be informative in future research analysis. Using the neonatal line as a point of reference and understanding the incremental growth period in teeth would allow future research to approximate a timeline of an individual's life history based on the deposition of elements within the hydroxyapatite lattice. This information could be utilized in understanding dietary change throughout development, as well

as cultural practices, such as discontinued use of kohl within the Nubian culture. This can be created through geospatial mapping to determine relationship of elements through spatial analysis.

Since trace element analysis is still considered a new method using technological advancements, the understanding of its uses and applications are still evolving. Future research on this sample combined with other methodologies, further literature review, and continual excavations on Sedeinga can attribute to researchers' knowledge of the people of Sedeinga. Topics to be considered further include: Nubian diet, prominent illnesses, burial practices, and cultural behaviors. This information can help bridge the gap of knowledge within the Nubian culture and attribute to understanding early practices of society and how modern-day civilizations have changed after centuries of cultural evolution have occurred.

APPENDIX A: ELEMENT MAPS

IIT 160-01_M1

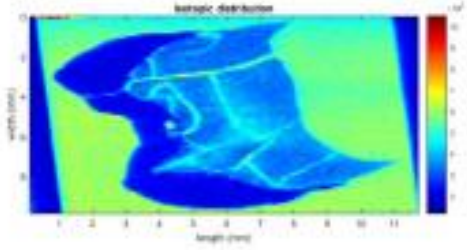

Carbon (C^{13}) detection

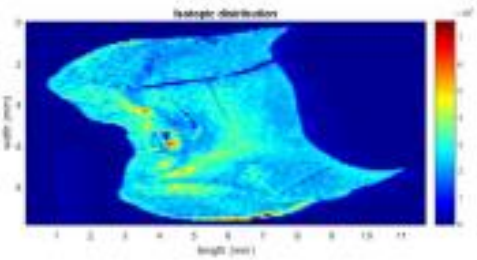

Calcium (Ca^{44}) detection

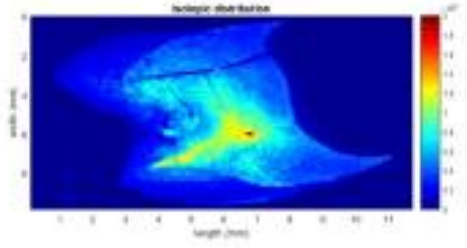

Magnesium (Mg^{24}) detection

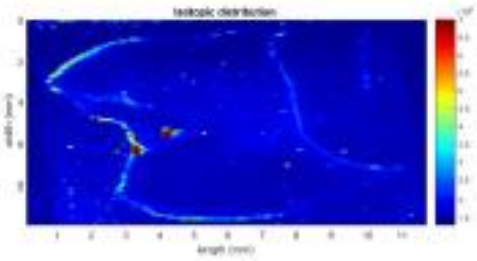

Iron (Fe^{56}) detection

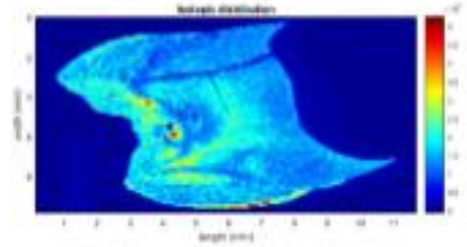

Phosphorus (P^{31}) detection

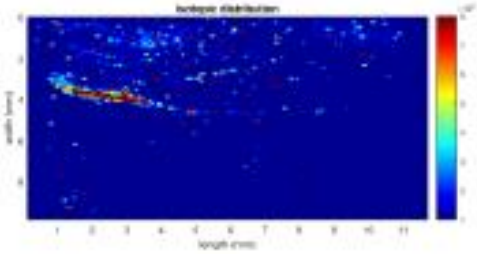

Copper (Cu^{63}) detection

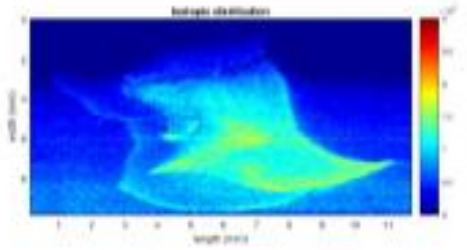

Sulfur (S^{32}) detection

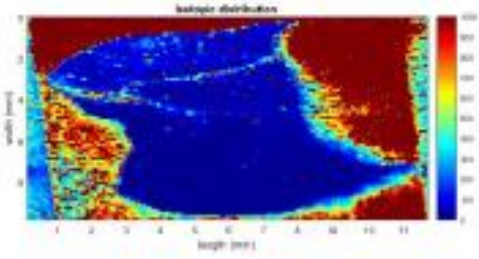

Copper (Cu^{63}) concentration

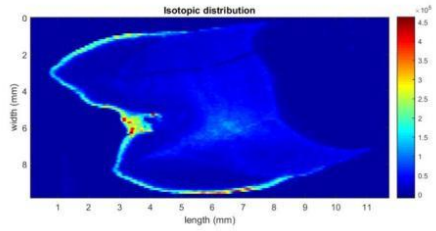

Zinc (Zn^{66}) detection

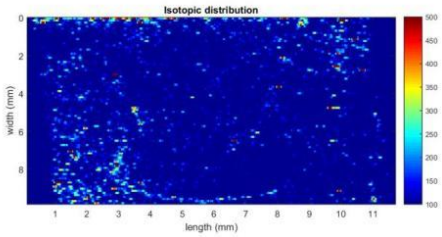

Antimony (Sb^{121}) detection

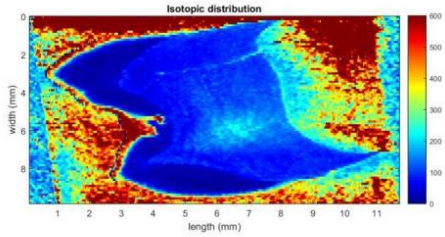

Zinc (Zn^{66}) concentration

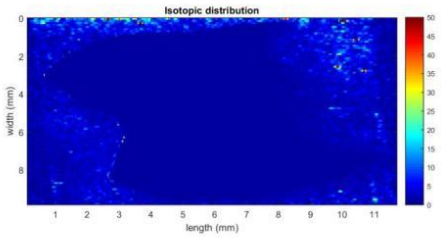

Antimony (Sb^{121}) concentration

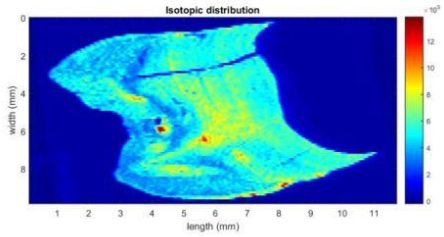

Strontium (Sr^{88}) detection

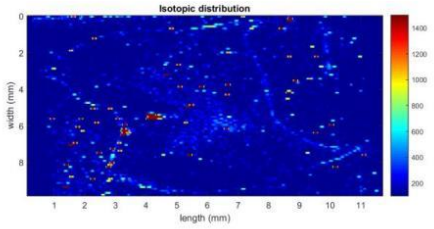

Lanthanum (La^{139}) detection

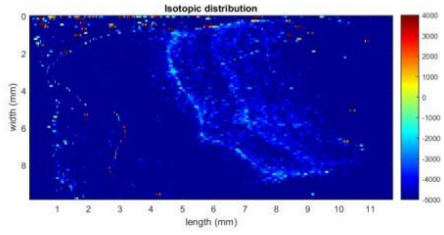

Strontium (Sr^{88}) concentration

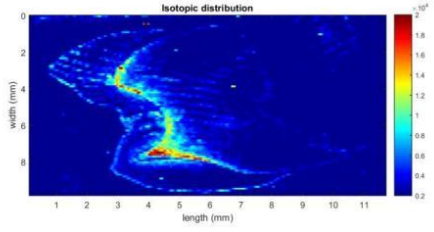

Lead (Pb^{208}) detection

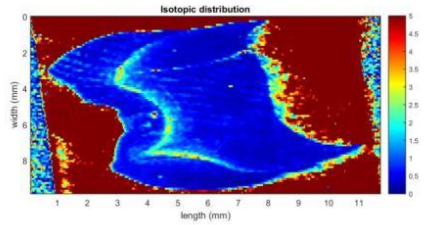

Lead (Pb^{208}) concentration

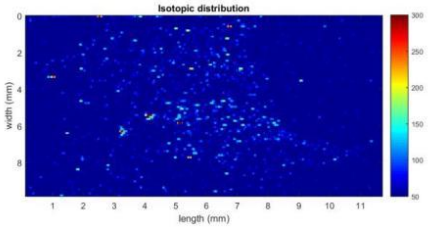

Uranium (U^{238}) detection

IIT 160-02_M2

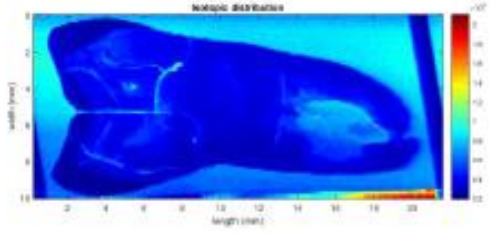

Carbon (C^{13}) detection

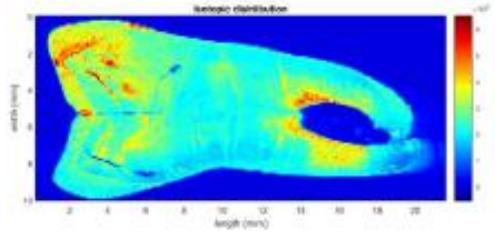

Calcium (Ca^{44}) detection

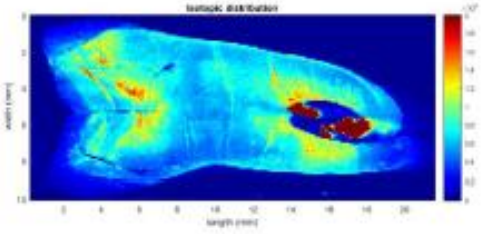

Magnesium (Mg^{24}) detection

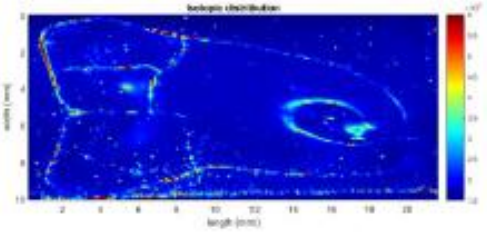

Iron (Fe^{56}) detection

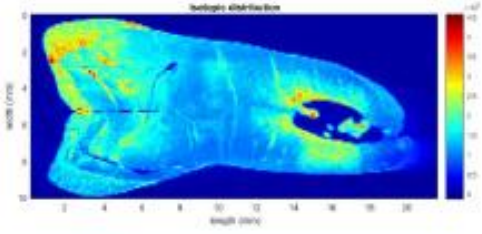

Phosphorus (P^{31}) detection

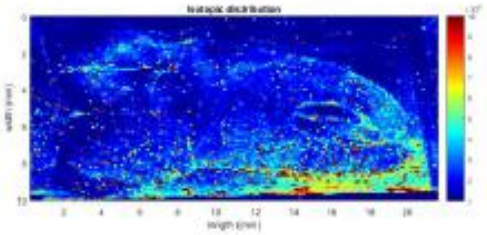

Copper (Cu^{63}) detection

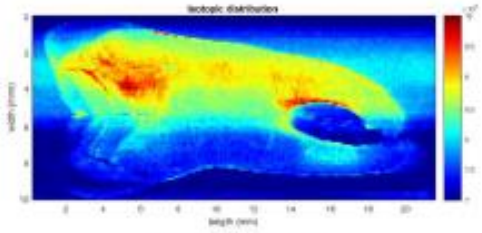

Sulfur (S^{32}) detection

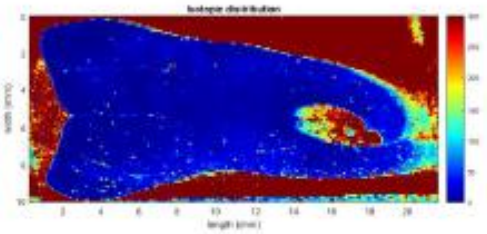

Copper (Cu^{63}) concentration

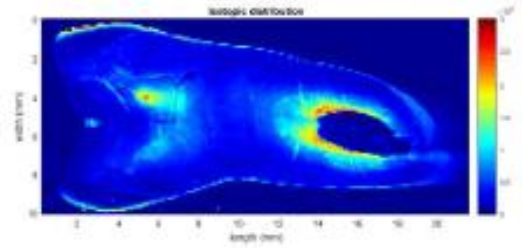

Zinc (Zn^{66}) detection

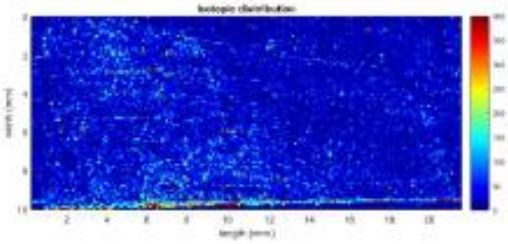

Antimony (Sb^{121}) detection

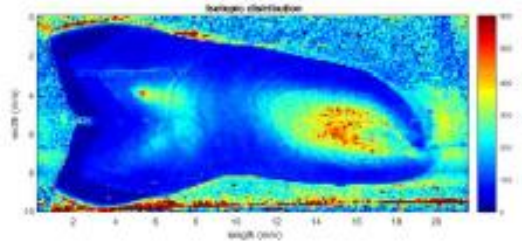

Zinc (Zn^{66}) concentration

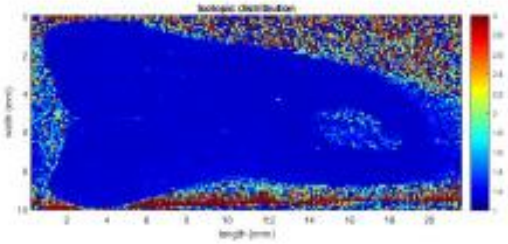

Antimony (Sb^{121}) concentration

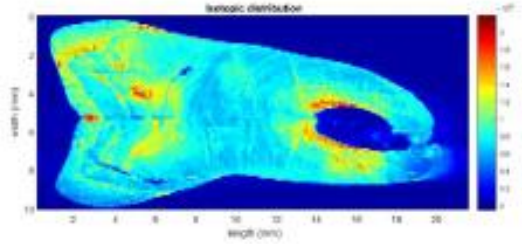

Strontium (Sr^{88}) detection

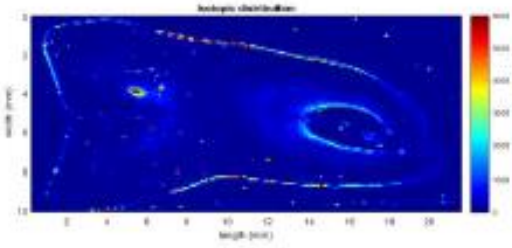

Lanthanum (La^{139}) detection

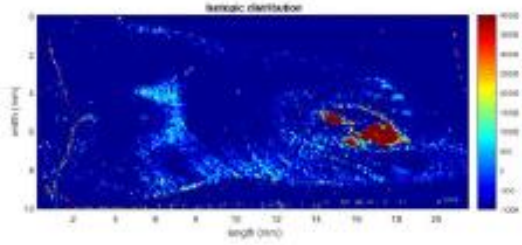

Strontium (Sr^{88}) concentration

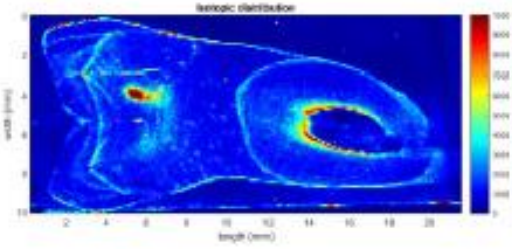

Lead (Pb^{208}) detection

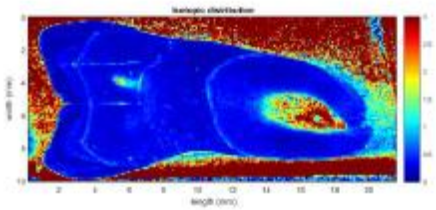

Lead (Pb^{208}) concentration

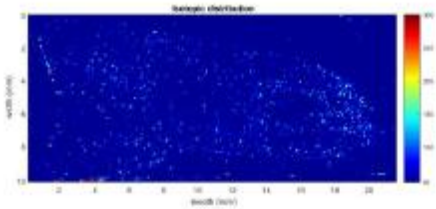

Uranium (U^{238}) detection

IIT 178-01_M1

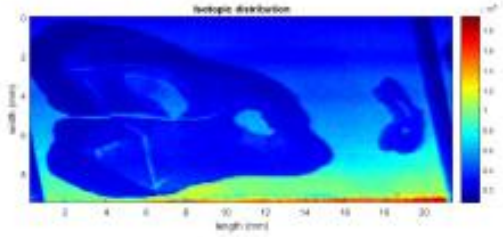

Carbon (C^{13}) detection

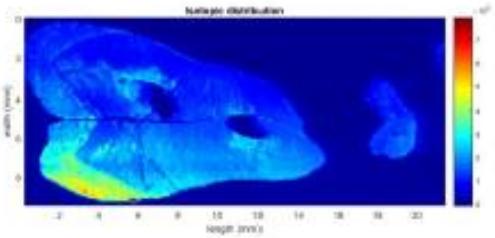

Calcium (Ca^{44}) detection

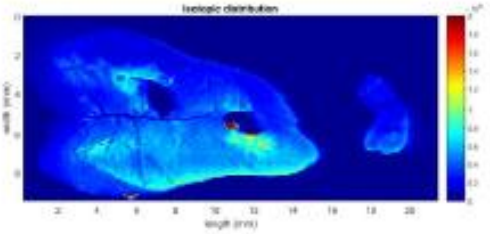

Magnesium (Mg^{24}) detection

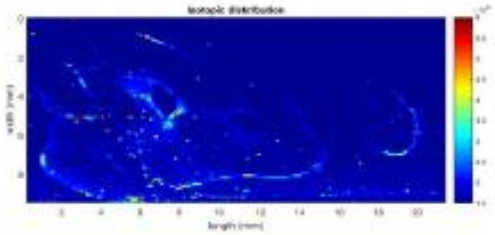

Iron (Fe^{56}) detection

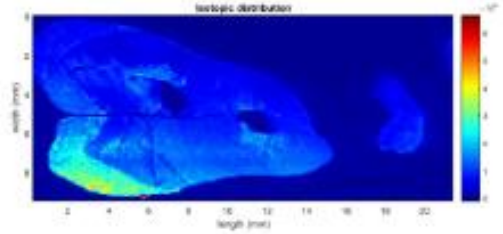

Phosphorus (P^{31}) detection

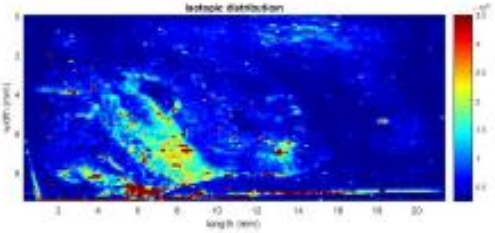

Copper (Cu^{63}) detection

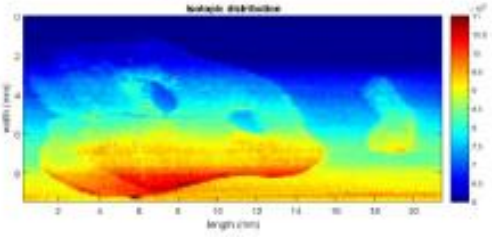

Sulfur (S^{32}) detection

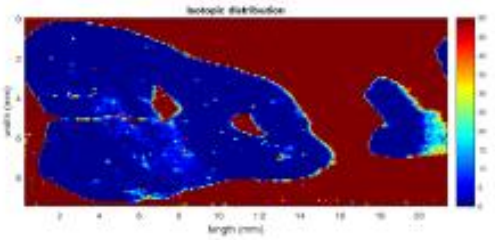

Copper (Cu^{63}) concentration

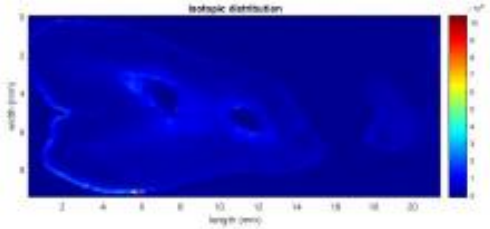

Zinc (Zn^{66}) detection

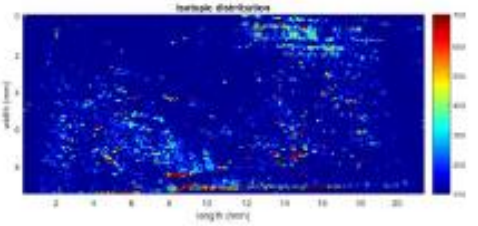

Antimony (Sb^{121}) detection

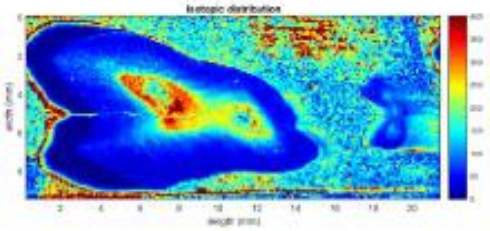

Zinc (Zn^{66}) concentration

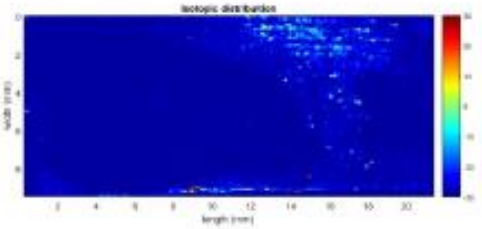

Antimony (Sb^{121}) concentration

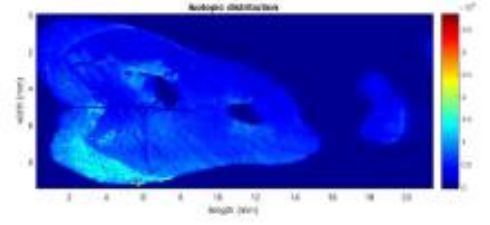

Strontium (Sr^{88}) detection

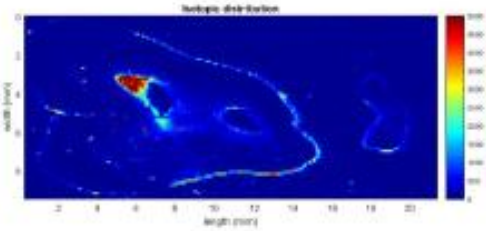

Lanthanum (La^{139}) detection

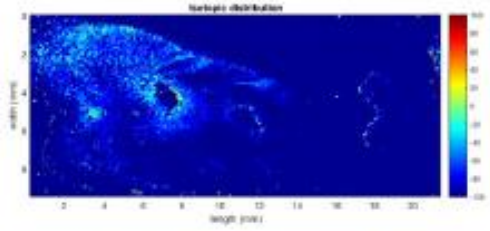

Strontium (Sr^{88}) concentration

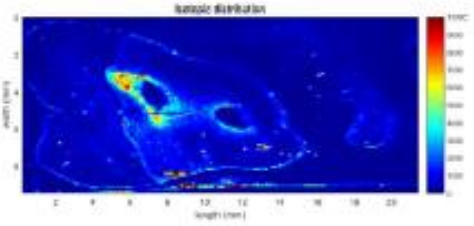

Lead (Pb^{208}) detection

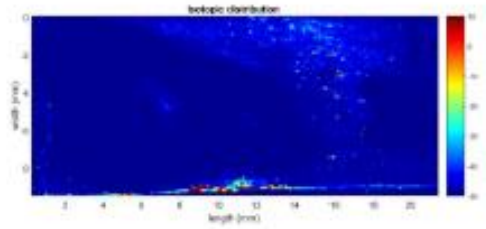

Lead (Pb^{208}) concentration

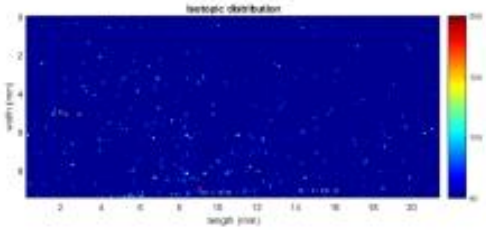

Uranium (U^{238}) detection

IIT 178-01_M3

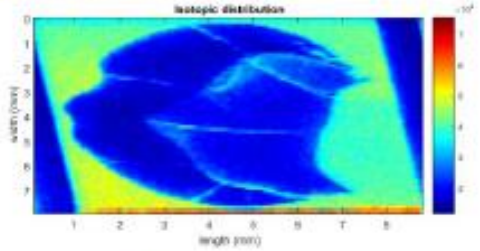

Carbon (C^{13}) detection

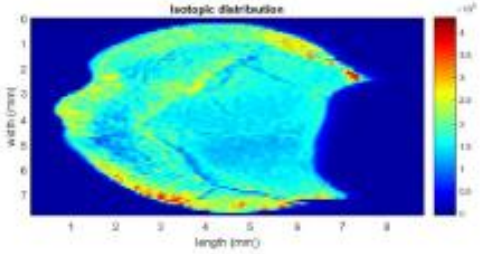

Calcium (Ca^{44}) detection

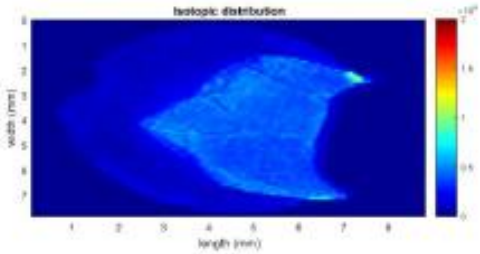

Magnesium (Mg^{24}) detection

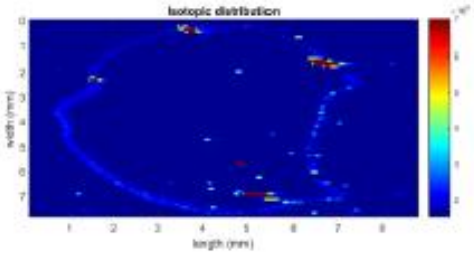

Iron (Fe^{56}) detection

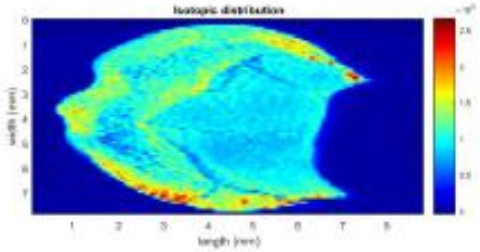

Phosphorus (P^{31}) detection

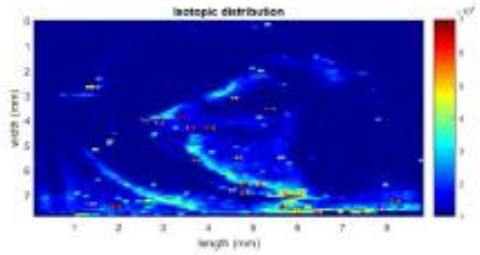

Copper (Cu^{63}) detection

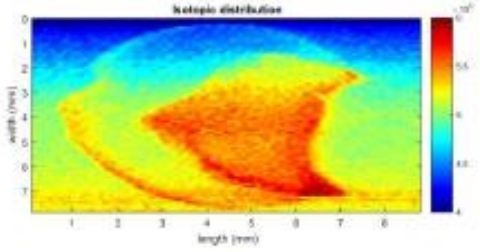

Sulfur (S^{32}) detection

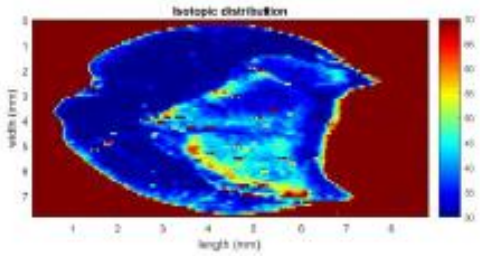

Copper (Cu^{63}) concentration

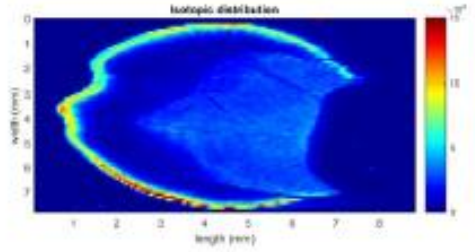

Zinc (Zn^{66}) detection

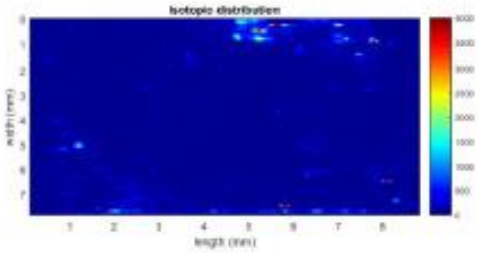

Antimony (Sb^{121}) detection

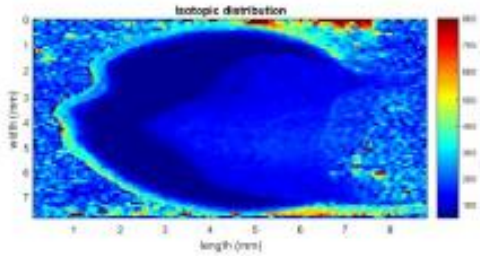

Zinc (Zn^{66}) concentration

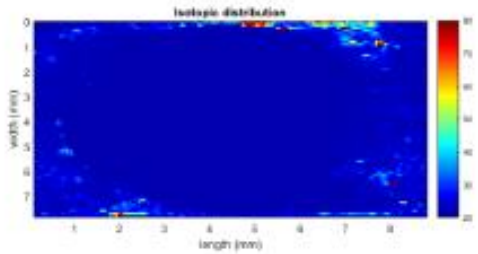

Antimony (Sb^{121}) concentration

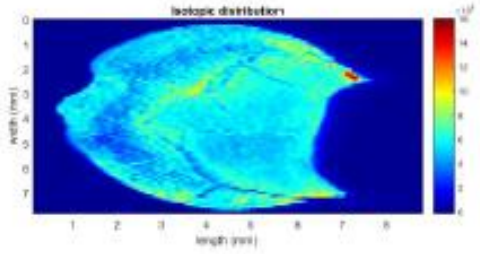

Strontium (Sr^{88}) detection

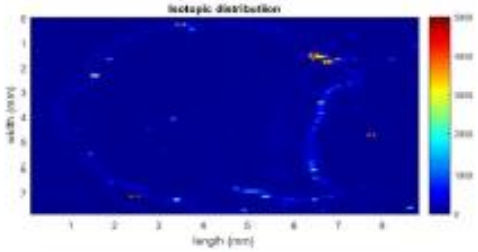

Lanthanum (La^{139}) detection

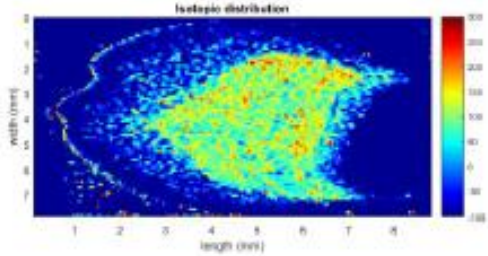

Strontium (Sr^{88}) concentration

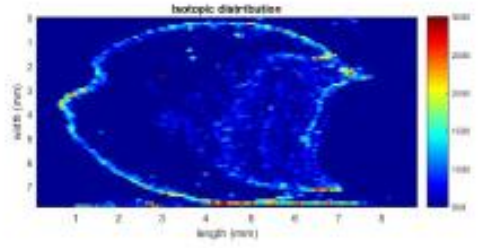

Lead (Pb^{208}) detection

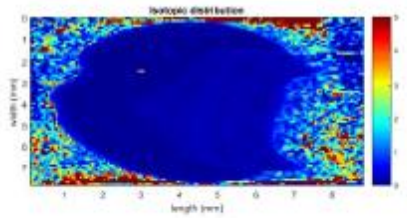

Lead (Pb^{208}) concentration

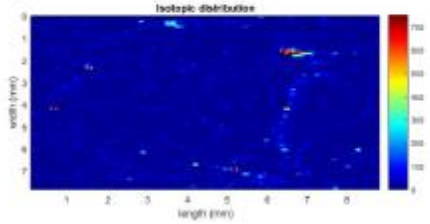

Uranium (U^{238}) detection

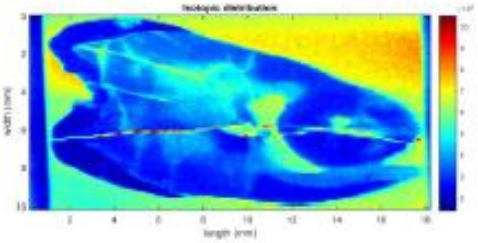

Carbon (C^{13}) detection

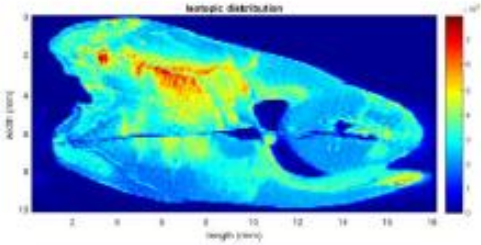

Calcium (Ca^{44}) detection

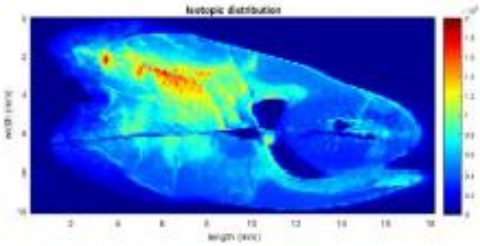

Magnesium (Mg^{24}) detection

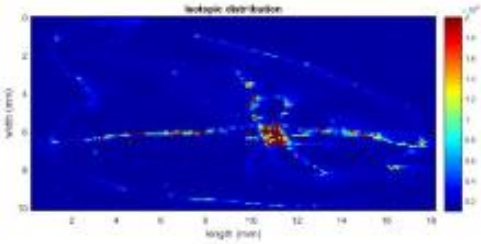

Iron (Fe^{56}) detection

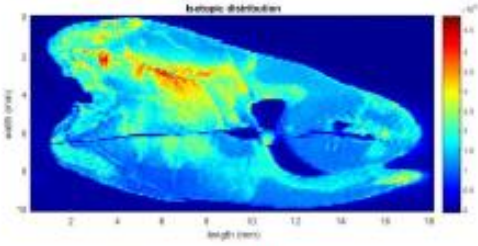

Phosphorus (P^{31}) detection

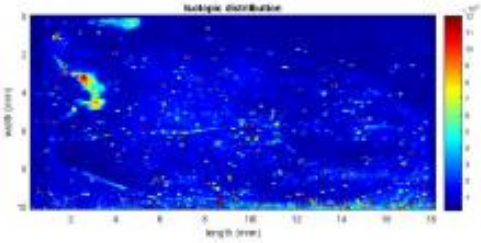

Copper (Cu^{63}) detection

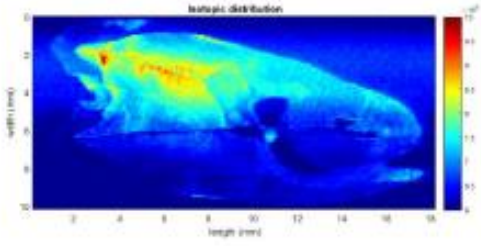

Sulfur (S^{32}) detection

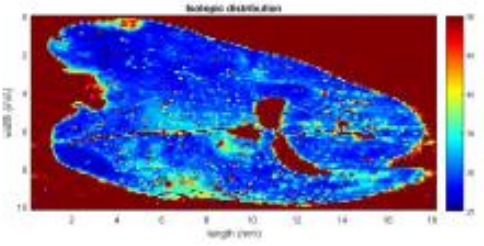

Copper (Cu^{63}) concentration

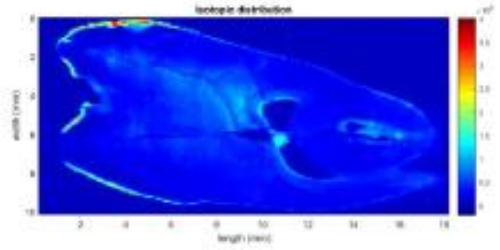

Zinc (Zn^{66}) detection

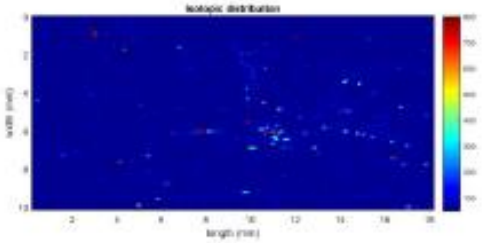

Antimony (Sb^{121}) detection

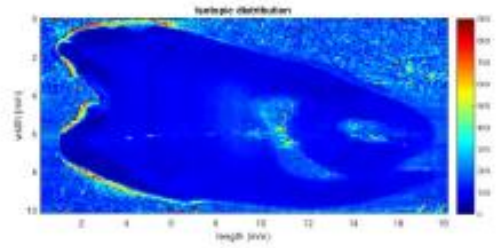

Zinc (Zn^{66}) concentration

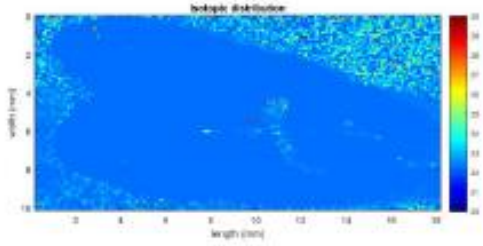

Antimony (Sb^{121}) concentration

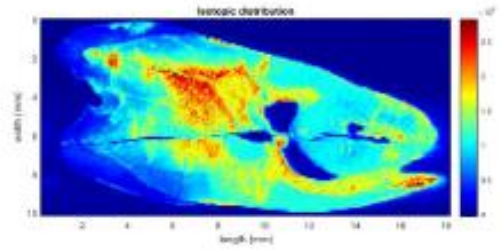

Strontium (Sr^{88}) detection

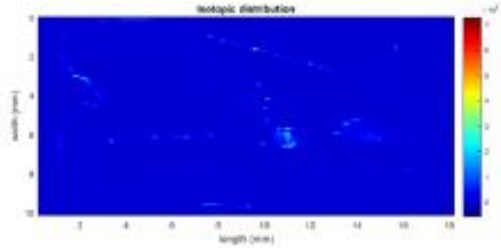

Lanthanum (La^{139}) detection

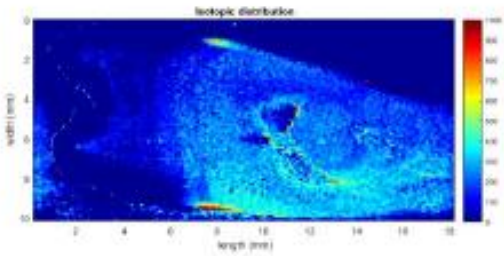

Strontium (Sr^{88}) concentration

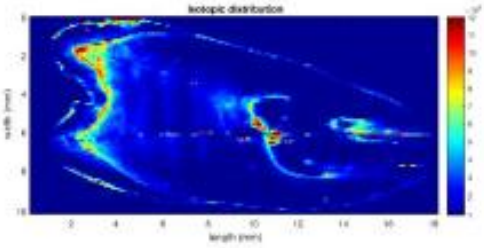

Lead (Pb^{208}) detection

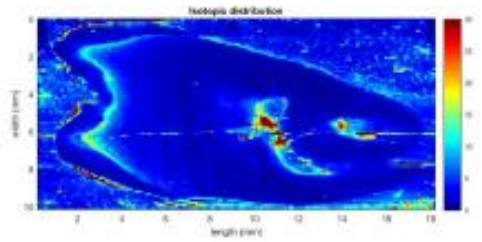

Lead (Pb^{208}) concentration

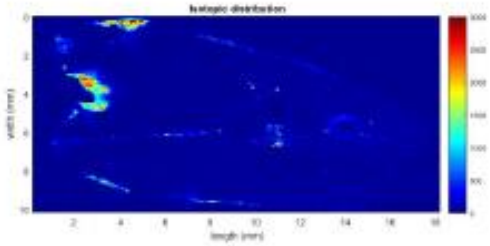

Uranium (U^{238}) detection

IIT 197-01_M1

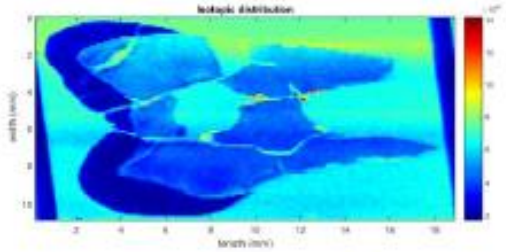

Carbon (C^{13}) detection

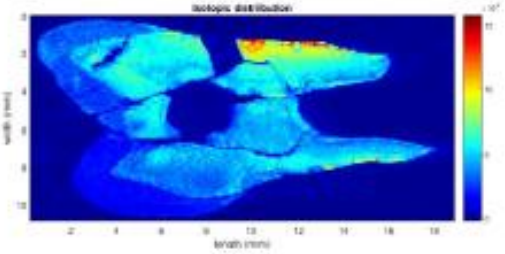

Calcium (Ca^{44}) detection

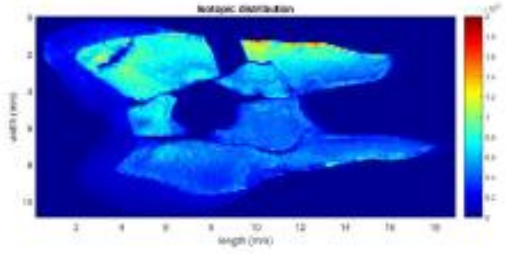

Magnesium (Mg^{24}) detection

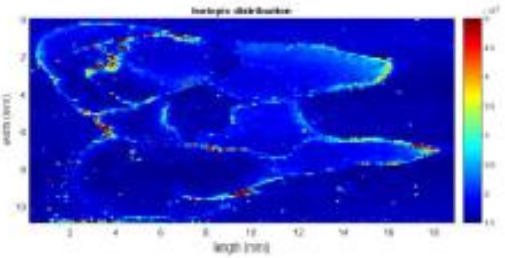

Iron (Fe^{56}) detection

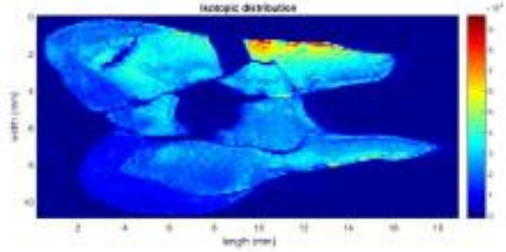

Phosphorus (P^{31}) detection

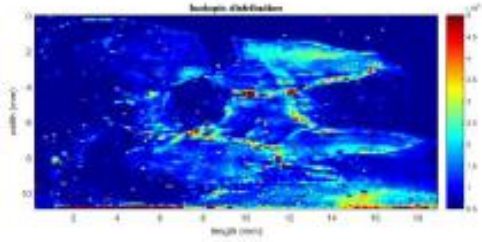

Copper (Cu^{63}) detection

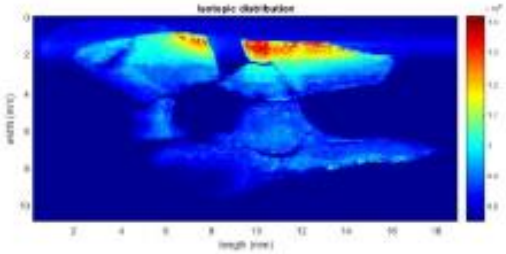

Sulfur (S^{32}) detection

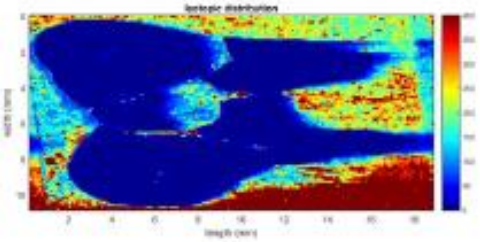

Copper (Cu^{63}) concentration

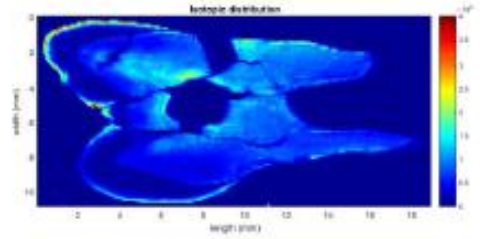

Zinc (Zn^{66}) detection

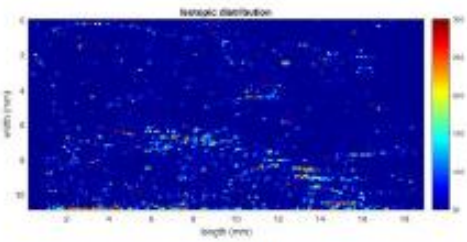

Antimony (Sb^{121}) detection

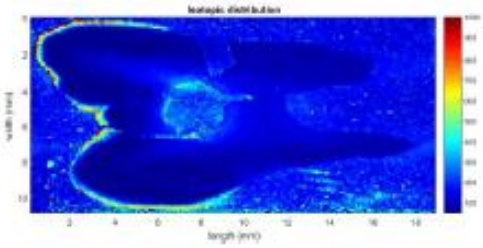

Zinc (Zn^{66}) concentration

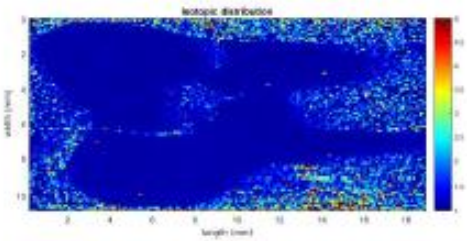

Antimony (Sb^{121}) concentration

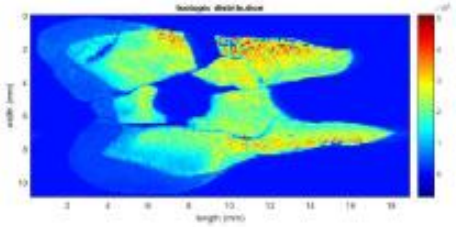

Strontium (Sr^{88}) detection

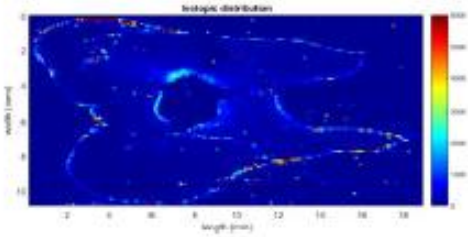

Lanthanum (La^{139}) detection

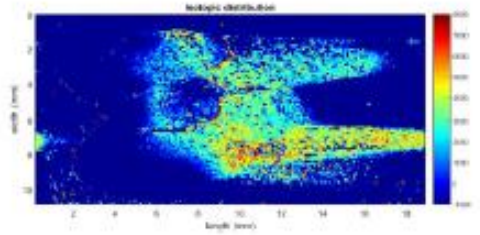

Strontium (Sr^{88}) concentration

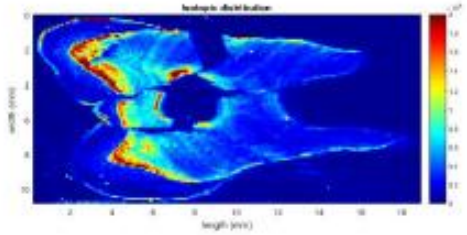

Lead (Pb^{208}) detection

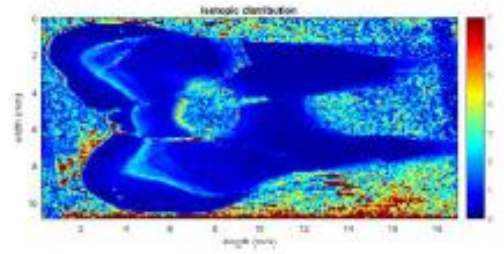

Lead (Pb^{208}) concentration

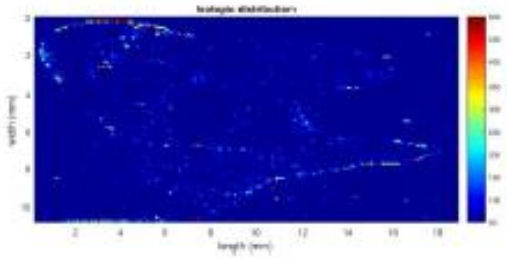

Uranium (U^{238}) detection

IIT 197-01_M2

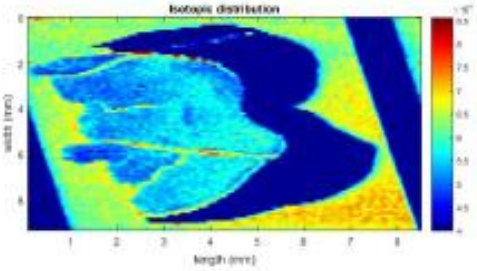

Carbon (C^{13}) detection

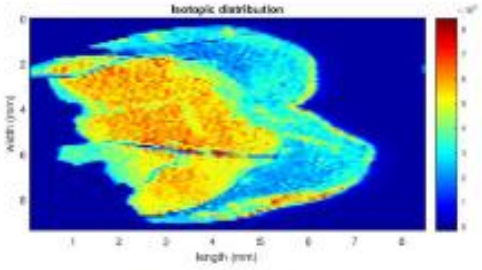

Calcium (Ca^{44}) detection

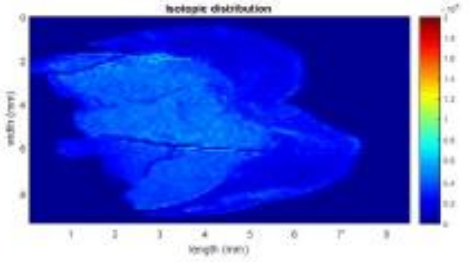

Magnesium (Mg^{24}) detection

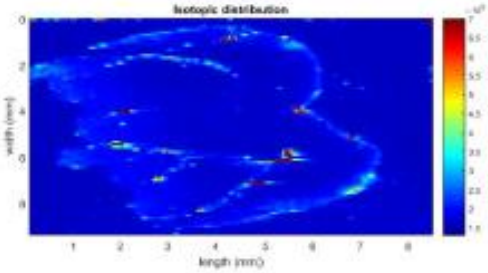

Iron (Fe^{56}) detection

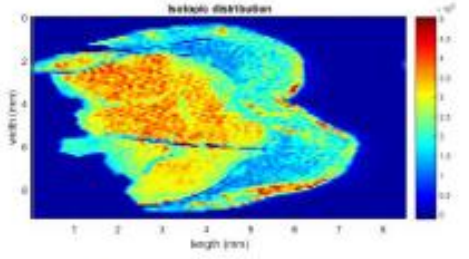

Phosphorus (P^{31}) detection

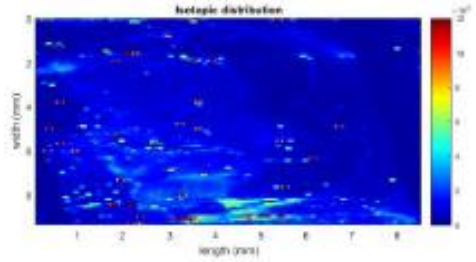

Copper (Cu^{63}) detection

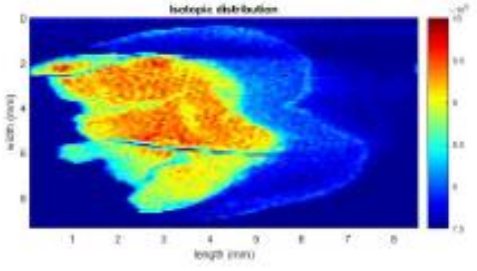

Sulfur (S^{32}) detection

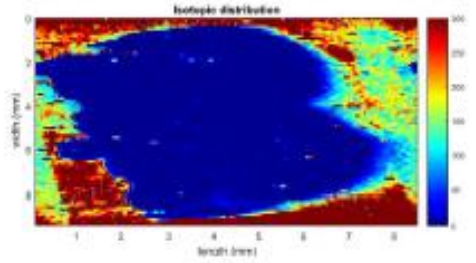

Copper (Cu^{63}) concentration

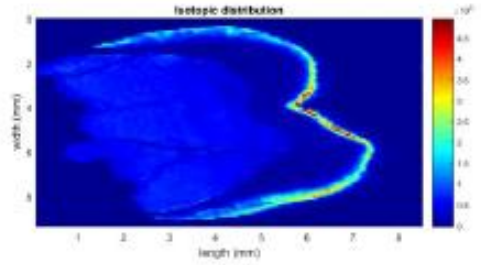

Zinc (Zn^{66}) detection

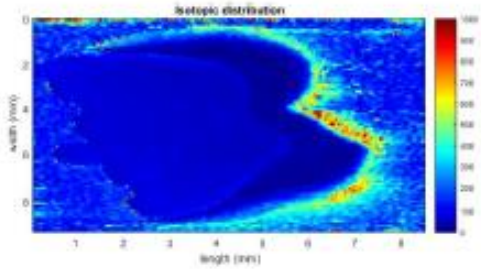

Zinc (Zn^{66}) concentration

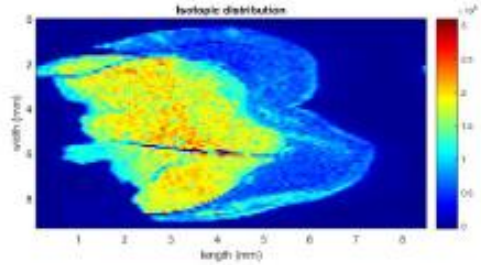

Strontium (Sr^{88}) detection

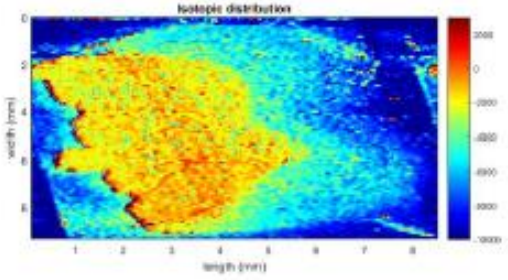

Strontium (Sr^{88}) concentration

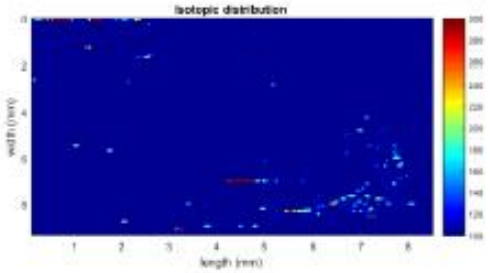

Antimony (Sb^{121}) detection

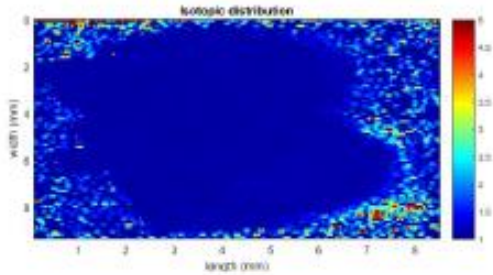

Antimony (Sb^{121}) concentration

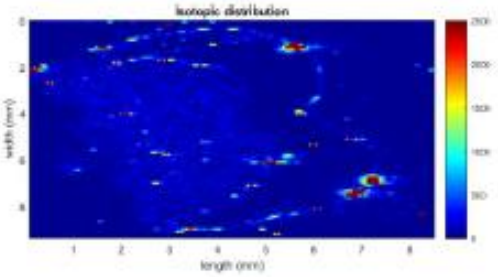

Lanthanum (La^{139}) detection

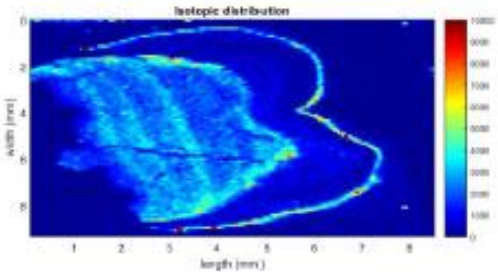

Lead (Pb^{208}) detection

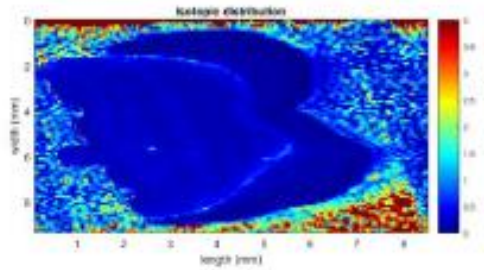

Lead (Pb^{208}) concentration

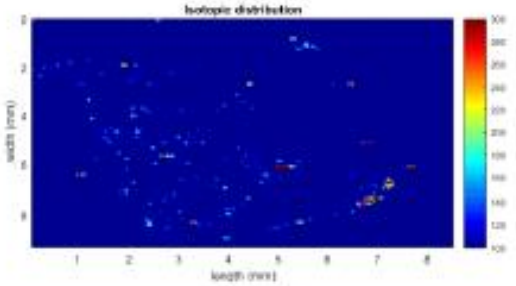

Uranium (U^{238}) detection

IIT 213-01_M1

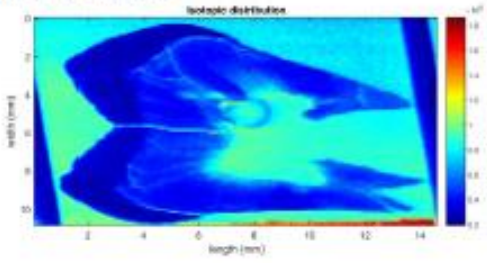

Carbon (C^{13}) detection

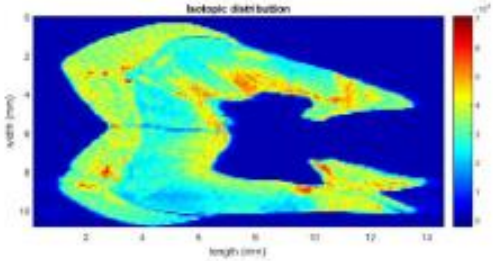

Calcium (Ca^{44}) detection

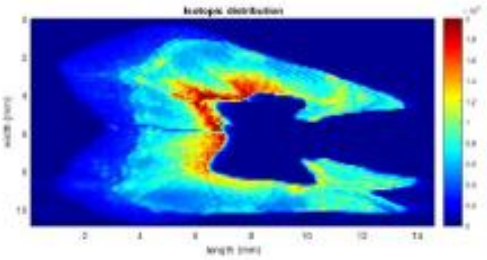

Magnesium (Mg^{24}) detection

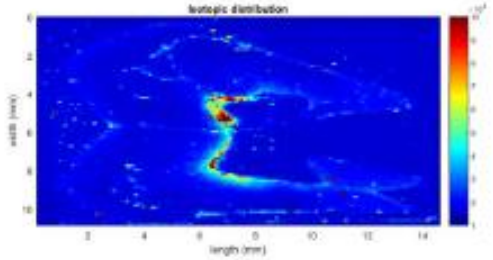

Iron (Fe^{56}) detection

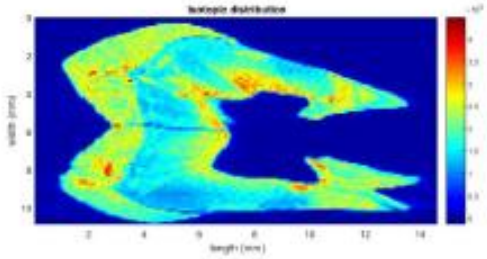

Phosphorus (P^{31}) detection

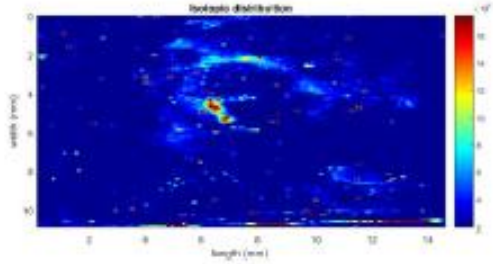

Copper (Cu^{63}) detection

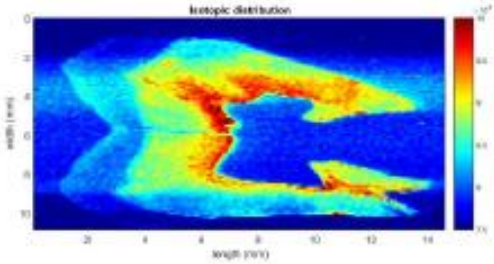

Sulfur (S^{32}) detection

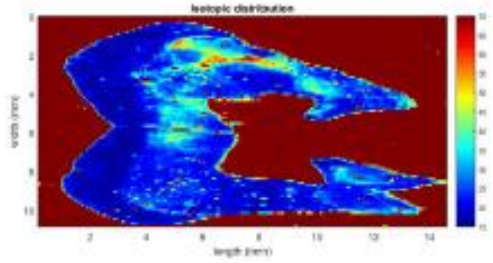

Copper (Cu^{63}) concentration

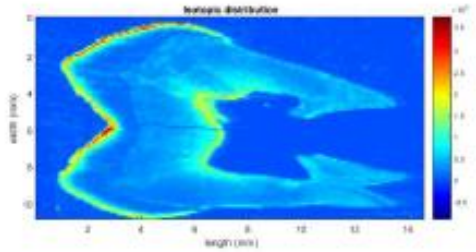

Zinc (Zn^{66}) detection

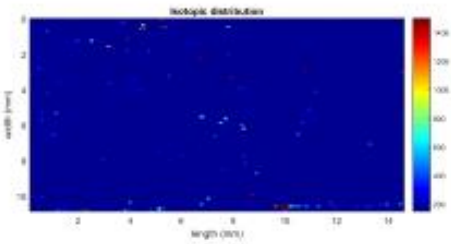

Antimony (Sb^{121}) detection

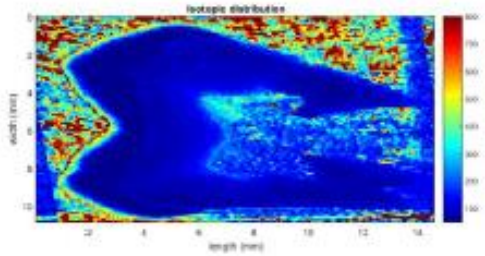

Zinc (Zn^{66}) concentration

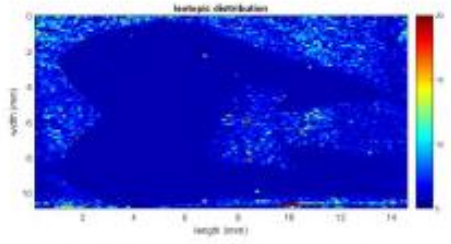

Antimony (Sb^{121}) concentration

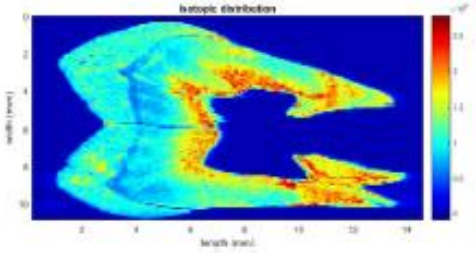

Strontium (Sr^{88}) detection

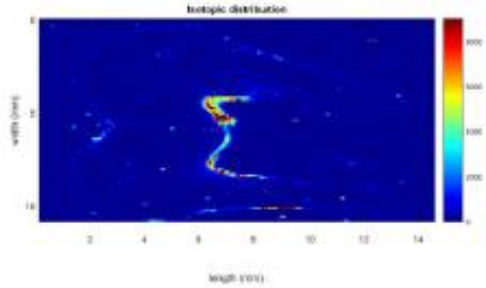

Lanthanum (La^{139}) detection

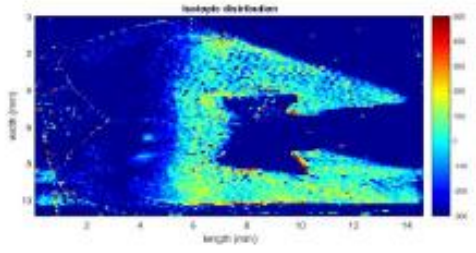

Strontium (Sr^{88}) concentration

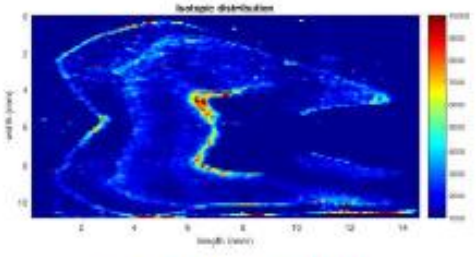

Lead (Pb^{208}) detection

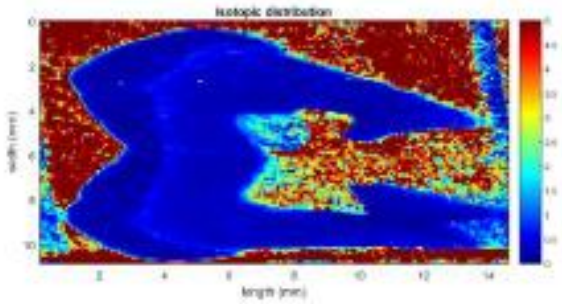

Lead (Pb^{208}) concentration

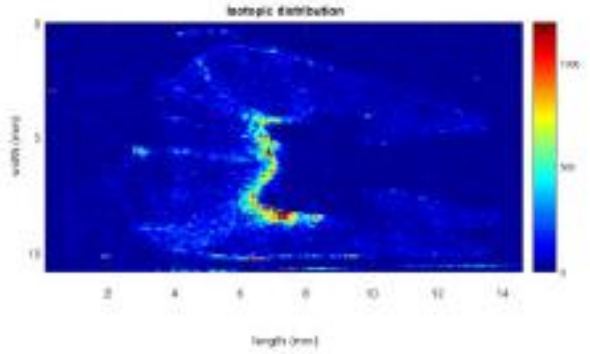

Uranium (U^{238}) detection

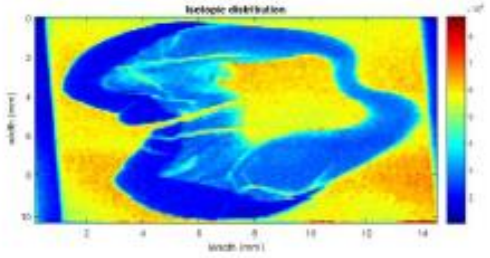

Carbon (C^{13}) detection

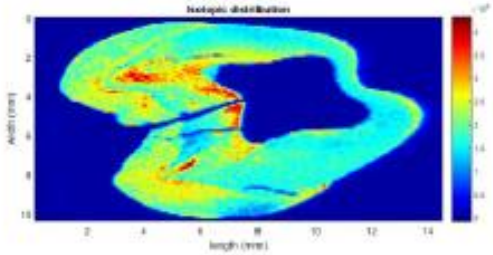

Calcium (Ca^{44}) detection

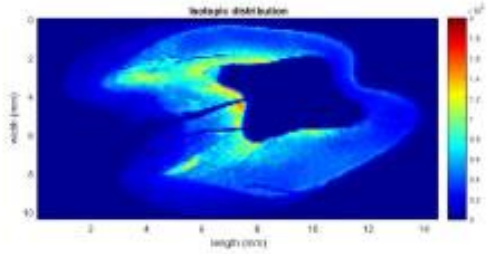

Magnesium (Mg^{24}) detection

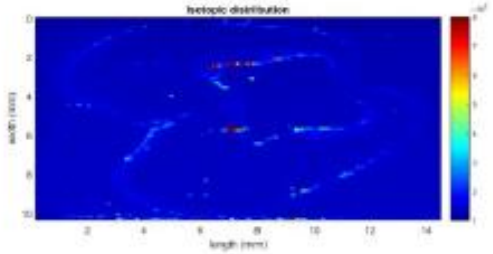

Iron (Fe^{56}) detection

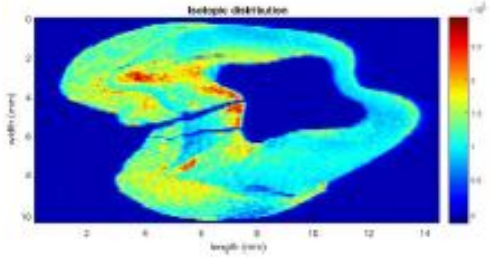

Phosphorus (P^{31}) detection

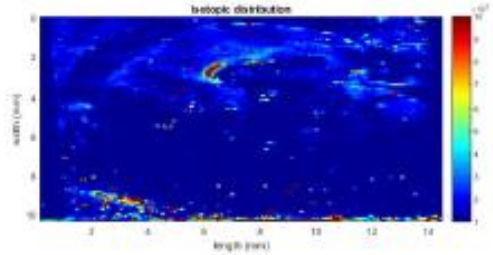

Copper (Cu^{63}) detection

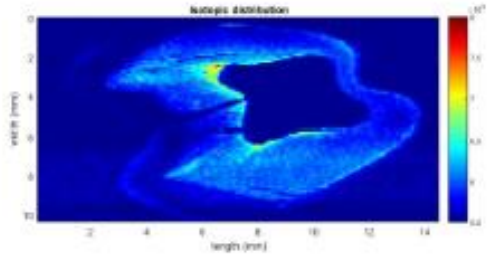

Sulfur (S^{32}) detection

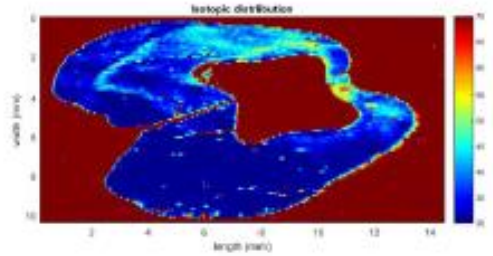

Copper (Cu^{63}) concentration

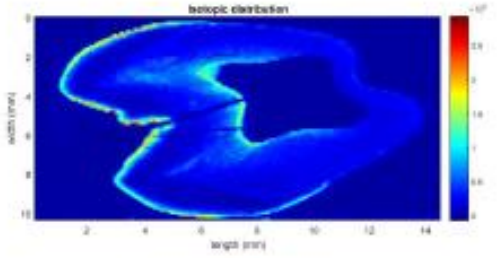

Zinc (Zn^{66}) detection

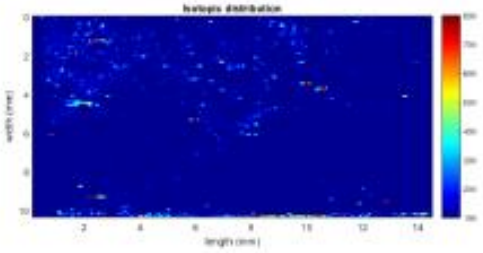

Antimony (Sb^{121}) detection

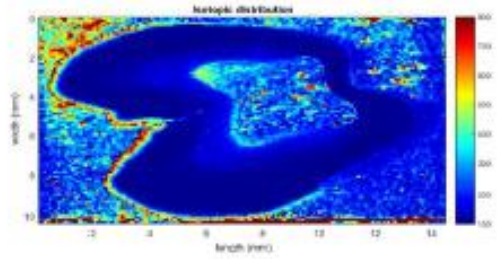

Zinc (Zn^{66}) concentration

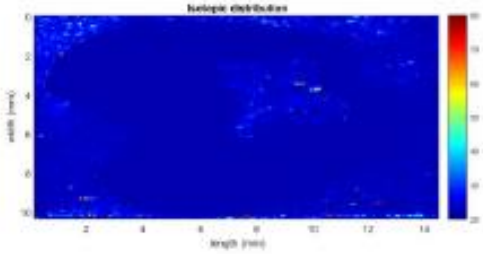

Antimony (Sb^{121}) concentration

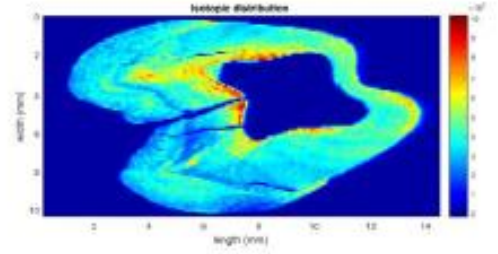

Strontium (Sr^{88}) detection

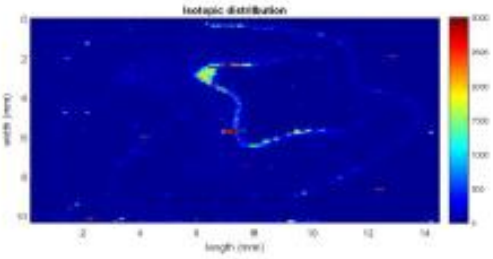

Lanthanum (La^{139}) detection

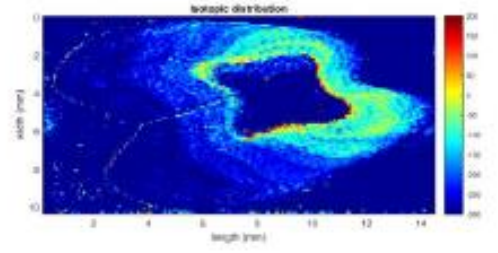

Strontium (Sr^{88}) concentration

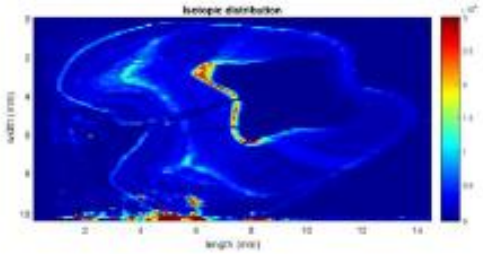

Lead (Pb^{208}) detection

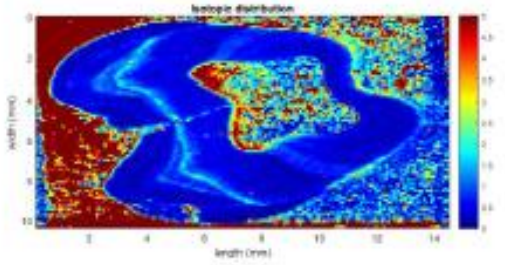

Lead (Pb^{208}) concentration

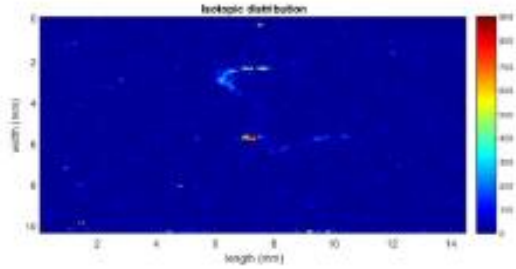

Uranium (U^{238}) detection

IIT 220-01_M1

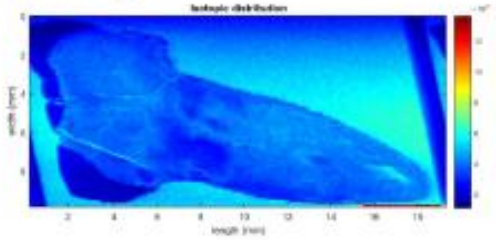

Carbon (C^{13}) detection

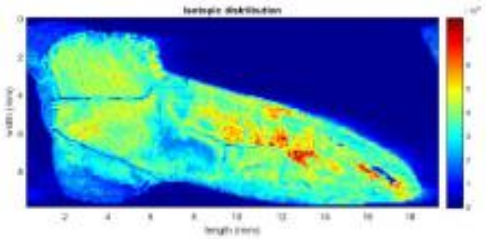

Calcium (Ca^{44}) detection

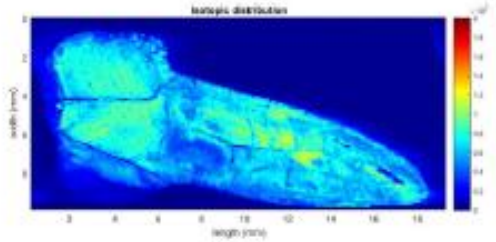

Magnesium (Mg^{24}) detection

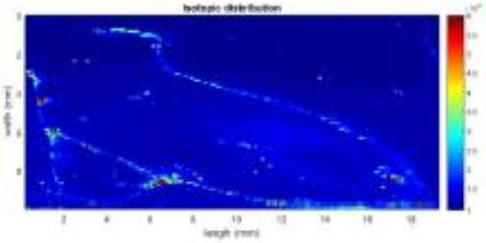

Iron (Fe^{56}) detection

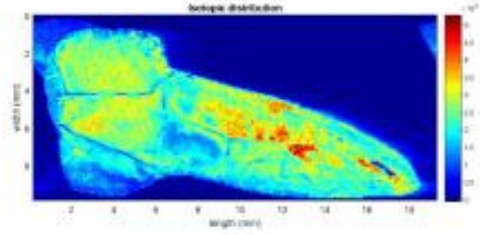

Phosphorus (P^{31}) detection

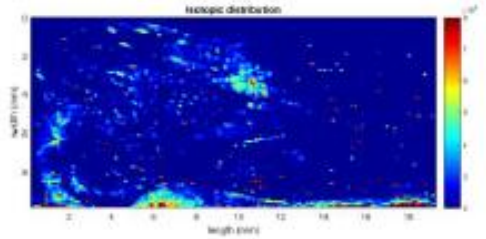

Copper (Cu^{63}) detection

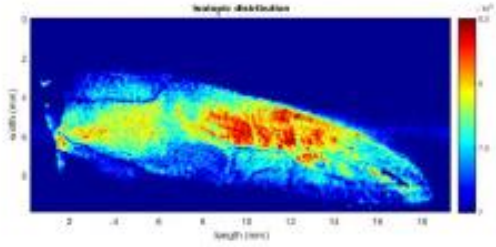

Sulfur (S^{32}) detection

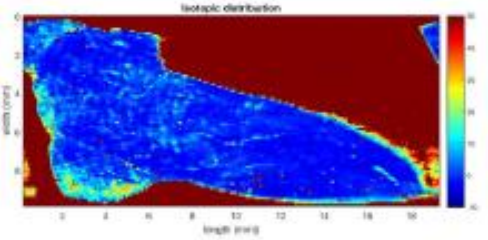

Copper (Cu^{63}) concentration

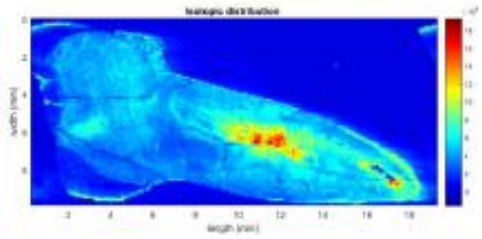

Zinc (Zn^{66}) detection

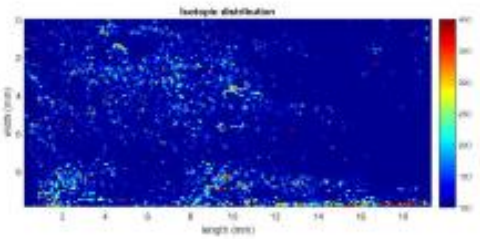

Antimony (Sb^{121}) detection

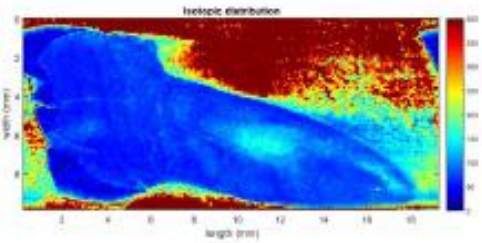

Zinc (Zn^{66}) concentration

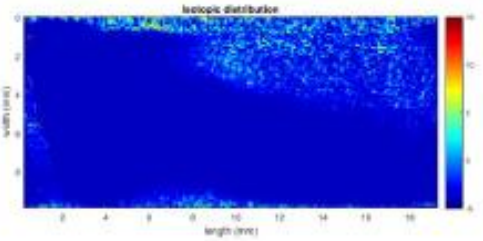

Antimony (Sb^{121}) concentration

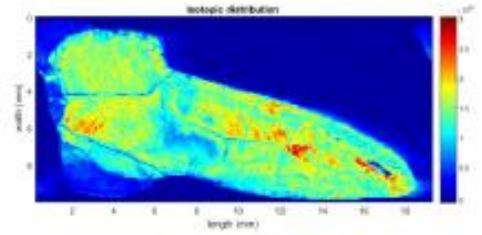

Strontium (Sr^{88}) detection

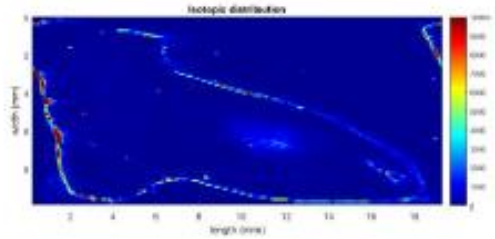

Lanthanum (La^{139}) detection

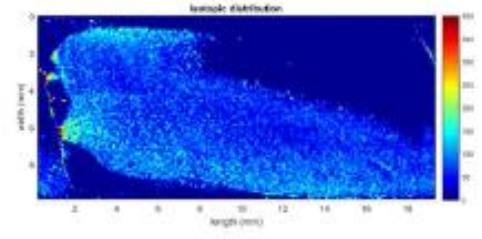

Strontium (Sr^{88}) concentration

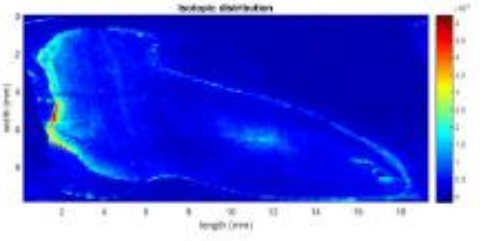

Lead (Pb^{208}) detection

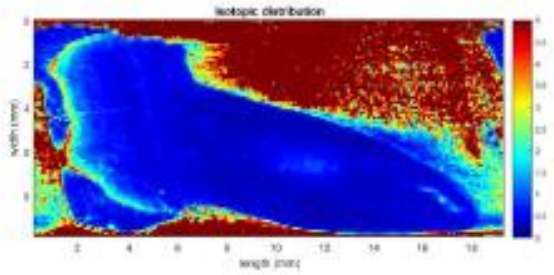

Lead (Pb^{208}) concentration

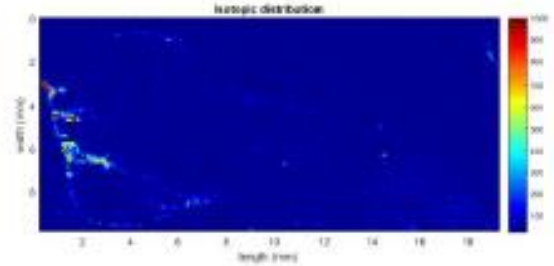

Uranium (U^{238}) detection

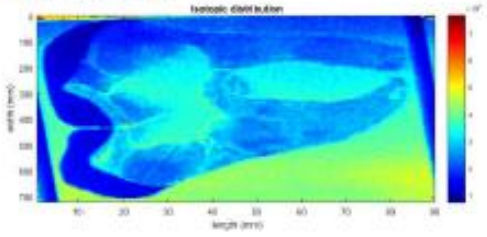

Carbon (C^{13}) detection

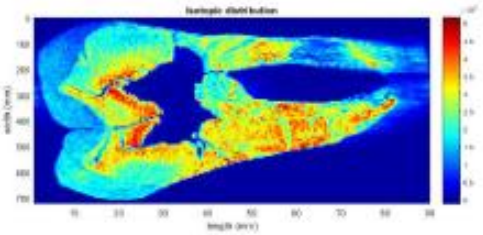

Calcium (Ca^{44}) detection

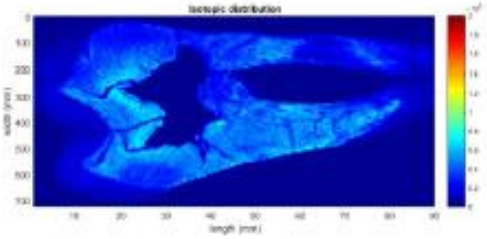

Magnesium (Mg^{24}) detection

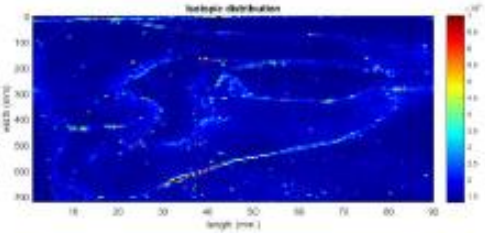

Iron (Fe^{56}) detection

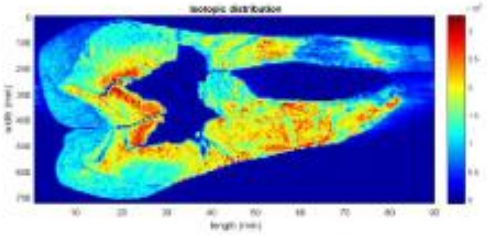

Phosphorus (P^{31}) detection

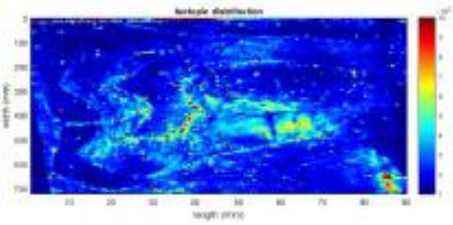

Copper (Cu^{63}) detection

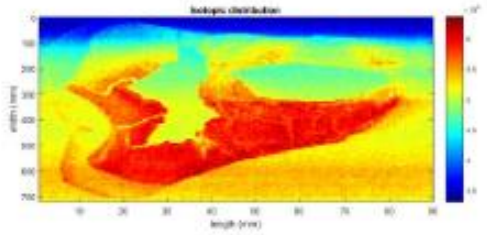

Sulfur (S^{32}) detection

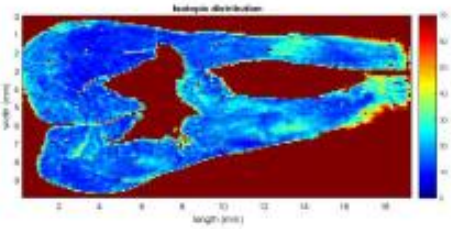

Copper (Cu^{63}) concentration

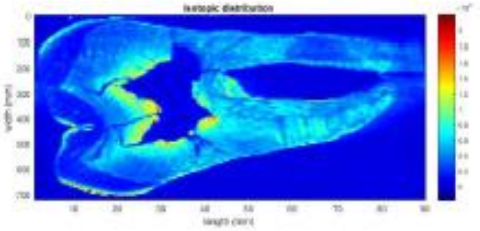

Zinc (Zn^{66}) detection

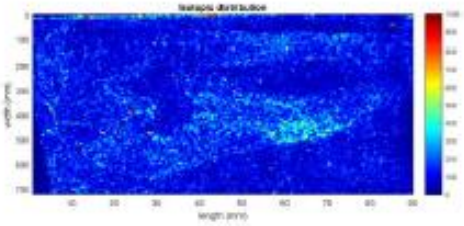

Antimony (Sb^{121}) detection

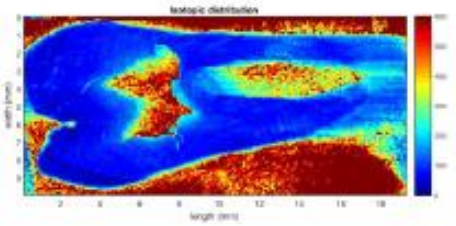

Zinc (Zn^{66}) concentration

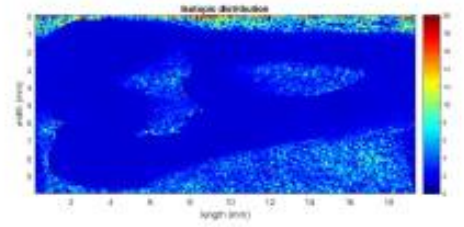

Antimony (Sb^{121}) concentration

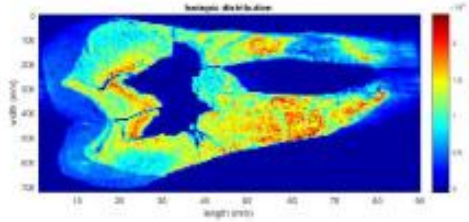

Strontium (Sr^{88}) detection

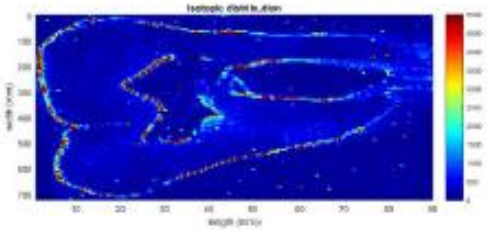

Lanthanum (La^{139}) detection

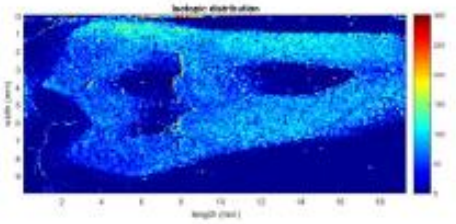

Strontium (Sr^{88}) concentration

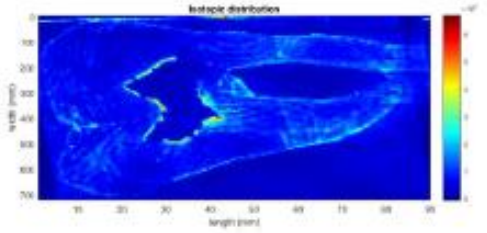

Lead (Pb^{208}) detection

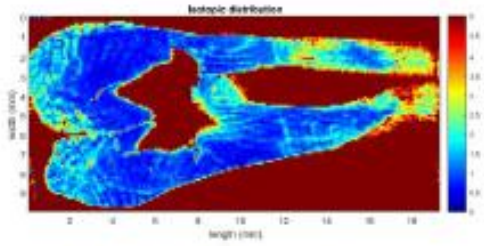

Lead (Pb^{208}) concentration

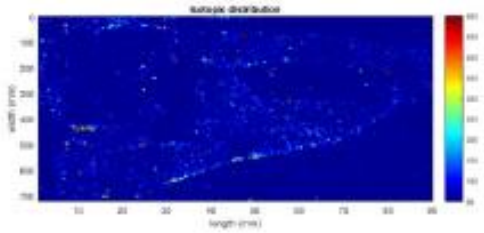

Uranium (U^{238}) detection

IIT 220-01_M3

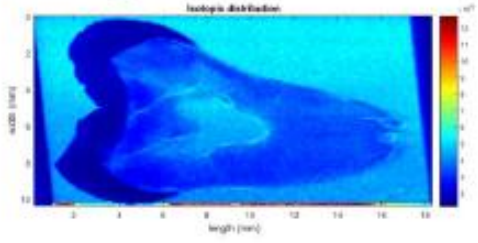

Carbon (C^{13}) detection

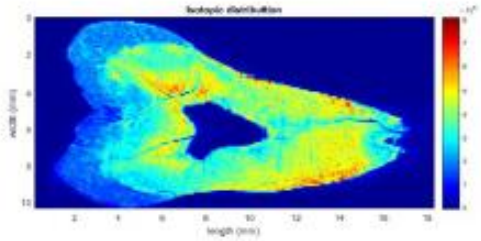

Calcium (Ca^{44}) detection

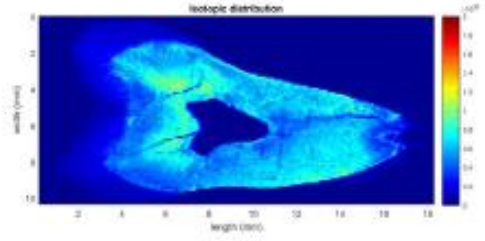

Magnesium (Mg^{24}) detection

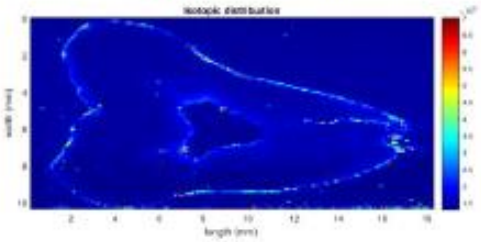

Iron (Fe^{56}) detection

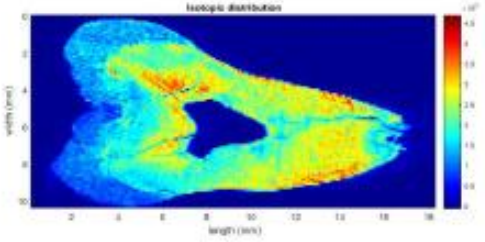

Phosphorus (P^{31}) detection

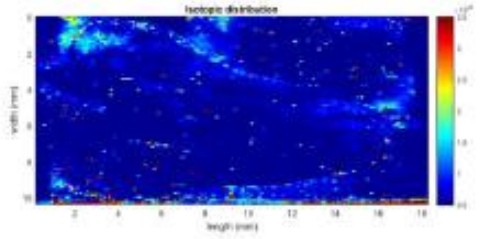

Copper (Cu^{63}) detection

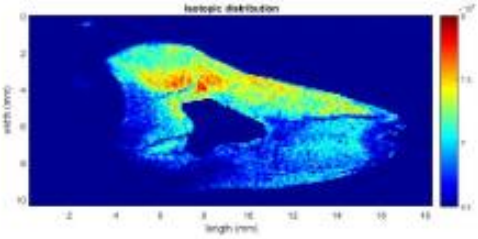

Sulfur (S^{32}) detection

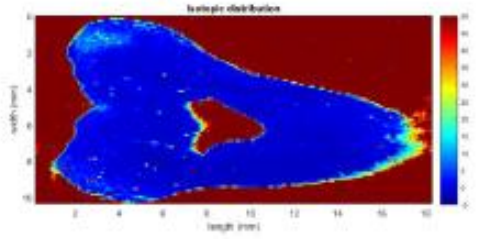

Copper (Cu^{63}) concentration

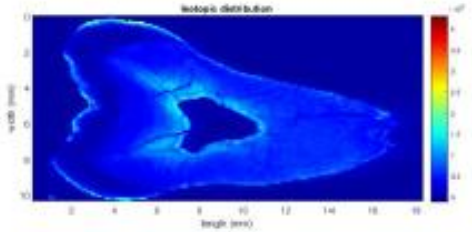

Zinc (Zn^{66}) detection

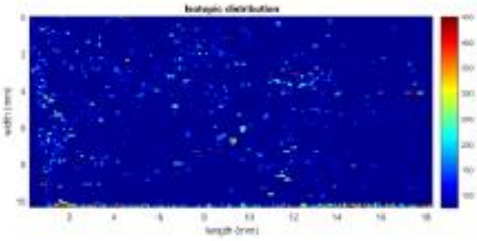

Antimony (Sb^{121}) detection

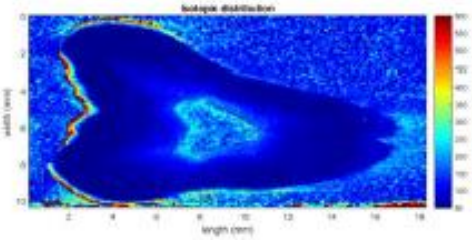

Zinc (Zn^{66}) concentration

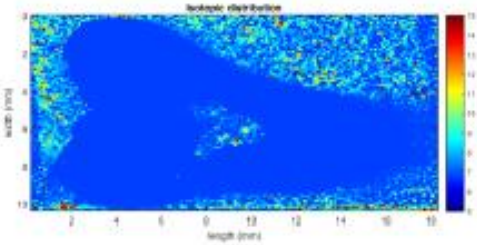

Antimony (Sb^{121}) concentration

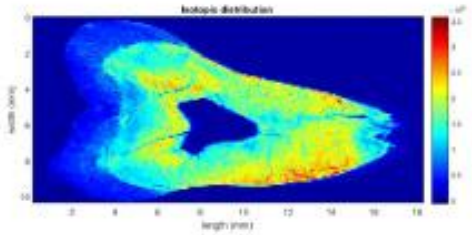

Strontium (Sr^{88}) detection

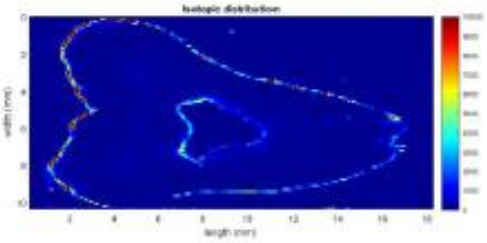

Lanthanum (La^{139}) detection

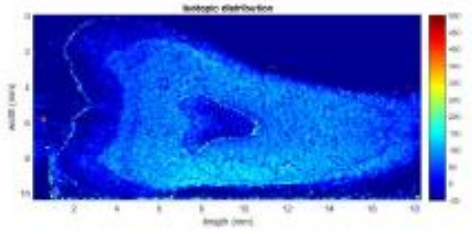

Strontium (Sr^{88}) concentration

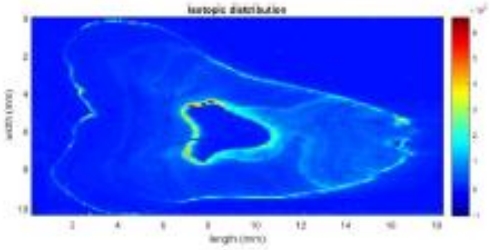

Lead (Pb^{208}) detection

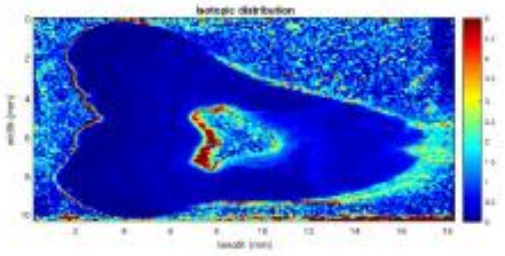

Lead (Pb^{208}) concentration

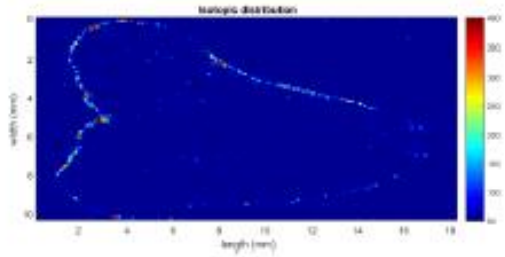

Uranium (U^{238}) detection

IIT 236-01_M1

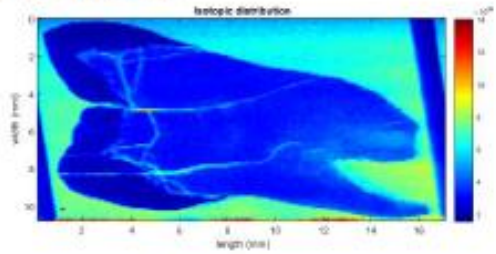

Carbon (C^{13}) detection

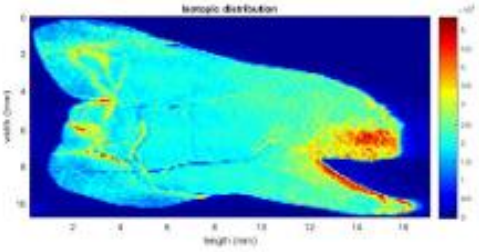

Calcium (Ca^{44}) detection

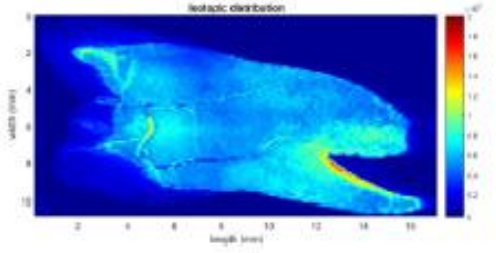

Magnesium (Mg^{24}) detection

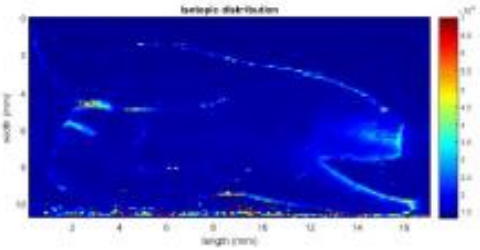

Iron (Fe^{56}) detection

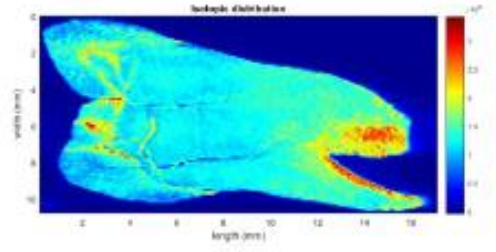

Phosphorus (P^{31}) detection

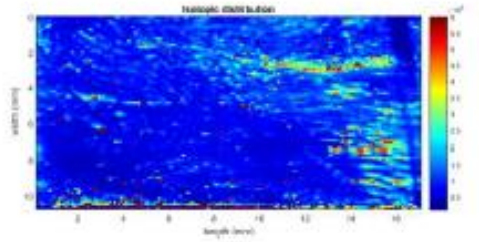

Copper (Cu^{63}) detection

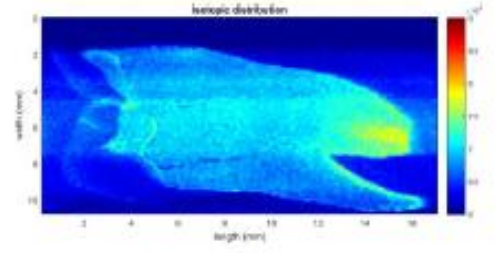

Sulfur (S^{32}) detection

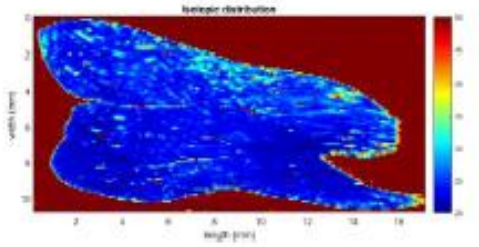

Copper (Cu^{63}) concentration

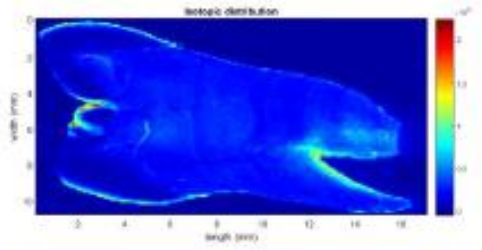

Zinc (Zn^{66}) detection

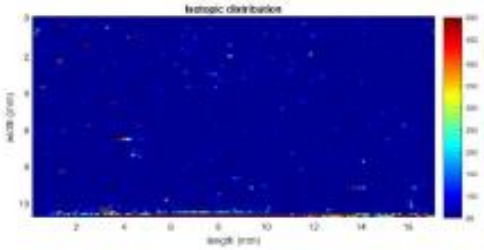

Antimony (Sb^{121}) detection

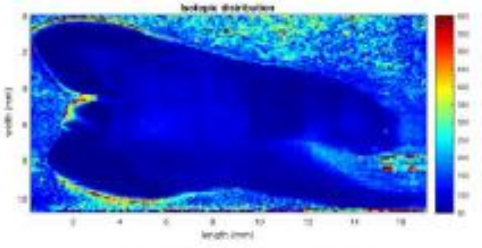

Zinc (Zn^{66}) concentration

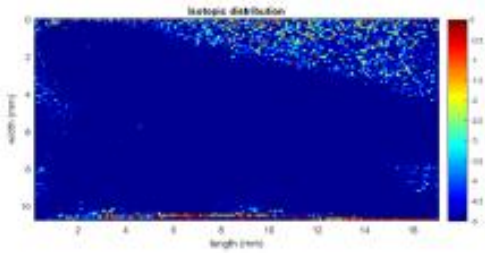

Antimony (Sb^{121}) concentration

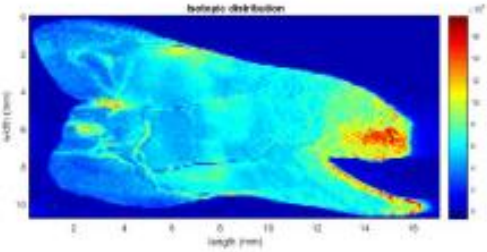

Strontium (Sr^{88}) detection

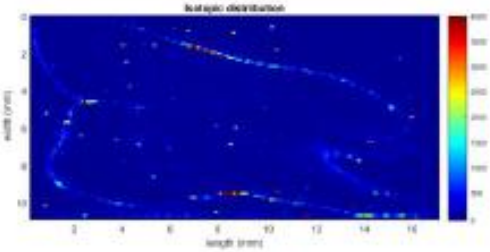

Lanthanum (La^{139}) detection

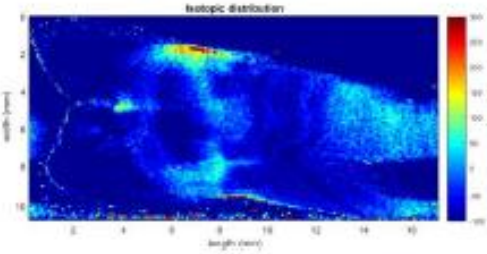

Strontium (Sr^{88}) concentration

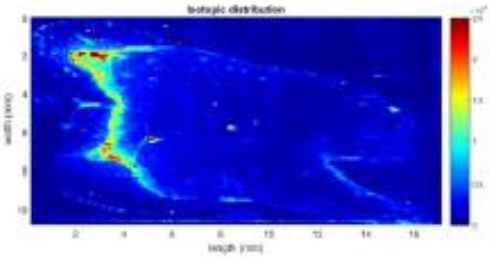

Lead (Pb^{208}) detection

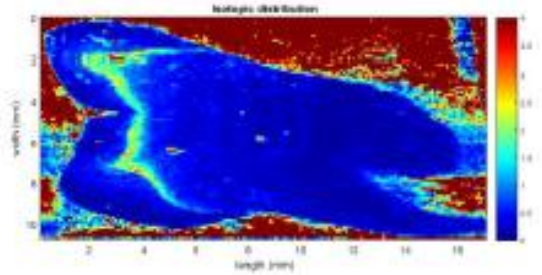

Lead (Pb^{208}) concentration

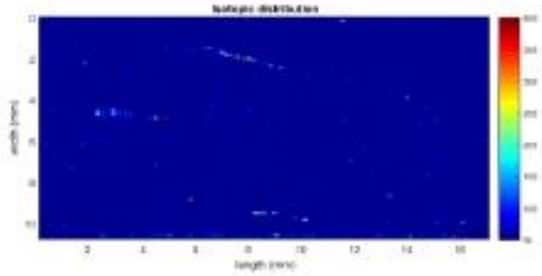

Uranium (U^{238}) detection

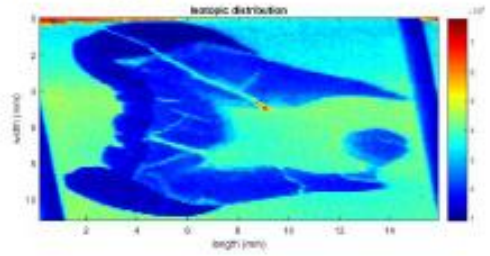

Carbon (C^{13}) detection

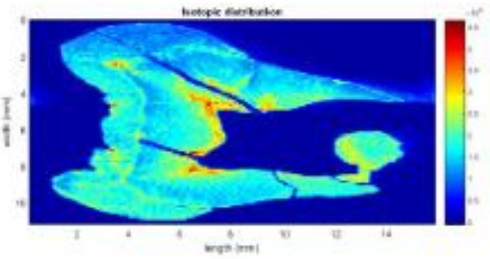

Calcium (Ca^{44}) detection

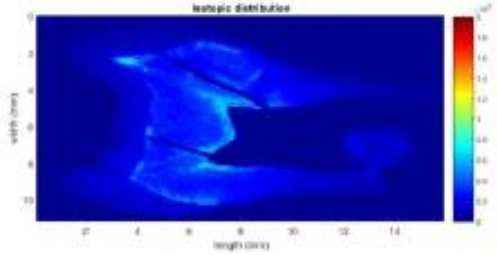

Magnesium (Mg^{24}) detection

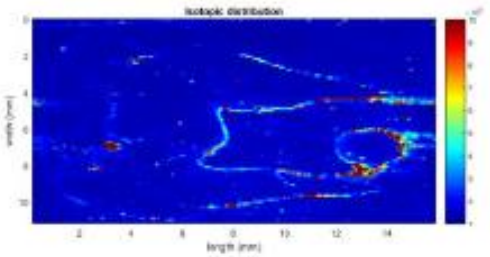

Iron (Fe^{56}) detection

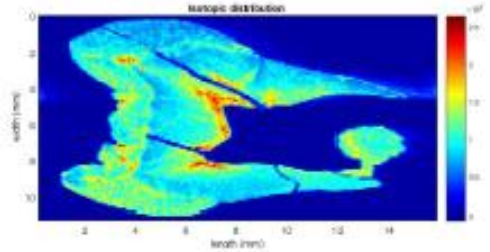

Phosphorus (P^{31}) detection

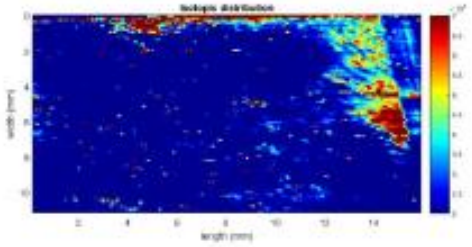

Copper (Cu^{63}) detection

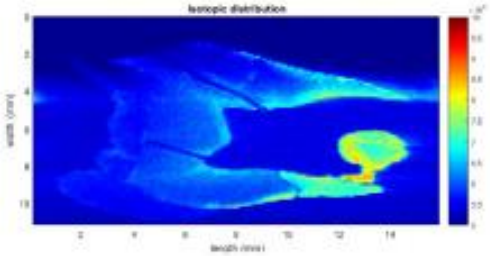

Sulfur (S^{32}) detection

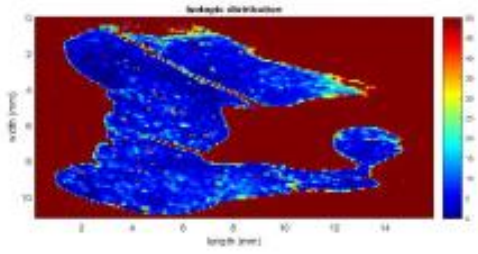

Copper (Cu^{63}) concentration

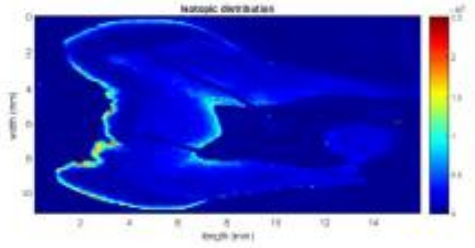

Zinc (Zn^{66}) detection

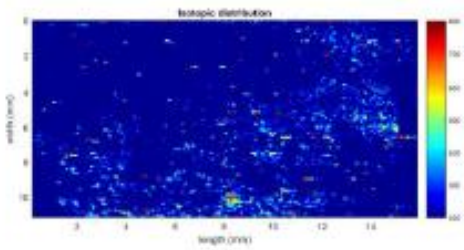

Antimony (Sb^{121}) detection

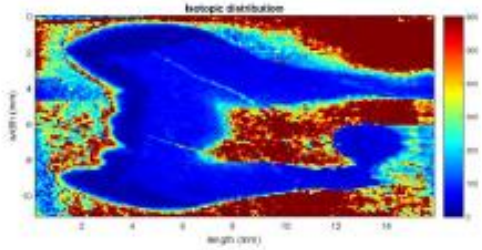

Zinc (Zn^{66}) concentration

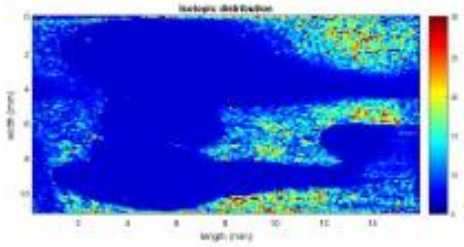

Antimony (Sb^{121}) concentration

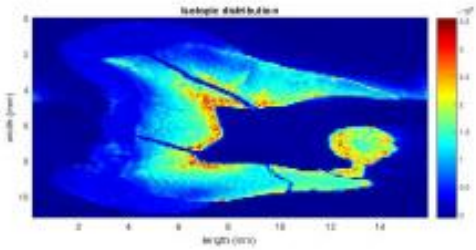

Strontium (Sr^{88}) detection

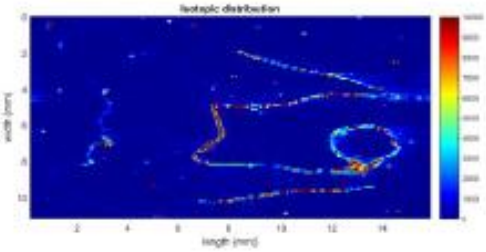

Lanthanum (La^{139}) detection

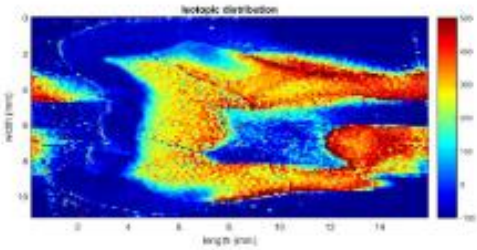

Strontium (Sr^{88}) concentration

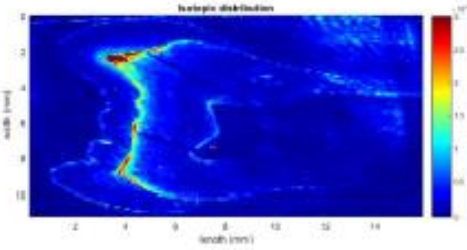

Lead (Pb^{208}) detection

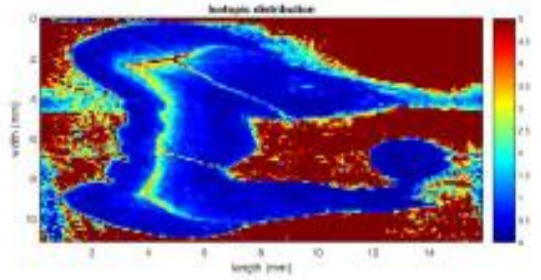

Lead (Pb^{208}) concentration

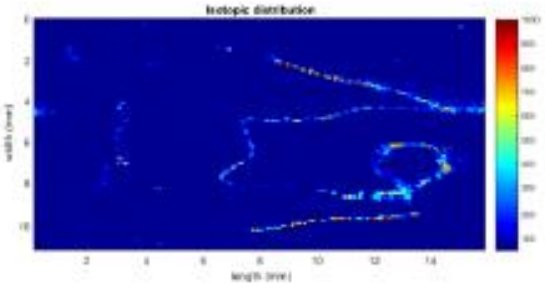

Uranium (U^{238}) detection

IIT 312-01_M1

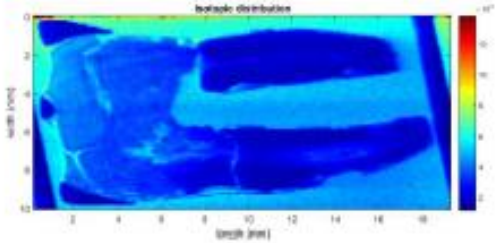

Carbon (C^{13}) detection

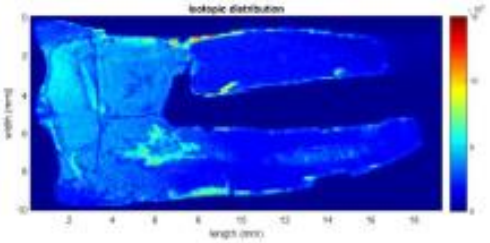

Calcium (Ca^{44}) detection

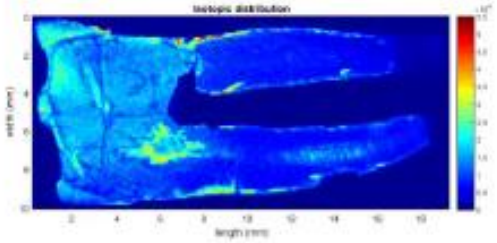

Magnesium (Mg^{24}) detection

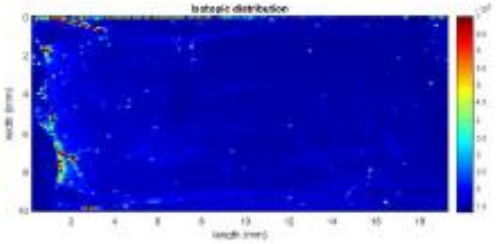

Iron (Fe^{56}) detection

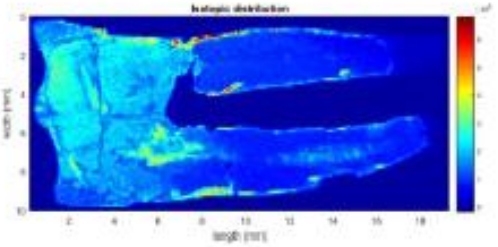

Phosphorus (P^{31}) detection

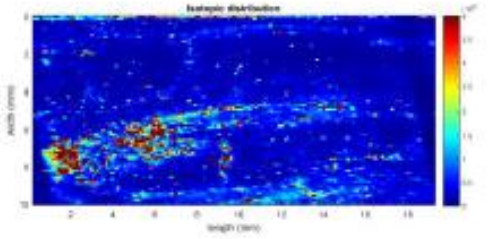

Copper (Cu^{63}) detection

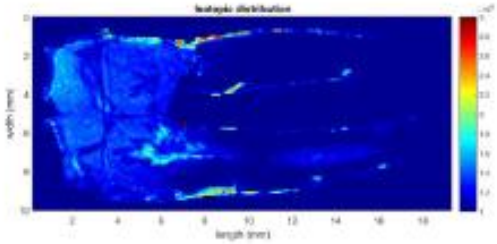

Sulfur (S^{32}) detection

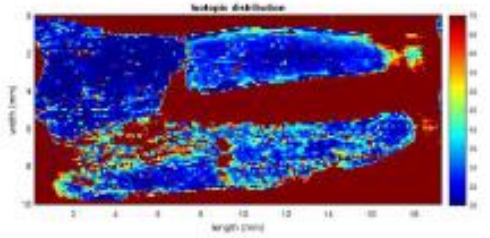

Copper (Cu^{63}) concentration

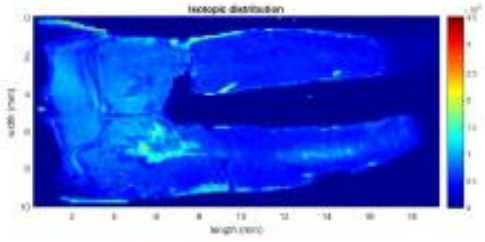

Zinc (Zn^{66}) detection

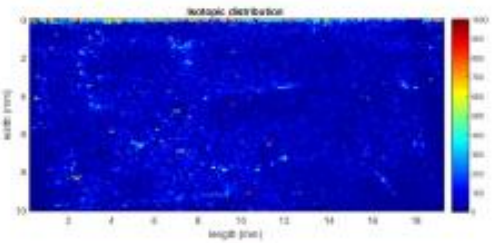

Antimony (Sb^{121}) detection

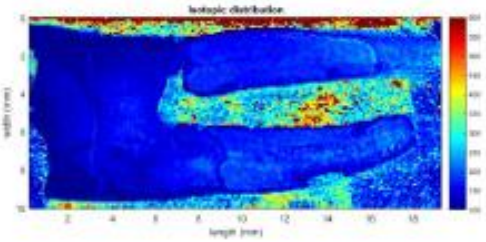

Zinc (Zn^{66}) concentration

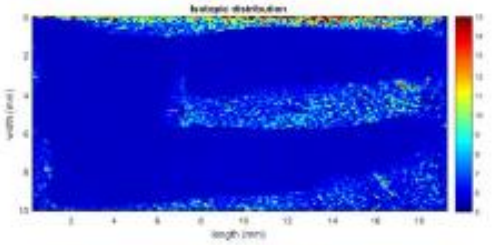

Antimony (Sb^{121}) concentration

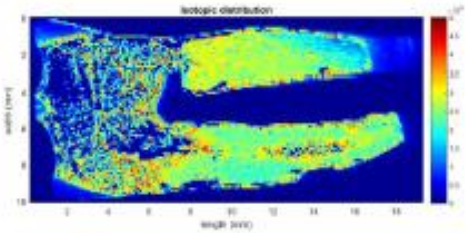

Strontium (Sr^{88}) detection

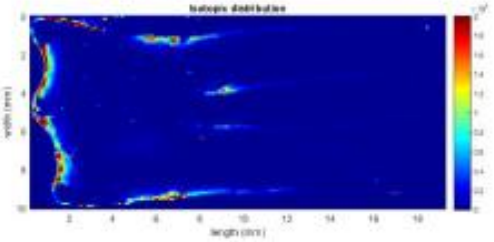

Lanthanum (La^{139}) detection

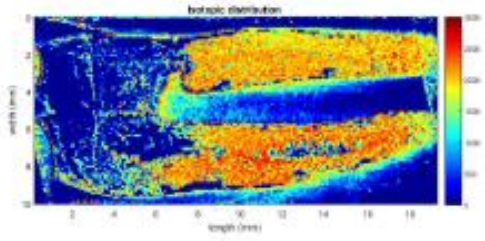

Strontium (Sr^{88}) concentration

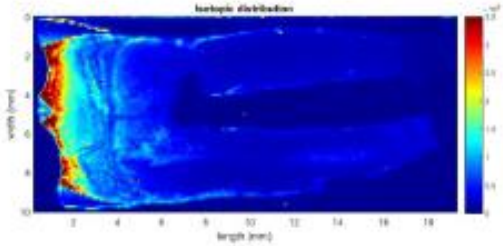

Lead (Pb^{208}) detection

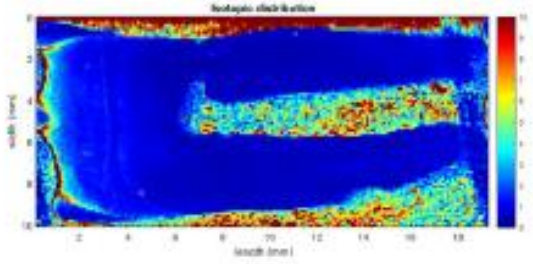

Lead (Pb^{208}) concentration

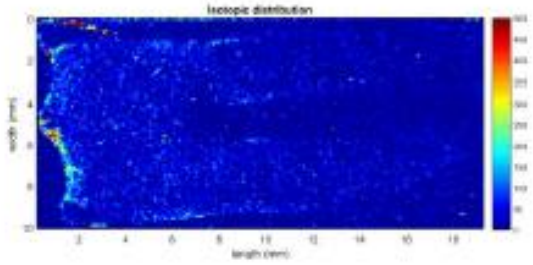

Uranium (U^{238}) detection

IIT 312-01_M3

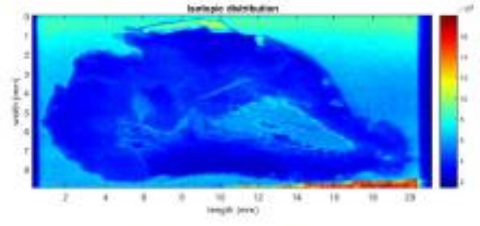

Carbon (C^{13}) detection

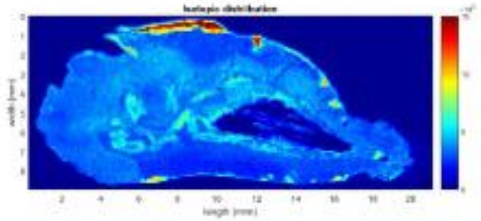

Calcium (Ca^{44}) detection

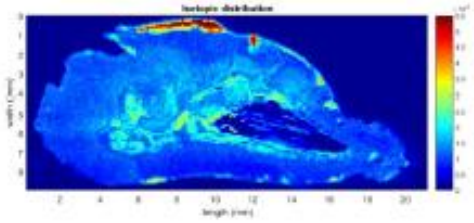

Magnesium (Mg^{24}) detection

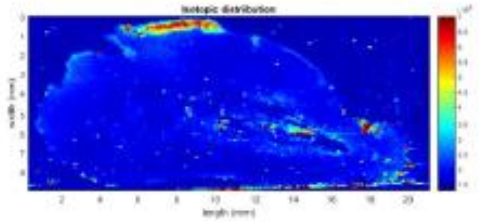

Iron (Fe^{56}) detection

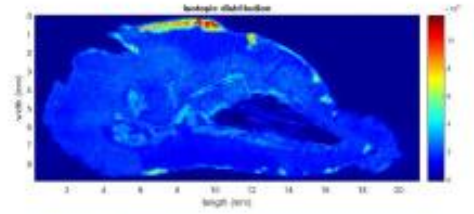

Phosphorus (P^{31}) detection

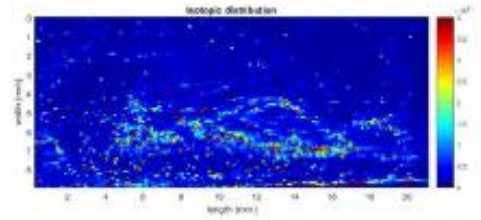

Copper (Cu^{63}) detection

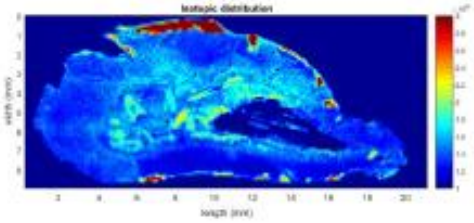

Sulfur (S^{32}) detection

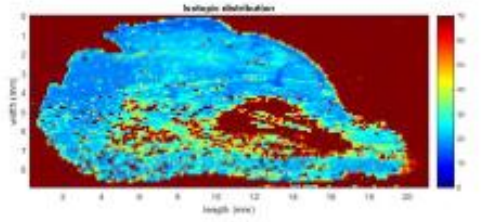

Copper (Cu^{63}) concentration

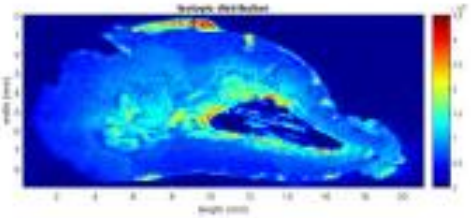

Zinc (Zn^{66}) detection

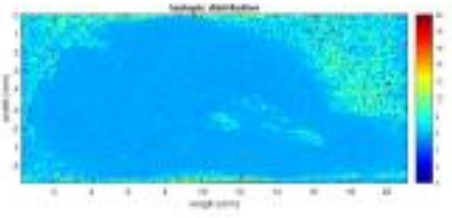

Antimony (Sb^{121}) concentration

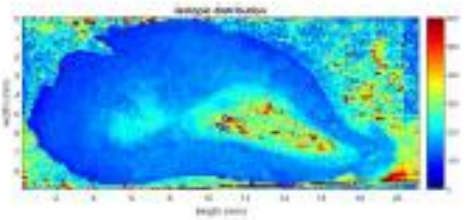

Zinc (Zn^{66}) concentration

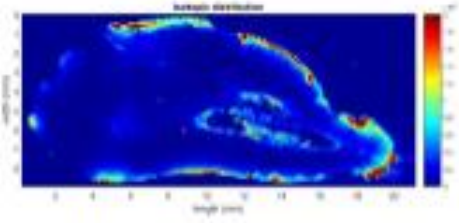

Lanthanum (La^{139}) detection

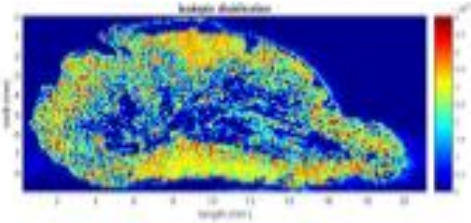

Strontium (Sr^{88}) detection

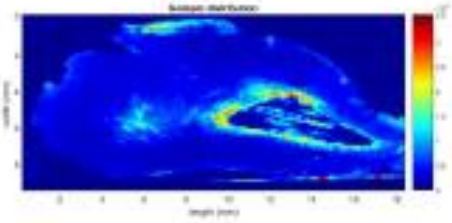

Lead (Pb^{208}) detection

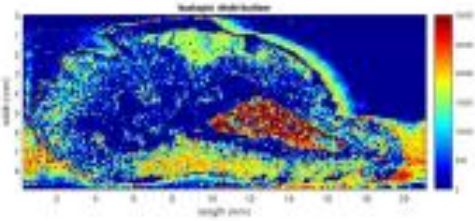

Strontium (Sr^{88}) concentration

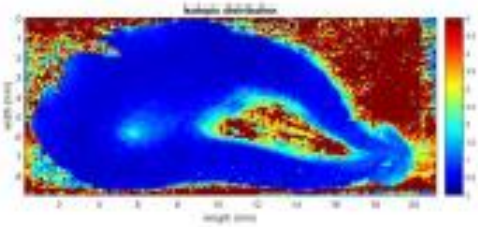

Lead (Pb^{208}) concentration

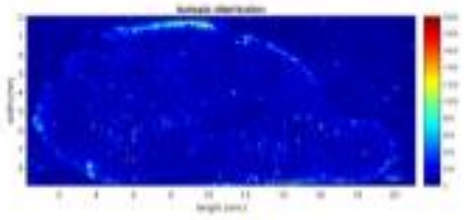

Antimony (Sb^{121}) detection

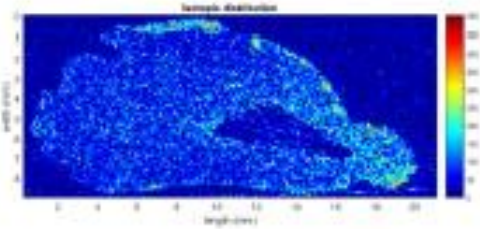

Uranium (U^{238}) detection

IIT 315-01_M1

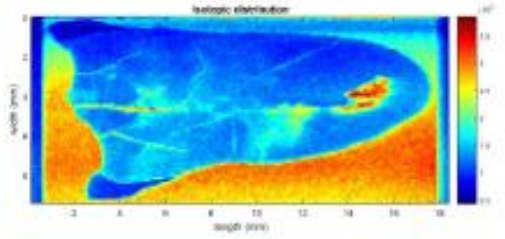

Carbon (C^{13}) detection

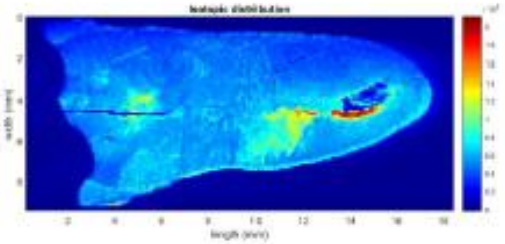

Calcium (Ca^{44}) detection

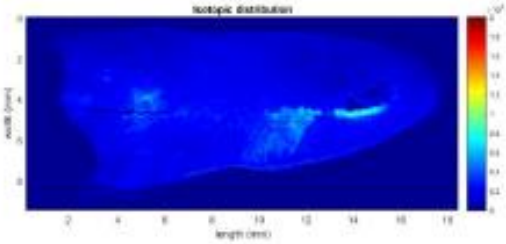

Magnesium (Mg^{24}) detection

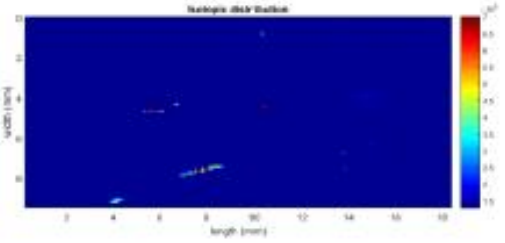

Iron (Fe^{56}) detection

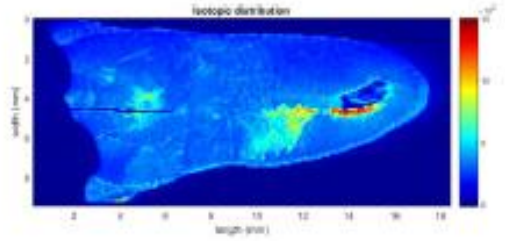

Phosphorus (P^{31}) detection

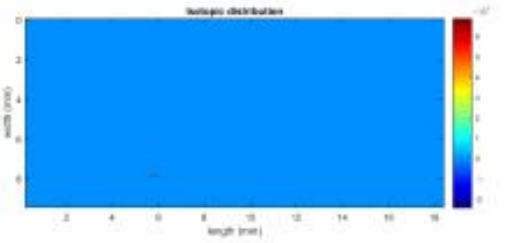

Copper (Cu^{63}) detection

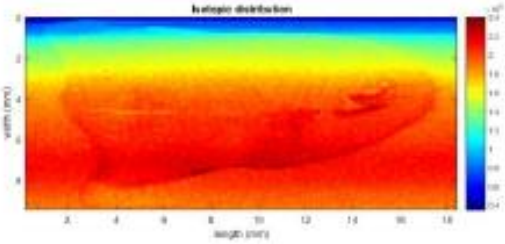

Sulfur (S^{32}) detection

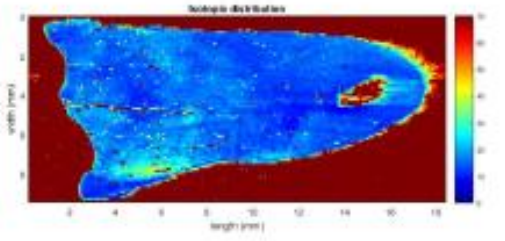

Copper (Cu^{63}) concentration

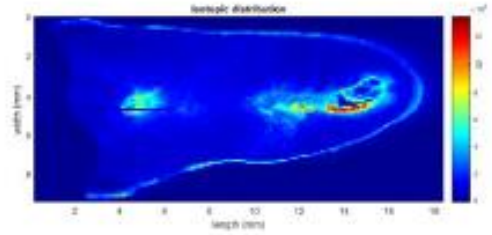

Zinc (Zn^{66}) detection

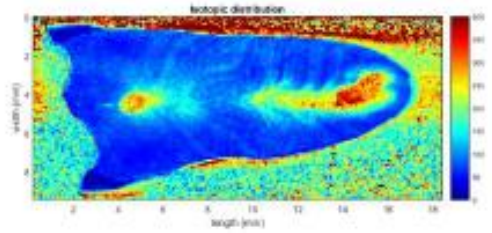

Zinc (Zn^{66}) concentration

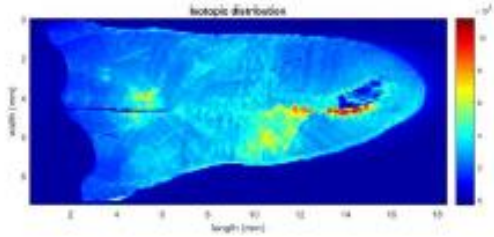

Strontium (Sr^{88}) detection

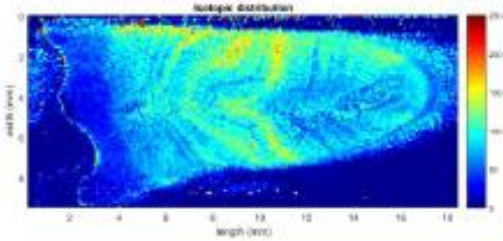

Strontium (Sr^{88}) concentration

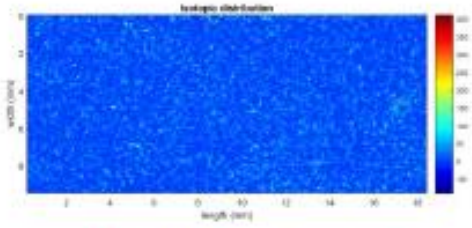

Antimony (Sb^{121}) detection

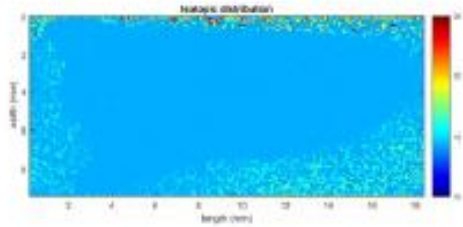

Antimony (Sb^{121}) concentration

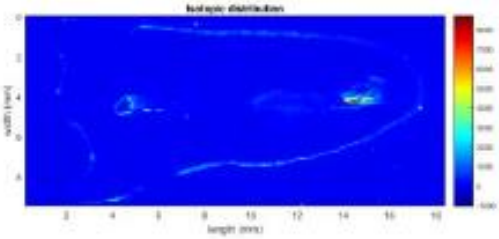

Lanthanum (La^{139}) detection

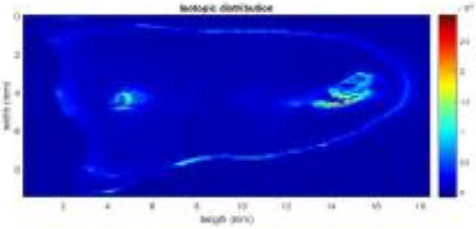

Lead (Pb^{208}) detection

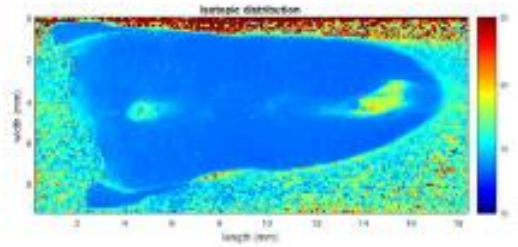

Lead (Pb^{208}) concentration

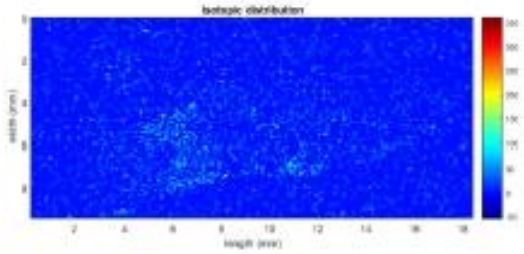

Uranium (U^{238}) detection

IIT 315-01_M2

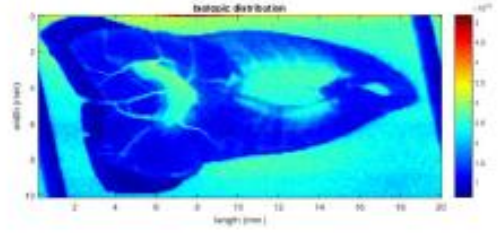

Carbon (C^{13}) detection

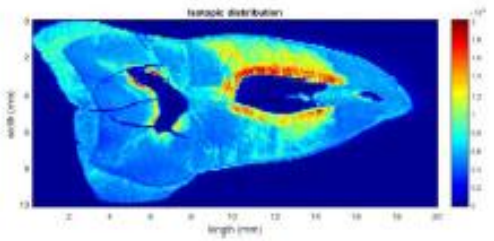

Calcium (Ca^{44}) detection

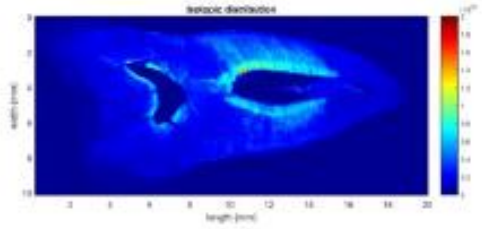

Magnesium (Mg^{24}) detection

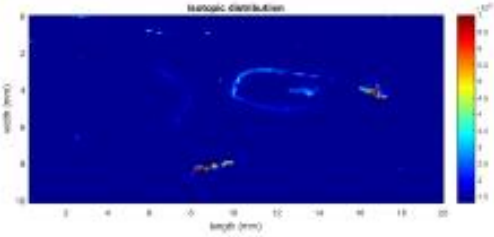

Iron (Fe^{56}) detection

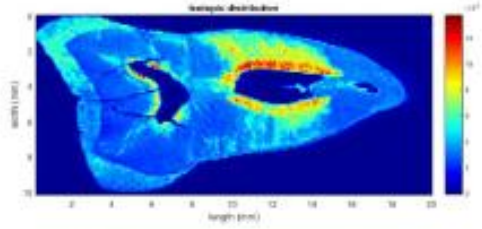

Phosphorus (P^{31}) detection

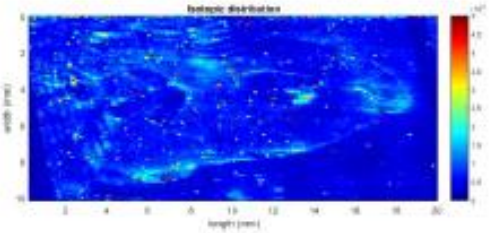

Copper (Cu^{63}) detection

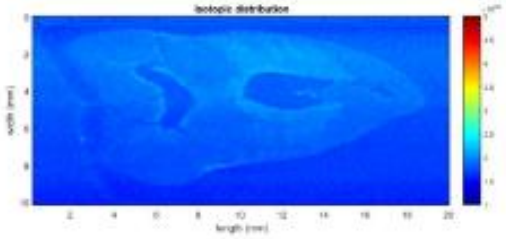

Sulfur (S^{32}) detection

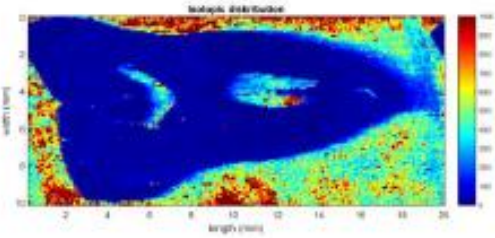

Copper (Cu^{63}) concentration

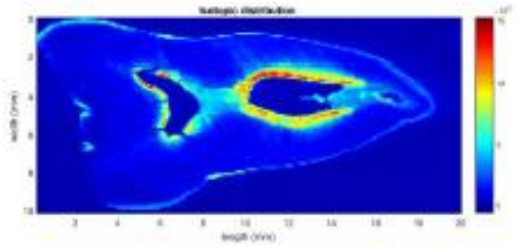

Zinc (Zn^{66}) detection

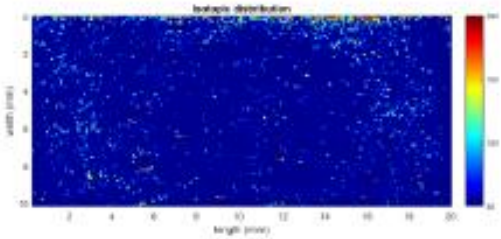

Antimony (Sb^{121}) detection

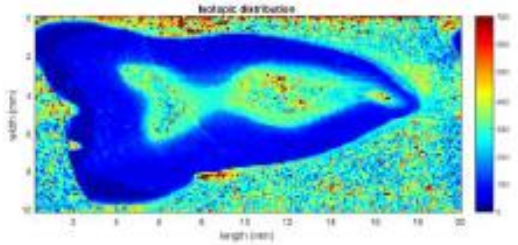

Zinc (Zn^{66}) concentration

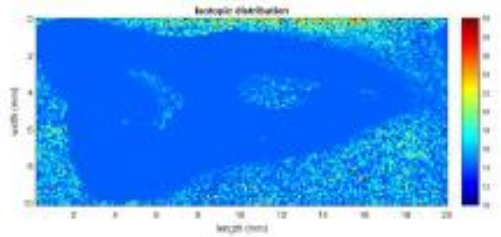

Antimony (Sb^{121}) concentration

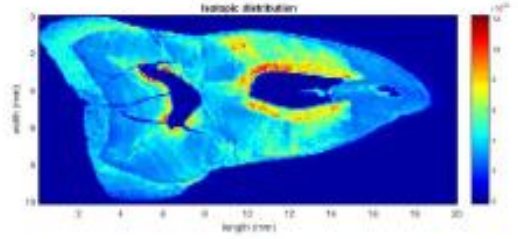

Strontium (Sr^{88}) detection

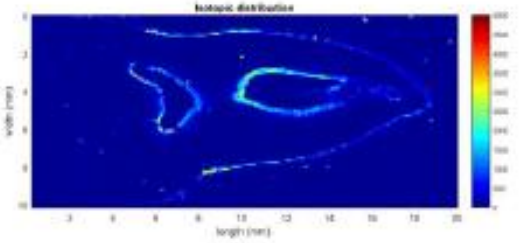

Lanthanum (La^{139}) detection

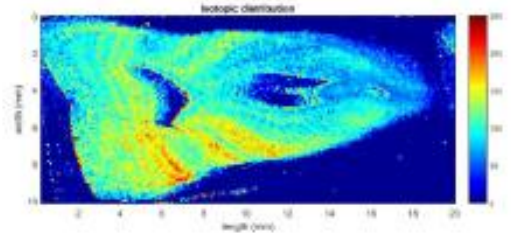

Strontium (Sr^{88}) concentration

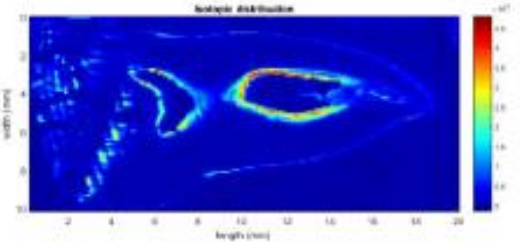

Lead (Pb^{208}) detection

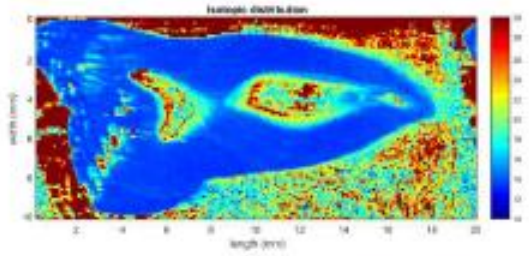

Lead (Pb^{208}) concentration

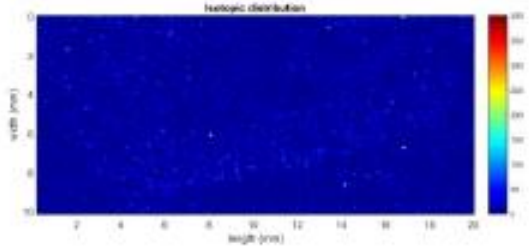

Uranium (U^{238}) detection

IIT 316-01_M2

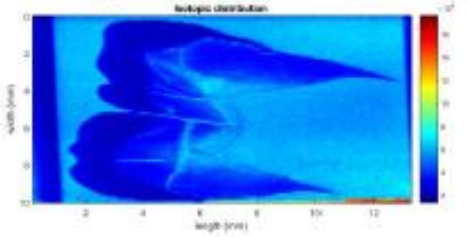

Carbon (C^{13}) detection

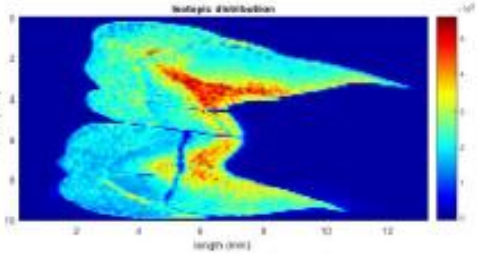

Calcium (Ca^{44}) detection

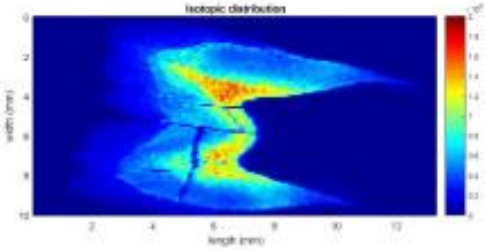

Magnesium (Mg^{24}) detection

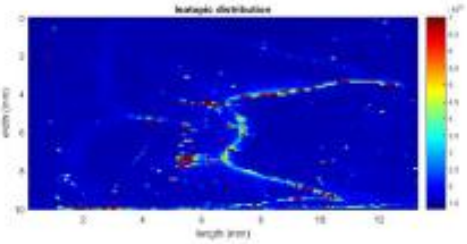

Iron (Fe^{56}) detection

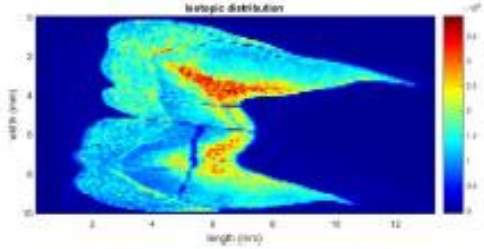

Phosphorus (P^{31}) detection

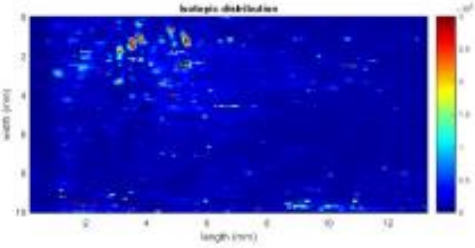

Copper (Cu^{63}) detection

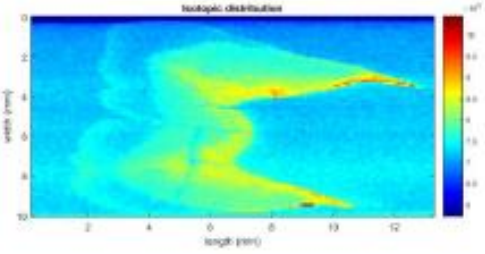

Sulfur (S^{32}) detection

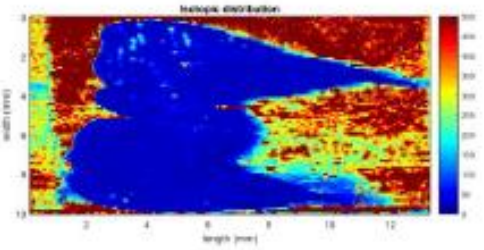

Copper (Cu^{63}) concentration

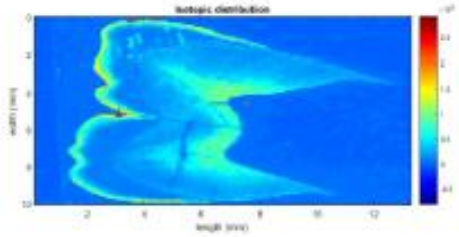

Zinc (Zn^{66}) detection

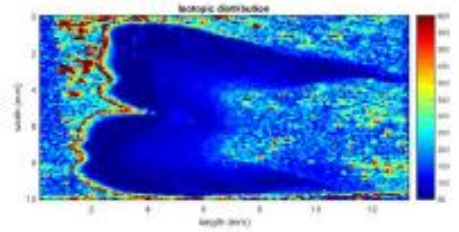

Zinc (Zn^{66}) concentration

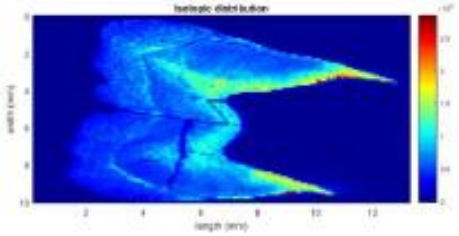

Strontium (Sr^{88}) detection

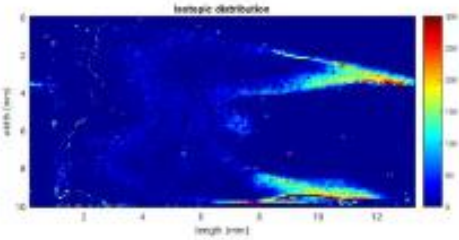

Strontium (Sr^{88}) concentration

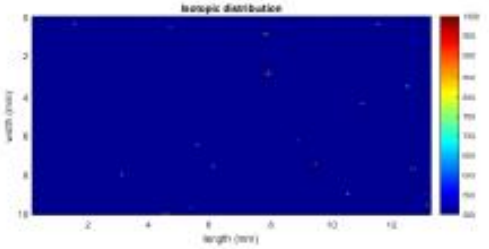

Antimony (Sb^{121}) detection

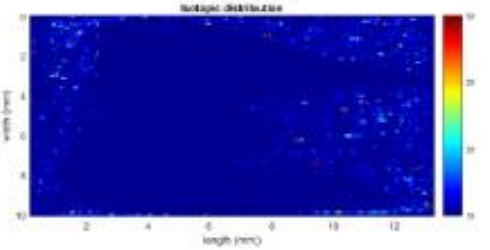

Antimony (Sb^{121}) concentration

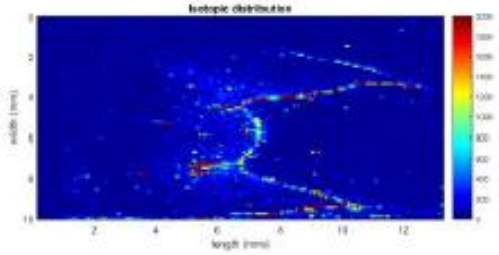

Lanthanum (La^{139}) detection

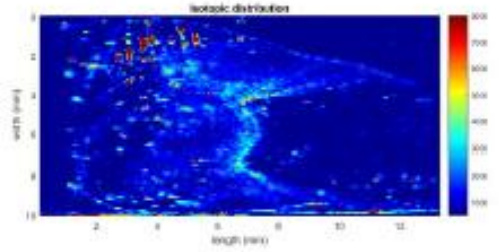

Lead (Pb^{208}) detection

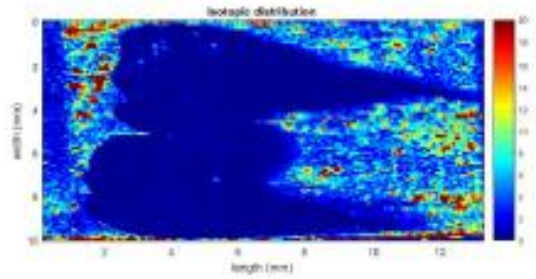

Lead (Pb^{208}) concentration

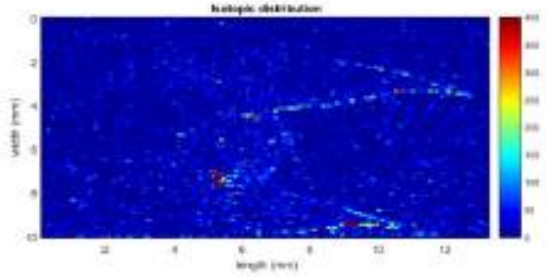

Uranium (U^{238}) detection

APPENDIX B: INTER- AND INTRA- INDIVIDUAL ELEMENT COMPARISONS BASED ON LITERATURE

Table 8. Inter- and intra- individual comparison of copper, zinc, and strontium to determine breastfeeding habits in M1 samples.

Individual	Copper (M1): Breastfed (BF) (Chandra, 1985)	Zinc (M1): Breastfed (BF) (Chandra, 1985)	Strontium (M1): Breastfed (BF) (Humphrey et al., 2014)
IIT 160-01	BF	Supplemented	Supplemented
IIT 160-02	N/A	N/A	N/A
IIT 178-01	Supplemented	BF	BF
IIT 190-01	Cow's milk	BF	BF
IIT 197-01	Supplemented	BF	Cow's milk/ Non-resident (Webb et al., 2005)
IIT 213-01	Cow's milk	BF	BF
IIT 217-01	Cow's milk	BF	BF
IIT 220-01	Deficient	Cow's milk	BF
IIT 236-01	Cow's milk	Supplemented	BF
IIT 263-01	Deficient	Supplemented	BF
IIT 312-01	Cow's milk	Cow's milk	Supplemented
IIT 315-01	Cow's milk	Cow's milk	BF
IIT 316-01	N/A	N/A	N/A

Table 9 Inter- and intra- individual variation of strontium and zinc to determine dietary consumption in M2 and M3.

Individual	Strontium (M2): Vegetarian (V) Omnivore (O) Carnivore (C) (Dolphin et al., 2005)	Strontium (M3): Vegetarian (V) Omnivore (O) Carnivore (C)	Zinc (M2): Vegetarian (V) Omnivore (O) Carnivore (C) (Kern and Mathiason, 2012)	Zinc (M3): Vegetarian (V) Omnivore (O) Carnivore (C)
IIT 160-01	N/A	N/A	N/A	N/A
IIT 160-02	V	C	V	V
IIT 178-01	O	O	C	O
IIT 190-01	N/A	N/A	N/A	N/A
IIT 197-01	V	N/A	C	**N/A**
IIT 213-01	N/A	N/A	N/A	N/A
IIT 217-01	N/A	N/A	N/A	N/A
IIT 220-01	O	O	O	O
IIT 236-01	N/A	N/A	N/A	N/A
IIT 263-01	N/A	N/A	N/A	N/A
IIT 312-01	N/A	V	N/A	O
IIT 315-01	O	N/A	O	N/A
IIT 316-01	O	N/A	O	N/A

Table 10. Inter- and intra- individual variation of exposure levels to antimony in M1, M2, and M3.

Individual	Antimony (M1)	Antimony (M2)	Antimony (M3)
IIT 160-01	No exposure	N/A	N/A
IIT 160-02	N/A	Indirect	No exposure
IIT 178-01	Exposed	No exposure	Exposed
IIT 190-01	Exposed	N/A	N/A
IIT 197-01	Indirect	Indirect	N/A
IIT 213-01	Indirect	N/A	N/A
IIT 217-01	Exposed	N/A	N/A
IIT 220-01	No exposure	No exposure	Indirect
IIT 236-01	No exposure	N/A	N/A
IIT 263-01	Indirect	N/A	N/A
IIT 312-01	Indirect	N/A	Indirect
IIT 315-01	Exposed	Exposed	N/A
IIT 316-01	N/A	Exposed	N/A

Table 11 Inter- and intra- individual variation of exposure levels of lead in M1, M2, and M3.

Individual	Lead (M1)	Lead (M2)	Lead (M3)
IIT 160-01	No exposure	N/A	N/A
IIT 160-02	N/A	Indirect	No exposure
IIT 178-01	No exposure	Indirect	No exposure
IIT 190-01	Exposed	N/A	N/A
IIT 197-01	No exposure	Indirect	N/A
IIT 213-01	No exposure	N/A	N/A
IIT 217-01	No exposure	N/A	N/A
IIT 220-01	No exposure	Indirect	Indirect
IIT 236-01	No exposure	N/A	N/A
IIT 263-01	No exposure	N/A	N/A
IIT 312-01	Indirect exposure	N/A	Indirect
IIT 315-01	Exposed	Exposure	N/A
IIT 316-01	N/A	Indirect	N/A

REFERENCES

Al-Ashban RM, Aslam M, Shah AH. 2004. Kohl (surma): a toxic traditional eye cosmetic study in Saudi Arabia. Public Health 118:292–298.

Al-Kaff A, Al-Rajhi A, Tabbara K, El-Yazigi A. 1993. Kohl-The Traditional Eyeliner: Use and Analysis. Annals of Saudi Medicine 13:26–30.

Al-Qutob MA, Alatrash HM, Abol-Ola S. 2013. Determination of different heavy metals concentrations in cosmetics purchased from the Palestinian markets by ICP/MS. AES Bioflux 5:287–293.

Anon. 1996. Trace elements in human nutrition and health. Geneva: World Health Organization.

Arora M, Hare D, Austin C, Smith DR, Doble P. 2011. Spatial distribution of manganese in enamel and coronal dentin of human primary teeth. Science of the Total Environment 409:1315–1319.

Asaduzzaman K, Khandaker MU, Baharudin NAB, Amin YBM, Farook MS, Bradley D, Mahmoud O. 2017. Heavy metals in human teeth dentin: A bio-indicator of metals exposure and environmental pollution. Chemosphere 176:221–230.

Bodnar DC, Dimitriu B. 2012. Tooth enamel trace elements. Metalurgia International 17:247-251.

Bogden JD, Klevay LM. 2010. Clinical nutrition of the essential trace elements and minerals: the guide for health professionals. Totowa, NJ: Humana Press.

Brown CJ, Chenery SR, Smith B, Mason C, Tomkins A, Roberts GJ, Sserunjogi L, Tiberindwa JV. 2004. Environmental influences on the trace element content of teeth—implications for disease and nutritional status. Archives of Oral Biology 49:705–717.

Budd P, Montgomery J, Cox A, Krause P, Barreiro B, Thomas R. 1998. The distribution of lead within ancient and modern human teeth: Implications for long-term and historical exposure monitoring. Science of the Total Environment 220:121–136.

Budd P, Montgomery J, Evans J, Barreiro B. 2000. Human tooth enamel as a record of the comparative lead exposure of prehistoric and modern people. Science of the Total Environment 263:1–10.

Chandra. 1985. Trace elements in nutrition of children. S.l.: Nestlé Nutrition.

Cox A, Keenan F, Cooke M, Appleton J. 1996. Trace element profiling of dental tissues using laser ablation-inductively coupled plasma-mass spectrometry. Fresenius Journal of Analytical Chemistry 354:254–258.

Crowder C, Heinrich J, Stout SD. 2012. Rib Histomorphometry for Adult Age Estimation. Methods in Molecular Biology Forensic Microscopy for Skeletal Tissues:109–127.

Dean MC. 2010. Incremental markings in enamel and dentine: what they can tell us about the way teeth grow. Development, Function and Evolution of Teeth:119–130.

Dean C. 2017. How the microstructure of dentin can contribute to reconstructing developing dentitions and the lives of hominoids and hominins. Comptes Rendus Palevol 16:557–571.

Dolphin AE, Goodman AH, Amarasiriwardena DD. 2005. Variation in elemental intensities among teeth and between pre- and postnatal regions of enamel. American Journal of Physical Anthropology 128:878–888.

Dupras TL, Schwarcz HP, Fairgrieve SI. 2001. Infant feeding and weaning practices in Roman Egypt. American Journal of Physical Anthropology 115:204–212.

Eerkens JW, Berget AG, Bartelink EJ. 2011. Estimating weaning and early childhood diet from serial micro-samples of dentin collagen. Journal of Archaeological Science 38:3101–3111.

Eerkens JW, Bartelink EJ. 2013. Sex-biased weaning and early childhood diet among middle holocene hunter-gatherers in Central California. American Journal of Physical Anthropology 152:471–483.

Eerkens JW, de Voogt A, Dupras TL, Rose SC, Bartelink EJ, Francigny V. 2014. Intra- and inter-individual variation in δ13C and δ15N in human dental calculus and comparison to bone collagen and apatite isotopes. Journal of Archaeological Science 52:64–71.

Eerkens JW, Sullivan K, Greenwald AM. 2016. Stable isotope analysis of serial samples of third molars as insight into inter- and intra-individual variation in ancient diet. Journal of Archaeological Science: Reports 5:656–663.

Eriksson G. 2013. Stable Isotope Analysis of Humans. Oxford Handbooks Online.

Failla ML. 2003. Trace elements and host defense: recent advances and continuing challenges. The Journal of Nutrition 133:1443S-1447S.

Fisher MM. 2012. Ancient Nubia: African kingdoms on the Nile. Cairo: The American University in Cairo Press.

Fraga CG. 2005. Relevance, essentiality, and toxicity of trace elements in human health. Molecular Aspects of Medicine 26:235–244.

Francigny V, David R, De Voogt A. 2014. Soleb & Sedeinga. Nubian Archaeological Development Organization.

Friese K, Markert B. 2000. Trace elements: their distribution and effects in the environment. Amsterdam: Elsevier.

Geissler C, Powers HJ. 2005. Human nutrition. Elsevier Churchill Livingstone.

Gibson RS. 1994. Zinc Nutrition in Developing Countries. Nutrition Research Reviews 7:151–173.

Gondal M, Dastageer M, Al-Adel F, Naqvi A, Habibullah Y. 2015. Detection of highly toxic elements (lead and chromium) in commercially available eyeliner (kohl) using laser induced break down spectroscopy. Optics & Laser Technology 75:99–104.

Grosvenor MB, Smolin LA. 2010. Visualizing nutrition: everyday choices. Hoboken, NJ: Wiley.

Gulson BL. 1996. Tooth analyses of sources and intensity of lead exposure in children. Environmental Health Perspectives 104:306–312.

Hardy AD, Walton RI, Vaishnav R. 2004. Composition of eye cosmetics (kohls) used in Cairo. International Journal of Environmental Health Research 14:83–91.

Hare D, Austin C, Doble P, Arora M. 2011. Elemental bio-imaging of trace elements in teeth using laser ablation-inductively coupled plasma-mass spectrometry. Journal of Dentistry 39:397–403.

Humphrey L, Dean M, Jeffries T. 2007. An evaluation of changes in strontium/calcium ratios across the neonatal line in human deciduous teeth. Vertebrate Paleobiology and Paleoanthropology Dental Perspectives on Human Evolution: State of the Art Research in Dental Paleoanthropology:303–319.

Humphrey LT. 2014. Isotopic and trace element evidence of dietary transitions in early life. Annals of Human Biology 41:348–357.

Kang D, Amarasiriwardena D, Goodman AH. 2004. Application of laser ablation-inductively coupled plasma-mass spectrometry (LA-ICP-MS) to investigate trace metal spatial distributions in human tooth enamel and dentin growth layers and pulp. Analytical and Bioanalytical Chemistry 378:1608–1615.

Kern J, Mathiason L. 2012. The determination of copper, zinc, and lead in human teeth using inductively coupled plasma atomic emission spectrometry (ICP-AES). Concordia College Journal of Analytical Chemistry 3:33-39.

Kumagai A, Fujita Y, Endo S, Itai K. 2012. Concentrations of trace element in human dentin by sex and age. Forensic Science International 219:29–32.

Lane D, Duffy C. 1996. The analysis of trace elements in human teeth collected from the Oxfordshire area in the UK. Nuclear Instruments and Methods in Physics Research Section B: Beam Interactions with Materials and Atoms 118:392–395.

Lee-Thorp JA, Sponheimer M, Van Der Merwe J. 2003. What do Stable Isotopes tell us about Hominid Dietary and Ecological Niches in the Pliocene? International Journal of Osteoarchaeology 13:104–113.

Lee-Thorp J, Sponheimer M. 2006. Contributions of Biogeochemistry to Understanding Hominin Dietary Ecology. Yearbook of Physical Anthropology 49:131–148.

Lekouch N, Sedki A, Nejmeddine A, Gamon S. 2001. Lead and traditional Moroccan pharmacopoeia. The Science of the Total Environment 280:39–43.

Lochner F, Appleton J, Keenan F, Cooke M. 1999. Multi-element profiling of human deciduous teeth by laser ablation-inductively coupled plasma-mass spectrometry. Analytica Chimica Acta 401:299–306.

Losee FL, Ludwig TG. 1970. Trace elements and caries. Journal of Dental Research 49:1229–1235.

Metkovic V. Badenhop NE. Ilich JZ. 2000. Trace Element and Mineral Nutrition during Lactation. Clinical Nutrition of the Essential Trace Elements and Minerals:153-181.

Moller J. 1967. Influence of Microelements on the Morphology of the Teeth. Journal of Dental Research 46:933–937.

Moorrees CF. Fanning EA. Hunt EE. 1963. Age Variation of Formation Stages for Ten Permanent Teeth. Journal of Dental Research 42:1490–1502.

Neufeld LM. 2004. Introduction to Laser Ablation ICP-MS for the Analysis of Forensic Samples. Forensic Toxicology.

Nir A. Tamir A. Zelnik N. Iancu TC. 1992. Is eye cosmetic a source of lead poisoning? Israel Journal of Medical Sciences 28:417–421.

O'Leary MH. 1988. Carbon Isotopes in Photosynthesis. BioScience 38:328–336.

Pais I, Jones JB. 1997. The handbook of trace elements. Boca Raton, FL: St. Lucie Press.

Papa S. Bartoli G. Fioretto A. 2012. Trace Metals in Fruit and Vegetable and Their Effects on Human Health. Trace Elements.

Picciano MF, Smiciklas-Wright H, Birch LL, Mitchell DC, Murray-Kolb L, Mcconahy KL. 2000. Nutritional Guidance Is Needed During Dietary Transition in Early Childhood. Pediatrics 106:109–114.

Reilly C. 2004. The nutritional trace metals. S.l.: Wiley InterScience.

Reitznerová E. Amarasiriwardena D. Kopčáková M. Barnes RM. 2000. Determination of some trace elements in human tooth enamel. Fresenius Journal of Analytical Chemistry 367:748–754.

Reynard B, Balter V. 2014. Trace elements and their isotopes in bones and teeth: Diet, environments, diagenesis, and dating of archeological and paleontological samples. Paleography, Palaeoclimatology, Palaeoecology 416:4–16.

Rilly C, Francigny V. 2010. Excavations at Sedeinga. A new start. Sudan and Nubia 14:62-68.

Rilly C, Francigny V. 2011. The late Meroitic cemetery at Sedeinga. Campaign 2010. Sudan and Nubia 15:72-79.

Rilly C, Francigny V. 2012. Excavations of the French archaeological mission in Sedeinga, 2011 season. Sudan and Nubia 16:60-71.

Rilly C, Francigny V. 2013. Sedeinga 2012. A season of unexpected discoveries. Sudan and Nubia 17:61-65.

Ruch JV, Lesot H. 2000. Molecules implicated in odontoblast terminal differentiation and dentinogenesis. Development, Function and Evolution of Teeth:22–36.

Schurr MR. 1998. Using stable nitrogen-isotopes to study weaning behavior in past populations. World Archaeology 30:327–342.

Sharp P. 2005. Minerals and Trace Elements. Human Nutrition:231-250.

Shellis RP, Dibdin GH. Enamel microporosity and its functional implications. Development, Function and Evolution of Teeth:242–251.

Shinnie PL. 1996. Ancient Nubia. London: Kegan Paul Internat.

Smith BH. 1991. Standards of human tooth formation and dental age assessment. Advances in Dental Anthropology:143-168.

Ten Cate. 1998. Oral histology: development, structure and function. Estados Unidos: Mosby.

Török L. Spuler B. Altenmüller H. 1997. The Kingdom of Kush handbook of the Napatan-Meroitic civilization. Leiden: Brill.

Uryu T, Yoshinaga J, Yanagisawa Y, Endo M, Takahashi J. 2003. Analysis of Lead in Tooth Enamel by Laser Ablation-Inductively Coupled Plasma-Mass Spectrometry. Analytical Sciences 19:1413–1416.

Webb E, Amarasiriwardena D, Tauch S, Green EF, Jones J, Goodman AH. 2005. Inductively coupled plasma-mass (ICP-MS) and atomic emission spectrometry (ICP-AES): Versatile analytical techniques to identify the archived elemental information in human teeth.

Williams A-MM, Siegele R. 2014. Iron deposition in modern and archaeological teeth. Nuclear Instruments and Methods in Physics Research B 335:19–23.